PROVENANCE AND DIAGENESIS OF THE MIOCENE BEAR LAKE FORMATION, BRISTOL BAY BASIN, ALASKA

A

THESIS

Presented to the Faculty

of the University of Alaska Fairbanks

in Partial Fulfillment of the Requirements

for the Degree of

MASTER OF SCIENCE

By

Cheryl Lynne Hartbauer

Fairbanks, Alaska

August 2010

ABSTRACT

The Miocene Bear Lake Formation (BLF) is a prospective hydrocarbon reservoir exposed on the southwestern Alaska Peninsula, extending into the subsurface to the northwest (reaching 2,360 m maximum thickness). This study comprehensively characterizes composition of BLF sandstones, and develops important implications for varying reservoir quality. Unique integration of standard petrographic methods, electron microprobe analysis (EMPA), and $^{40}Ar/^{39}Ar$ dating of detrital hornblende strengthens interpretations by providing multiple lines of evidence and a more complete picture of composition, source units and terrane, and diagenetic history than possible with petrography alone. EMPA provides superior classification of volcanic rock fragments and identification of diagenetic minerals. Results indicate a pressure-controlled diagenetic system, and a provenance more complicated than recycling of older strata, as currently interpreted. Simultaneous derivation from the Meshik Volcanics and recycling of Tolstoi, Chignik, and Naknek formations suggests erosion of a structurally-deformed source terrain (e.g. reverse-faulted anticlines). Abundance patterns of pore-filling zeolites, calcite, albite, and kaolinite likely represent variations in P_{CO2} caused by variations in burial depth. Optimal reservoir quality is likely present in the subsurface upper BLF along the northwestern coast (and deeper in the basin), where sandstone composition is presumably more quartz-rich, less volcaniclastic, and has experienced higher P_{CO2} fluid migration.

TABLE OF CONTENTS

Page

Signature Page i

Title Page ii

Abstract iii

Table of Contents iv

List of Figures vii

List of Tables xi

List of Appendices xii

Acknowledgements xiii

Chapter 1. Introduction 1

Chapter 2. Materials 7

Chapter 3. Geologic Background 12

3.1 Regional Stratigraphy 12

3.1.1 Mesozoic 12

3.1.2 Tertiary 15

3.1.3 Bear Lake Formation 16

3.1.3.1 Recent Studies of the Bear Lake Formation 18

3.2 Magmatic Arcs of the Alaska Peninsula 19

3.3 Regional Geologic Structure 20

3.3.1 Bristol Bay Basin 20

3.3.2 Bruin Bay Fault and Ugashik Lakes Fault System 21

3.3.3 Ugashik Sub-Basin 21

3.3.4 Structure of the Herendeen Bay - Port Moller Area 22

Chapter 4. Petrography 23

4.1 Introduction 23

4.2 Methods 24

Page

4.3 Results 31
4.3.1 Point Count Data 31
4.3.2 Ternary Diagrams 43
4.3.2.1 Quartz, Feldspar, and Lithic Grains 43
4.3.2.2 Monocrystalline Components 49
4.3.2.3 Composition of Lithic Grains 52
4.3.2.4 Intergranular Components 55
4.3.2.5 Tectonic Provenance Diagrams 59
4.4 Discussion 59
4.5 Conclusions 66
Chapter 5. Electron Microprobe Analysis 67
5.1 Introduction 67
5.2 Methods 67
5.2.1 Analytical Routine and Strategy 67
5.2.2 Criteria for Naming Clays 73
5.2.3 Potential Sources of Error 75
5.3 Results 76
5.3.1 Diagenetic Mineralogy 76
5.3.2 Volcanic Rock Fragments 84
5.3.2.1 Mineralogy and Alteration 84
5.3.2.2 Composition 90
5.3.3 Detrital Plagioclase Clasts 100
5.4 Discussion 104
5.4.1 Evaluation of Petrographic Identifications of Diagenetic Minerals 104
5.4.2 Classification of Volcanic Rock Fragments 105
5.4.2.1 Potential Volcanic Provenance 107

Page

5.4.3 Detrital Plagioclase Clast Provenance 111
5.5 Conclusions 111
Chapter 6. Geochronology 114
6.1 Introduction 114
6.2 Methods 114
6.3 Results 116
6.4 Discussion 134
6.4.1 Potential Igneous Source Rocks on the Alaska Peninsula 134
6.4.2 Sources of Detrital Hornblende in the Upper Bear Lake Formation 139
6.4.2.1 Jurassic 139
6.4.2.2 Early Cretaceous 140
6.4.2.3 Paleocene to Early Eocene 140
6.4.2.4 Eocene to Oligocene 141
6.5 Conclusions 142
Chapter 7. Provenance 144
Chapter 8. Diagenesis 151
8.1 Introduction 151
8.2 Thermal maturity 151
8.3 Mineral stability 154
8.3.1 Heulandite-Laumontite-Calcite 154
8.3.2 Kaolinite-Laumontite-Calcite 158
8.4 Summary and Conclusions 165
Chapter 9. Summary and Conclusions 170
References Cited 177
Appendicies 185

LIST OF FIGURES

Page

1.1 Location of study area 2

1.2 Cartoon illustrating progressive erosion of older strata 3

1.3 Photomicrographs showing varying porosity in the Bear Lake Formation 5

2.1 Sample locality map 8

2.2 Chronostratigraphic correlation of measured stratigraphic sections of the Bear Lake Formation 9

3.1 Map of generalized geologic units and structure of the Alaska Peninsula 13

3.2 Stratigraphic column of the Alaska Peninsula 14

3.3 Distribution of the Bear Lake Formation on the Alaska Peninsula 17

4.1 Proportion of authigenic components identified in outcrop samples during point count analysis 42

4.2 Summary of petrographically identified pore-filling and replacement components in outcrop samples 44

4.3 Summary of petrographically identified pore-filling and replacement components in well samples 45

4.4 Quartz/Feldspar/Lithic Grains ternary diagrams 46

4.5 Ratio of stable quartzose lithic grains to total quartz 47

4.6 Ratio of chert to total stable quartzose lithic grains 48

4.7 Monocrystalline Quartz/Plagioclase/K-Feldspar (QmPK) ternary diagram 50

4.8 Ratio of plagioclase to total feldspar 51

4.9 Ternary diagrams of the lithic components 53

4.10 Ratio of undifferentiated quartz (Qu) to total lithics including chert and undifferentiated quartz (L + Qu) 54

4.11 Proportion of plutonic and volcanic rock fragments in the igneous lithic portion of the framework 56

4.12 Proportion of petrographically determined volcanic rock compositions in the volcanic lithic portion of the framework 57

4.13 Ternary diagrams of the framework and intergranular portions of samples 58

4.14 Ternary diagrams with tectonic provenance fields 60

4.15 Framework percentages of key components distinguishing the lower Bear Lake Formation from upper Bear Lake Formation 62

Page

5.1 Photomicrographs of plutonic rock fragments 72

5.2 Summary of pore-filling and replacement components of detrital minerals identified in outcrop samples using electron microprobe analysis 81

5.3 Summary of pore-filling and replacement components of detrital minerals identified in well samples using electron microprobe analysis 82

5.4 Photomicrographs of volcanic rock fragments with porphyritic texture 85

5.5 Photomicrographs of volcanic rock fragments with trachytic texture 86

5.6 Photomicrographs of volcanic rock fragments with mosaic textures 87

5.7 Photomicrographs of volcanic rock fragments with calcite replacement 89

5.8 Groundmass compositions of volcanic rock fragments from the Bear Lake Formation 91

5.9 Percent phenocrysts versus SiO_2 and Na_2O+K_2O 93

5.10 Total alkali-silica diagram showing groundmass and corrected groundmass compositions 95

5.11 Corrected groundmass compositions of volcanic rock fragments from the Bear Lake Formation 96

5.12 Weight percent SiO_2 versus TiO_2 of groundmass in volcanic rock fragments from the Bear Lake Formation 97

5.13 Composition of plagioclase phenocrysts in volcanic rock fragments from Bear Lake Formation outcrop samples 98

5.14 Composition of plagioclase phenocrysts in volcanic rock fragments from Bear Lake Formation well samples 99

5.15 Composition of detrital plagioclase clasts from Bear Lake Formation outcrop samples 101

5.16 Composition of detrital plagioclase clasts from Bear Lake Formation well samples 102

5.17 Photomicrographs of detrital plagioclase clasts 103

5.18 Distribution of potential volcanic provenance units for the Bear Lake Formation 108

5.19 Quadrangle location map of the Alaska Peninsula 110

5.20 Comparison of detrital and phenocryst plagioclase compositions 112

6.1 $^{40}Ar/^{39}Ar$ ages of representative detrital hornblende grains from the Bear Lake Formation 120

6.2 ^{39}Ar release versus Ca/K plot for samples BL5-95, LH1-182, and LH1-164 121

6.3 Atmospheric ^{40}Ar versus calculated age plot for grains analyzed from sample BL5-95 122

Page

6.4 ^{39}Ar release versus calculated age plot for grains analyzed from sample BL5-95 123

6.5 Ca/K versus calculated age plot for grains analyzed from sample BL5-95 124

6.6 Flowchart illustrating parameters used for filtering of $^{40}Ar/^{39}Ar$ data for sample BL5-95 125

6.7 Atmospheric ^{40}Ar versus calculated age plot for grains analyzed from sample LH1-182 126

6.8 ^{39}Ar release versus calculated age plot for samples BL5-95, LH1-182, and LH1-164 128

6.9 Flowchart illustrating parameters used for filtering of $^{40}Ar/^{39}Ar$ data for sample LH1-182 129

6.10 Atmospheric ^{40}Ar versus calculated age plot for grains analyzed from sample LH1-164 130

6.11 Ca/K versus calculated age plot for grains analyzed from sample LH1-164 131

6.12 ^{39}Ar release versus calculated age plot for sample LH1-164 132

6.13 Flowchart illustrating parameters used for filtering of $^{40}Ar/^{39}Ar$ data for sample LH1-164 133

6.14 Probability distribution of detrital hornblende ages 135

6.15 Plot of ages for Bear Lake Formation hornblende and igneous rocks of the Alaska Peninsula 136

6.16 Map showing generalized location of Meshik arc rocks and the Alaska-Aleutian Range batholith .. 138

7.1 Progressive erosion of older strata during deposition of the Bear Lake Formation 146

7.2 Cartoons illustrating possible structural deformation of source area 147

7.3 Simple model of erosion and corresponding deposition of the Bear Lake Formation 148

7.4 Cartoon illustrating the fault-controlled Ugashik sub-basin 150

8.1 Summary of diagenetic mineralogy 152

8.2 Vitrinite reflectance (R_o) versus depth 153

8.3 Heulandite-Laumontite-Quartz stability diagram 156

8.4 Kaolinite-Laumontite-Prehnite stability related to P_{CO2} and temperature 157

8.5 Weight percent CaO and Na_2O versus burial depth in the Bear Lake Formation 159

8.6 Kaolinite-Muscovite-K-feldspar stability diagram 160

8.7 Kaolinite-Muscovite-K-feldspar-Albite stability diagram 161

8.8 Relationship of Ca^{2+} concentration in solution, P_{CO2}, and pH 163

8.9 Fe-bearing mineral stability diagram 164

Page

8.10 Summary diagram of the pressure-dependant diagenetic system in the Bear Lake Formation 166

8.11 Schematic illustration of P_{CO2} effects on precipitation of kaolinite versus calcite..... 167

8.12 Schematic representation of relative temperatures experienced by measured sections of the Bear Lake Formation 169

9.1 Diagenetic variation of the Bear Lake Formation..... 173

A-1 Outcrop exposure of the Unga Formation..... 186

LIST OF TABLES

Page

2.1 List of samples and analyses 10

4.1 Classification scheme of original point count categories 25

4.2 Petrographic parameters used in ternary calculations based on traditional point counts 29

4.3 Explanation of ternary diagram parameters based on Gazzi-Dickinson approximations 30

4.4 Lithologic description of samples based on petrographic analysis 33

4.5 Summary of compositional point count data 34

4.6 Detailed point count category framework percentages 35

4.7 Detailed point count category whole-rock percentages 36

4.8 Pore-filling minerals identified during point count analysis 39

4.9 Replacement minerals identified during point count analysis 40

5.1 Electron microprobe analysis analytical routine details 68

5.2 Standard assignments used for peaking and measuring intensities 70

5.3 Average analytical error of electron microprobe analyses of feldspar 74

5.4 Clay and mica mineral formulas 74

5.5 Pore-filling components identified using electron microprobe analysis 77

5.6 Alteration and replacement of detrital minerals identified using electron microprobe analysis 78

5.7 Alteration and replacement mineralogy of volcanic rock fragments identified using electron microprobe analysis 79

5.8 Summary of feldspar clasts analyzed using electron microprobe analysis 80

6.1 $^{40}Ar/^{39}Ar$ single grain fusion data for detrital hornblende grains from sample BL5-95 117

6.2 $^{40}Ar/^{39}Ar$ single grain fusion data for detrital hornblende grains from sample LH1-182 118

6.3 $^{40}Ar/^{39}Ar$ single grain fusion data for detrital hornblende grains from sample LH1-164 119

B-1 Description of volcanic rock fragments analyzed by electron microprobe analysis 193

C-1 Major oxide chemistry of Bear Lake Formation sandstones 212

C-2 Minor element chemistry of Bear Lake Formation sandstones 213

LIST OF APPENDICES

Page

A Bear Lake Formation Bibliography 185

B Description of Volcanic Rock Fragments in Sandstones of the Bear Lake Formation 191

C X-Ray Fluorescence Analytical Methods and Data 211

ACKNOWLEDGEMENTS

This study was funded as part of the four-year (2004-2007) Bristol Bay – Alaska Peninsula energy program completed by the Alaska Division of Geological and Geophysical Surveys, Alaska Division of Oil and Gas, and Bristol Bay Native Corporation. My research was funded in part by a U.S. Department of Energy grant through the Arctic Energy Technology Development Laboratory at the University of Alaska Fairbanks, provided to Rocky Reifenstuhl (Alaska Division of Geological and Geophysical Surveys) and Paul McCarthy (University of the Alaska Fairbanks). Kenneth Helmold provided additional funds from the Alaska Division of Oil and Gas to support the electron microprobe analyses completed during this study.

There are several people who deserve many thanks for their support throughout this project. First, I would like to thank my advisors and committee members for their guidance, patience, and enthusiasm. I very much appreciate the time that Rocky Reifenstuhl and Kate Bull volunteered outside of their daily careers at the Alaska Division of Geological and Geophysical Surveys in order to serve on my committee. I must also thank Paul McCarthy and Rainer Newberry, my co-advisors, for the great balance of calm and excitement that their partnership as advisors provided. Working with the two was quite a bit like day and night, which offered me the best of both worlds – and 24 hour support on occasion.

Emily Finzel deserves a thank you for her help with brainstorming project ideas early on, and providing me with many resources to familiarize myself with general geology and stratigraphy of the Bristol Bay basin during my first semester as a graduate student. I am thankful for the expertise that Kenneth Helmold provided throughout my project, and his willingness to answer my many questions. I also appreciate the time that Christopher Nye (Alaska Volcano Observatory) took to meet with me on multiple occasions. I would also like to thank Paul Decker (Alaska Division of Oil and Gas) for taking time out of his very busy schedule to talk with me about structure of the Alaska Peninsula, and Frederic Wilson (U.S. Geological Survey) for sharing his insight and knowledge of the geology of the Alaska Peninsula. I also want to thank Paul Layer, who was willing to run many more samples than I expected for a geochronology class project, which ultimately became it's own chapter in my thesis. And last, but not least, I would like to thank my fellow graduate students who gave our office the right combination of motivation and distraction.

CHAPTER 1. INTRODUCTION

The Bear Lake Formation is a Middle to Late Miocene sedimentary unit exposed in outcrops on the southwest end of the Alaska Peninsula near Port Moller, and in several wells near the Port Moller area and in the Bristol Bay lowlands along the northwestern coast of the peninsula (Fig. 1.1). The Bear Lake Formation is considered to be a prospective hydrocarbon reservoir in the region (Lyle et al., 1979; Decker et al., 2005; Finzel et al., 2005; Decker et al., 2006; Sherwood et al., 2006; Helmold et al., 2008). The State of Alaska has conducted the most recent studies of the Bear Lake Formation as part of a four-year program that focused on petroleum system characterization of Bristol Bay and the Alaska Peninsula (Reifenstuhl and Decker, 2008).

There is agreement among most authors that the Bear Lake Formation is more quartz-rich, and contains a greater abundance of non-volcanic clasts, than other Tertiary sedimentary units on the Alaska Peninsula as a result of recycling of Mesozoic sedimentary rocks (Burk, 1965; Wisehart, 1971; Lyle et al., 1979; Nilsen, 1984; Wilson, 1985; Detterman, 1990; Wilson et al., 1995; Detterman et al., 1996; Wilson et al., 1999). Although this interpretation is commonly accepted, no detailed studies have addressed the framework composition or diagenetic mineralogy of the Bear Lake Formation, with one exception – a recent study by Helmold et al. (2008) on reservoir quality of Tertiary sandstones from wells of the Bristol Bay basin included petrogrpahic anlaysis of 28 subsurface samples from the Bear Lake Formation. Although the Bear Lake Formation may be less volcanic-rich than other Tertiary units, Helmold et al. (2008) report sandstone framework compositions containing as much as 25% volcanic rock fragments and show that these volcanic rock fragments are the primary lithic component in some samples. Additionally, ternary diagrams presented by Helmold et al. (2008) indicate a compositional range in sandstones of the Bear Lake Formation.

Given the recycled origin of the Bear Lake Formation, one might expect its composition to record progressive erosion reflecting an inverse stratigraphy of older strata (Fig. 1.2). In that case, compositional changes within the Bear Lake Formation would occur up-section, and these changes would affect reservoir quality. In order to identify compositional variation within the Bear Lake Formation, and

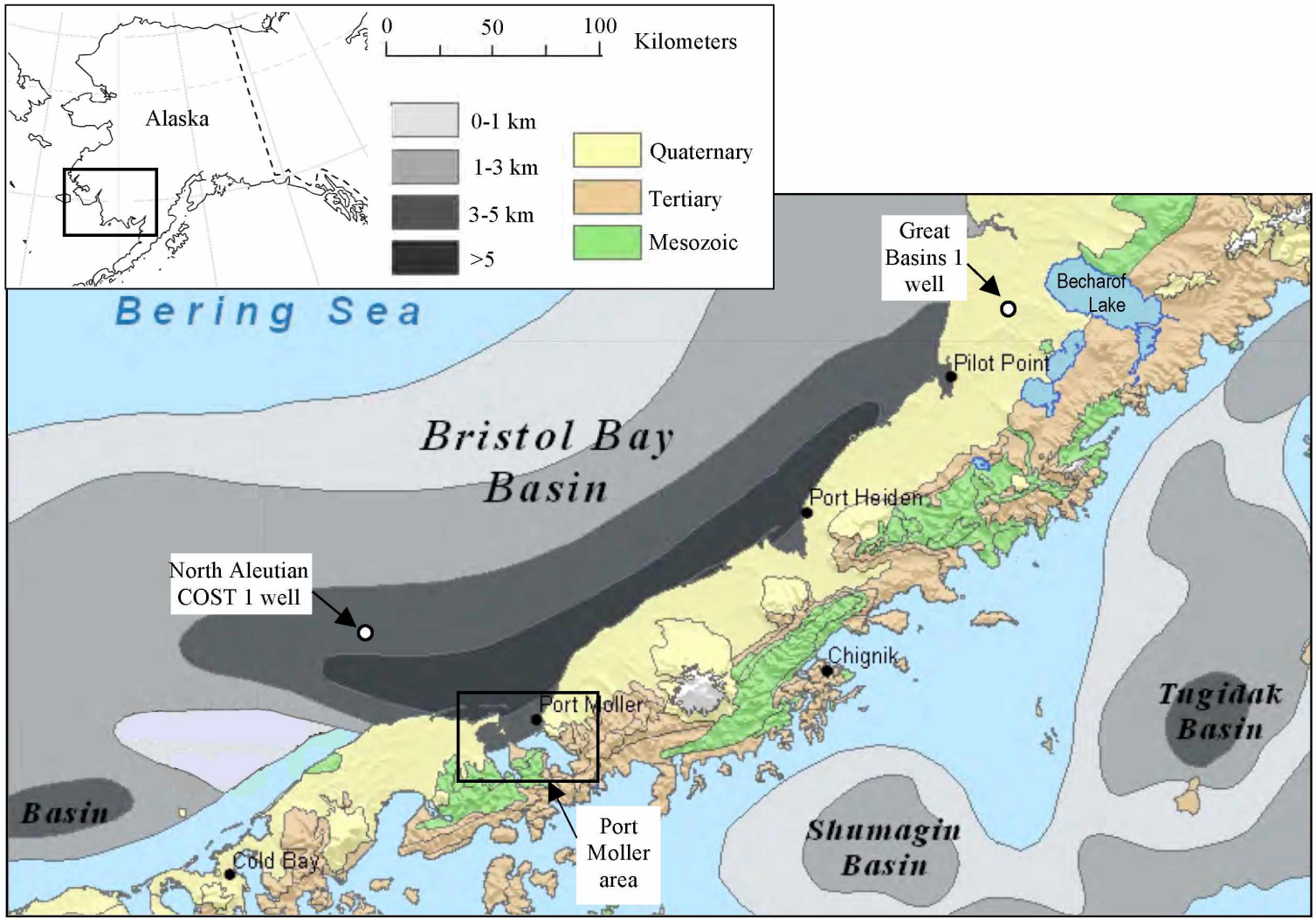

Fig. 1.1 Location of study area. Map shows generalized geology of the region and sedimentary basin thickness. Modified from Finzel et al. (2005).

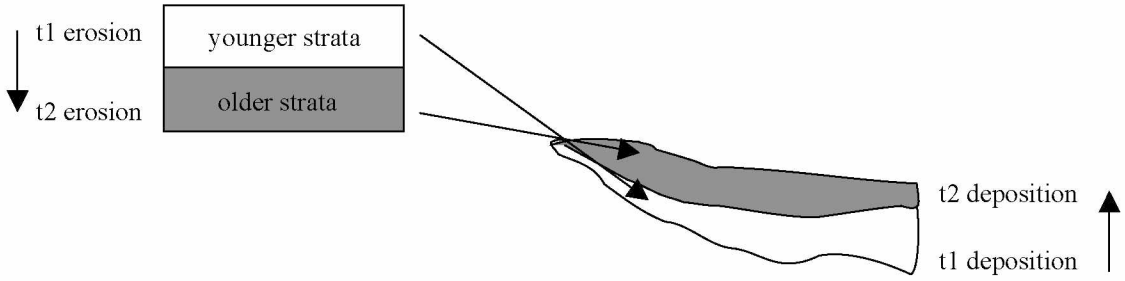

Fig. 1.2 Cartoon illustrating progressive erosion of older strata. The erosion results in an inverse stratigraphy during deposition.

to understand the pattern of variation, a more in-depth compositional characterization and a more detailed provenance interpretation are needed.

Porosity directly impacts reservoir quality, and one factor that affects porosity is diagenetic mineralogy (Boggs, 2003). Diagenetic mineralogy is, in turn, controlled by temperature, pressure and fluid conditions (Faure, 1998; Boggs, 2003). Petrographic comparison of samples used in this study indicates that porosity of the Bear Lake Formation is greater in the North Aleutian COST 1 and the Great Basins 1 wells than in outcrops near Port Moller (Fig. 1.1 and Fig. 1.3). Available thermal maturation data (Flett, 1988; Molenaar, 1996; Bergman et al., 2008) also indicate differing diagenetic conditions between these locations. A better understanding of the diagenetic mineralogy of the formation, therefore, is needed in order to determine the factors controlling the diagenetic system, and thus the variation in, and distribution of reservoir quality.

The purpose of this study is to definitively characterize the composition of sandstones in the Bear Lake Formation in order to refine existing provenance interpretations and to determine diagenetic conditions. I integrated multiple tools, going beyond standard petrographic analysis, in order to characterize the composition. I combined petrographic point counting with electron microprobe analysis (EMPA) and geochronology. Point counts were performed for all samples that I analyzed using the electron microprobe. Point count data provided identification and abundance of compositional components. I used EMPA to characterize the composition of volcanic rock fragments in the formation, which have largely been overlooked by previous studies. I also performed analyses on detrital plagioclase clasts to obtain anorthite percentages to aid in provenance determination, and to identify albite which is diagenetically significant. I also analyzed pore-filling components to supplement the point count data. $^{40}Ar/^{39}Ar$ dates for detrital hornblende from three samples were obtained to identify ages of source units.

This thesis is organized into nine chapters. Following this introduction, Chapter 2 presents information on the materials I used and provides sample names and locations. Chapter 3 summarizes the geologic background of the Alaska Peninsula and Bristol Bay basin. I address the regional stratigraphy, history of magmatic arcs, and regional structure. Chapter 4 outlines petrographic methods and reports point

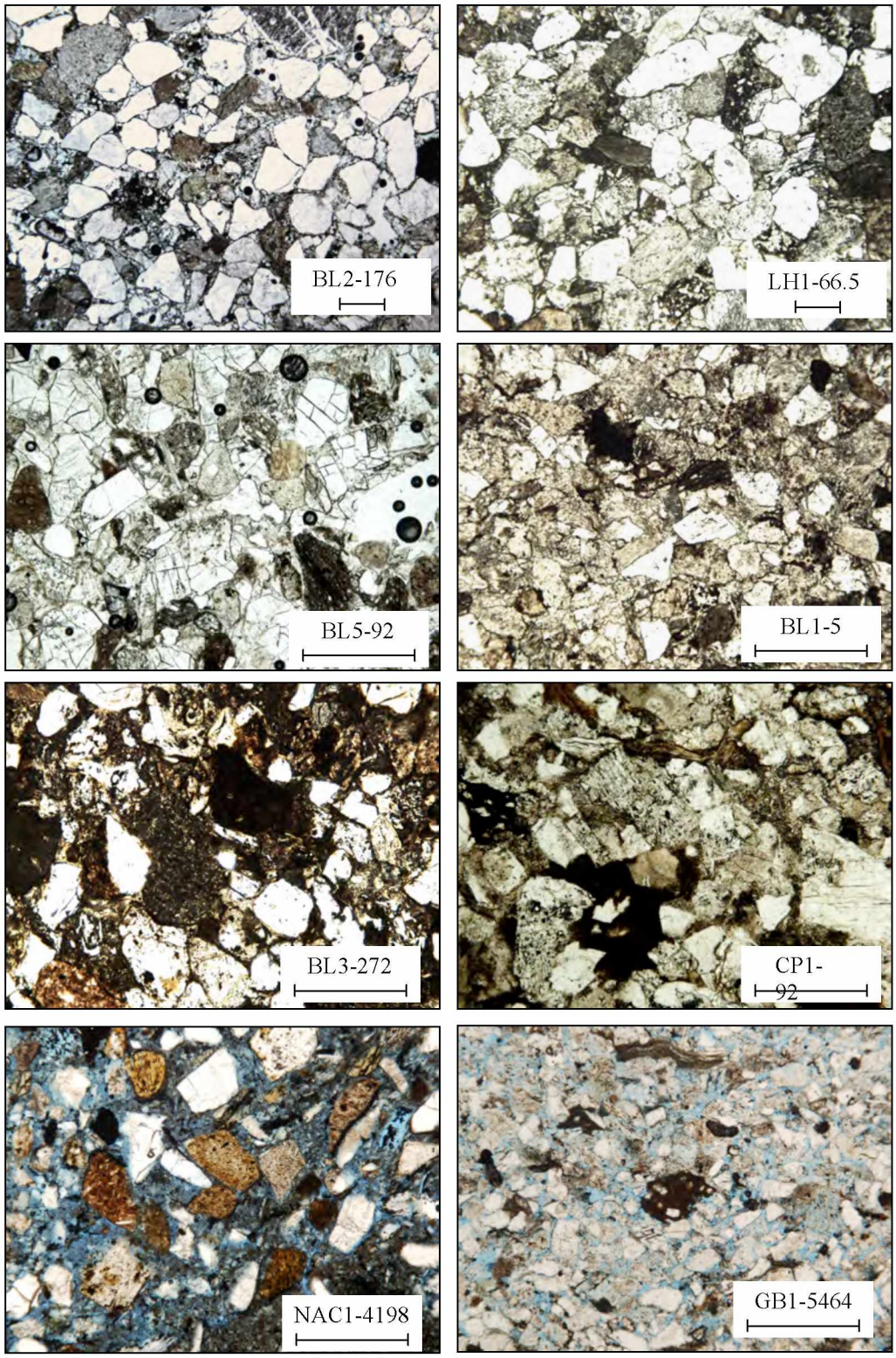

Fig. 1.3 Photomicrographs showing varying porosity in the Bear Lake Formation. All scale bars represent 0.5 mm. Samples are from outcrops in the Port Moller area (BL2-176, LH1-66.5, BL5-92, BL1-5, BL3-272, and CP1-92), and the North Aleutian COST 1 (NAC1-4198) and Great Basins 1 (GB1-5464) wells. Blue-dyed epoxy fills pores, and indicates greater porosity in the well samples.

count results in tables and on ternary diagrams in order to illustrate compositional differences that I identified. The petrographic discussion and conclusions focus on provenance interpretation. Chapter 5 describes the methods I used for EMPA and reports the diagenetic mineralogy, composition of volcanic rock fragments, and composition of detrital plagioclase clasts. The EMPA discussion and conclusions focuses on evaluating petrographic identifications as compared to EMPA identifications, classification of volcanic rock fragments in the Bear Lake Formation, and interpretation of provenance. Chapter 6 presents $^{40}Ar/^{39}Ar$ analysis methods and results. The geochronology discussion and conclusions focus on provenance interpretation. Chapter 7 summarizes provenance interpretations based on petrography, EMPA, and geochronology. Chapter 8 addresses diagenesis of the Bear Lake Formation. Discussion of thermal maturity indicators and diagenetic mineralogy identified by petrography and EMPA identifies the major factors controlling the diagenetic system in the Bear Lake Formation. Chapter 9 summarizes provenance and diagenetic interpretations and presents implications for reservoir quality and recommendations for future work.

CHAPTER 2. MATERIALS

The Alaska Division of Geological and Geophysical Surveys (ADGGS) collected samples of the Bear Lake Formation that I used in this study during the 2004 through 2006 field seasons from outcrops in the Herendeen Bay and Port Moller area of the Alaska Peninsula (Fig. 2.1). This study presents analyses of eighteen samples from seven different measured stratigraphic sections (Fig. 2.1). Emily Finzel and Rocky Reifenstuhl of the ADGGS provided these samples. Rocky Reifenstuhl provided additional samples from outcrops of the Bear Lake Formation which I used during preliminary stages of my research (Hartbauer, 2008). Samples from measured sections became the primary focus of my analyses because these samples have a known stratigraphic context which facilitated my objective of evaluating compositional variation up-section as related to changes in provenance and diagenetic environment. Locality details, stratigraphy and sedimentology, depositional environment, and structural deformation pertaining to the measured stratigraphic sections are given by Decker et al. (2005) and Finzel et al. (2005). Palynomorph and megafauna fossils provide age and environmental constraints for measured sections (Finzel et al., 2005; Blodgett et al., 2008). Chronostratigraphic correlation of the seven measured sections by Decker et al. (2005) is key to this study (Fig. 2.2).

I included several subsurface samples of the Bear Lake Formation in addition to outcrop samples. Kenneth Helmold of the Alaska Division of Oil and Gas (DOG) provided thin sections and sample billets of sandstones from the North Aleutian COST 1 and Great Basins 1 wells (Fig. 2.1). Samples from the North Aleutian COST 1 well provide a view of the Bear Lake Formation at the center of the depositional basin (Bristol Bay basin). The three samples I studied from this well are the only material that was available. Samples made available to me by the DOG from the Great Basins 1 well are distributed through the entire interval of the Bear Lake Formation in the well (3,700 ft to 10,320 ft; Mickey et al., 2005; Decker et al., 2008a). The completeness of the sample distribution made Great Basins 1 well a good resource of sample material for the purposes of evaluating up-section formation changes. The Great Basins 1 well is located in the Ugashik sub-basin at the northern end of the greater Bristol Bay basin (see Chapter 3).

Table 2.1 lists samples and corresponding analyses. Names of the measured section samples use the section abbreviation as a prefix, followed by the sample height from the base of the section in meters.

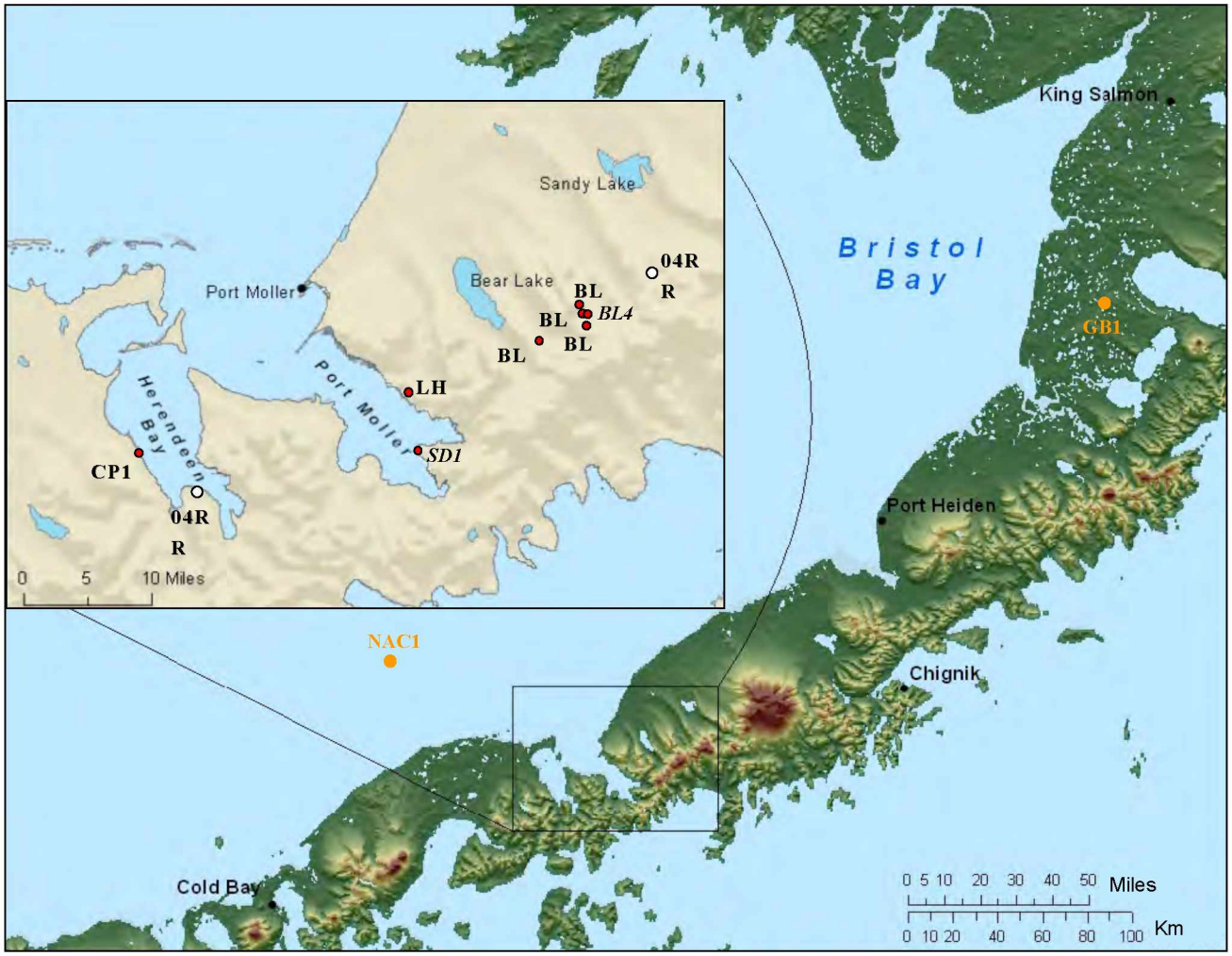

Fig 2.1 Sample locality map. Red dots on inset indicate measured stratigraphic section locations: Bear Lake 1 (BL1), Bear Lake 2 (BL2), Bear Lake 3 (BL3), Bear Lake 4 (BL4), Bear Lake 5 (BL5), Coal Point 1 (CP1), Left Head 1 (LH1), and Sundean (SD1). Samples from BL4 and SD1 were not included in this study. White dots on inset indicate outcrop samples used for preliminary analyses. Orange dots on the map indicate well locations: Great Basins 1 (GB1) and North Aleutian COST 1 (NAC1). Measured section locations given by Finzel et al. (2005) and Decker et al. (2005). Modified from Finzel et al. (2005). See Fig. 2.2 for chronostratigraphic correlation of measured stratigraphic sections (Decker et al., 2005).

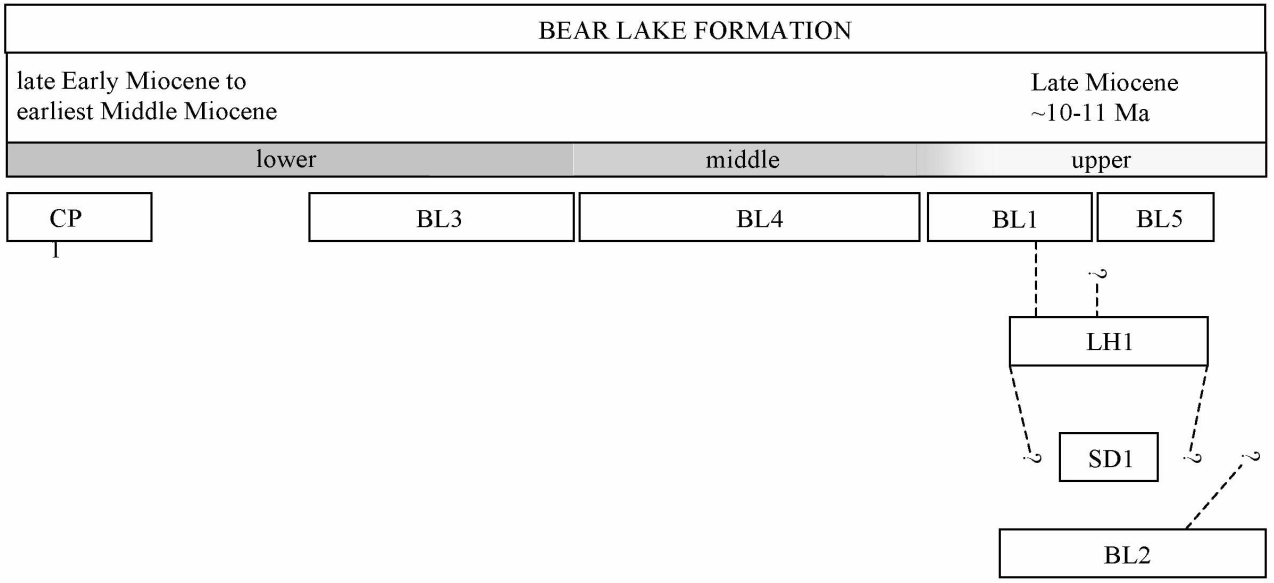

Fig. 2.2 Chronostratigraphic correlation of measured stratigraphic sections of the Bear Lake Formation. Correlations are from Decker et al. (2005), and based on palynological or macrofossil (bivalve and gastropod) interpretations (Finzel et al., 2005; Blodgett et al., 2008). Lower, middle, and upper designations are informal and based on Decker et al. (2005). Abbreviations of measured sections are as follows: Bear Lake 1 (BL1), Bear Lake 2 (BL2), Bear Lake 3 (BL3), Bear Lake 4 (BL4), Bear Lake 5 (BL5), Coal Point 1 (CP1), Left Head 1 (LH1), and Sundean 1 (SD1). See Fig. 2.1 for measured section locations. Modified from Decker et al. (2005).

Table 2.1 List of samples and analyses. Names of measured section samples use the section abbreviation as the prefix, followed by the sample height from the base of the section in meters. Abbreviations are defined as follows: Bear Lake 1 (BL1), Bear Lake 2 (BL2), Bear Lake 3 (BL3), Bear Lake 4 (BL4), Bear Lake 5 (BL5), Coal Point 1 (CP1), electron microprobe analysis (EMPA), Great Basins 1 well (GB1), Left Head 1 (LH1), and North Aleutian COST 1 well (NAC1). See Fig. 2.1 for a map of sample locations.

Sample Name (this study)	Location		Notes	Analyses			Preliminary Study
				Point Count	EMPA	$^{40}Ar/^{39}Ar$	
BL2-176	measured section BL2			x	x		x
LH1-182	measured section LH1			x	x	x	
LH1-164	measured section LH1			x	x	x	
LH1-120	measured section LH1			x	x		
LH1-66.5	measured section LH1			x	x		
LH1-2	measured section LH1			x	x		
BL5-95	measured section BL5					x	
BL5-92	measured section BL5			x	x		x
BL5-52	measured section BL5			x	x		
BL1-155	measured section BL1		original sample name = 06RR124a	x	x		
BL1-5	measured section BL1		original sample name = 06RR121a	x	x		
BL3-272	measured section BL3			x	x		
BL3-205	measured section BL3			x	x		x
BL3-193	measured section BL3			x	x		
BL3-36	measured section BL3			x	x		
CP1-185	measured section CP1			x	x		
CP1-92	measured section CP1			x	x		
CP1-11	measured section CP1			x	x		
04RR163b	outcrop		preliminary study only	x	x		x
04RR152b	outcrop		preliminary study only	x	x		x
	Well	**Depth (ft)**					
GB1-3890	GB1	3890-91	well core chip	x	x		
GB1-4945	GB1	4945-46	well core chip	x	x		
GB1-5464	GB1	5464-65	well core chip	x	x		
GB1-6083	GB1	6083-84	well core chip	x	x		
GB1-8236	GB1	8236-37	well core chip	x	x		
GB1-9823	GB1	9823-24	well core chip	x	x		
NAC1-4195	NAC1	4195	well core plug	x	x		
NAC1-4197	NAC1	4197	well core plug	x	x		
NAC1-4198	NAC1	4198	well core plug	x	x		

For example, sample BL2-176 is from measured section Bear Lake 2, 176 meters up-section from the base. Samples 06RR121a and 06RR124a are from measured section BL1, and I refer to them as BL1-5 and BL1-155 to conform to the sample naming convention used for other samples from measured sections. For the well samples, I use the prefixes "NAC1" to indicate samples from the North Aleutian COST 1 well and "GB1" to indicate samples from the Great Basins 1 well. I refer to well samples without noting the depth range for brevity. For example, I refer to sample 3890-91 from the Great Basins 1 well as GB1-3890.

CHAPTER 3. GEOLOGIC BACKGROUND

3.1 Regional Stratigraphy

Mesozoic and Cenozoic rocks form a well-exposed succession covering the Alaska Peninsula with an average thickness of 7,000 m to 8,000 m (Fig. 3.1 and Fig. 3.2; Detterman et al., 1996). A thorough report on the stratigraphy of the Alaska Peninsula is given by Detterman et al. (1996). Geologic mapping of the Alaska Peninsula has been compiled by Wilson et al. (1999) into a digital regional geologic map of the peninsula with accompanying text that provides a stratigraphic and brief structural overview of the Alaska Peninsula terrane, divided into the Iliamna and Chignik subterranes.

3.1.1 Mesozoic

The backbone of the Alaska Peninsula is composed of 8,500 m of Mesozoic sedimentary rocks of the Chignik subterrane that are predominantly of marine origin (Fig. 3.1 and Fig. 3.2; Detterman et al., 1996). The oldest Mesozoic rocks on the Alaska Peninsula are limestone of the Late Triassic Kamishak Formation (Burk, 1965; Detterman et al., 1996). Jurassic volcaniclastic sandstones, siltstones, and shales of the Talkeetna Formation, and sandstones, siltstones, and shales of the Kialagvik and Shelikof formations record the development and subsequent erosion of an Early Jurassic magmatic arc (Wilson et al., 1999).

The Late Jurassic Nakenk Formation, composed of arkosic sandstones and conglomerates, is the most prevalent Mesozoic unit on the Alaska Peninsula and is subdivided into five members: the basal Chisik Conglomerate Member, Northeast Creek Sandstone Member, Sung Harbor Siltstone Member, Indecision Creek Sandstone Member, and Katolinat Conglomerate Member (Detterman et al., 1996; Wilson et al., 1999). The Naknek Formation contains the first significant contribution of granitic detritus, recording rapid uplift and erosion of the Jurassic portion of the Alaska-Aleutian Range batholith and older sedimentary rocks (Burk, 1965; McLean, 1979; Wilson, 1980; Detterman et al., 1996; Wilson et al., 1999).

The siltstones and sandstones of the Staniukovich Formation and thin calcareous sandstones of the Herendeen Formation were deposited during the Early Cretaceous, and their compositions continue to reflect input from the Alaska-Aleutian Range batholith and reworking of older sedimentary units (Wilson, 1980; Wilson et al., 1999). The mid-Cretaceous section on the Alaska Peninsula is missing as a result of

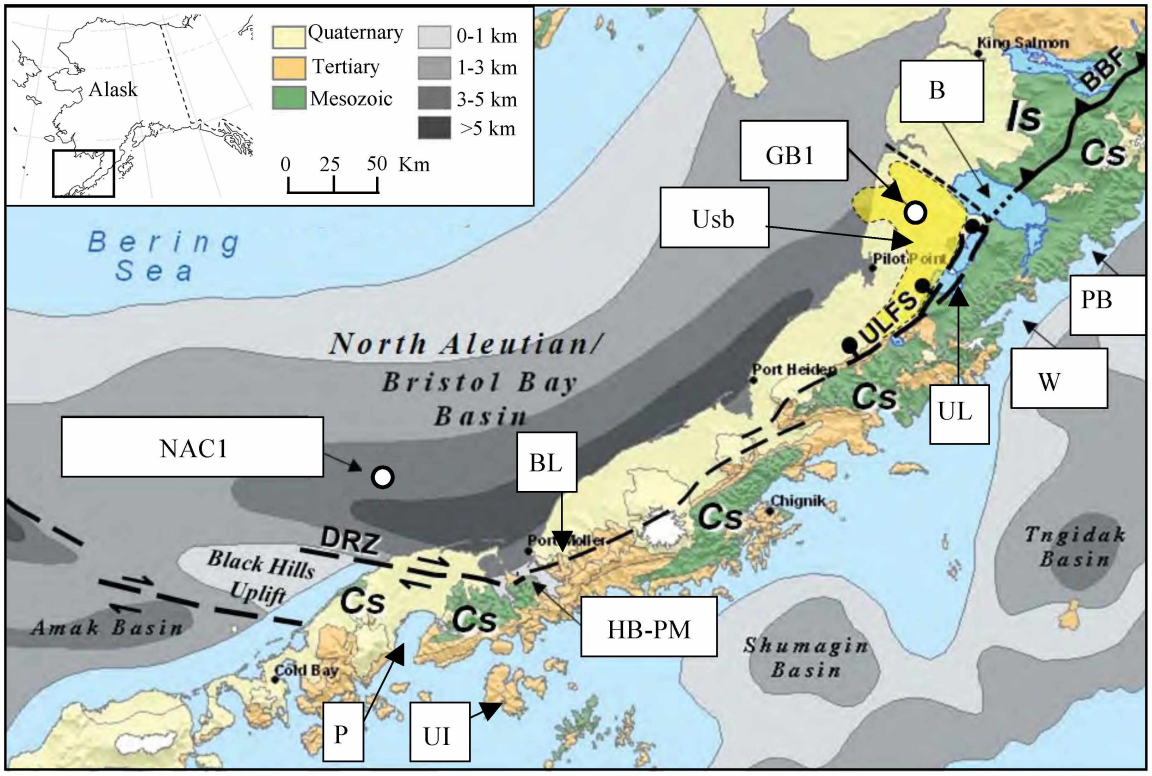

Fig. 3.1 Map of generalized geologic units and structure of the Alaska Peninsula. Abbreviations of locations and geologic features are as follows: Becharof Lake (B), Bruin Bay fault (BBF), Bear Lake (BL), Chignik subterrane (Cs), David River zone (DRZ), Great Basins 1 well (GB1), Herendeen Bay – Port Moller area (HB-PM), Iliamna subterrane (Is), North Aleutian COST 1 well (NAC1), Pavlof Bay (P), Puale Bay (PB), Unga Island (UI), Ugashik Lakes (UL), Ugashik Lakes fault system (ULFS), Ugashik sub-basin (Usb), Wide Bay (WB). Modified from Decker (2008).

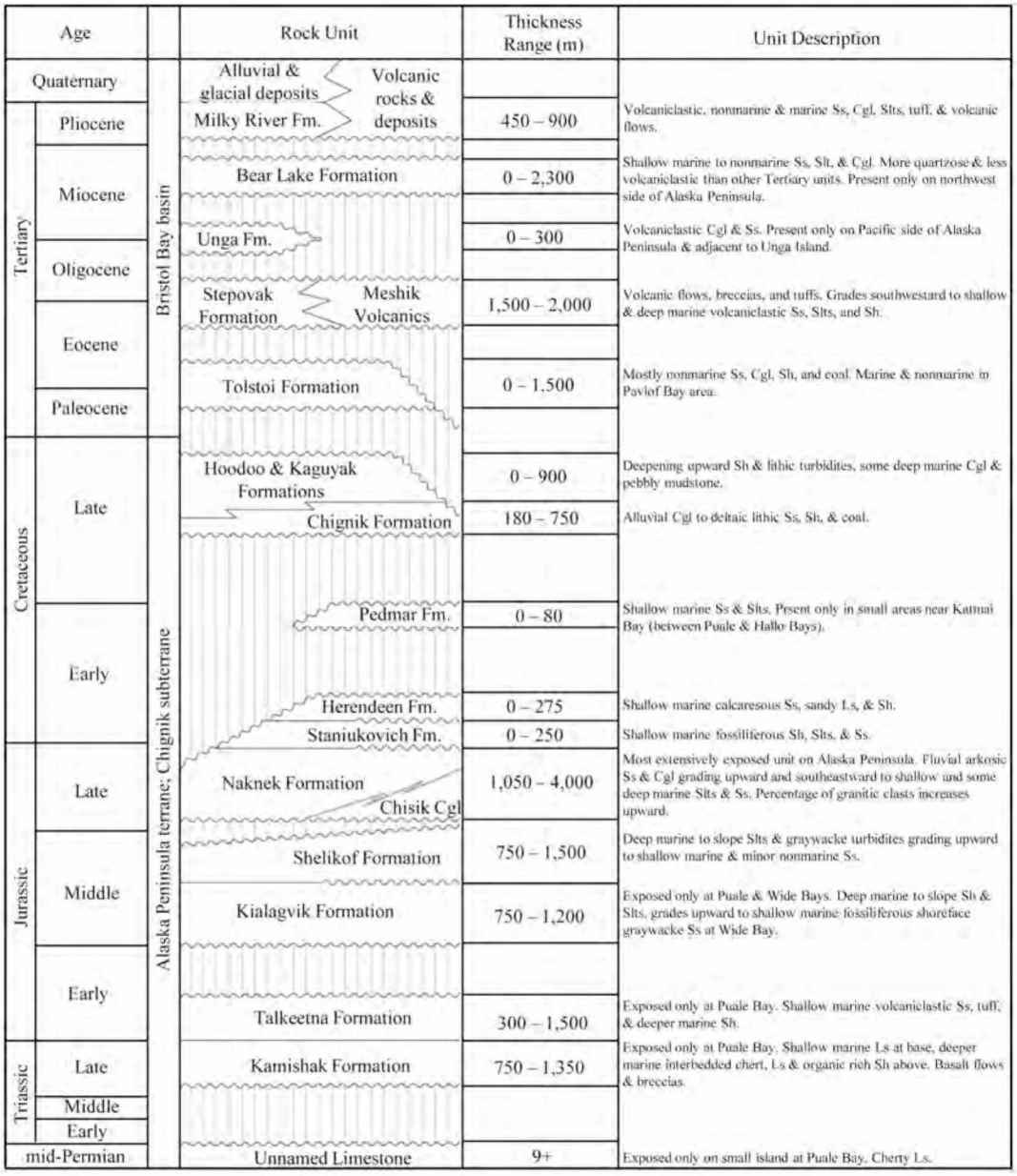

Fig. 3.2 Stratigraphic column of the Alaska Peninsula. Abbreviations are as follows: Sandstone (Ss), conglomerate (Cgl), Siltstone (Slts), Shale (Sh), and Limestone (Ls). See Fig. 3.1 for localities mentioned in unit descriptions. Modified from Reifenstuhl et al. (2004) and Decker et al. (2008a), after Detterman et al. (1996).

uplift and erosion during this time period, including partial erosion of the Herendeen, Staniukivich, and Naknek formations (Burk, 1965; Wilson et al., 1999). Erosion was followed by Late Cretaceous deposition of sandstones and siltstones of the Chignik Formation, and siltstones and shales of the Hoodoo Formation – both of which reflect erosion of a plutonic source and reworking of older strata (Mancini, 1978; Wilson, 1980; Wilson et al., 1999).

3.1.2 Tertiary

Tertiary sedimentary rocks blanket the southwest end of the Alaska Peninsula and consist of mainly volcaniclastic sedimentary rocks that are interlayered with volcanic rocks (Fig. 3.1 and Fig. 3.2; Detterman et al., 1996). The Tertiary strata unconformably overlie the Mesozoic section (Detterman et al., 1996). The Mesozoic section and Alaska-Aleutian Range batholith served as the main sediment source for rocks of the Paleocene to Eocene Tolstoi and Middle to Late Miocene Bear Lake formations, as reflected by their largely nonvolcanic composition (>50% nonvolcanic materials; Detterman, 1990; Wilson et al., 1994; Detterman et al., 1996; Wilson et al., 1999). In contrast, the remainder of the Tertiary sedimentary section contains rocks derived from contemporaneous volcanic debris (Detterman et al., 1996). Sandstones and conglomerates of the Eocene to Oligocene Stepovak Formation contain unaltered volcanic clasts, distinct from the altered volcanic material of the underlying Tolstoi Formation which is commonly chloritized (Detterman, 1990; Detterman et al., 1996). Siltstones and sandstones of the Stepovak Formation are coeval with volcanic flows, tuffs, and breccia of the Meshik Volcanics (Detterman et al., 1996). These two units interfinger along the southwest side of the Alaska Peninsula (Wilson et al., 1995; Detterman et al., 1996; Wilson et al., 1999). The Late Oligocene to earliest Middle Miocene Unga Formation is restricted mainly to Unga Island, and the majority of the unit is composed of locally derived volcanic clasts (Wisehart, 1971; Detterman et al., 1996). The Tertiary succession is capped by the Milky River Formation, consisting of volcaniclastic sandstones and conglomerates interlayered with volcanic flows and sills which become thicker and more abundant up-section where lahar deposits and tuff beds are also present (Wilson et al., 1999).

3.1.3 Bear Lake Formation

The Bear Lake Formation was first defined by Burk (1965) and described as a thick sequence of interbedded sandstones, conglomerates, and a few siltstones, exposed on the eastern shores of Port Moller and in the mountains to the northeast, well beyond Bear Lake (Fig. 3.3). Exposures reach northeast to the Upper and Lower Ugashik Lake area (Detterman et al., 1996). The type locality was designated by Detterman et al. (1981) as the southeast slope of the mountains 10 km east of Bear Lake. The Bear Lake Formation is also present in subsurface, appearing in several onshore wells and in the North Aleutian COST 1 well in Bristol Bay (Fig. 3.3; Detterman, 1990). The maximum thickness of the Bear Lake Formation is considered to be 1,000 m (Detterman et al., 1996; Decker et al., 2005). Anomalous thicknesses, such as the 2,360 m observed in the Sandy River Federal 1 well (Fig. 3.3), are thought to result from structural thickening due to thrust faulting (Detterman et al., 1996).

As originally defined by Burk (1965), the Bear Lake Formation included the Unga Conglomerate Member as the basal member of the formation. However, this unit is now defined as a separate formation. Detterman et al. (1996) revised the previous assignment of the Unga Conglomerate Member, defining it as the Unga Formation because it is a mappable unit that is lithologically distinct from the Bear Lake Formation and geographically restricted to the Unga Island area.

The Bear Lake Formation is locally underlain by the Meshik Volcanics, Stepovak Formation, and Tolstoi Formation, with contacts that are disconformities and angular unconformities (Fig. 3.2; Wilson et al., 1995; Detterman et al., 1996; Wilson et al., 1999). Disconformities and, less commonly, angular unconformities also separate the Bear Lake Formation from overlying volcanic and sedimentary strata of the Milky River Formation (Fig. 3.2; Wilson et al., 1995; Detterman et al., 1996; Wilson et al., 1999).

The Bear Lake Formation has been assigned a Middle to Late Miocene age based on identification of macrofauna and palynomorphs (Detterman et al., 1996; Finzel et al., 2005; Blodgett et al., 2008). The majority of preserved marine invertebrates lived in shallow, near-shore environments in water depths less than 100 m (Marincovich, 1983; Marincovich, written communication, 1978 and 1985 *in* Detterman et al., 1996; Blodgett et al., 2008). The depositional environment has been interpreted to be a regional

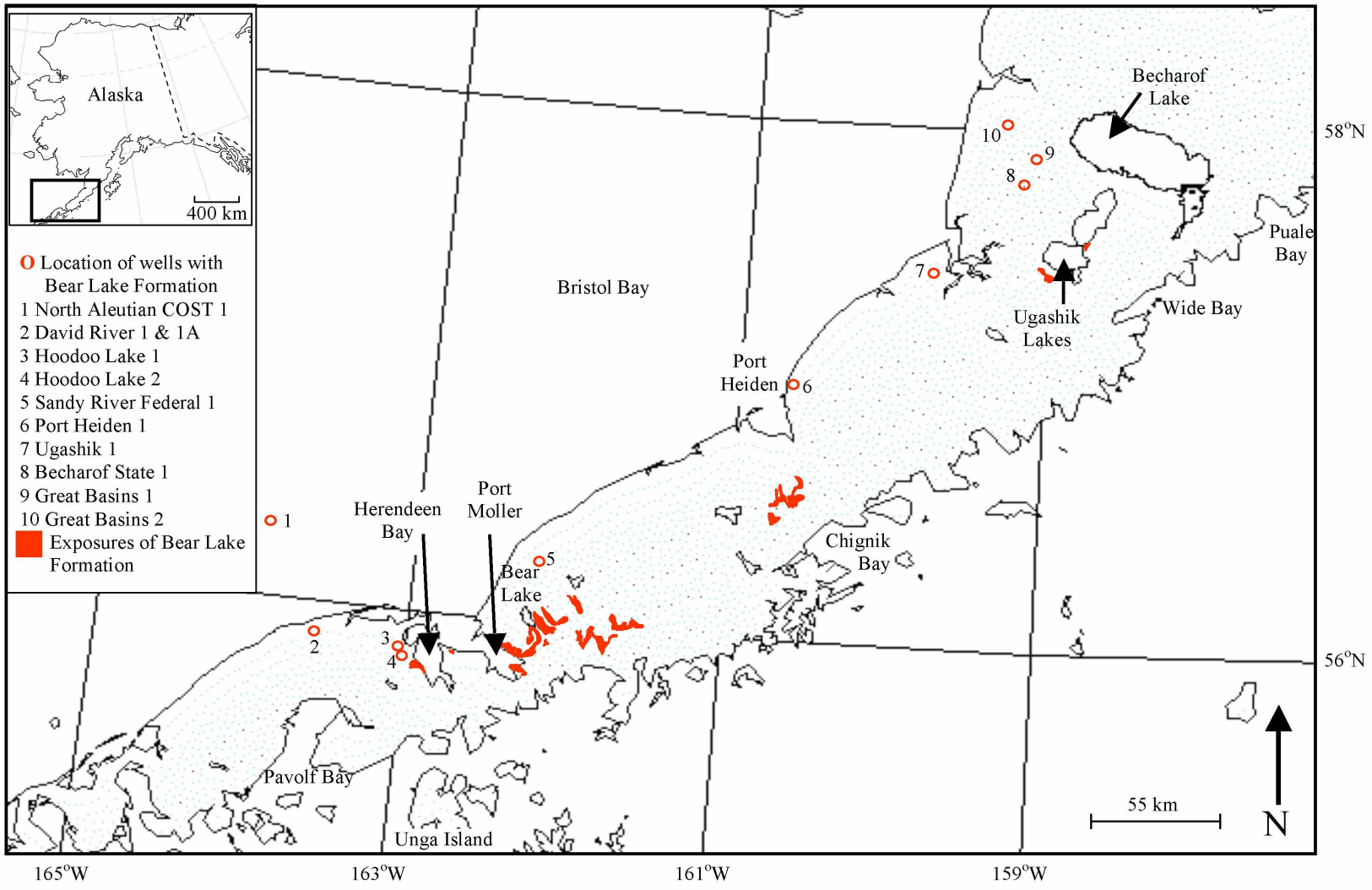

Fig. 3.3 Distribution of the Bear Lake Formation on the Alaska Peninsula. Well locations from Detterman (1990). Outcrop exposures of the Bear Lake Formation from Wilson et al. (1999) and Decker et al. (2008b).

estuarine/tidal flat system with tidal flats and channels, fluvial channels, and brackish marshes (Decker et al., 2005; Finzel et al., 2005).

The Bear Lake Formation contains a greater abundance of non-volcanic material than other Tertiary sedimentary units on the Alaska Peninsula, with the exception of the Tolstoi Formation (Burk, 1965; Detterman, 1990; Detterman et al., 1996; Wilson et al., 1999). In particular, quartz and chert are common in the Bear Lake Formation (Burk, 1965; Wisehart, 1971; Lyle et al., 1979; Detterman et al., 1996). Pore-filling and grain-replacement components include iron oxide, clay minerals, carbonate, silica, and zeolite (Wisehart, 1971; Lyle et al., 1979; Helmold and Brizzolara, 2005; Helmold et al., 2008). Clays consist of glauconite, chlorite, montmorillonite, illite, and kaolinite (Wisehart, 1971; Helmold and Brizzolara, 2005; Helmold et al., 2008). Wilson (1980) suggests that the relatively minor amount of volcanic detritus in the Bear Lake Formation indicates a hiatus in volcanic activity on the Alaska Peninsula during the Middle to Late Miocene.

3.1.3.1 Recent Studies of the Bear Lake Formation

Previous studies of the Bear Lake Formation include information on stratigraphy and sedimentology, petrography, biostratigraphy, depositional environment, and reservoir quality (Appendix A). Most recent studies of the Bear Lake Formation were carried out by the Alaska Division of Geological and Geophysical Surveys and Alaska Division of Oil and Gas, beginning in 2004 (including Decker et al., 2005; Finzel et al., 2005; Mickey et al., 2005; Blodgett et al., 2008; Decker et al., 2008a; Decker et al., 2008b; Helmold et al., 2008). Finzel et al. (2005) addressed sedimentology and stratigraphy of the Bear Lake Formation. Eight measured sections of the Bear Lake Formation from the Port Moller – Herendeen Bay area of the Alaska Peninsula are presented by Finzel et al. (2005) and Decker et al. (2005) with interpretation of depositional environments. Decker et al. (2005) provide a chronostratigraphic correlation of these measured sections based on megafauna and palynomorphs.

Structural deformation of the Bear Lake Formation near Coal Point, on the western coast of Herendeen Bay, and near Bear Lake is reported by Decker et al. (2005). An important revision in geologic mapping of the Herendeen Bay area has been made by Decker et al. (2008b). They reinterpret the outcrop

distribution of the Bear Lake Formation on the east coast of Herendeen Bay with significant implications for a new structural interpretation of the area (see section 3.3.4).

Recent megafossil (primarily mollusks) and palynomorph identifications constraining age, depositional environment, and stratigraphic correlations are reported by Finzel et al. (2005), Decker et al. (2005), Blodgett et al. (2008), and Mickey et al. (2005). Current interpretation of subsurface formation boundaries of the Bear Lake Formation, and other Tertiary strata, are based on the findings of Mickey et al. (2005). Most notably, for the Bear Lake Formation, the lower contact of the formation in the Great Basins 1 well has been assigned to a greater depth (10,320 ft) than previously interpreted (5,600 ft by Brockway et al., 1975; McLean, 1977; Detterman, 1990). Finzel et al. (2005) and Sherwood et al. (2006) have assigned formation names, including the Bear Lake Formation, to seismically defined stratigraphic intervals identified in the North Aleutian COST 1 well by Turner et al. (1988).

Helmold and Brizzolara (2005) and Helmold et al. (2008) report on the petrography of the Bear Lake Formation with regard to reservoir quality. Other studies addressing the role of the Bear Lake Formation in the petroleum system of Bristol Bay basin include Finzel et al. (2005), Decker et al. (2006), Sherwood et al. (2006), Loveland et al. (2007), Bolger and Reifenshtuhl (2008), and Decker (2008).

3.2 Magmatic Arcs of the Alaska Peninsula

A large part of the exposed stratigraphic sequence on the Alaska Peninsula consists of volcanic and intrusive rocks, most of which were deposited during three time intervals: Early to Middle Jurassic, Late Eocene to Early Miocene, and Late Miocene(?) to Holocene (Detterman et al., 1996).

The Jurassic arc is represented by the Talkeetna Formation and Mesozoic intrusive rocks of the Alaska-Aleutian Range batholith (Detterman et al., 1996). The Tertiary stratigraphy of the peninsula records two main magmatic episodes. The first Tertiary magmatic episode formed the Meshik arc, and the second formed the currently active Aleutian arc (Wilson, 1985).

Radiometric K-Ar dates indicate that the first Tertiary magmatic episode occurred between 22 and 48 Ma (Wilson et al., 1981; Wilson, 1985). This activity is recorded in the volcaniclastic Stepovak Formation and in the Meshik Volcanics that consists of basalt to dacite flows, agglomerates and breccias, and volcaniclastic sediments (Wilson, 1980; 1985). Middle Tertiary plutonic rocks of the Alaska-Aleutian

Range batholith are also associated with the Meshik arc (Reed and Lanphere, 1973; Wilson, 1980). Volcanic activity on the Alaska Peninsula subsided by Early Miocene and a period of volcanic quiescence is marked by deposition of the Bear Lake Formation (Wilson, 1980; Detterman et al., 1996). The second Tertiary magmatic episode formed the modern day Aleutian arc beginning at the end of the Miocene, when volcanic activity was re-initiated and recorded by deposition of volcaniclastic sediments, lava flows, and lahars of the Milky River Formation (Wilson, 1980; Wilson et al., 1994; Wilson et al., 1995).

3.3 Regional Geologic Structure

3.3.1 Bristol Bay Basin

The Bristol bay basin (also known as the North Aleutian basin) is a northeast trending sediment-filled structural depression with a gently dipping northwest flank and a steeply dipping southeastern margin (Fig. 3.1; Kirschner, 1988; Marlow et al., 1994; Walker et al., 2003). The majority of the basin lies offshore beneath the Bering Sea shelf, and the southern flank is exposed on the northern edge of the Alaska Peninsula (Marlow et al., 1994). The basin formed in a back-arc setting after emplacement of the Peninsular terrane at the end of the Mesozoic (Marlow et al., 1994; Walker et al., 2003). Subsidence has occurred in three phases: 1) Paleocene to Eocene extensional and strike-slip faulting between the Black Hills uplift and southern margin of the basin; 2) Late Eocene to Middle Miocene flexural subsidence; and 3) Late Miocene to Holocene asymmetric subsidence driven by sediment loading associated with renewed volcanism on the Alaska Peninsula (Worrall, 1991; Walker et al., 2003; Decker et al., 2005; Finzel et al., 2005). Phase three may have been facilitated by down-to-northwest normal faulting on the Alaska Peninsula (Finzel et al., 2005).

The sedimentary section consists of more than 6,000 m of Cenozoic deposits which are thickest in the southeast part of the basin, characterized by horsts and grabens (Marlow et al., 1994; Walker et al., 2003; Finzel et al., 2005). The North Aleutian COST 1 well is located in one of the deepest grabens, and bottomed in Early and Middle Eocene strata of the Tolstoi Formation (Fig. 3.1 and Fig. 3.2; Turner et al., 1988; Finzel et al., 2005; Mickey et al., 2005).

3.3.2 Bruin Bay Fault and Ugashik Lakes Fault System

The Bruin Bay fault is a northeast-trending, high-angle reverse fault with probable left lateral motion that is recognized north of Becharof Lake extending approximately 500 km northeast to the Castle Mountain fault, near Mt. Susitna (Burk, 1965; Detterman and Hartsock, 1966; Detterman et al., 1976; Detterman and Reed, 1980; Detterman et al., 1987; Wilson et al., 1999). Offset along the fault system is as much as 3 km of stratigraphic separation and 19 km of possible left-lateral displacement (Detterman and Hartsock, 1966; Detterman et al., 1976). The fault juxtaposes plutonic and related metamorphic rocks of the Iliamna subterrane against Mesozoic sedimentary units of the Chignik subterrane (Fig. 3.1; Detterman and Reed, 1980; Detterman et al., 1987; Detterman et al., 1996; Wilson et al., 1999). On the Alaska Peninsula, near Becharof Lake, Jurassic plutonic rocks of the Alaska-Aleutian Range batholith are exposed in the uplifted northwest fault block, whereas the Jurassic Naknek Formation is exposed to the southeast in the downthrown block (Wilson et al., 1999). Movement along the fault during Late Jurassic time may have been responsible for uplift and erosion of the Alaska-Aleutian Range batholith and resulting deposition of arkosic and granitic sedimentary rocks of the Naknek Formation (McLean, 1979; Detterman and Reed, 1980); movement likely ceased by Miocene time (Detterman and Reed, 1980).

Immediately southwest of Becharof Lake, the structural regime of the Bruin Bay fault continues into that of the Ugashik Lakes fault system (ULFS; Fig. 3.1), which was introduced by Decker et al. (2008a). The ULFS consists of down-to-the northwest normal or normal-oblique faults, opposite of the up-to-the northwest reverse Bruin Bay fault; this structural readjustment causes uplift to the north and subsidence to the south (Decker et al., 2008a). The ULFS juxtaposes Mesozoic sedimentary rocks to the southeast with Tertiary sedimentary rocks of the Bristol Bay basin to the northwest and defines the southeast margin of the Ugashik sub-basin (Fig. 3.1; Decker et al., 2008a).

3.3.3 Ugashik Sub-Basin

The Ugashik sub-basin is a fault-controlled Neogene depocenter west of Ugashik Lakes and southwest of Becharof Lake (Fig. 3.1; Decker et al., 2008a). Based on publicly-available geophysical data, the sub-basin is bound to the north and southeast by normal faults, and separated from the greater Bristol Bay bay basin to the southwest by an Eocene to Oligocene extrusive complex of the Meshik Formation

(Decker et al., 2008a). Uplift along the Bruin Bay fault has exposed Jurassic plutonic rocks of the Alaska-Aleutian Range batholith (Iliamna subterrane) north of the sub-basin, and Mesozoic sedimentary rocks of the Chignik subterrane are exposed to the east (Fig. 3.1). The Great Basins 1 well provides a stratigraphic section nearest the center of the sub-basin and bottoms in Oligocene strata of the Stepovak Formation (Mickey et al., 2005; Decker et al., 2008a).

3.3.4 Structure of the Herendeen Bay - Port Moller Area

The David River zone is a complex structural boundary that separates Tertiary rocks of the Bristol Bay basin to the north and uplifted Mesozoic sedimentary rocks to the south (Fig. 3.1; Worrall, 1991; Decker et al., 2005; Decker et al., 2008b). In the vicinity of Herendeen Bay and Port Moller, folding and reverse faulting were active between Late Cretaceous and late Middle Eocene time with subsequent uplift during the Late Miocene (Decker et al., 2008b). More recent uplift cannot be ruled out (Decker, P.L., personal communication, 2010). Most current geologic mapping of this area by Decker et al. (2008b) shows no evidence for exposure of the Bear Lake Formation on the eastern coastline of Herendeen Bay, and does not support the low angle thrusting mapped by Wilson et al. (1995) and Wilson et al. (1999) . Alternatively, Decker et al. (2008b) interpret high-angle reverse faults to be present that formed in relation to overstepping right lateral strike-slip faults. West of Herendeen Bay, reverse faulting has placed the Jurassic Naknek Formation in contact with the Miocene Bear Lake Formation (Wilson et al., 1995; Wilson et al., 1999; Decker et al., 2008b). Down-to-the north normal faults mark the northward transition from onshore uplift to offshore subsidence and reflect syndepositional Miocene subsidence of the offshore Bristol Bay basin (Decker et al., 2008b).

CHAPTER 4. PETROGRAPHY

4.1 Introduction

Petrographic quantification of detrital modes of sandstones via point count analysis is a standard approach used to characterize the composition of sandstones, and as a means of provenance interpretation. Ternary diagrams are frequently employed to illustrate detrital modes using various combinations of grain parameters (such as quartz, feldspar, and lithic grains illustrated on a QFL ternary diagram). Ternary diagrams are an effective tool for evaluating large datasets often obtained during point count analysis. In addition to ternary calculations, ratios such as plagioclase to total feldspar, and polycrystalline quartz to total quartz (Dickinson, 1970; Dickinson and Rich, 1972), are useful in compositional characterization of sandstones. However, ratios and ternary diagrams display relative abundances, and not absolute framework percentages. In conjunction with ratios and ternary plots, plotting framework percentages in relation to stratigraphic height is a useful approach to evaluate up-section compositional changes.

Such stratigraphic compositional changes commonly reflect changing tectonic setting through time, or erosional modification of source terrains (Dickinson, 1985). Major provenance types related to tectonic setting contribute distinctive detritus to associated sedimentary basins (Dickinson, 1985). Ternary diagrams can be used to relate sandstone composition to tectonic setting (Dickinson and Suczek, 1979; Dickinson et al., 1983) and are useful for evaluating stratigraphic compositional changes as a function of provenance (see, for example, early studies by Dickinson and Rich, 1972; Ingersoll, 1978; Ingersoll, 1983).

A recent study by Helmold et al. (2008), focusing on reservoir characterization, included petrogrpahic anlaysis of 28 subsurface samples of Bear Lake Formation sandstones and indicates compositional variation within the formation (Fig. 3 in Helmold et al., 2008). In order to petrographically evaluate diagenetic and framework compositional changes in stratigraphic context, I obtained traditional point count data for 26 samples from a combination of wells and chronostratigraphically-correlated measured sections (Fig. 2.1 and Fig. 2.2). For provenance interpretation, I used a series of ternary diagrams, parameter ratios, and framework percentage plots to identify compositional groupings related to stratigraphic position within the Bear Lake Formation and to illustrate compositional variation between subsurface well samples and outcrops.

4.2 Methods

Mark Mercer (Petrographic Services, Montrose, Colorado) prepared the thin sections that I used for point count analysis. He impregnated samples with blue epoxy and half-stained them for K-feldspar and carbonates. Mercer prepared North Aleutian COST 1 well thin sections from 1 inch diameter core plugs, and Great Basins 1 well thin sections from large core chips. Michael Wilson (Wilson & Associates, Lakewood, Colorado) completed all point counts for this study.

Kenneth Helmold at Alaska Division of Oil and Gas provided point count data for all well samples, which existed prior to this study. The petrographer (Michael Wilson) used the same methods to analyze the outcrop samples as he used for the existing well sample counts in order to keep the datasets consistent and comparable. He counted a total of 300 grains per sample for composition using the traditional point count method. Counting 300 points yields a $2\sigma < 6\%$ with 95% confidence (Van der Plas and Tobi, 1965). He also conducted grain size analyses for 200 grains in thin section, consisting of long-axis measurements made using a Microplan II digitizer tablet.

Point count categories used by Wilson are specific to this sample set in order to collect detailed data pertinent to the rocks being analyzed. A means of standardization is necessary in order to more easily compare these detailed counts with other datasets. Recently published petrographic data from Bristol Bay basin sandstones (Helmold and Brizzolara, 2005; Helmold et al., 2008) convert original counts by Wilson to Decker-Helmold format, which is based on a hierarchical scheme (Decker, 1985) for classifying sandstone point count data (Helmold, K.P., written communication, 2008). I used a set of Excel macros provided by Helmold to classify the original categories into this hierarchy. Details of my classifications are outlined in Table 4.1.

The Gazzi-Dickinson point count method (Dickinson, 1970) is component-based. It is designed to reflect framework composition independent of grain size by counting monominerallic crystals >0.0625 mm (lower limit of sand) that occur in phaneretic lithic grains (rock fragments with components >0.0625 mm) as the constituent crystal rather than a lithic grain, as is done in the traditional method (Dickinson, 1970; Ingersoll et al., 1984; Dickinson, 1985). Decker and Helmold (1985) suggest that grain size effects be controlled by restricting the grain size of samples analyzed to medium- to coarse-sand, rather than by

Table 4.1 Classification scheme of original point count categories. Main classifications, shown in bold, are subdivided to show their components in detail. Any original categories that were used during point counting that yielded 0 counts are excluded (Rock fragments: Extensively deformed metasiltstone/metamudstone, Extensively deformed mica/chlorite schist, Gneissic fragment (>40% feldspars); Detrital minerals: Pyroxene, Extensively fractured amphibole; Cement: Dolomite, Ankerite, K-feldspar overgrowths, Chlorite, Mixed layer illite-smectite, Clinoptilolite, Analcite; Porosity: Macropore in cements, Pores replacing detrital calcite, Mesopore in chert, Transparticulate pore [>20 microns]; Laminae/Burrow-Fill: Burrow fill; Other: Drilling Mud, Laumontite fracture fill, Pore concentric with grain boundaries). Any categories assigned to a main classification are represented by the "undifferentiated" modifier used in calculating ternary diagram parameters (for example, undifferentiated quartz).

	ORIGINAL POINT COUNT CATAGORIES		
CLASSIFICATION	**Grain Type Identified in Both Sample Sets**	**Grain Type Identified in Outcrop Only**	**Grain Type Identified in Wells Only**
Quartz		Quartz with trace-very minor mica/chlorite	Extensively Fractured Quartz
Monocrystalline	Monocrystalline Quartz		
Polycrystalline	Polycrystalline Quartz		
Feldspar			
Alkali	Extensively Fractured K-Feldspar K-Feldspar (<33% dissolution)		
Dissolved			K-Feldspar (>33% dissolution)
Plagioclase	Extensively Fractured Plagioclase Plagioclase (<33% dissolution)		
Dissolved	Plagioclase (>33% dissolution)		
Sedimentary Rock Fragment			
Chert		Extensively Fractured Chert	
Common (Microcrystalline)	Dense Chert		
Cherty Argillite	Argillaceous Chert		
Microporous Chert	Porous Chert (>33% visible porosity)		
Argillite	Highly Quartzose Argillite		
Slate/Shale	Undeformed Shale/Mudstone Fragments Slightly Deformed Shale/Mudstone Fragments Extensively Deform. Shale/Mudstone Fragments		
Siltstone	Feldspathic Siltstone/Mudstone		
Sandstone		Lithic Sandstone	
Quartz	Quartzose Sandstone Fragment		
Feldspar	Feldspathic Sandstone Fragment		
Detrital Carbonate	Carbonate Fragments (incl. fossil fragments)		
Volcanic Rock Fragment		Indeterminate Volcanic Fragment	
Felsic	Siliceous Volcanic Fragment Porous Silicic Volcanic Fragment		Plastically Deformed Silicic Volcanic Fragment
Vitric/Cryptocrystalline	Glass Shards		
Intermediate		Intermediate Volcanic Fragment Porous Intermediate Volcanic Fragment	*
Tuffaceous		Devitrified Tuff Fragments	
Mafic	Basic Volcanic Fragment Porous Basic Volcanic Fragment		Plastically Deformed Basic Volcanic Fragment

Table 4.1 continued

CLASSIFICATION	ORIGINAL POINT COUNT CATAGORIES Grain Type Identified in Both Sample Sets	Grain Type Identified in Outcrop Only	Grain Type Identified in Wells Only
Metamorphic Rock Fragment			
Felsic			
Unfoliated Metaclastic (Quartzite)	Micaceous Quartzite (5-15% mica)		
Quartz-Mica Phyllite	Undeformed Metasiltstone/Metamudstone Slightly Deformed Metasiltstone/Metamudstone Undeformed Phyllite Fragment Slightly Deformed Phyllite Fragment	Extensively Deformed Phyllite Fragment	
Quartz-Mica Schist/Gneiss	Undeformed Mica/Chlorite Schist		
	Slightly Deform. Mica/Chlorite Schist		
Plutonic Rock Fragment			
Felsic	Granitic Fragment (>40% Feldspars)	Granitic Fragment (<40% Feldspars)	
Mafic	Diorite/Gabbro Fragments		
Detrital Mineral	Stable Heavy Minerals (Zircon etc.) Unstable Heavy Minerals (Epidote etc.)		
Biotite	Undeformed Biotite Slightly Deformed Biotite	Extensively Deformed Biotite	
White Mica	Undeformed Muscovite Extensively Deformed Muscovite		Slightly Deformed Muscovite
Chlorite	Extensively Deformed Chlorite		Undeformed Chlorite Slightly Deformed Chlorite
Amphibole	Amphibole		
Garnet			Garnet
Undifferentiated Grain	Unknown Framework Component		
Matrix			
Argillaceous	Detrital Clay Rims		
Clay	Clay & Mud Matrix		
Pseudomatrix	Slightly Deformed Indeterminate Ductile Extensively Deformed Indeterminate Ductile	Undeformed Indeterminate Ductile	
Cement/Overgrowths		Indeterminate & Miscellaneous Pore Fillers	
Silica			
Quartz	Quartz Overgrowths		
Chert		Chert Cement	
Carbonate			
Calcite		Calcite Ferroan Calcite Plagioclase Replaced by Calcite Basic Volcanic Replaced by Calcite or Fe-Calcite Unknown Replaced by Ferroan Calcite	
Siderite	Siderite		Siderite Dilating Biotite

Table 4.1 continued

CLASSIFICATION	ORIGINAL POINT COUNT CATAGORIES Grain Type Identified in Both Sample Sets	Grain Type Identified in Outcrop Only	Grain Type Identified in Wells Only
Argillaceous			
Kaolinite	Kaolinite	Plagioclase Replaced by Kaolinite	Muscovite Replaced by Kaolinite
Smectite/Mixed-Layer	Volcanic Glass Replaced by Smectite	Smectite Corrensite	
Authigenic Mineral			
Pyrite	Pyrite		
Anatase/Rutile			Anatase
Laumontite		Laumontite Plagioclase Replaced by Laumontite Amphibole Replaced by Laumontite	
Heulandite		Heulandite	
Intrabasinal Grain			
Pellet (Non-Glauconite)	Undeformed Clay Peloid/Volcanic Vug Fill? Slightly Deformed Clay Peloid/Volcanic Vug Fill?	Extensively Deformed Clay Peloid./Volcanic Vug Fill?	
Organic Material	Undeformed Organic Fragment Slightly Deform Organic Fragment Extensively Deform. Organic Fragment		
Oversize Grain			
Shell Fragment		Carbonate Fragments (incl. fossil frags.)**	
Porosity			
Intergranular	Intergranular Pore (2-20um) Intergranular Pore (>20um)		
Intragranular			
Secondary	Macropore in Plagioclase Macropore in Unknown		Mesopore in K-Feldspar
Fracture		Transparticulate pore (2-20um)	
Laminae/Burrow-Fill			
Clay Laminae/Burrow-Fill	Clay Laminae		

*Volcanic rock fragments in well samples were counted as either felsic or mafic. The intermediate volcanic category was added for point counting of the outcrop sample set.
**Sample LH1-66.5 has an appreciable amount of carbonate counts that mostly occur in one large bivalve fragment, and have been assigned to the oversize grain category to prevent them from impacting framework ternary calculations.

employing the Gazzi-Dickinson method. They argue that valuable provenance information held within phaneritic rock fragments is lost in the Gazzi-Dickinson method by counting genetically significant rock fragments as monominerallic crystals. Ingersoll et al. (1985) suggest that the information is transformed rather than lost, posing the question: "Is more information conveyed by saying a sandstone consists of 100% plutonic fragments (traditional) or by saying it consists of 40% monocrystalline quartz, 30% potassium feldspar, and 30% plagioclase feldspar (Gazzi-Dickinson)?"

The genetic-based, traditional method, is an appropriate choice for this study for three main reasons: 1) Newly obtained data for the outcrop sample set need to conform to methods used for the pre-existing well sample dataset. A single petrographer performed all the point counts, and using consistent methodology reduces error in interpreting compositional differences within the combined sample set; 2) Samples in this study are all within the very fine- to coarse-grained sand size range. Therefore, I expected differences in composition to be minimally impacted by differing grain sizes; 3) For the purposes of this study, it is more helpful to know what the origin of phaneritic rock fragments are than their constituent mineralogy. The Bear Lake Formation may contain components of recycled sedimentary units as well as primary or recycled plutonic detritus. Therefore, for example, it is valuable to distinguish between a quartzose sandstone fragment and a quartz-rich granite fragment in determining potential source units. Such a distinction is only made using the traditional method.

Dickinson et al. (1983) derived provenance fields empirically from datasets counted by the Gazzi-Dickinson method. Given the differences between the traditional and Gazzi-Dickinson point count methods it is unacceptable to simply plot data based on traditional counts in fields derived from Gazzi-Dickinson data. The relatively small grain size of this sample set suggests that the values would be similar between the two methods (Ingersoll et al., 1984). Nevertheless, I addressed this difference in methodology by recalculating the data to approximate Gazzi-Dickinson methodology. I used the original dataset (traditional point count method) to identify compositional variation within the sample set. I used the recalculated dataset that approximates Gazzi-Dickinson methodology to relate sample compositions to tectonic provenance. The parameters that I used in the diagrams which are based on each dataset represent different definitions of grain types (Table 4.2 and Table 4.3).

Table 4.2 Petrographic parameters used in ternary calculations based on traditional point counts.

Parameter	Calculations	Definition
f	quartz + feldspar + rock fragments + detrital minerals + undifferentiated grains + intrabasinal grains	Total framework
Qu	(Qu/f)*100	Undifferentiated quartz
Qm	(Qm/f)*100	Monocrystalline quartz
Qp	(Qp/f)*100	Polycrystalline quartz
C	(C/f)*100	Chert
Qp+	Qp + Qu + C	Total stable rock fragments
Q	Qm + Qp + Qu	Total quartz
Q+	Q + C	Total quartz including chert
K	(K/f)*100	Total K-feldspar
P	(P/f)*100	Total plagioclase
F	P + K	Total feldspar
Ls-	differentiated SRF – C	Sedimentary rock fragments excluding chert
Ls+	differentiated SRF + C	Sedimentary rock fragments including chert
Ls	Ls+ + undifferentiated SRF	Total sedimentary rock fragments
Ls*	Ls- + Lms	Sedimentary and metasedimentary rock fragments, excludes chert
Lvf	(Lvf/f)*100	Felsic volcanic rock fragments
Lvi	(Lvi/f)*100	Intermediate volcanic rock fragments
Lvm	(Lvm/f)*100	Mafic volcanic rock fragments
Lv	undifferentiated + differentiated VRF	Total volcanic rock fragments
Lv*	Lv + Lmv	Volcanic and metavolcanic rock fragments
Lms	(Lms/f)*100	Metasedimentary rock fragments
Lmv	(Lmv/f)*100	Metavolcanic rock fragments
Lm	Lms + Lmv	Total metamorphic rock fragments
Lp	(Lp/f)*100	Total plutonic rock fragments
Li	Lv + Lp	Total igneous rock fragments
L	Ls + Lv + Lm + Lp	Rock fragments including chert
L-	Ls- + Lv + Lm + Lp	Total unstable rock fragments, excludes chert
Lt	Qp+ + Ls- + Lv + Lp	Total rock fragments, includes all stable rock fragments

Table 4.3 Explanation of ternary diagram parameters based on Gazzi-Dickinson approximations. These definitions are those outlined by Graham et al. (1976) and used by Dickinson and Suczek (1979) and Dickinson et al. (1983).

Parameters	**Definition**	**Calculations**
Q	Total quartzose grains	Qm + Qp
Qm	Monocrystalline quartz	
Qp	Polycrystalline quartzose lithic fragments (chert, quartzite, etc.)	
F	Monocrystalline feldspar grains	P + K
P	Plagioclase feldspar	
K	K-feldspar	
Lt	Total aphanitic lithic fragments	L + Qp
L	Unstable polycrystalline lithic fragments	Lv + Ls
Lv	Volcanic-metavolcanic-hypabyssal lithic fragments	
Ls	Aphanitic sedimentary-metasedimentary lithic fragments	

I used a set of diagrams based on the traditional point count method to identify compositional variation within the sample set. Parameters that I used in ternary calculations are defined in Table 4.2. The total framework calculation includes undifferentiated framework grains, intrabasinal grains, and detrital minerals along with quartz, feldspar, and rock fragments (after Decker, 1985). Inclusion of these components with the lithic parameters may be valuable in reservoir quality studies (Helmold et al., 2008), but they have a minimal impact on illustrating compositional differences between the samples used in this study. Although the total framework calculation includes undifferentiated framework grains, intrabasinal grains, and detrital minerals, they are not included with any other parameter (Table 4.2). I normalized all ternary calculations so that the sum of the three pole parameters equals 100%.

A second set of diagrams is based on the recalculated dataset approximating Gazzi-Dickinson methodology, and relates the sample compositions to tectonic provenance using the fields of Dickinson et al. (1983). I made all ternary calculations using the recalculated dataset with the parameter definitions of Table 4.3. I approximated a Gazzi-Dickinson count by re-appropriating phaneretic lithic grains (rock fragments) in the following manner: 1) classified granitic rock fragments with less than 40% feldspars as monocrystalline quartz, and those with >40% feldspars and diorite/gabbro as feldspar; 2) classified mica/chlorite schist as mica; 3) classified quartzose sandstone rock fragments as monocrystalline quartz, and feldspathic sandstone rock fragments as feldspar; and 4) classified argillaceous chert and quartz with trace mica/chlorite as sedimentary lithic grains. This recalculated dataset represents a reconstructed composition (that is, the original framework composition prior to alteration) by classifying replaced grains as their appropriate framework category when the original clast is identifiable. For example, a plagioclase clast replaced by calcite is classified as plagioclase and not calcite. Undifferentiated framework grains, intrabasinal grains, and detrital minerals are excluded entirely from these calculations.

4.3 Results

4.3.1 Point Count Data

Michael Wilson (Wilson & Associates, Lakewood, Colorado) collected all point count data, and the results I present in this sub-section reflect his interpretations – with the exception of his designation of "limonite/hematite". It is my interpretation, based on my own petrographic examination, that hematite is

not present in the samples and that Wilson's designation of "limonite/hematite" in fact indicates the presence of limonite and not hematite. Therefore, where Wilson noted "limonite/hematite" I have represented it as limonite. Limonite is an amorphous or cryptocrystalline, fine-grained mixture of Fe-oxides and hydroxides, whereas geothite is a crystalline Fe-oxyhydroxide (Nesse, 1991). It is likely that some percentage of geothite is present in addition to limonite.

Samples range from very fine- to coarse-grained sandstones of feldspathic and lithic composition with moderately well- to very well-sorted framework grains (Table 4.4). The smallest grain sizes occur in the Great Basins 1 well. Table 4.5 provides a summary of compositional point count data. I report detailed category framework percentages in Table 4.6, and whole-rock percentages in Table 4.7. Refer to the classification scheme of original point count categories (Table 4.1) for the specific grain types included in the detailed categories. The results below note specific details of the data in these three compositional point count tables (Table 4.5, Table 4.6, and Table 4.7).

Monocrystalline quartz in BL3-193 is all volcanic, as is some in BL3-36 (at least 25%). In all North Aleutian COST 1 well samples, the polycrystalline quartz category includes some quartz clasts with traces of aligned, fine-grained muscovite and/or chlorite.

One third of the total sandstone fragments are cemented by chert. The one tuffaceous grain counted in LH1-120 is extensively altered to corrensite.

Epidote and opaque minerals are the typical undifferentiated detrital minerals. A few samples contain rutile (BL1-155, CP1-185, GB1-4945, and GB1-8236). CP1-185 contains an anatase-altered, opaque mineral. BL2-176 contains a possible prehnite clast. Biotite in CP1-92, and some in CP1-11, is partially altered to corrensite or siderite. The siderite has altered to limonite. Undifferentiated detrital minerals predominate in about 40% of the samples where detrital minerals were identified. Hornblende and/or micaceous minerals (biotite, muscovite and (or) chlorite) are prevalent in the remaining samples. Where hornblende is present, it is equal to, or greater than the abundance of the micaceous component. Hornblende is the primary detrital mineral in LH1. Micaceous minerals are the principal detrital mineral in the Great Basins 1 well.

Table 4.5 Summary of compositional point count data.

Framework Percentages	**BL1-5**	**BL1-155**	**BL2-176**	**BL3-36**	**BL3-193**	**BL3-205**	**BL3-272**	**BL5-52**	**BL5-92**	**CP1-11**	**CP1-92**	**CP1-185**	**LH1-2**	**LH1-66.5**	**LH1-120**	**LH1-164**	**LH1-182**	**NAC1-4195**	**NAC1-4197**	**NAC1-4198**	**GB1-3890**	**GB1-4945**	**GB1-5464**	**GB1-6083**	**GB1-8236**	**GB1-9823**
Undifferentiated Quartz	3.2	6.1	4.9	0.5	0.4	4.1	1.2	3.6	2.7	2.6	2.5	0.8	3.1	3.6	4.1	5.5	5.9	0.0	0.7	0.0	1.0	0.0	0.0	0.0	0.0	1.3
Monocrystalline Quartz	9.7	22.4	21.6	9.4	0.4	12.9	5.3	15.8	18.9	23.1	17.4	9.6	17.2	20.2	21.8	24.5	20.5	21.8	12.8	23.6	13.0	26.8	15.2	18.7	31.0	10.3
Polycrystalline Quartz	4.9	6.1	15.4	1.4	1.2	5.1	2.8	10.7	8.1	6.4	7.4	2.1	9.2	9.3	10.7	11.5	10.5	9.5	7.4	11.4	6.7	10.0	5.2	7.7	7.9	9.9
Plagioclase	13.5	13.9	3.1	20.2	13.1	19.8	21.9	5.6	10.8	31.6	30.2	15.9	8.0	19.7	14.4	6.0	15.1	10.9	10.8	12.2	11.9	8.9	6.3	6.7	9.2	32.3
K-Feldspar	2.2	1.8	2.5	0.0	0.0	1.8	2.8	4.1	5.4	2.6	7.9	0.8	2.3	1.6	9.1	7.0	6.8	5.4	7.4	4.9	1.0	8.9	8.9	8.6	4.8	5.2
Plutonic Rock Fragment	3.8	3.0	6.2	2.3	2.5	3.7	4.9	9.7	4.3	3.4	14.9	7.9	9.2	9.8	8.2	6.0	5.0	6.1	3.4	1.6	9.3	0.0	3.7	6.7	1.7	30.2
Volcanic Rock Fragment	26.5	17.0	11.1	48.4	61.1	16.6	33.6	6.6	9.7	7.3	7.9	57.3	29.5	16.1	18.5	13.0	9.6	13.6	12.2	8.1	12.4	6.8	13.6	15.3	2.6	4.3
Metamorphic Rock Fragment	9.7	4.8	1.2	0.5	1.2	1.8	2.0	3.6	4.3	1.7	0.0	0.0	1.5	3.1	1.6	3.5	4.1	7.5	9.5	10.6	9.3	3.2	13.6	8.6	6.1	1.3
Sedimentary Rock Fragment	2.2	1.2	3.1	1.4	2.9	2.8	5.3	4.6	4.3	2.1	0.4	0.0	2.3	1.0	0.8	1.5	0.9	6.8	4.1	2.4	9.8	0.5	4.7	4.3	5.7	0.0
Chert	17.3	12.1	25.3	10.8	12.7	21.2	15.8	31.6	21.1	12.8	1.7	0.8	14.9	14.5	8.2	13.0	14.6	10.2	15.5	11.4	18.1	14.7	17.8	16.7	13.1	0.9
Mica	0.0	0.0	0.0	0.0	0.0	0.5	0.0	0.5	0.0	0.9	5.4	0.0	0.0	0.0	0.0	0.5	1.4	0.0	2.0	2.4	0.5	4.7	3.7	1.4	7.0	1.3
Heavy Mineral	0.0	7.3	1.2	0.0	0.4	3.7	0.0	1.0	7.0	0.4	0.8	1.7	0.4	0.5	2.5	3.5	3.2	2.7	5.4	3.3	2.1	1.1	0.0	0.0	1.3	0.0
Organic material	0.0	0.0	0.0	0.5	0.8	0.5	1.2	0.0	1.1	0.4	1.2	0.0	0.0	0.0	0.0	0.0	0.0	0.7	1.4	0.0	1.0	6.3	1.0	2.4	2.6	0.4
Other Intrabasinal	1.6	0.0	0.6	0.9	1.2	0.0	0.8	0.0	0.0	0.4	0.4	1.7	0.0	0.5	0.0	2.5	0.0	0.7	2.0	2.4	1.0	0.0	0.5	0.0	0.9	0.0
Undifferentiated grain	5.4	4.2	3.7	3.8	2.0	5.5	2.4	2.6	2.2	4.3	2.1	1.3	2.3	0.0	0.0	2.0	2.3	4.1	5.4	5.7	2.6	7.9	5.8	2.9	6.1	2.6
Whole Rock Percentages*																										
Undifferentiated Quartz	2.0	3.3	2.7	0.3	0.3	3.0	1.0	2.3	1.7	2.0	2.0	0.7	2.7	2.7	3.3	3.7	4.3	0.0	0.3	0.0	0.7	0.0	0.0	0.0	0.0	1.0
Monocrystalline Quartz	6.0	12.3	11.7	6.7	0.3	9.3	4.3	10.3	11.7	18.0	14.0	7.7	15.0	14.8	17.7	16.3	15.0	10.7	6.3	9.7	8.3	17.0	9.7	13.0	23.7	8.0
Polycrystalline Quartz	3.0	3.3	8.3	1.0	1.0	3.7	2.3	7.0	5.0	5.0	6.0	1.7	8.0	6.8	8.7	7.7	7.7	4.7	3.7	4.7	4.3	6.3	3.3	5.3	6.0	7.7
Plagioclase	8.3	7.7	1.7	14.3	10.7	14.3	18.0	3.7	6.7	24.7	24.3	12.7	7.0	14.4	11.7	4.0	11.0	5.3	5.3	5.0	7.7	5.7	4.0	4.7	7.0	25.0
K-Feldspar	1.3	1.0	1.3	0.0	0.0	1.3	2.3	2.7	3.3	2.0	6.3	0.7	2.0	1.1	7.3	4.7	5.0	2.7	3.7	2.0	0.7	5.7	5.7	6.0	3.7	4.0
Plutonic Rock Fragment	2.3	1.7	3.3	1.7	2.0	2.7	4.0	6.3	2.7	2.7	12.0	6.3	8.0	7.2	6.7	4.0	3.7	3.0	1.7	0.7	6.0	0.0	2.3	4.7	1.3	23.3
Volcanic Rock Fragment	16.3	9.3	6.0	34.3	49.7	12.0	27.7	4.3	6.0	5.7	6.3	45.7	25.7	11.8	15.0	8.7	7.0	6.7	6.0	3.3	8.0	4.3	8.7	10.7	2.0	3.3
Metamorphic Rock Fragment	6.0	2.7	0.7	0.3	1.0	1.3	1.7	2.3	2.7	1.3	0.0	0.0	1.3	2.3	1.3	2.3	3.0	3.7	4.7	4.3	6.0	2.0	8.7	6.0	4.7	1.0
Sedimentary Rock Fragment	1.3	0.7	1.7	1.0	2.3	2.0	4.3	3.0	2.7	1.7	0.3	0.0	2.0	0.8	0.7	1.0	0.7	3.3	2.0	1.0	6.3	0.3	3.0	3.0	4.3	0.0
Chert	10.7	6.7	13.7	7.7	10.3	15.3	13.0	20.7	13.0	10.0	1.3	0.7	13.0	10.6	6.7	8.7	10.7	5.0	7.7	4.7	11.7	9.3	11.3	11.7	10.0	0.7
Mica	0.0	0.0	0.0	0.0	0.0	0.3	0.0	0.3	0.0	0.7	4.3	0.0	0.0	0.0	0.0	0.3	1.0	0.0	1.0	1.0	0.3	3.0	2.3	1.0	5.3	1.0
Heavy Mineral	0.0	4.0	0.7	0.0	0.3	2.7	0.0	0.7	4.3	0.3	0.7	1.3	0.3	0.4	2.0	2.3	2.3	1.3	2.7	1.3	1.3	0.7	0.0	0.0	1.0	0.0
Undifferentiated grain	3.3	2.3	2.0	2.7	1.7	4.0	2.0	1.7	1.3	3.3	1.7	1.0	2.0	0.0	0.0	1.3	1.7	2.0	2.7	2.3	1.7	5.0	3.7	2.0	4.7	2.0
Organic material	0.0	0.0	0.0	0.3	0.7	0.3	1.0	0.0	0.7	0.3	1.0	0.0	0.0	0.0	0.0	0.0	0.0	0.3	0.7	0.0	0.7	4.0	0.7	1.7	2.0	0.3
Other Intrabasinal	1.0	0.0	0.3	0.7	1.0	0.0	0.7	0.0	0.0	0.3	0.3	1.3	0.0	0.4	0.0	1.7	0.0	0.3	1.0	1.0	0.7	0.0	0.3	0.0	0.7	0.0
Detrital Matrix	2.7	2.3	5.0	3.0	0.7	8.3	1.7	9.3	0.7	11.0	8.7	3.7	0.3	0.4	0.0	1.7	5.7	5.0	11.7	9.0	7.3	16.3	15.3	12.0	9.7	5.7
Silica Cement	0.0	0.0	0.0	0.0	0.0	0.0	0.0	0.0	0.0	0.3	0.0	1.3	0.0	0.0	0.0	0.0	0.0	0.0	0.0	0.0	0.0	0.0	0.0	0.3	0.0	0.3
Feldspar Cement	0.0	0.0	0.0	0.0	0.0	0.0	0.0	0.0	0.0	0.0	0.0	0.0	0.0	0.0	0.0	0.0	0.0	0.0	0.0	0.0	0.0	0.0	0.0	0.0	0.0	0.0
Carbonate Cement	33.7	41.3	0.0	14.0	0.0	0.0	0.0	0.0	35.3	0.3	1.7	5.3	7.0	16.3	13.3	30.3	0.0	0.0	0.0	0.0	0.7	1.0	6.0	0.7	0.3	0.0
Clay Cement	0.0	0.0	4.7	9.7	12.0	11.7	14.0	2.7	0.0	5.3	5.3	5.0	5.7	9.1	4.3	1.3	4.3	0.0	0.0	0.0	0.7	0.7	1.7	1.0	3.7	6.7
Analcite Cement	0.0	0.0	0.0	0.0	0.0	0.0	0.0	0.0	0.0	0.0	0.0	0.0	0.0	0.0	0.0	0.0	0.0	0.0	0.0	0.0	0.0	0.0	0.0	0.0	0.0	0.0
Other Cement	2.0	1.3	25.3	2.3	4.0	4.3	0.7	20.3	1.0	2.0	3.0	4.3	0.0	0.4	1.3	0.0	17.0	0.3	0.7	0.7	0.0	0.0	0.0	0.3	0.0	0.3
Porosity	0.0	0.0	11.0	0.0	2.0	0.7	0.7	2.3	0.0	2.3	0.0	0.0	0.0	0.4	0.0	0.0	0.0	6.0	9.7	6.0	16.0	9.7	13.3	7.0	9.3	5.7
Laminae/Burrow-Fill	0.0	0.0	0.0	0.0	0.0	2.7	0.7	0.0	1.3	0.7	0.7	0.7	0.0	0.0	0.0	0.0	0.0	39.7	28.7	43.3	11.0	9.0	0.0	9.0	0.7	4.0

*LH1-66.5 whole rock percentages have been normalized excluding the large shell fragment.

Table 4.6 Detailed point count category framework percentages. Empty cells represent 0%.

	BL1-5	BL1-155	BL2-176	BL3-36	BL3-193	BL3-205	BL3-272	BL5-52	BL5-92	CP1-11	CP1-92	CP1-185	LH1-2	LH1-66.5	LH1-120	LH1-164	LH1-182	NAC1-4195	NAC1-4197	NAC1-4198	GB1-3890	GB1-4945	GB1-5464	GB1-6083	GB1-8236	GB1-9823
Quartz	3.2	6.1	4.9	0.5	0.4	4.1	1.2	3.6	2.7	2.6	2.5	0.8	3.1	3.6	4.1	5.5	5.9		0.7		1.0					1.3
Monocrystalline	9.7	22.4	21.6	9.4	0.4	12.9	5.3	15.8	18.9	23.1	17.4	9.6	17.2	20.2	21.8	24.5	20.5	21.8	12.8	23.6	13.0	26.8	15.2	18.7	31.0	10.3
Polycrystalline	4.9	6.7	15.4	1.5	1.2	5.1	2.8	10.7	8.1	6.4	7.4	2.1	9.2	9.3	10.7	11.5	10.5	9.5	7.4	11.4	6.7	10.0	5.2	7.7	7.9	9.9
Feldspar																										
Alkali	2.2	1.8	2.5			1.8	2.8	4.8	5.4	2.6	7.9	0.8	2.3	1.6	9.1	7.0	6.8	5.4	7.4	4.9	1.0	8.9	8.9	8.6	4.4	3.0
Dissolved																									0.4	2.2
Plagioclase	13.5	13.9	3.1	20.2	13.1	19.4	21.9	5.6	10.8	28.6	30.2	15.9	8.0	19.7	14.0	6.0	15.1	10.9	10.8	11.4	11.9	8.9	6.3	6.2	8.7	31.5
Dissolved						0.5				3.0					0.4					0.8				0.5	0.4	0.9
Sedimentary Rock Fragment																										
Chert		1.2						2.6		0.4			1.9	0.5												
Common (Microcrystalline)	14.6	9.1	19.1	9.9	11.9	17.5	13.0	26.5	17.8	11.5	1.7		11.1	13.0	7.0	10.5	14.2	7.5	12.8	10.6	14.0	14.7	16.2	14.4	11.8	0.4
Cherty Argillite	2.7	1.8	6.2	0.9	0.8	3.2	2.4	2.6	3.2	0.9		0.8	1.9	1.0	0.4	1.5		2.7	2.7	0.8	4.1		1.0	1.9	0.9	
Microporous Chert						0.5	0.4								0.8	1.0	0.5						0.5	0.5	0.4	0.4
Argillite	0.5								0.5				0.4	0.5	0.4		0.5	2.0	1.4	1.6	1.6	0.5	2.1	1.9	1.7	
Slate/Shale	0.5	0.6	1.2	0.5	0.4	2.8	4.0	2.6	1.6	2.1					0.4		0.5	0.7	0.7		5.7		2.1	1.4	3.9	
Siltstone			1.2					1.2					0.8	0.5				1.4	0.7	0.8	1.0		0.5	0.5		
Sandstone	1.1				1.2			0.5					0.4			1.0										
Quartz			0.6		0.4				2.2				0.8					0.7						0.5		
Feldspar		0.6		0.5	0.8		1.2	0.5			0.4					0.5		2.0	1.4							
Detrital Carbonate				0.5																	1.6					
Volcanic Rock Fragment	3.8	4.8	1.9	9.9	4.5	1.4	2.8	1.5	1.6	0.9	0.4	3.8	1.5	2.1	1.6	2.0	0.9									
Felsic	17.8	8.5	6.8	3.3	16.8	11.5	17.8	2.6	3.8	4.7	7.0	1.7	13.8	8.3	11.1	5.5	4.6	8.8	8.8	4.1	10.4	6.8	13.1	15.3	2.2	3.9
Vitric/Cryptocrystalline									0.5									0.7								
Intermediate	4.9	3.6	2.5	26.8	34.4	2.8	10.9	1.5	1.1	0.4	0.4	28.5	10.3	2.6	3.7	3.5	1.4	*	*	*	*	*	*	*	*	*
Tuffaceous				0.5								0.4			0.4	0.5										
Mafic				8.0	5.3	0.9	2.0	1.2	2.7	1.3		23.0	3.8	3.1	1.6	1.5	2.7	4.1	3.4	4.1	2.1		0.5		0.4	0.4
Metamorphic Rock Fragment																										
Felsic																										
Unfoliated Metaclastic (Quartzite)	4.3	1.2	0.6		0.4	0.5	0.9		0.5	0.9			0.4	1.0		1.5	0.5	0.7	1.4	2.4	3.1	1.6	5.2	4.8	2.6	
Quartz-Mica Phyllite	5.5	1.8	0.6	0.5	0.8	1.4	1.2	3.6	3.8	0.9			0.8	1.6	0.4	1.5	2.7	6.8	8.1	8.1	6.2	1.6	8.4	3.8	2.6	
Quartz-Mica Schist/Gneiss		1.8											0.4	0.5	1.2	0.5	0.9								0.9	1.3
Plutonic Rock Fragment																										
Felsic	3.8	3.0	6.2	2.3	2.5	3.7	4.9	9.7	4.3	3.4	14.9	7.1	9.2	9.8	8.2	6.0	5.0	6.1	2.7	1.6	8.8		3.7	6.7	1.7	30.2
Mafic												0.8							0.7		0.5					
Detrital Mineral		3.0	1.2		0.4	3.7		1.2	4.9	0.4	0.8	1.7			1.6	1.5	1.4	1.4	2.7	0.8	1.6	1.1			1.3	
Biotite								0.5			4.5					0.5	1.4		0.7			2.6	0.5		1.7	
White Mica						0.5				0.4	0.8										0.5	1.1	2.6	0.5	4.4	
Chlorite										0.4									1.4	2.4		1.1	0.5	1.0	0.9	1.3
Amphibole		4.2							2.2				0.4	0.5	0.8	2.0	1.8	1.4	2.0	2.4	0.5					
Garnet																			0.7							
Undifferentiated Grain	5.5	4.2	3.7	3.8	2.0	5.5	2.4	2.6	2.2	4.3	2.1	1.3	2.3			2.0	2.3	4.1	5.4	5.7	2.6	7.9	5.8	2.9	6.1	2.6
Intrabasinal Grain																										
Pellet (Non-Glauconite)	1.6		0.6	0.9	1.2		0.9			0.4	0.4	1.7		0.5		2.5		0.7	2.0	2.4	1.0		0.5		0.9	
Organic Material				0.5	0.8	0.5	1.2		1.1	0.4	1.2							0.7	1.4		1.0	6.3	1.0	2.4	2.6	0.4

*Volcanic rock fragments in well samples were counted as either felsic or mafic. The intermediate volcanic category was added for point counting of the outcrop sample set.

Table 4.7 Detailed point count category whole-rock percentages. Empty cells represent 0%.

	BL1-5	BL1-155	BL2-176	BL3-36	BL3-193	BL3-205	BL3-272	BL5-52	BL5-92	CP1-11	CP1-92	CP1-185	LH1-2	LH1-66.5	LH1-120	LH1-164	LH1-182	NAC1-4195	NAC1-4197	NAC1-4198	GB1-3890	GB1-4945	GB1-5464	GB1-6083	GB1-8236	GB1-9823
Quartz	2.0	3.3	2.7	0.3	0.3	3.0	1.0	2.3	1.7	2.0	2.0	0.7	2.7	2.3	3.3	3.7	4.3		0.3		0.7					1.0
Monocrystalline	6.0	12.3	11.7	6.7	0.3	9.3	4.3	10.3	11.7	18.0	14.0	7.7	15.0	13.0	17.7	16.3	15.0	10.7	6.3	9.7	8.3	17.0	9.7	13.0	23.7	8.0
Polycrystalline	3.0	3.3	8.3	1.0	1.0	3.7	2.3	7.0	5.0	5.0	6.0	1.7	8.0	6.0	8.7	7.7	7.7	4.7	3.7	4.7	4.3	6.3	3.3	5.3	6.0	7.7
Feldspar																										
Alkali	1.3	1.0	1.3			1.3	2.3	2.7	3.3	2.0	6.3	0.7	2.0	1.0	7.3	4.7	5.0	2.7	3.7	2.0	0.7	5.7	5.7	6.0	3.3	2.3
Dissolved																									0.3	1.7
Plagioclase	8.3	7.7	1.7	14.3	10.7	14.0	18.0	3.7	6.7	22.3	24.3	12.7	7.0	12.7	11.3	4.0	11.0	5.3	5.3	4.7	7.7	5.7	4.0	4.3	6.7	24.3
Dissolved						0.3				2.3					0.3					0.3				0.3	0.3	0.7
Sedimentary Rock Fragment																										
Chert		0.7						1.7		0.3			1.7	0.3												
Common (Microcrystalline)	9.0	5.0	10.3	7.0	9.7	12.7	10.7	17.3	11.0	9.0	1.3		9.7	8.3	5.7	7.0	10.3	3.7	6.3	4.3	9.0	9.3	10.3	10.0	9.0	0.3
Cherty Argillite	1.7	1.0	3.3	0.7	0.7	2.3	2.0	1.7	2.0	0.7		0.7	1.7	0.7	0.3	1.0		1.3	1.3	0.3	2.7		0.7	1.3	0.7	
Microporous Chert						0.3	0.3								0.7	0.7	0.3						0.3	0.3	0.3	0.3
Argillite	0.3								0.3				0.3	0.3	0.3		0.3	1.0	0.7	0.7	1.0	0.3	1.3	1.3	1.3	
Slate/Shale	0.3	0.3	0.7	0.3	0.3	2.0	3.3	1.7	1.0	1.7					0.3		0.3	0.3	0.3		3.7		1.3	1.0	3.0	
Siltstone			0.7					0.7					0.7	0.3				0.7	0.3	0.3	0.7		0.3	0.3		
Sandstone	0.7				1.0			0.3					0.3			0.7										
Quartz			0.3		0.3				1.3				0.7					0.3						0.3		
Feldspar		0.3		0.3	0.7		1.0	0.3			0.3					0.3		1.0	0.7							
Detrital Carbonate				0.3																	1.0					
Volcanic Rock Fragment	2.3	2.7	1.0	7.0	3.7	1.0	2.3	1.0	1.0	0.7	0.3	3.0	1.3	1.3	1.3	1.3	0.7									
Felsic	11.0	4.7	3.7	2.3	13.7	8.3	14.7	1.7	2.3	3.7	5.7	1.3	12.0	5.3	9.0	3.7	3.3	4.3	4.3	1.7	6.7	4.3	8.3	10.7	1.7	3.0
Vitric/Cryptocrystalline									0.3									0.3								
Intermediate	3.0	2.0	1.3	19.0	28.0	2.0	9.0	1.0	0.7	0.3	0.3	22.7	9.0	1.7	3.0	2.3	1.0	*	*	*	*	*	*	*	*	*
Tuffaceous				0.3								0.3			0.3	0.3										
Mafic				5.7	4.3	0.7	1.7	0.7	1.7	1.0		18.3	3.3	2.0	1.3	1.0	2.0	2.0	1.7	1.7	1.3		0.3		0.3	0.3
Metamorphic Rock Fragment																										
Felsic																										
Unfoliated Metaclastic (Quartzite)	2.7	0.7	0.3		0.3	0.3	0.7		0.3	0.7			0.3	0.7		1.0	0.3	0.3	0.7	1.0	2.0	1.0	3.3	3.3	2.0	
Quartz-Mica Phyllite	3.3	1.0	0.3	0.3	0.7	1.0	1.0	2.3	2.3	0.7			0.7	1.0	0.3	1.0	2.0	3.3	4.0	3.3	4.0	1.0	5.3	2.7	2.0	
Quartz-Mica Schist/Gneiss		1.0											0.3	0.3	1.0	0.3	0.7								0.7	1.0
Plutonic Rock Fragment																										
Felsic	2.3	1.7	3.3	1.7	2.0	2.7	4.0	6.3	2.7	2.7	12.0	5.7	8.0	6.3	6.7	4.0	3.7	3.0	1.3	0.7	5.7		2.3	4.7	1.3	23.3
Mafic												0.7							0.3		0.3					
Detrital Mineral		1.7	0.7		0.3	2.7		0.7	3.0	0.3	0.7	1.3			1.3	1.0	1.0	0.7	1.3	0.3	1.0	0.7			1.0	
Biotite								0.3			3.7					0.3	1.0		0.3			1.7	0.3		1.3	
White Mica						0.3				0.3	0.7										0.3	0.7	1.7	0.3	3.3	
Chlorite										0.3									0.7	1.0		0.7	0.3	0.7	0.7	1.0
Amphibole		2.3							1.3				0.3	0.3	0.7	1.3	1.3	0.7	1.0	1.0	0.3					
Garnet																			0.3							
Undifferentiated Grain	3.3	2.3	2.0	2.7	1.7	4.0	2.0	1.7	1.3	3.3	1.7	1.0	2.0			1.3	1.7	2.0	2.7	2.3	1.7	5.0	3.7	2.0	4.7	2.0

Table 4.7 continued

	BL1-5	BL1-155	BL2-176	BL3-36	BL3-193	BL3-205	BL3-272	BL5-52	BL5-92	CP1-11	CP1-92	CP1-185	LH1-2	LH1-66.5	LH1-120	LH1-164	LH1-182	NAC1-4195	NAC1-4197	NAC1-4198	GB1-3890	GB1-4945	GB1-5464	GB1-6083	GB1-8236	GB1-9823
Matrix																										
Argillaceous				0.3																					0.7	
Clay				0.3	0.3	6.3	0.3			4.7		0.3					5.0	5.0	11.7	9.0	7.0	13.3	7.0	12.0	3.3	5.3
Pseudomatrix	2.7	2.3	5.0	2.3	0.3	2.0	1.3	9.3	0.7	6.3	8.7	3.3	0.3	0.3		1.7	0.7				0.3	3.0	8.3		5.7	0.3
Cement/Overgrowths**	2.0	0.7	11.0	2.3	4.0	4.3	0.7	4.7		2.0	3.0	4.3					3.3									
Silica																										
Quartz										0.3														0.3		0.3
Chert												1.3														
Carbonate																										
Calcite	33.7	41.3		14.0					35.3	0.3	1.3	4.7	7.0	14.3	13.3	30.3										
Siderite											0.3	0.7									0.7	1.0	6.0	0.7	0.3	
Argillaceous																										
Kaolinite										5.3	2.7											0.3	1.7	0.3	3.7	6.7
Smectite/Mixed-Layer			4.7	9.7	12.0	11.7	14.0	2.7			2.7	5.0	5.7	8.0	4.3	1.3	4.3				0.7	0.3		0.7		
Authigenic Mineral																										
Pyrite		0.3							0.3								0.7	0.3	0.7	0.7				0.3		
Anatase/Rutile																										0.3
Zeolite																										
Laumontite														0.3	1.3		13.0									
Heulandite		0.3	14.3					15.7	0.7																	
Intrabasinal Grain																										
Pellet (Non-Glauconite)	1.0		0.3	0.7	1.0		0.7			0.3	0.3	1.3		0.3		1.7		0.3	1.0	1.0	0.7		0.3		0.7	
Organic Material				0.3	0.7	0.3	1.0		0.7	0.3	1.0							0.3	0.7		0.7	4.0	0.7	1.7	2.0	0.3
Oversize Grain																										
Shell Fragment														12.3												
Porosity																										
Intergranular			7.3		2.0	0.3		1.3		0.7				0.3				5.3	9.3	6.0	15.7	9.0	13.0	5.3	9.0	3.0
Intragranular																										
Secondary			3.7			0.3	0.7	0.7		1.7								0.7	0.3		0.3	0.7	0.3	1.7	0.3	2.7
Fracture								0.3																		
Laminae/Burrow-Fill																										
Clay Laminae/Burrow-Fill						2.7	0.7		1.3	0.7	0.7	0.7						39.7	28.7	43.3	11.0	9.0		9.0	0.7	4.0

*Volcanic rock fragments in well samples were counted as either felsic or mafic. The intermediate volcanic category was added for point counting of the outcrop sample set.
**The undifferentiated Cement/Overgrowths category represents mostly limonite (which likely includes geothite).

The undifferentiated framework grains likely include hornfels in BL1-155, BL5-92, and LH Some undifferentiated grains in CP1-92 may be extensively sericite-altered plagioclase clasts. Intrab components consist of clay pellets and/or organic material. The clay pellets in the North Aleutian C well samples are all olive-green and rounded. They may be glauconite in GB1-8236. In BL3-36, BI and LH1-66.5, the clay pellets are corrensite vug filling. These two BL3 samples also contain volca rock fragments with corrensite vug filling.

In many samples, altered micas compose the pseudomatrix (discontinuous interstitial materi formed by deformation of ductile detrital grains, as defined by Dickinson, 1970). Some of the pseudomatrix in CP1-185 is composed of argillaceous fragments with abundant siderite. Pseudomat few samples (BL2-176, BL5-92, and LH1-164) appears to be of volcanic origin, and likely consists c severely altered volcanic fragments in BL2-176, clay-altered pellets or smectite-altered volcanic glas BL5-92, and may be tuffaceous in LH1-164.

In addition to clay and carbonate cements, GB1-8236 contains traces of quartz overgrowths kaolinite in GB1-9823 is probably dickite. The undifferentiated cement/overgrowths category (Tabl represents limonite and includes dead oil in BL2-176.

The petrographer (Michael Wilson) identified several pore-filling, alteration, and replaceme minerals (Table 4.8 and Table 4.9). Zeolite cements (heulandite and laumontite) are restricted to the Bear Lake Formation, measured sections BL1, BL5, LH1, and BL2 (Table 4.8). Laumontite has repl plagioclase and amphibole in LH1 (Table 4.9). Calcite is present only in outcrop samples, and occur both a cement (Table 4.8) and replacement component (Table 4.9) in every measured section except Calcite has replaced plagioclase, mafic volcanic fragments, glass, and unknown framework clasts (T 4.9). Smectite, corrensite, and limonite occur as pore-filling components in outcrop samples and are conspicuously absent in well samples (Table 4.8). However, volcanic glass is replaced by smectite i several Great Basins 1 well samples and in the lower Bear Lake Formation measured sections CP1 a (Table 4.9). Well samples, and BL3 outcrop samples, contain clay and mud matrix (Table 4.8). Pyri occurs, as a minor component, in BL1, BL5, LH1, and both wells (Table 4.8).

Table 4.8 Pore-filling minerals identified during point count analysis. Abbreviations in the zeolite column indicate laumontite (L) and heulandite (H).

	Zeolite	Smectite	Corrensite	Limonite	Ferroan Calcite	Calcite	Chert	Pyrite	Clay & Mud matrix	Detrital clay rims	Siderite	Kaolinite	Quartz overgrowths	Anatase
BL2-176	H	x		x										
LH1-182	L		x	x				x	x					
LH1-164			x		x	x								
LH1-120	L		x			x								
LH1-66.5			x		x	x								
LH1-2			x		x	x								
BL5-92	H				x			x						
BL5-52	H	x		x										
BL1-155	H			x	x			x						
BL1-5				x	x									
BL3-272			x	x					x					
BL3-205			x	x					x					
BL3-193			x	x					x					
BL3-36			x	x	x	x			x	x				
CP1-185		x	x	x	x		x		x		x			
CP1-92			x	x	x							x		
CP1-11				x					x			x	x	
GB1-3890									x		x			
GB1-4945									x		x			
GB1-5464									x		x	x		
GB1-6083								x	x		x	x	x	
GB1-8236									x	x		x		
GB1-9823									x			x	x	x
NAC1-4195								x	x					
NAC1-4197								x	x					
NAC1-4198								x	x					

Table 4.9 Replacement minerals identified during point count analysis. Abbreviations indicate the detrital grains that have been altered and (or) replaced and are defined as follows: plagioclase (P), mafic volcanic rock fragments (V), amphibole (A), glass (G), muscovite (M), biotite (B), unknown (U).

	Ferroan Calcite	Calcite	Ferroan calcite or calcite	Laumontite	Smectite	Kaolinite	Siderite
BL2-176							
LH1-182				P, A			
LH1-164	P, V	P, V					
LH1-120		P		P			
LH1-66.5	U		V	P			
LH1-2	U						
BL5-92	U						
BL5-52							
BL1-155	U		V				
BL1-5	U	P					
BL3-272					G		
BL3-205							
BL3-193							
BL3-36	U	P			G		
CP1-185	U		G				
CP1-92	U				G	P	
CP1-11	U					P	
GB1-3890					G		
GB1-4945					G	M	B
GB1-5464						M	B
GB1-6083					G		
GB1-8236							B
GB1-9823							
NAC1-4195							
NAC1-4197							
NAC1-4198							

The Great Basins 1 well samples contain clay and mud matrix, siderite, and kaolinite (Table 4.8). Muscovite has been replaced by kaolinite in GB1-5464 and biotite has altered to siderite in both GB1-5464 and GB1-8236 (Table 4.9). Volcanic glass in GB1-3890, GB1-4945, and GB1-6083 has been replaced by smectite (Table 4.9). The petrographer (Michael Wilson) did not identify pore-filling kaolinite in the uppermost samples, GB1-3890 and GB1-4945 (Table 4.8), but he did identify kaolinite replacement of muscovite in GB1-4945 (Table 4.9). The North Aleutian COST 1 well samples are characterized by clay and mud matrix with subordinate pyrite (Table 4.8).

The authigenic component in BL2-176 is predominately heulandite with lesser clay and limonite (Fig. 4.1A). LH1 samples are predominantly cemented by calcite and subordinate clay with the notable exception of the uppermost sample, LH1-182 (Fig. 4.1B). Zeolite (laumontite) is the primary cement in LH1-182, with lesser amounts of clay and limonite (Fig. 4.1B and Table 4.7.). Plagioclase is replaced by both calcite and laumontite throughout LH1 (Table 4.9). Mafic volcanic rock fragments are replaced by both ferroan calcite and calcite (Table 4.9). The two BL5 samples are distinctly different from one another (Fig. 4.1C). BL5-52 is similar to BL2-176 (Fig. 4.1A and Fig. 4.1C). Zeolite (heulandite) is the predominant cement with lesser clay and limonite in BL5-52, whereas calcite accounts for nearly the entire authigenic component in BL5-92 with very minor heulandite (Fig. 4.1C and Table 4.7). Both BL1 samples are primarily cemented by calcite with a very minor limonite component (Fig. 4.1D). Ferroan calcite and (or) calcite has replaced plagioclase, volcanic rock fragments, and unknown framework grains in BL1 (Table 4.9).

Clay is the principal authigenic component in most BL3 samples, with lesser amounts of limonite (Fig. 4.1E). Calcite accounts for approximately half of the cement in the lowermost sample, BL3-36. The remainder is composed of clay with lesser limonite. Glass is replaced by smectite in this measured section (Table 4.9). CP1 samples contain various combinations of several authigenic minerals (Fig. 4.1F). Calcite, clay, and siderite become more pervasive from the lowermost (CP1-11) to uppermost (CP1-185) samples. Kaolinite shows the opposite trend. Kaolinite is the primary cement in CP1-11, diminishes in CP1-92, and is absent in CP1-185. All CP1 samples contain limonite. Ferroan calcite has replaced unknown framework grains in CP1 (Table 4.9). Glass is replaced by ferroan calcite or calcite in CP1-185, and by smectite in

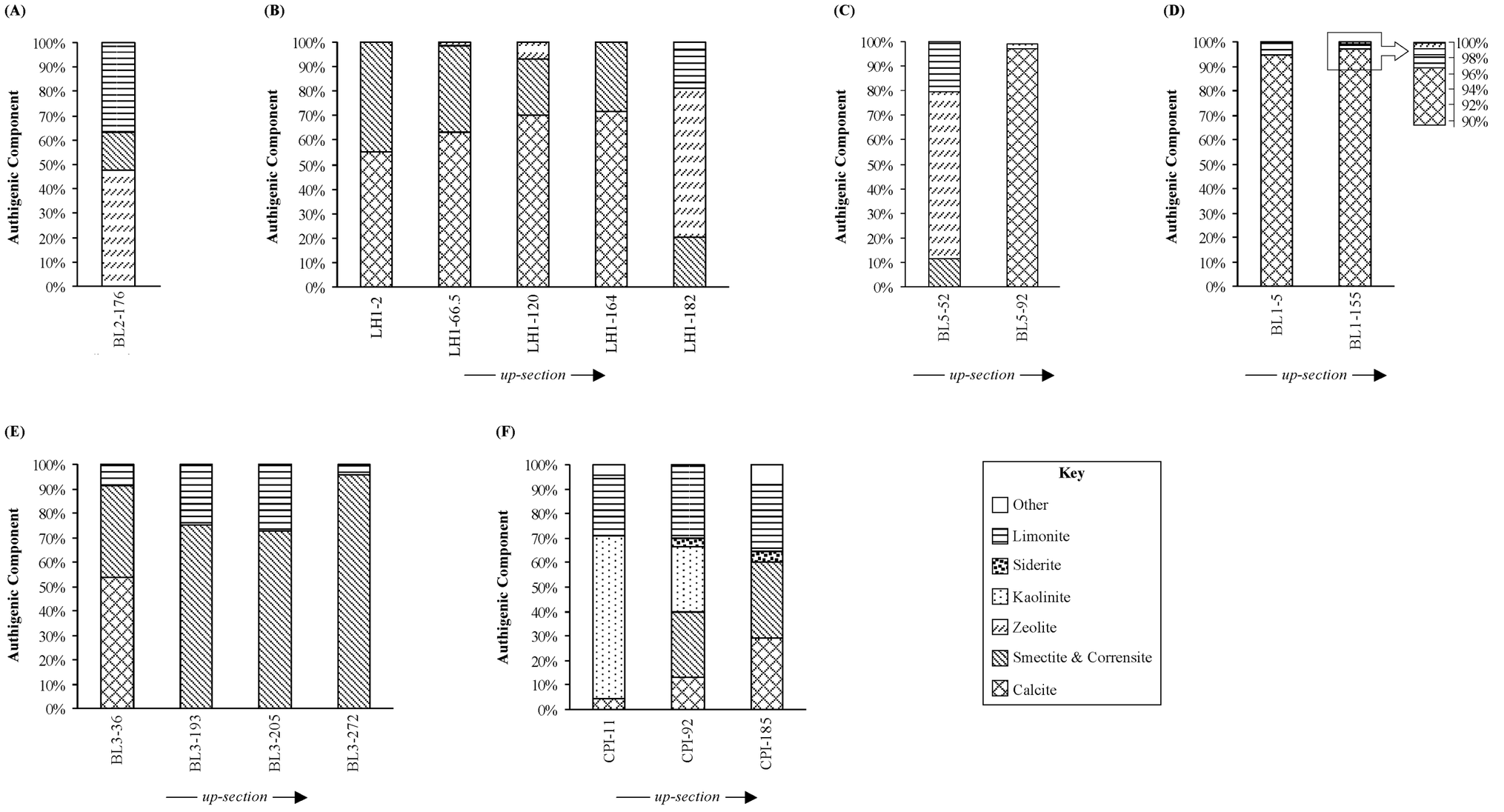

Fig. 4.1 Proportion of authigenic components identified in outcrop samples during point count analysis. (A) Measured section BL2. (B) Measured section LH1. (C) Measured section BL5. (D) Measured section BL1. (E) Measured section BL3. (F) Measured section CP1. For stratigraphic positions of measured sections and samples see Fig. 4.2.

CP1-92 (Table 4.9). Kaolinite has replaced plagioclase in CP1-11 and CP1-92 (Table 4.9).

Fig. 4.2 summarizes the petrographically identified pore-filling and replacement componen outcrop samples. Each measured section shows a fairly consistent mineralogy. The lower Bear Lak Formation sections all contain matrix and authigenic clays. The upper Bear Lake Formation measur sections generally lack matrix and contain both zeolites and calcite. Features of note include the pre of kaolinite in lower CP1, calcite near the base of BL3, laumontite in LH1, and heulandite in BL1, B and BL2. Fig. 4.3 summarizes the petrographically identified pore-filling and replacement compone well samples. All well samples contain clay and mud matrix. The Great Basins 1 well shows no significant change in authigenic mineralogy with depth. In addition to clay and mud matrix, the sam from the Great Basins 1 well contain kaolinite and siderite.

4.3.2 Ternary Diagrams

I plotted petrographic data on a series of ternary diagrams to illustrate the composition of sa from the Bear Lake Formation, and to identify compositional variation within the sample set. The diagrams show no systematic compositional changes between samples within individual measured s or either well. However, compositional differences do occur when all measured sections are conside chronostratigraphic order (see Fig. 2.2). Compositional differences also occur between outcrop and samples.

4.3.2.1 Quartz, Feldspar, and Lithic Grains

Fig. 4.4 shows detrital components plotted on two ternary diagrams illustrating the distribution of qu feldspar, and lithic grains. Comparison of the Quartz/Feldspar/Unstable lithic grains (Q+FL-) and Monocrystalline Quartz/Feldspar/Stable lithic grains (QmFLt) diagrams shows a notable shift from t pole (Fig. 4.4A) toward the Lt pole (Fig. 4.4B). This illustrates the parameter C/Q (ratio of chert, in polycrystalline quartz to total quartz) of Dickinson (1970) which reflects a change by moving stable grains to the lithic pole when placing emphasis on source rather than stability. Dickinson's paramet is equivalent to Qp+/Q+ as defined in Table 4.2. Qp+/Q+ is quantified in Fig. 4.5 and shows that sta lithic grains account for greater than 40% of the quartzose component in nearly all sandstones. Plott ratio C/Qp+ reveals that much of the stable lithic component is chert (Fig. 4.6).

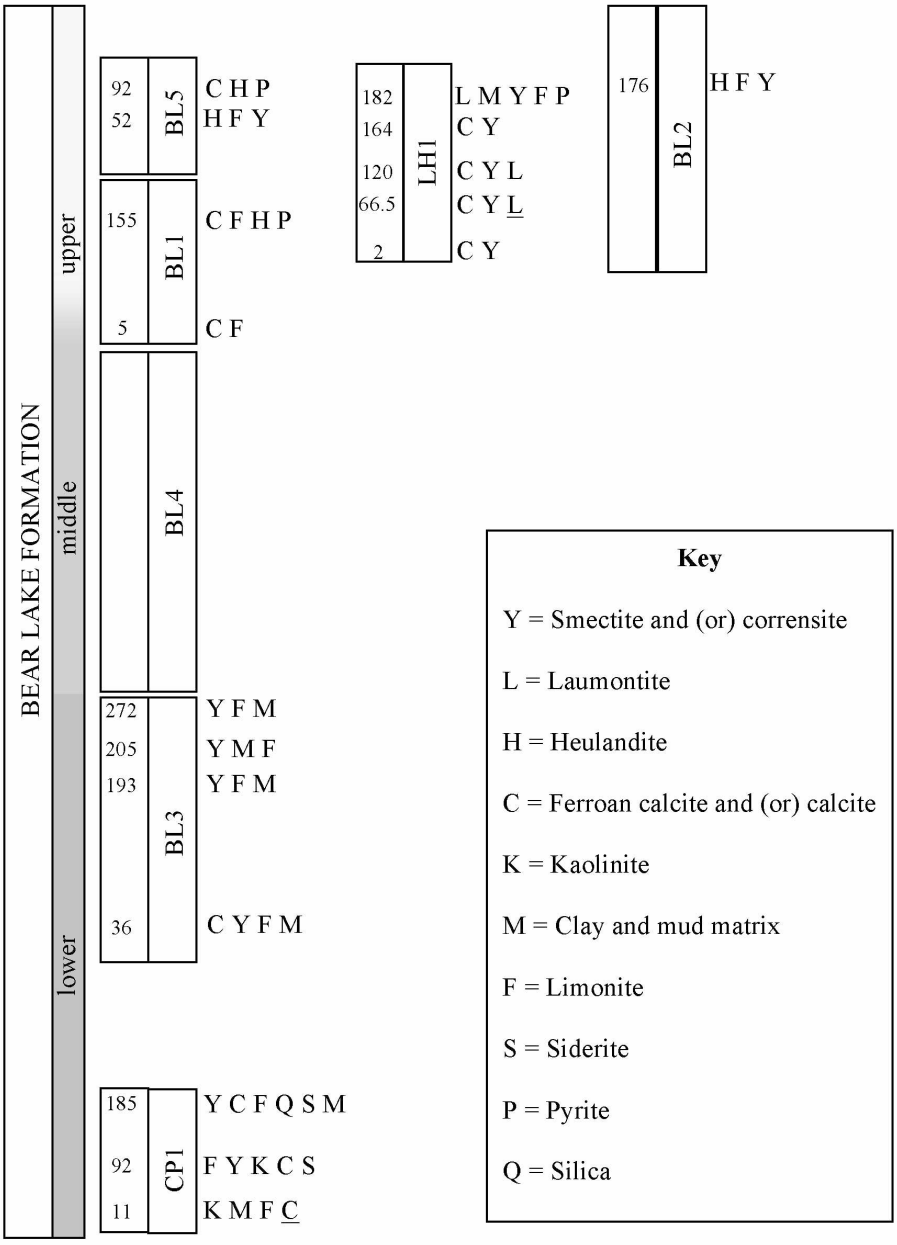

Fig. 4.2 Summary of petrographically identified pore-filling and replacement components in outcrop samples. Underline indicates that the mineral is only present as a replacement component, and not a pore-filling component. This figure summarizes data from Table 4.8 and Table 4.9. Minerals are listed in order of decreasing abundance. The measured sections are displayed in chronostratigraphic order (Decker et al., 2005; Finzel et al., 2005). The lower, middle, and upper designations are based on Decker et al. (2005).

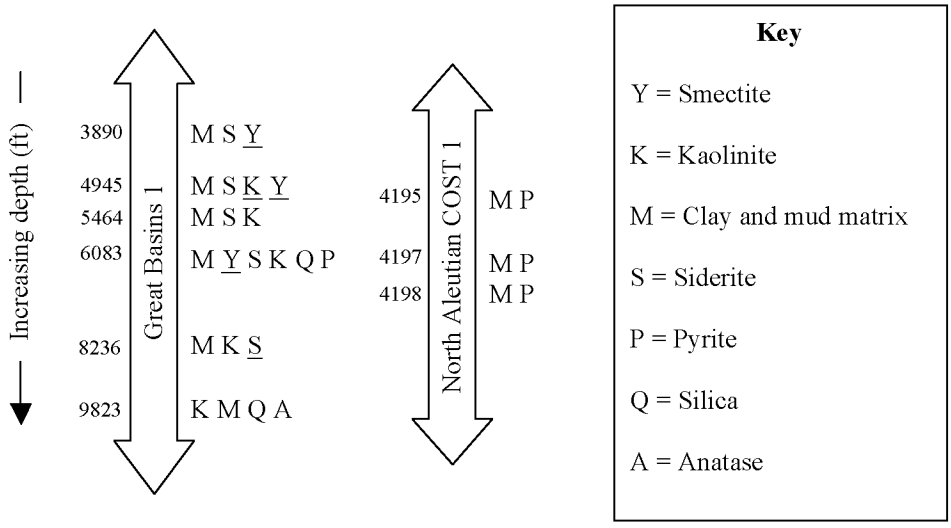

Fig. 4.3 Summary of petrographically identified pore-filling and replacement components in well samples. Underline indicates that the mineral is only present as a replacement component, and not a pore-filling component. Minerals are listed in order of decreasing abundance. This figure summarizes data from Table 4.8 and Table 4.9.

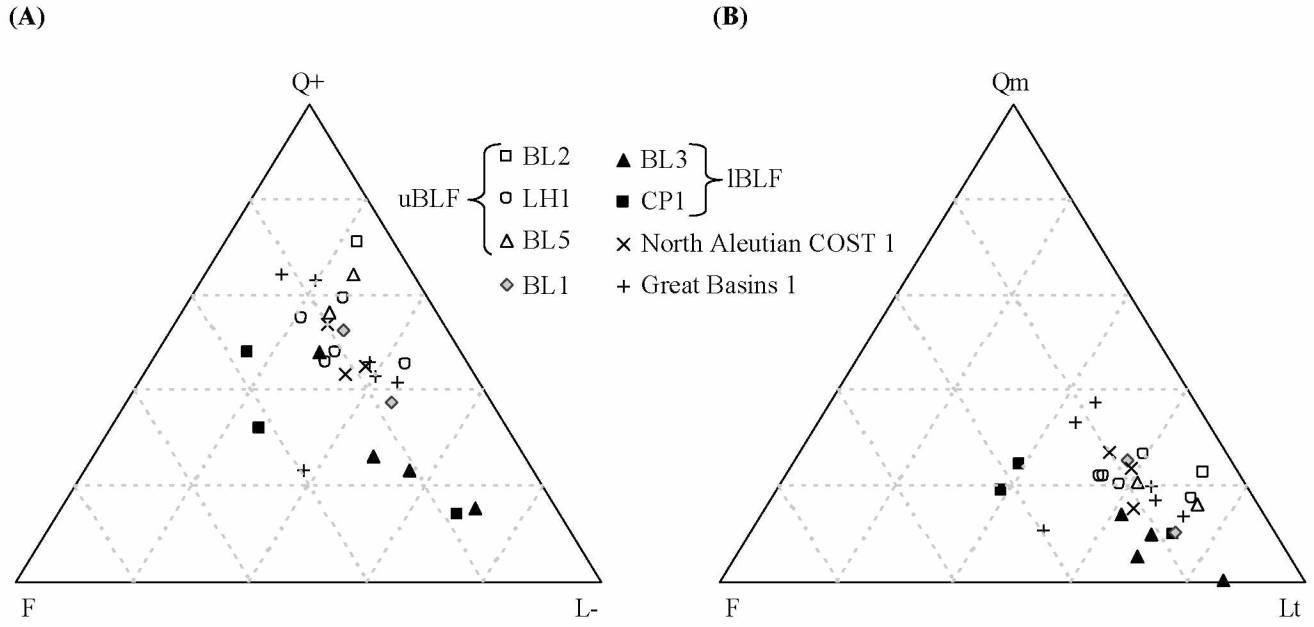

Fig. 4.4 Quartz/Feldspar/Lithic Grains ternary diagrams. (A) Quartz/Feldspar/Unstable Lithic Grains (Q+FL-) ternary diagram. Stable lithic components are assigned to the quartz pole to emphasize stability. (B) Monocrystalline Quartz/Feldspar/Stable Lithic Grains (QmFLt) ternary diagram. Only monocrystalline quartz is included at the quartz pole, and stable lithic grains are assigned to the lithic pole to emphasize source over stability. uBLF refers to samples from measured sections BL2, LH1, and BL5, and lBLF refers to samples from measured sections BL3 and CP1 (see section 4.4). See Table 4.2 for parameter definitions

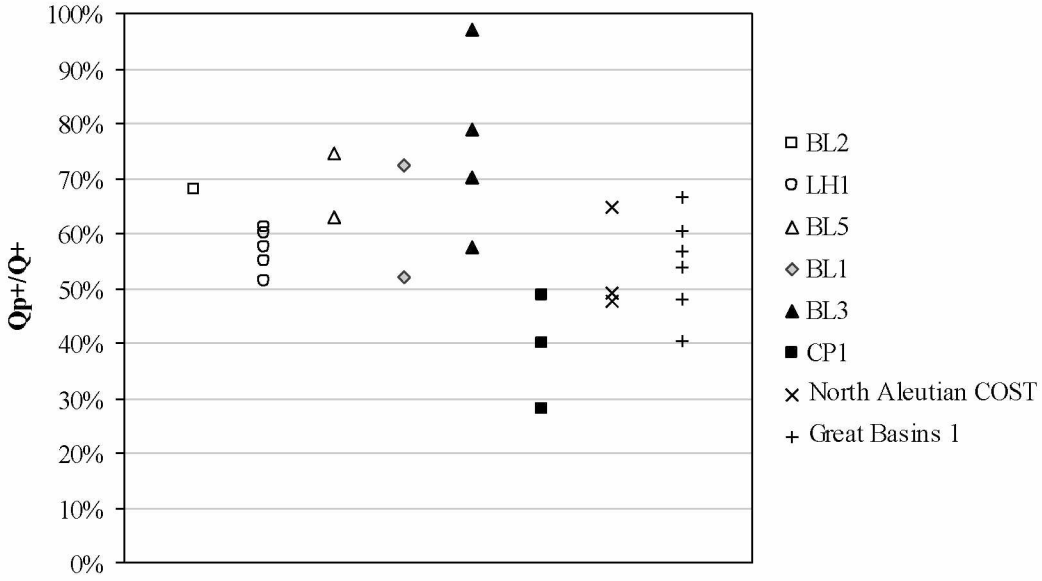

Fig. 4.5 Ratio of stable quartzose lithic grains to total quartz. The vertical axis represents the percent of stable lithic grains (Qp+) in the total quartz component (Q+). The horizontal axis does not represe parameter and is only used for clarity by separating samples from different measured sections and wel See Table 4.2 for parameter definitions.

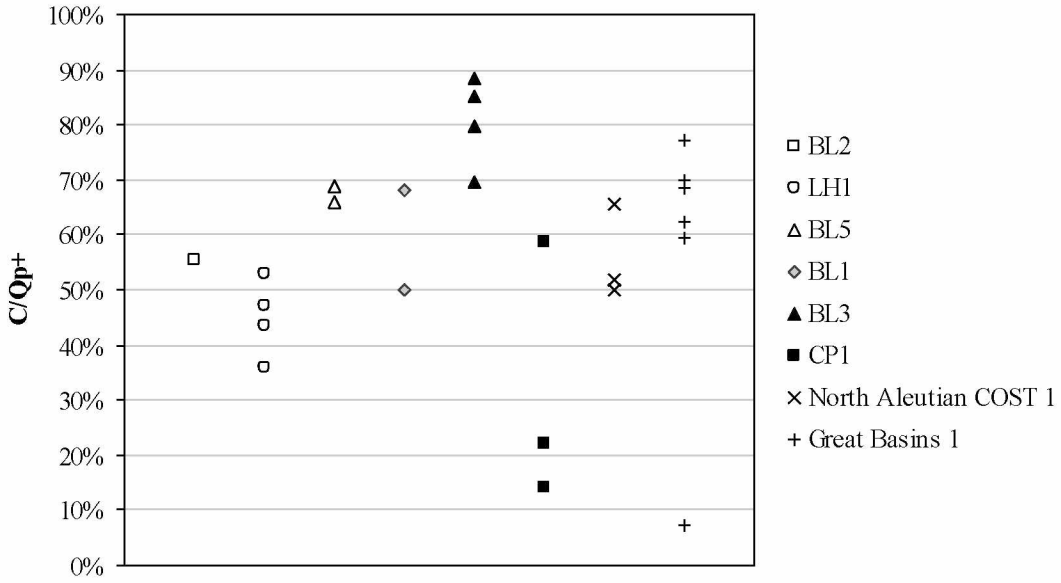

Fig. 4.6 Ratio of chert to total stable quartzose lithic grains. The vertical axis represents the percentage of chert (C) in the stable lithic component (Qp+). The horizontal axis does not represent any parameter and is only used for clarity by separating samples from different measured sections and wells. Sample GB1-9823 is an outlier (C/Qp+ = 7%) compared to other samples form the Great Basins 1 well. See Table 4.2 for parameter definitions.

The average framework compositions of the entire sample set are $Q+_{45}F_{20}L-_{35}$ and $Qm_{19}F_{20}Lt_{61}$, however components do show a significant range of $Q+_{14-71}F_{6-42}L-_{13-71}$ and $Qm_{0-38}F_{6-42}Lt_{39-86}$. The Q+FL- diagram (Fig. 4.4A) shows that outcrop samples from the upper Bear Lake Formation (measured sections BL5, LH1, and BL2) group together and are more quartz-rich. Other outcrop samples show less consistency, but generally shift toward the lithic pole, becoming depleted in quartz components. Samples from the lower Bear Lake Formation (measured sections CP1 and BL3) are distinctly set apart from the upper grouping (Fig. 4.4A). Two CP1 samples (CP1-11 and CP1-92) are more feldspathic than all other outcrop samples and represent the lowermost Bear Lake Formation. The well samples group with outcrop samples from the upper Bear Lake Formation (BL5, LH1, and BL2), except for one feldspathic outlier from the Great Basins 1 well (GB1-9823). The QmFLt diagram (Fig. 4.4B) shows a similar pattern, but samples plot closer to the lithic pole. The same three samples (CP1-11, CP1-92, and GB1-9823) are still set apart by their more feldspathic nature.

4.3.2.2 Monocrystalline Components

Fig. 4.7 shows monocrystalline components on the Monocrystalline Quartz/Plagioclase/K-Feldspar (QmPK) diagram (Dickinson and Suczek, 1979). This diagram is designed to show the quartzose and feldspathic monocrystalline components of the framework grains and shows that plagioclase-rich sandstones have less monocrystalline quartz, and that plagioclase is generally more abundant than K-feldspar.

As seen on the detrital component diagrams (Fig. 4.4A and Fig. 4.4B), outcrop samples from the upper Bear Lake Formation (BL5, LH1, and BL2) group together and are more quartz-rich, as are most well samples (Fig. 4.7). The QmPK diagram (Fig. 4.7) shows that quartz accounts for more than 40% of the monocrystalline component, whereas plagioclase represents less than 40% in this grouping. Outcrop samples from the lower Bear Lake Formation (CP1 and BL3) plot closer to the plagioclase pole. Quartz accounts for less than 40% of the monocrystalline component, whereas plagioclase represents more than 50% in this grouping . The two BL1 samples are split between the two groups.

A plot of the ratio of plagioclase to total feldspar (P/F) also sets the lower Bear Lake Formation samples apart (Fig. 4.8). Plagioclase predominates in CP1, BL3 and BL1. All of these samples have a

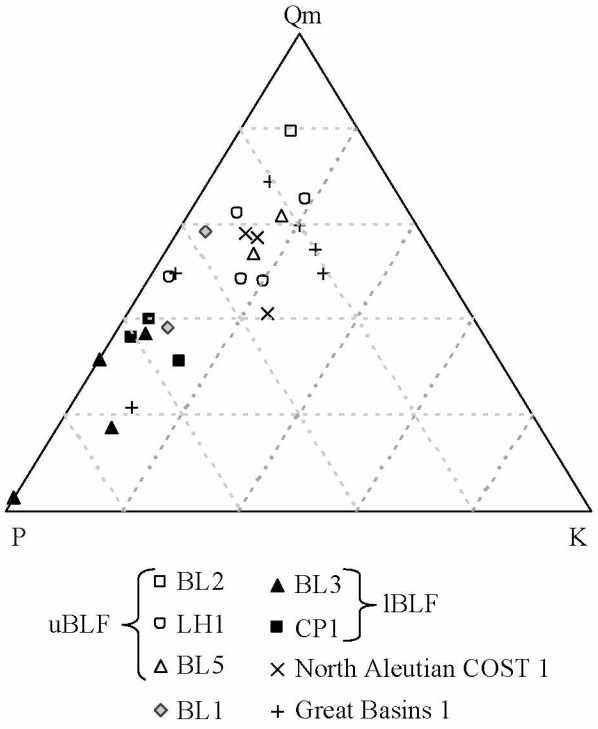

Fig. 4.7 Monocrystalline Quartz/Plagioclase/K-Feldspar (QmPK) ternary diagram. This diagram shows the monocrystalline composition of the framework. uBLF refers to samples from measured sections BL2, LH1, and BL5, and lBLF refers to samples from measured sections BL3 and CP1 (see section 4.4). See Table 4.2 for parameter definitions.

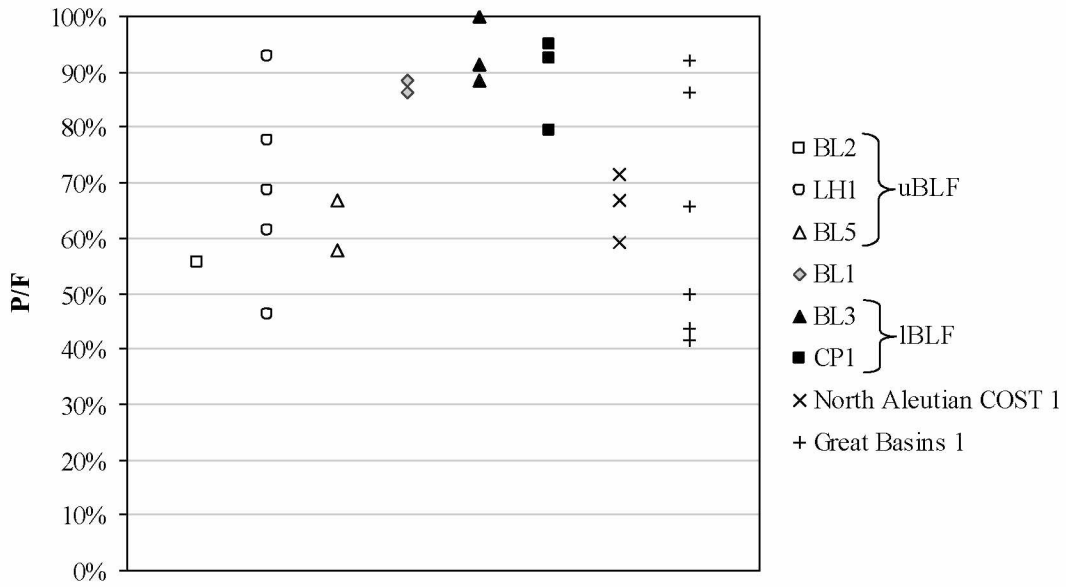

Fig. 4.8 Ratio of plagioclase to total feldspar. The vertical axis represents the percentage of plagioclase (P) in the monocrystalline feldspar (F) component. The horizontal axis does not represent any parameter and is only used for clarity by separating samples from different measured sections and wells. uBLF refers to samples from measured sections BL2, LH1, and BL5, and lBLF refers to samples from measured sections BL3 and CP1 (see section 4.4). See Table 4.2 for parameter definitions.

feldspathic component of 80% plagioclase or more. Plagioclase is the primary feldspar in most of the other samples, but K-feldspar can be as much as half of the feldspathic component.

4.3.2.3 Composition of Lithic Grains

The Sedimentary/Volcanic/Metamorphic lithic grains (Ls+LvLm) diagram (Fig. 4.9A) shows the lithic components (Helmold et al., 2008). The lithic portion is chiefly sedimentary and volcanic. Chert is included at the sedimentary pole to emphasize its sedimentary origin. Plutonic rock fragments are not represented. Removing chert from the diagram shows an obvious shift to the volcanic pole, illustrating that chert is the major sedimentary contributor (Fig. 4.9B). The minor portion of the sedimentary lithic component is composed of argillite, mudstone (shale and siltstone), and sandstone (Table 4.1 and Table 4.6). The metamorphic lithic grains include micaceous quartzite, phyllite, and schist (Table 4.1 and Table 4.6). According to Suttner and Basu (1985), quartz-mica aggregates may be derived from either plutonic or metamorphic sources and should not be included with the metamorphic lithic grains. Therefore, I have excluded the Qu parameter (undifferentiated quartz defined in Table 4.2, which represents quartz with trace-very minor mica/chlorite in outcrop samples according to Table 4.1) from these lithic diagrams due to their generally ambiguous origin (for example, metamorphic versus plutonic). Only quartz-mica aggregates with aligned micaceous minerals (classified as micaceous quartzite in Table 4.1) are included at the metamorphic poles.

The Sedimentary/Igneous/Metamorphic lithic grains (Ls+LiLm) diagram (Fig. 4.9C) includes both plutonic and volcanic lithic grains at the igneous pole in my attempt to represent the plutonic portion of rock fragments. Qu is still excluded from the diagram due to uncertainty of plutonic or metamorphic origin, but the ratio Qu/(L+Qu) (undifferentiated quartz to total lithcs including chert and undifferentiated quartz) represents the maximum amount of shift away from the sedimentary pole that would occur if Qu were assigned to either the igneous or metamorphic poles. Plotting this ratio (Fig. 4.10) indicates that the sedimentary representation on the lithic ternary diagrams (Fig. 4.9) would be reduced by less than 15% (less than 10% for most samples).

Ternary diagrams of lithic components (Fig. 4.9) show that the well samples have a higher percentage of metamorphic rock fragments. This is most pronounced on the Ls-LvLm diagram (Fig. 4.9B).

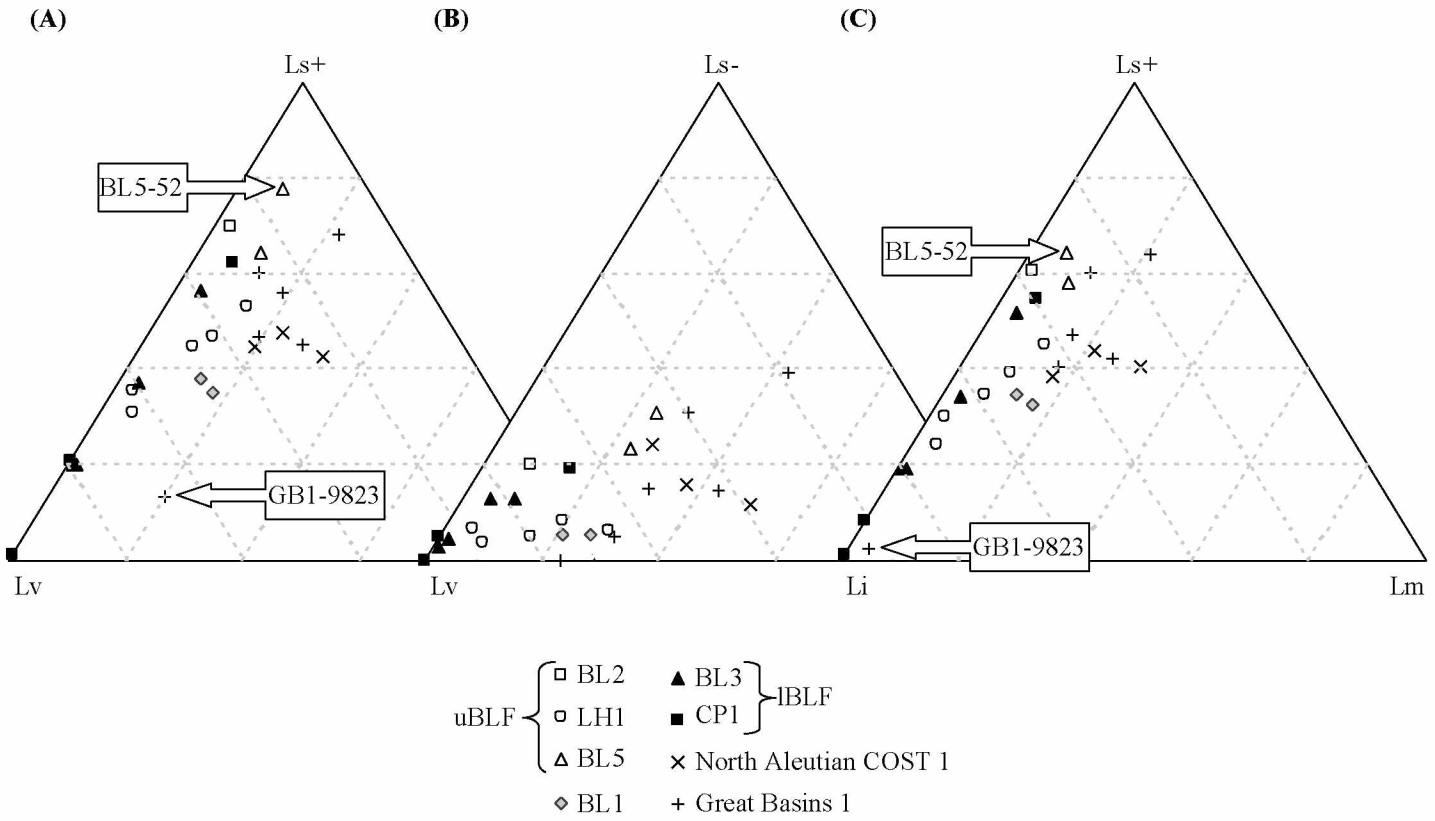

Fig. 4.9 Ternary diagrams of the lithic components. (A) Sedimentary/Volcanic/Metamorphic lithic (Ls+LvLm) ternary diagram. Chert is included at the sedimentary pole in this diagram. (B) Sedimentary/Volcanic/Metamorphic lithic (Ls-LvLm) ternary diagram. Chert is not represented on this diagram. (C) Sedimentary/Igneous/Metamorphic lithic (Ls+LiLm) ternary diagram. Both volcanic and plutonic lithic grains are represented at the igneous pole. Chert is included at the sedimentary pole. uBLF refers to samples from measured sections BL2, LH1, and BL5, and lBLF refers to samples from measured sections BL3 and CP1 (see section 4.4). See Table 4.2 for parameter definitions.

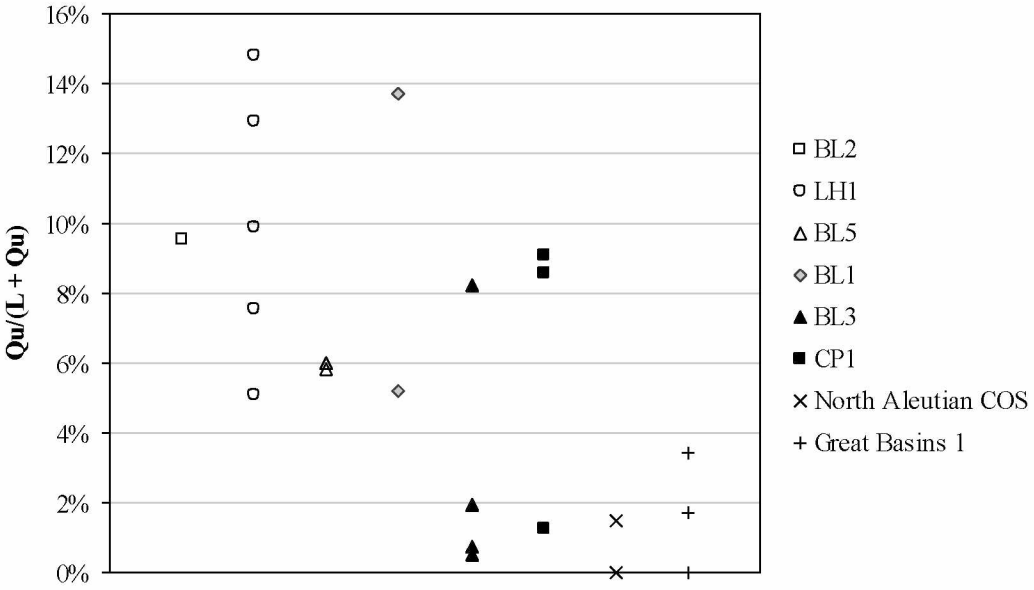

Fig. 4.10 Ratio of undifferentiated quartz (Qu) to total lithcs including chert and undifferentiated qu (L + Qu). The horizontal axis does not represent any parameter and is only used for clarity by separa samples from different measured sections and wells. Four samples from the Great Basins 1 well plot of one another at 0%, as do two samples from the North Aleutian COST 1 well. See Table 4.2 for parameter definitions

Comparison of the Ls+LvLm and Ls+LiLm diagrams (Fig. 4.9A and Fig. 4.9C) shows that accounting for plutonic fragments in the total lithic population causes a transfer toward the igneous pole and a shift toward the Ls+Li join that are more pronounced for some samples than others. The most substantial shift occurs for the sedimentary-rich BL5 sample (BL5-52) and the igneous-rich Great Basins 1 well sample (GB1-9823). Outcrop samples from measured sections (BL2, LH1, BL5, BL1, BL3, and CP1) cluster more toward the igneous pole (generally ≥ 40% Li) and all contain a greater amount of igneous lithic grains than metamorphic lithic grains on the Ls+LiLm diagram (Fig. 4.9C). However, there is no significant change in the overall proportion of sedimentary lithic grains between the two diagrams. The same samples plot above and below about 50% sedimentary lithic grains on both diagrams (Fig. 4.9A and Fig. 4.9C). This comparison indicates that the igneous lithic component is predominately volcanic. A stacked column graph that illustrates the relative proportions of volcanic and plutonic lithic grains in each sample (Fig. 4.11) confirms this relationship. Major exceptions, which have a ratio of plutonic to volcanic clasts greater than 60%, are samples GB1-9823, CP1-92, and BL5-52.

A stacked column graph illustrates that the volcanic component of the Bear Lake Formation is predominately felsic and intermediate with varying amounts of mafic volcanic rock fragments (Fig. 4.12). The graph also shows the amount of undifferentiated volcanic grains, which are grains counted as volcanic rock fragments by the petrographer, but not classified as felsic, intermediate, or mafic. They range from 6% to 30% (average 13%) of the total volcanic component. This high percentage is an indication of the difficulty in petrographically distinguishing the composition of volcanic rock fragments within sandstones, and calls into question the distinctions made between felsic and intermediate volcanic rock fragments as reported in Table 4.6 and Table 4.7. I address the nature of the volcanic clasts in greater detail through electron microprobe analysis in Chapter 5.

4.3.2.4 Intergranular Components

Framework/Cement/Matrix (FCM) and Porosity/Cement/Matrix (PCM) diagrams (Fig. 4.13) illustrate the framework and intergranular portions of the sandstones (Helmold et al., 2008). Both diagrams show distinction of pore-filling components (cement versus matrix) between outcrop and well samples.

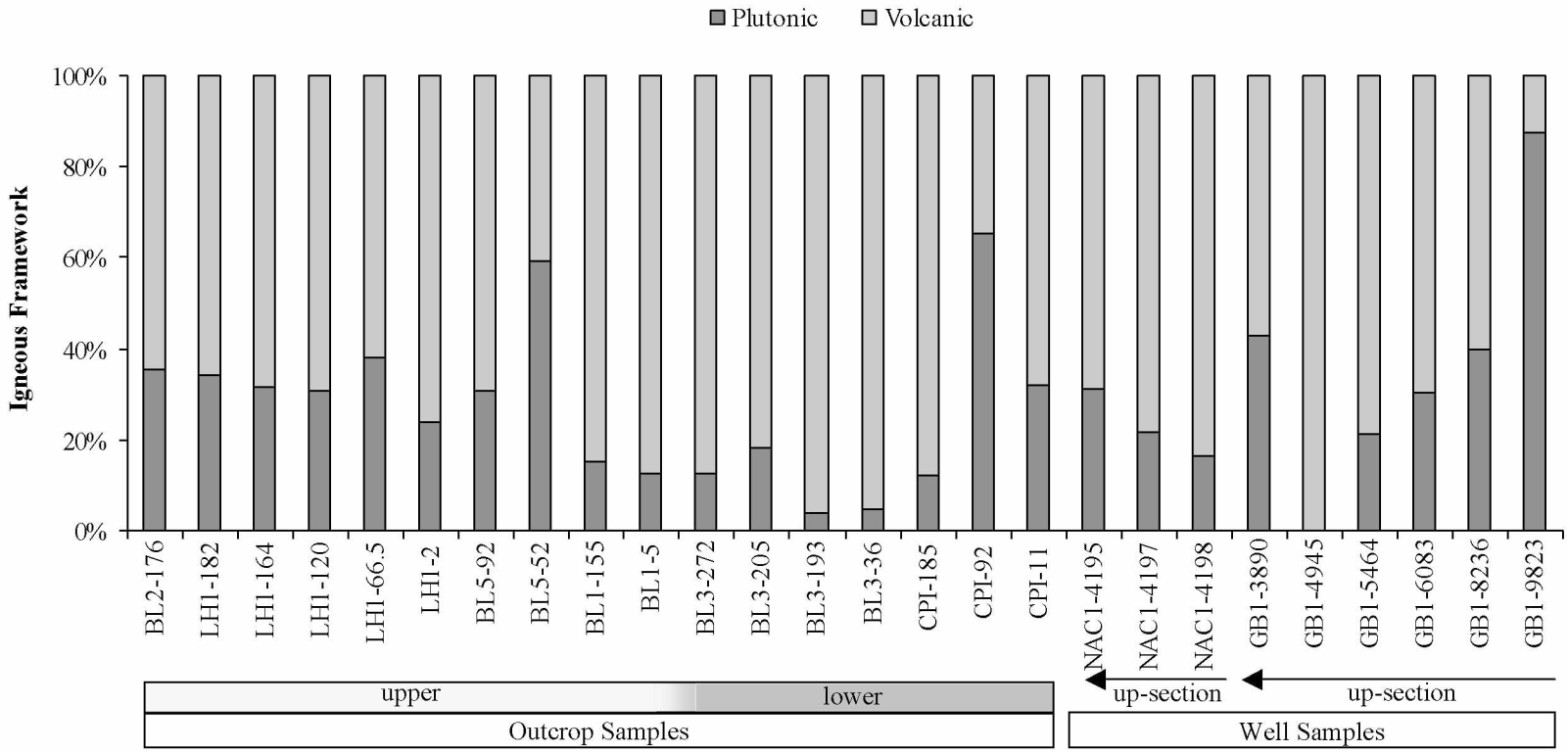

Fig. 4.11 Proportion of plutonic and volcanic rock fragments in the igneous lithic portion of the framework. Outcrop samples are arranged with lower measured sections at the right. See Fig. 2.2 for chronostratigraphic correlation of measured sections

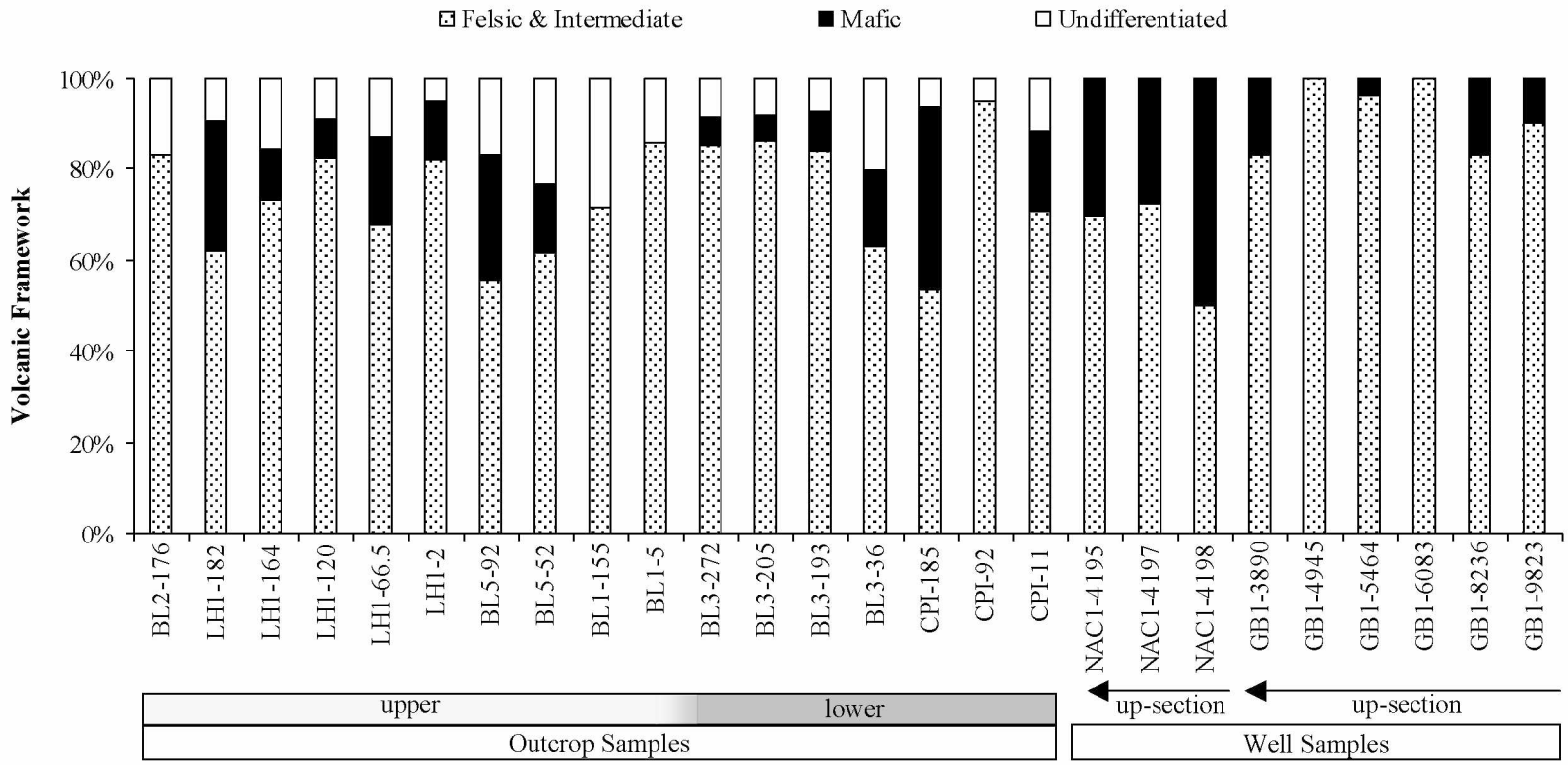

Fig. 4.12 Proportion of petrographically determined volcanic rock compositions in the volcanic lithic portion of the framework. Undifferentiated volcanic rock fragments are those that the petrographer identified as volcanic clasts, but did not classify as felsic, intermediate, or mafic. Outcrop samples are arranged with lower measured sections at the right. See Fig. 2.2 for chronostratigraphic correlation of measured sections.

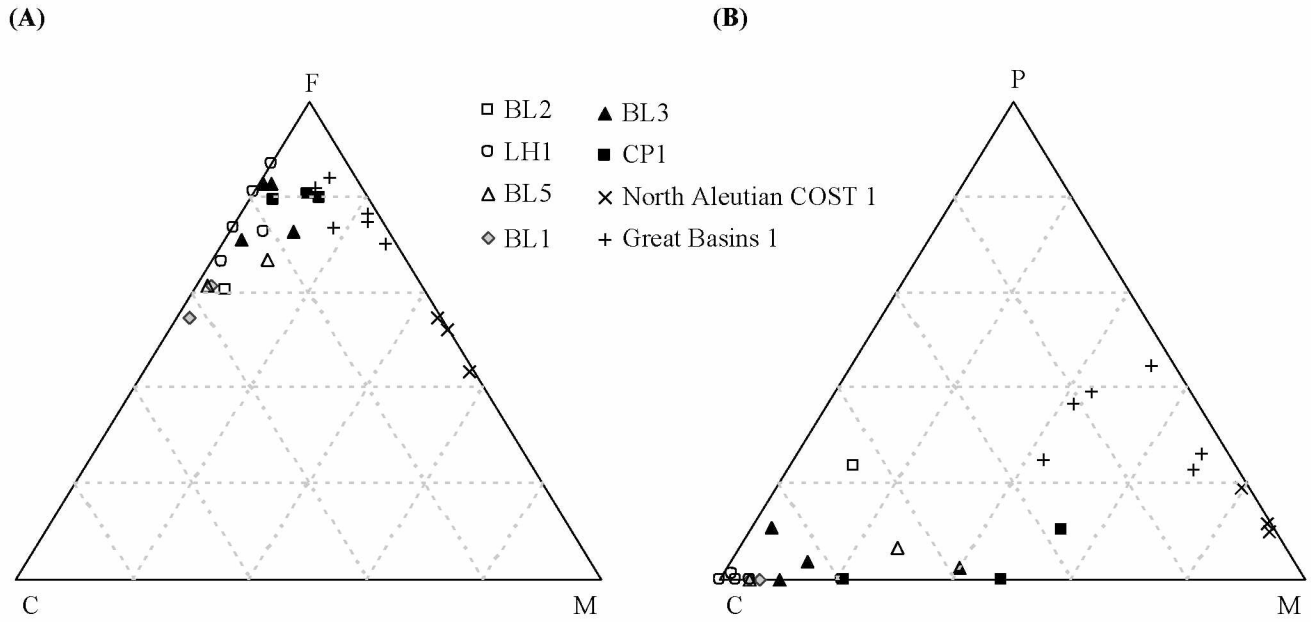

Fig. 4.13 Ternary diagrams of the framework and intergranular portions of samples. (A) Framework/Cement/Matrix (FCM) ternary diagram showing the composition of the solid components of each sample. (B) Porosity/Cement/Matrix (PCM) ternary diagram showing the composition of interstitial components of each sample

The FCM diagram (Fig. 4.13A) shows that framework and cement are the main components of the outcrop samples, whereas the well samples are composed chiefly of framework and matrix. The PCM diagram (Fig. 4.13B) also illustrates greater matrix content in the well samples. Outcrop samples plot closer to the cement pole and well samples plot closer to the matrix pole. North Aleutian COST 1 samples have the greatest amount of matrix. This diagram also indicates that Great Basins 1 samples have the greatest porosity.

4.3.2.5 Tectonic Provenance Diagrams

QFL and QmFLt diagrams (Fig. 4.14) with the tectonic provenance fields of Dickinson et al. (1983) show data that I recalculated to approximate the Gazzi-Dickinson methodology. These diagrams illustrate how compositional differences between samples of the Bear Lake Formation affect their placement in different provenance fields. Samples from the upper Bear Lake Formation (BL2, LH1, and BL5) plot in the recycled field of the QFL diagram (Fig. 4.14A), whereas samples from the lower Bear Lake Formation (BL3 and CP1) plot in arc fields. Most well samples plot in the recycled field, excep for the lowermost Great Basins 1 sample (GB1-9823), which plots in the basement uplift field. However, when stable lithic components are moved to the lithic pole on the QmFLt diagram (Fig. 4.14B), almost all samples plot in arc fields. BL2-176 remains in a recycled field, and the lowermost Great Basins 1 sample (GB1-9823) remains in the basement uplift field.

4.4 Discussion

Compositional variation of framework grains between samples from the different measured sections illustrated on ternary diagrams divides the outcrop sample set into two consistent groupings. For the purpose of this discussion, “upper Bear Lake Formation” (uBLF) refers to the group of compositionally similar samples (n=8) from measured sections BL2, LH1, and BL5. The “lower Bear Lake Formation" (lBLF) refers to the group of samples (n=7) from measured sections BL3 and CP1. BL1 is not included in either group because the two samples from this measured section often lie between, or are split between the uBLF and lBLF groups.

Several variables demonstrate a shift in provenance between the lBLF and uBLF. Most notable are the abundance of quartz, feldspar composition, and composition of the igneous component.

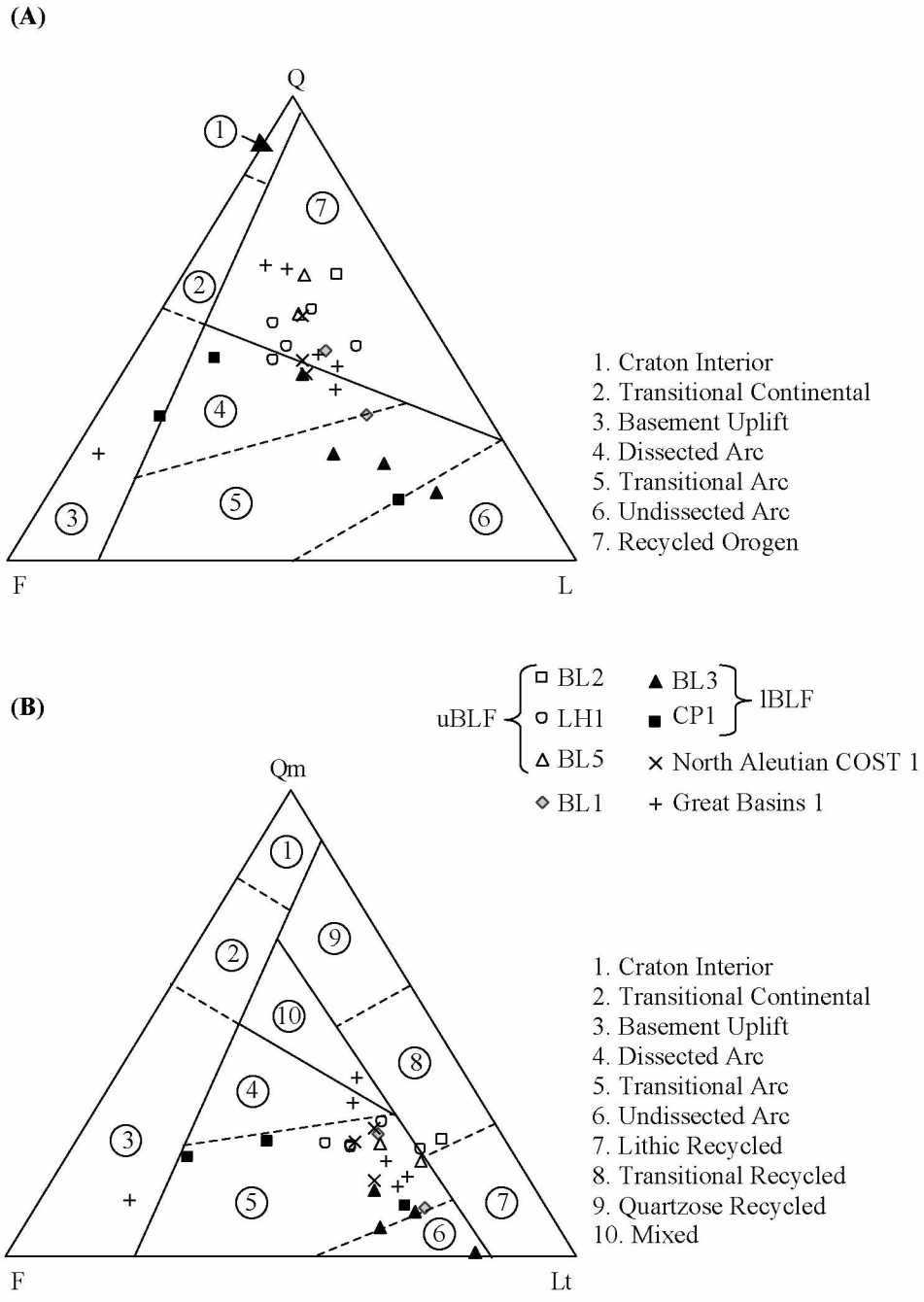

Fig. 4.14 Ternary diagrams with tectonic provenance fields. (A) QFL diagram. (B) QmFLt diagram. Provenance fields are from Dickinson et al. (1983). Data are approximated to conform to Gazzi-Dickinson methodology (refer to section 4.2). See Table 4.3 for parameter definitions.

Compositional differences between samples of the uBLF and lBLF expressed on ternary diagrams are also reflected in the framework percentages. Quartz is more common in the uBLF and its abundance varies correspondingly with the ratio of K-feldspar to total feldspar (K/F; Fig. 4.15A). The variability of plutonic rock fragments is similar to the K-feldspar abundance (Fig. 4.15B). Volcanic detritus decreases up-section and becomes less prevalent than quartz (Fig. 4.15C). Additionally, an increase in the ratio of plutonic to volcanic clasts occurs up-section (Fig. 4.15D). Relative to the lBLF, the uBLF is characterized by a notable increase in total quartz and ratio of K-feldspar to total feldspar, and a decrease of volcanic rock fragments (Fig. 4.15).

The volcanic content and high proportion of plagioclase relative to K-feldspar (low K/F) in the lBLF is consistent with arc derivation (Dickinson and Suczek, 1979; Dickinson, 1985). Although two of the lBLF samples have less volcanic rock fragments than others within the lBLF, their K/F ratios are low and one sample has a relatively high percentage of plutonic rock fragments. These characteristics are in agreement with the arc classification according to the tectonic discrimination diagrams (Fig. 4.14). The occurance of chert in the lBLF suggests recycling. The percentage and grain types within the lBLF suggest derivation primarily from volcanic sources, with less input from plutonic sources and chert-bearing sedimentary sources.

The arc affinity apparent from tectonic discrimination diagrams may point to a primary source for igneous detritus, whereas the presence of chert is likely indicative of recycled input (assuming that it is sedimentary chert and not microcrystalline quartz from silicic alteration of volcanic rocks). It is possible that the igneous detritus is recycled as well, and the arc affinity reflects the original source unit (Mack, 1984). There are three units that are geologically most likely to source the lBLF volcanic clasts: the Meshik Volcanics, Stepovak Formation, and Tolstoi Formation. The Meshik Volcanics are Late Eocene to Early Oligocene volcanic deposits associated with the Stepovak Formation, the sedimentary equivalent that consists of siltstone and volcaniclastic sandstone (Detterman et al., 1996). These two units, in conjunction with associated intrusive rocks, represent the Eocene to earliest Miocene Meshik arc (Wilson, 1985). The Tolstoi Formation is a Upper Paleocene to Middle Eocene sedimentary succession that contains chloritized volcanic clasts (Detterman et al., 1996). Volcanic detritus in the Tolstoi Formation is less abundant than in

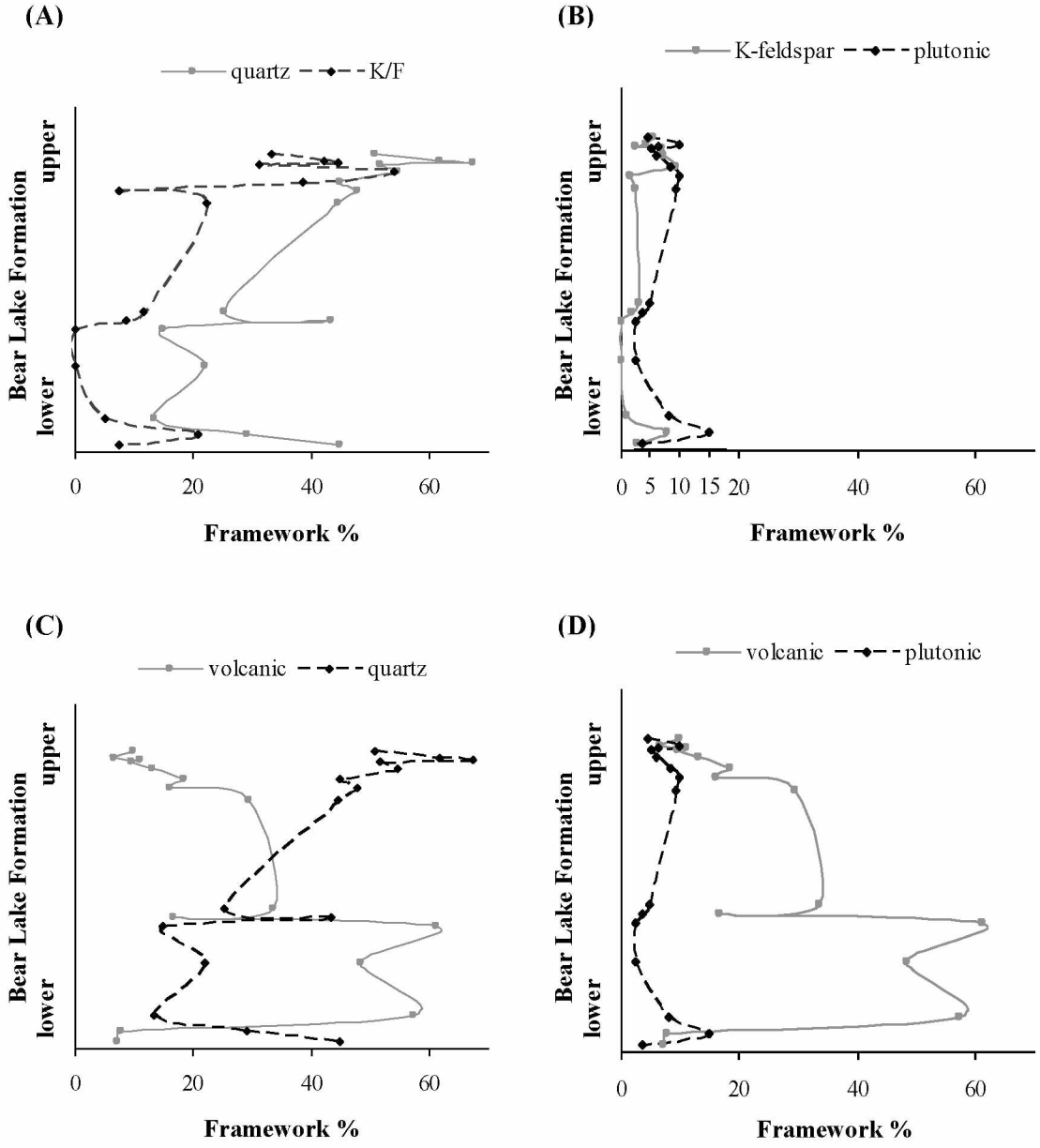

Fig. 4.15 Framework percentages of key components distinguishing the lower Bear Lake Formation from upper Bear Lake Formation. Lower and upper Bear Lake Formation labels represent samples in the lBLF and uBLF compositional groups as discussed in text (section 4.4). (A) Total quartz (Q+ as defined in Table 4.2) and ratio of K-feldspar to total feldspar. (B) K-feldspar and plutonic rock fragments. (C) Volcanic rock fragments and total quartz (Q+ as defined in Table 4.2). (D) Volcanic rock fragments and plutonic rock fragments.

the overlying Stepovak Formation, and is substantially more altered in comparison (Detterman et al., 1996). Wilson et al. (1994) suggest that the volcanic clasts in the Tolstoi Formation are recycled from Mesozoic strata. Igneous rocks of mafic compositions are only moderately durable (Abbot and Peterson, 1978), therefore the chloritized volcanic clasts in the Tolstoi Formation likely would not survive subsequent recycling and incorporation into the Bear Lake Formation.

Based on the regional stratigraphy and chloritized nature of volcanic clasts in the Tolstoi Formation, Tertiary deposits of the Meshik arc are the most likely candidates for contributing volcanic material to the Bear Lake Formation. Other formations on the Alaska Peninsula that include considerable amounts of volcanic material are the Early Jurassic Talkeetna Formation and the Late Triassic Cottonwood Bay Greenstone. The Talkeetna Formation is not widespread on the peninsula, and volcanic rocks in the Cottonwood Bay Greenstone are metamorphosed (Wilson et al., 1999).

Discrepancy of provenance indications between the QFL and QmFLt diagrams (Fig. 4.14) for the uBLF is somewhat more complex. Feldspar is present in high enough percentages in the uBLF to preclude the majority of samples plotting in the recycled fields on the QmFLt diagram (Fig. 4.14B). However, the percentage of stable lithic grains is significant enough to draw samples down into the transitional arc field. This may indicate a quartz-rich plutonic source for the feldspar and polycrystalline quartz framework grains. Similar variability in the quartz, K-feldspar, and plutonic clasts (Fig. 4.15A and Fig. 4.15B) suggests that these constituents are genetically related. The interpretation of quartz and K-feldspar as being related to a plutonic source is consistent with a genetic link. However, it is important to note that it is the *proportion* of plutonic clasts in the igneous component that markedly increases in the uBLF (Fig. 4.15D). This is not accompanied by a significant increase in the percentage of plutonic framework clasts.

Transitional arcs are more deeply eroded than undissected arcs and provide local intermittent exposure of plutons (Dickinson and Suczek, 1979). Dissected arcs are deeply eroded arcs where both the volcanic strata and plutonic roots serve as source sediment, resulting in a less lithic and more quartzo-feldspathic composition (Dickinson and Suczek, 1979; Dickinson et al., 1983). It is problematic that stable lithic grains are the parameter controlling the shift into the transitional arc field when comparing the QFL and QmFLt diagrams (Fig. 4.14). Polycrystalline quartz, present in such influential percentages, should be

accompanied by a higher feldspar content than is observed in the uBLF if sediment was shed from a predominantly plutonic source in an arc setting. Furthermore, the lithic constituents derived from arc settings should be dominated by volcaniclastic debris (Dickinson and Suczek, 1979). In cotrast, it is the stable lithic grains (polycrystalline quartz and chert) that form the majority of the lithic component in the uBLF.

My alternative, and preferred, interpretation for the compositional characteristics identified in the uBLF is recycling of older arc-derived sedimentary units. Recycling accounts for a higher stable lithic population than is expected for typical arc derivation. Sediments are enriched in quartzose components through recycling while retaining clast types inherited from the original arc source, such as the high feldspar content, which is too high for samples to plot in recycled fields on the QmFLt diagram (Fig. 4.14B). The decrease in volcanic rock fragments (Fig. 4.15D) and high K/F ratio (Fig. 4.15A) in the uBLF may reflect a sedimentary source originally derived from a plutonic terrane.

Lower Tertiary sedimentary units on the Alaska Peninsula were derived from erosion of Mesozoic sediments and the Alaska-Aleutian Range batholith (Detterman et al., 1996). Mesozoic sedimentary units were derived mainly from the Alaska-Aleutian Range batholith with minor contributions from older volcaniclastic rocks (Detterman et al., 1996). Possible sources for the high percentage of chert clasts in the Bear Lake Formation are limited. The very few primary sources of chert present on the Alaska Peninsula are late Paleozoic and early Mesozoic in age, and are geographically restricted (Detterman et al., 1996; Wilson et al., 1999). Clasts of chert, however, occur in many sedimentary formations, making them potential sources of recycled sediment in the Bear Lake Formation. The Late Jurassic Naknek Formation is widespread on the Alaska Peninsula with an average thickness of approximately 1,700 to 2,000 m (Detterman et al., 1996). It contains abundant chert clasts in conglomerates of the basal Chisik Conglomerate Member, and in conglomerates and sandstones of the Katolinat Conglomerate Member (Detterman et al., 1996; Wilson et al., 1999). The Naknek Formation also contains a high percentage of plutonic rock clasts and that were derived mainly from the Alaska-Aleutian Range batholith (Wilson et al., 1999). The abundance of chert and plutonic rock clasts, and the Naknek Formation's widespread

distribution, make the Naknek Formation a prime candidate as the source of recycled clasts present in the Bear Lake Formation.

The Late Cretaceous Chignik and Hoodoo formations were derived from a plutonic source and the Chignik Formation contains clasts recycled from the Naknek Formation (Detterman, 1990). Conglomerates in both formations contain chert clasts in addition to plutonic rock fragments and quartz, but conglomerates are a very minor component in the otherwise fine-grained Hoodoo Formation (Wilson et al., 1999). Exposures of the Chignik Formation are prevalent on the Alaska Peninsula and the Hoodoo Formation crops out between Pavolf Bay and Herendeen Bay (Wilson et al., 1999). The Chignik Formation is, therefore, another potential source of recycled sediment present in the Bear Lake Formation.

Samples from the North Aleutian COST 1 well, which is located roughly 75-115 km from the Bear Lake Formation measured sections (Fig. 2.1), have framework compositions similar to samples from the uBLF. The most identifiable difference in the framework composition is that the well samples contain a higher percentage of metamorphic rock fragments (phyllite and metamudstone; Fig. 4.9 and Table 4.5). The three North Aleutian COST 1 samples plot in the recycled orogen field and near the border between the recycled orogen and dissected arc fields on the QFL diagram (Fig. 4.14A). Similar to the uBLF samples, the North Aleutian COST 1 well samples plot in the transitional arc field on the QmFLt diagram (Fig. 4.14B). I interpret the North Aleutian COST 1 samples to have the same source terrain as the uBLF due to the compositional similarities between samples from the North Aleutian COST 1 well and uBLF. However, given that the North Aleutian COST 1 well is located a significant distance from the depositional system of the marginal marine uBLF, the abundance of phyllite and metamudstone clasts may be a function of clast hydrodynamics and more distal basin location relative the samples of the uBLF.

A distinctive change in composition occurs within the Bear Lake Formation between 9,823 ft and 8,236 ft in the Great Basins 1 well. Sample GB1-9823 is notably coarser grained than other samples (Table 4.4) and plots in the basement uplift field on both tectonic discrimination diagrams (Fig. 4.14). All other samples analyzed from the Great Basins 1 well plot in the same fields as the uBLF samples: mostly in the recycled orogen field on the QFL diagram, and mostly within arc fields on the QmFLt diagram (Fig. 4.14). The coarse-grained feldspathic sample (GB1-9823) is rich in plutonic rock

fragments and contains relatively little chert (Fig. 4.6, Fig. 4.11, and Table 4.5). The high abundance of both feldspar and plutonic rock fragments coupled with a lack of chert suggests derivation mainly from a primary plutonic source rather than a recycled sedimentary unit. Additionally, the metamorphic rock fragments present in this sample are schist (compared to phyllite in other samples from the well). The low durability of schist (Abbot and Peterson, 1978; Boggs, 2003) also suggests primary derivation rather than a recycled source. This basal stratigraphic section of the Great Basins 1 well may represent part of a tectonic event that resulted in opening of the Ugashik sub-basin of Decker (2008a), directly to the south of uplifted Iliamna subterrane rocks (Fig. 3.1). The Iliamna subterrane is composed of the Alaska-Aleutian Range batholith and high grade metamorphic rocks including schist and gneiss (Wilson et al., 1999).

4.5 Conclusions

Petrographic analysis of sandstone samples (n=17) from outcrops of the Bear Lake Formation near Port Moller (Fig. 2.1) shows an increase of recycled input up-section, accompanied by a decrease in volcanic input that reflects a provenance shift from a predominantly arc-derived source to a primarily recycled source. Tertiary deposits of the Meshik arc (Meshik Volcanics and Stepovak Formation) provided a substantial portion of the detritus deposited in the lower Bear Lake Formation near Port Moller. Recycling of Mesozoic sedimentary units containing chert and plutonic rock fragments (Naknek and Chignik formations) contributed material throughout deposition of the Bear Lake Formation. This recycled source became a more prominent source of sediment during deposition of the upper Bear Lake Formation in the Port Moller area. The recycled source terrain was also the main source during deposition of the rocks analyzed from the North Aleutian COST 1 well. In the Great Basins 1 well, the composition of the Bear Lake Formation near its base records erosion of a primary plutonic and metamorphic source (Iliamna subterrane). Up-section, within the Bear Lake Formation in the Great Basins 1 well, the source terrain shifts to recycled Mesozoic sedimentary units.

CHAPTER 5. ELECTRON MICROPROBE ANALYSIS

5.1 Introduction

Petrographic recognition of volcanic rock fragments in sandstones, such as the Bear Lake Formation, is challenging. Clasts can show a range of volcanic textures (porphyritic, mosaic, trachyitic), but, commonly, alteration of the volcanic fragments obscures diagnostic volcanic textures. Sodium cobaltinitite staining of thin sections enables identification of K-feldspar versus plagioclase, but plagioclase compositions in the clasts can rarely be determined by standard petrographic techniques. Poor phenocryst representation in fine- to coarse-sand clasts and clay-altered ferromagnesian crystals makes distinction between felsic and intermediate compositions tenuous, especially when coupled with a lack of knowledge regarding plagioclase composition. Consequently, the petrographic determination of whether a given volcanic clast is of felsic, intermediate, or mafic composition, or even if it *is* a volcanic rock fragment frequently comes down to a best guesstimate.

EMPA allows quantitative identification of plagioclase composition (and compositional zoning) as a guide to classification of volcanic rock type. In addition, the whole-rock composition of a volcanic rock fragment can be estimated from the EMPA-based groundmass composition of the clast. I measured phenocryst plagioclase compositions and average groundmass compositions for volcanic rock fragments, and classified the volcanic rock fragments based on these data. I also measured compositions and zoning of detrital plagioclase clasts in order to identify provenance. Finally, I used EMPA to investigate and positively identify diagenetic minerals identified during petrographic examination.

5.2 Methods

5.2.1 Analytical Routine and Strategy

I analyzed carbon-coated, polished thin sections using the Cameca SX-50 electron microprobe at the Advanced Instrumentation Laboratory at the University of Alaska Fairbanks. The Cameca SX-50 is equipped with four multi-crystal wavelength-dispersive spectrometers (WDS) and one energy-dispersive spectrometer (EDS). I used a 15 KeV beam with a 10nA current and 1 micron diameter. Table 5.1 gives details of the analytical routine that I created using Probe for Windows. The count times allowed each

Table 5.1 Electron microprobe analysis analytical routine details.

Element	**Spectrometer Setup**		**Count Times (seconds)**			**Acquisition Order**
	Spec. #	***Crystal***	***On-Peak***	***Hi-Peak***	***Lo-Peak***	
Ca	1	PET	21	7.5	7.5	1
K	1	PET	21	7.5	7.5	2
Si	2	TAP	21	7.5	7.5	1
Al	2	TAP	21	7.5	7.5	2
Fe	3	LIF	10	5	5	1
Ti	3	LIF	10	5	5	2
Mn	3	LIF	10	5	5	3
Mg	4	TAP	21	7.5	7.5	1
Na	4	TAP	21	7.5	7.5	2

spectrometer equal motion and acquisition time. Acquisition order of the elements is based on ascending angstroms since no volatiles were measured.

Standard assignments that I used for measuring intensities are the same as those that I used for peaking (Table 5.2). I used the Interval Halving method to find peak centers and used the "quick standards" option to measure standard intensities. I measured five points on each standard and, when necessary, deleted outliers to bring the percent relative standard deviation below 2.5% for the element(s) of interest in each standard (Table 5.2). To check the calibration, I analyzed two additional standards as unknowns (228 Plagioclase Labradorite -USNM 115900 and 219 Hornblende HB2 - USNM 143965) and compared the results to published compositions in the Probe for Windows standard database. When I was satisfied that my analytical routine gave adequate results, I analyzed Bear Lake Formation samples. I chose a hornblende standard to run as an unknown because it is a mineral that contains all the major elements found in clays and volcanic rocks (Si, Al, Fe, Mg, Ca, Na, K, and Ti), which were the primary focus of my EMPA. I also used the labradorite standard as an unknown because I especially wanted to ensure that the plagioclase analyses were of high quality.

I obtained major oxide compositions for volcanic rock fragments, feldspar clasts, and pore-filling components in 26 samples (Table 2.1). The number of volcanic rock fragments that I examined depended on their abundance in each sample. I analyzed an average of six feldspar clasts per sample as well as representative examples of pore-filling components. I outlined a polygonal area of each thin section to examine so that I analyzed each volcanic rock fragment within the polygon. Polygon size varied depending on the abundance of volcanic rock fragments in each sample. Generally, polygon size was on the order of 1 cm^2. I used this polygon approach in order to minimize the risk of skewing my results by bypassing the more highly altered (and less recognizable) volcanic rock fragments. This would possibly exclude an entire population of volcanic rock composition in the sample.

I focused the analyses of samples from the Great Basins 1 well on pore-filling components due to the lower percentage of volcanic rock fragments and the smaller grain size, with the exception of sample

Table 5.2 Standard assignments used for peaking and measuring intensities. The percent relative standard deviation (% Rel SD) reported here is an average from multiple election microprobe analysis sessions.

Element	Standard	% Rel SD
Ca	333 Wollastonite (CaSiO3)	0.7
K	302 OR10 CT	1.4
Si	333 Wollastonite (CaSiO3)	0.7
Al	615 (TALBITE)	0.5
Fe	211 Garnet, USNM 87375	1.3
Ti	307 SPHENE1A	2.3
Mn	328 Willimite	1.9
Mg	339 Spinel	0.6
Na	615 (TALBITE)	1.8

GB1-3890. Additionally, I analyzed several plutonic rock fragments in sample GB1-9823. The grain size in this sample is larger and a substantial proportion of the framework grains are plutonic rock fragments (Fig. 5.1).

To analyze volcanic rock fragments, I measured points on suitably large phenocrysts where present (larger than the 1 micron beam diameter), and at least four groundmass points. Calculating whole-rock compositions of these fragments was not viable because averaging the phenocryst analyses with the groundmass analyses does not accurately reflect the whole-rock composition. The main challenges in calculating the whole-rock composition in this fashion are: 1) representation of the parent rock is severely limited, both in terms of grain size and number of analyses, and 2) the error involved in guessing the correct proportion of groundmass and phenocryst to include in such an average is substantial (especially considering a lack of phenocryst representation in fine- to medium-grained sand clasts). In light of these challenges, I used plagioclase phenocryst composition as a guide to classify the volcanic rock fragments instead of calculating an approximate whole-rock composition by combining phenocryst and groundmass compositions. I compared plagioclase phenocryst compositions in volcanic rock fragments of the Bear Lake Formation to literature values for plagioclase compositions of specific volcanic rock types (Brown, 1967; Marsh, 1976; Ewart, 1982; Marsh, 1982; Durant, 1989; McBirney, 1989; Tappen et al., 2009), and used these guidelines to identify volcanic rock fragments as felsic, intermediate, or mafic. In addition, I considered the mineralogy of other phenocrysts (where present) in conjunction with the plagioclase phenocryst compositions to aid my classification of the volcanic rock fragments in the Bear Lake Formation.

I described the groundmass composition as felsic, intermediate, or mafic based on the groundmass mineralogy and the average chemical composition of multiple analyses of groundmass in each volcanic rock fragment, and adjusted for the percentage of phenocrysts (see section 5.3.2.2). I described the compositions independent of phenocryst compositions. I plotted the groundmass averages of each rock fragment on a total-alkali silica diagram, and also compared the groundmass averages to the composition of volcanic rocks, placing emphasis on the relatively non-mobile elements Si and Ti by using a weight percent

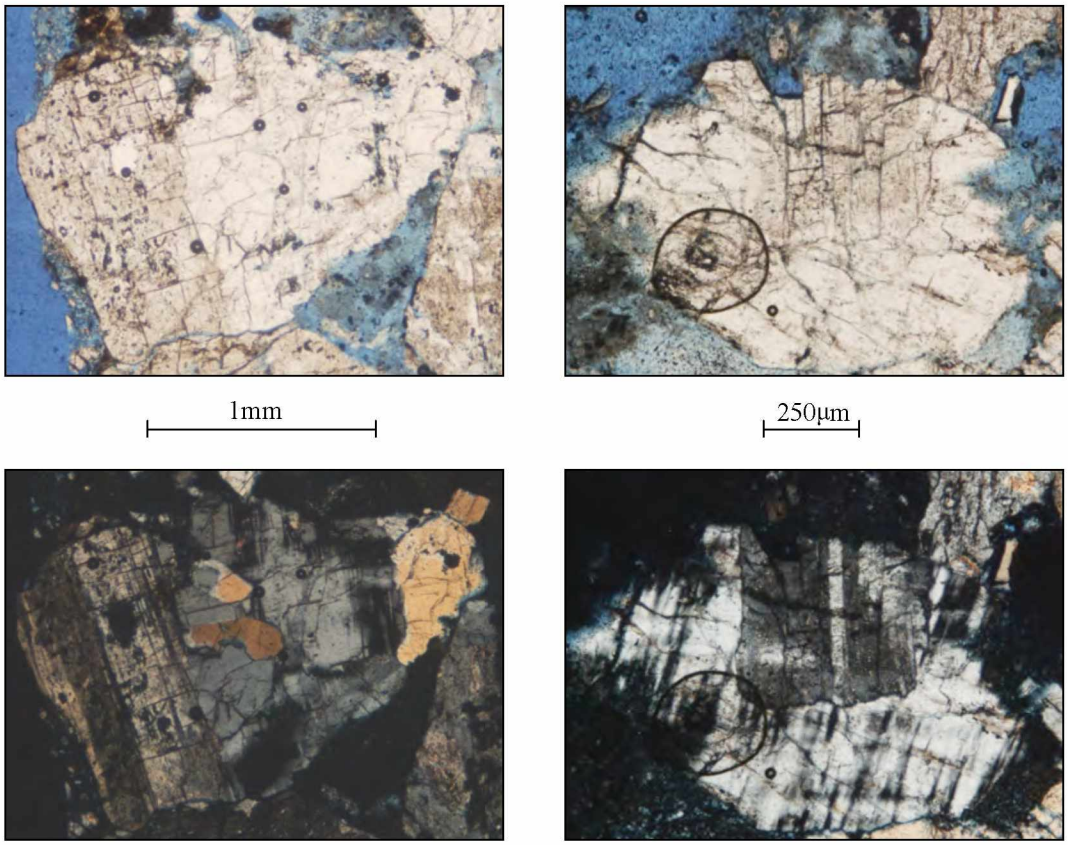

Fig. 5.1 Photomicrographs of plutonic rock fragments. Plane polarized light (above) and crossed-polars (below). Sample GB1-9823.

SiO_2 versus TiO_2 diagram. I used average volcanic rock compositions based on the GEOROC online database (http://georoc.mpch-mainz.gwdg.de/georoc/Start.asp) and major-oxide compositions of rocks from Aleutian arc volcanoes for comparison with my calculated groundmass averages. Christopher Nye of the Alaska Volcano Observatory provided an unpublished compilation of data from Aleutian arc volcanoes (Nye, C.J., written communication, 2009).

I analyzed most feldspar clasts and feldspar phenocrysts using the EDS. I measured each point until the energy spectra stabilized. By comparing analyses of a single point with increasing count times, I found that waiting for the spectra to stabilize was sufficient time to obtain a reliable composition. Using the EDS in lieu of the WDS proved a useful approach to conserve analytical time and yielded comparable results. Table 5.3 reports average analytical error percentages for feldspar analyses.

5.2.2 Criteria for Naming Clays

Due to the incredible difficulty of physically separating mixtures of clays from individual clasts, I did not employ X-ray diffraction (XRD) for identification of clays. Clay names that I assigned are solely based on chemical composition. I designated a mineral as clay if the chemical composition fit a formula for smectite, celadonite, illite, or close to that of chlorite (Table 5.4).

Mixtures of di- and tri-octahedral layers of smectite occur with an intermediate chemistry (Deer et al., 1992). I have therefore used $(Al,Mg,Fe)_{4\text{-}6}$ and $(Si,Al)_8$ as criteria for what I labeled smectite. I use "Na-smectite" to note smectite clay in which the Na cation total is notably greater than that of Ca. "Fe-smectite" is meant to imply an Fe-rich clay. It may be a true Fe-smectite such as nontronite, but may also be a mixed-layer smectite or chlorite-smectite (corrensite for example), and in some cases may be a mixture of smectite and limonite. Nontronite generally has greater than three Fe^{2+} cations, whereas other di-octahedral varieties have less than three per formula unit (Deer et al., 1992). All clays that I named "Fe-smectite" have three Fe+Mg cations or greater. I combined Fe and Mg, considering the possibility of cation substitution. The weight percent FeO generally ranges from 14% to 23% in "Fe-smectites". "Chloritic clay" may also be a mixed-layer chlorite-smectite, but has an octahedral site cation total greater than those that I designated as "Fe-smectites" (compared using equal oxygen). However, on the basis of 28 oxygens, the octahedral site cation total is too low to fit chlorite (Table 5.4). I designated "chlorite" to have

Table 5.3 Average analytical error of electron microprobe analyses of feldspar.

Oxide	Average Weight % Error
SiO_2	0.22
Al_2O_3	0.13
K_2O	0.04
Na_2O	0.11
CaO	0.05

Table 5.4 Clay and mica mineral formulas. Formulas for chlorite, smectite, illite, and muscovite are taken from Deer et al. (1992). The formula for celdanonite is from Boles and Coombs (1975).

Clay Mineral	Formula
Chlorite	$(Mg,Fe,Mn,Al)_{12}[(Si,Al)_8O_{20}](OH)_{16}$
Smectite	$(0.5Ca,Na)_{0.7}(Al,Mg,Fe)_4[(Si,Al)_8O_{20}](OH)_4 \cdot nH_2O$ di-octahedral $(0.5Ca,Na)_{0.7}(Mg,Fe,Al)_6[(Si,Al)_8O_{20}](OH)_4 \cdot nH_2O$ tri-octahedral
Illite	$K_{1.5\text{-}1.0}Al_4[Si_{6.5\text{-}7.0}Al_{1.5\text{-}1.0}O_{20}](OH)_4$
Muscovite	$K_2Al_4[Si_6Al_2O_{20}](OH,F)_4$
Celadonite	$(K,Na,Ca)_{1.2\text{-}2.0}(Mg,Fe,Al)_4(Si,Al)_8O_{20}(OH)_4$

a cation total in the octahedral site greater or equal to 11 on the basis of 28 oxygens. I used a total of 11 cations instead of the 12 in the chemical formula for chlorite (Table 5.4), in order to allow for error resulting from low analyses totals.

I named "mixed-layer" clays with caution. The material appears to be clay in thin section and the chemical formula fits my criteria for smectite, but has more K than expected for true smectite. The mixed-layer clay names I used are Fe-K, K-Ca, and K-Na to indicate the notable cations. In some instances I simply noted "mixed-layer clay." XRD data presented by Helmold et al. (2008) show that mixed-layer illite-smectite is present in samples from the North Aleutian COST 1 well and Great Basins 1 well; these samples are included in this study (Table 2.1). Therefore, it is likely that the clays I named "mixed-layer" are illite-smectites. Additionally, the Fe-K clays may represent mixed-layer chlorite-illite or a mixture of illitic clay and limonite. The approximate ranges in weight percent FeO and K_2O are 10% to 23%, and 2% to 5% respectively. I refrained from using the Fe-K designation for clay-like analyses with a greater amount of FeO and equal or greater K_2O, and assumed that these are a mixture of illitic clay and limonite. This assumed mixture yields approximate ranges in weight percent FeO and K_2O of 24% to 30%, and 3% to 6% respectively.

All clays that I named "illite" fit the formula very closely (Table 5.4). I used "illitic clay" when the analyses are close to the formula of celadonite (Table 5.4). All illitic clays have about 1 to 1.5 K cations per formula unit. Where necessary, I used the term "sericite" to describe a colorless mica whose composition is in the vicinity of illite to muscovite, fitting neither perfectly (Table 5.4).

5.2.3 Potential Sources of Error

Error sources associated with my analytical approach include misidentification of volcanic clasts in thin section, inaccurate averaging of groundmass compositions, misinterpretation of geochemical data, and analytical error. I identified volcanic rock fragments in thin section by looking for mineralogical and textural evidence (quartz, feldspar, hornblende, pyroxene; porphyritic, trachytic, mosaic textures, glass shards). The alteration state of volcanic clasts in many samples made identifying textures difficult. I considered the mineralogy and chemistry identified by EMPA in conjunction with features identified in thin section in order to confirm volcanic origin of clasts.

Groundmass compositions that I report (felsic, intermediate, and mafic) are based on averaging of multiple analyses of the groundmass in each volcanic rock fragment. For most clasts, I only analyzed four groundmass points. I made the assumption that the points I analyzed are an accurate representation of both 1) the minerals present, and 2) the ratios of minerals present. The mineralogy of the groundmass that I identified supports the groundmass composition that I averaged in most cases. For instance, the averaged analyses of groundmass in a volcanic rock fragment containing quartz, albite, and K-feldspar indicated a felsic chemical composition, whereas the averaged analyses of groundmass in a volcanic rock fragment containing smectite, chloritic clay, calcite, and Ti-oxide indicated an intermediate chemical composition.

Clay mineral analyses proved to be the most difficult to interpret. To reduce errors in interpreting clay mineralogy I devised a protocol for classifying clay minerals (section 5.2.2). This protocol allowed consistency when identifying clays and assigns informal names in order to avoid misrepresentation. Although I may have misidentified some analyses, the misidentifications are consistent. For example, as stated above (section 5.2.2), "Fe-smectite" is meant to imply an Fe-rich clay. It may be a true Fe-smectite such as nontronite, but may also be a mixed-layer smectite or chlorite-smectite, and in some cases may be a mixture of smectite and limonite. Regardless, I consistently refer to it as "Fe-smectite."

Analytical error associated with plagioclase analyses is the most important analytical error in terns of my classification of volcanic rock fragments. Errors in the Ca and Na analyses may affect the calculated end-member compositions which I used to guide my classification of volcanic clasts. However, the analytical error for Ca and Na (Table 5.3) is small enough that calculations of anorthite percentages are not significantly affected.

5.3 Results

5.3.1 Diagenetic Mineralogy

I documented several pore-filling, alteration, and replacement minerals using EMPA (Table 5.5, Table 5.6, Table 5.7, and Table 5.8). Identifications of diagenetic components that I made using EMPA generally agree with the petrographic identifications (Table 4.8, Table 4.9, Fig. 4.2, and Fig. 4.3). Fig. 5.2 and Fig. 5.3 summarize the pore-filling, alteration, and replacement components of detrital minerals that I identified using EMPA. In this section, I present comparison of results from both methods in order to

Table 5.5 Pore-filling components identified using electron microprobe analysis. Abbreviations are defined as follows: laumontite (L), heulandite (H), Fe-smectite (F), and Mg-rich siderite (Mg). In the smectite column, an "x" indicates smectite and an F indicates Fe-smectite.

Sample	Zeolite	Smectite	Mixed layer clay	Chloritic Clay	Chlorite	Illite and (or) Illitic Clay	Kaolinite	Calcite	Siderite	Limonite	Ti-oxide	Pyrite	Ilmenite	Clay & Mud Matrix
BL2-176	H	x	K-Ca			x				x				
LH1-182	L	x		x	x					x	x			
LH1-164		x						x						
LH1-120				x	x			x						
LH1-66.5				x	x			x						
LH1-2		F			x			x						
BL5-92	H							x						
BL5-52	H	F								x				
BL1-155				x				x				x	x	
BL1-5		x		x	x			x		x	x			
BL3-272				x	x									
BL3-205		F		x										
BL3-193		F		x	x									
BL3-36		F			x			x			x			
CP1-185		F			x			x			x			
CP1-92		F, x	Fe-K	x		x	x							
CP1-11		F		x			x				x			
GB1-3890									Mg		x			?
GB1-4945							x			x				x
GB1-5464							x		x					x
GB1-6083							x		Mg			x		x
GB1-8236							x	x						x
GB1-9823							x							x
NAC1-4195														x
NAC1-4197												x		x
NAC1-4198														x

Table 5.6 Alteration and replacement of detrital minerals identified using electron microprobe analysis An "x" indicates that the mineral listed in the header row occurs as a replacement mineral in the corresponding sample. Abbreviations are used to indicate that the mineral listed in the header row has altered or replaced hornblende (H) and biotite (B) in the corresponding sample. Detrital feldspar alteration is excluded from this table. See Table 5.8 for feldspar mineralogy.

Sample	Calcite	Kaolinite	Chlorite and (or) Chloritic Clay	Mixed Layer Fe-K Clay	Sericite and (or) Illite	Siderite	Ti-oxide
BL2-176							
LH1-182							
LH1-164							
LH1-120	H						
LH1-66.5							
LH1-2							
BL5-92							
BL5-52					B?		
BL1-155							
BL1-5							
BL3-272							
BL3-205							
BL3-193							
BL3-36							
CP1-185			B				
CP1-92							
CP1-11		x	B				
GB1-3890		x				x	
GB1-4945		x			x		
GB1-5464		x			x		x
GB1-6083		x			x		
GB1-8236			B?				
GB1-9823							
NAC1- 4195				B?			
NAC1-4197							
NAC1-4198							

Table 5.7 Alteration and replacement mineralogy of volcanic rock fragments identified using electron microprobe analysis. An "x" indicates that the mineral listed in the header row occurs as a replacement mineral in the corresponding sample. Abbreviations are used to indicate that the mineral listed in the header row has altered and (or) replaced groundmass (g) and phenocrysts (p) in the corresponding sample. Fine-grained siliceous material refers to dark (usually brownish) non-crystalline material with high weight percent SiO_2 (commonly greater than about 85 wt %).

Sample	Calcite	Laumontite	Kaolinite	Albite	Chlorite and (or) Chloritic Clay	Fe-Smectite (*smectite)	Mixed Layer K Clay and (or) Illitic Clay	Sericite and (or) Illite	Fine-grained Silicous Material	Sphene	Ilmenite	Fe-oxide	Ti-oxide
BL2-176				g	g	*g	g, p						g
LH1-182		p		g	p	*g	g			p			
LH1-164	g, p				p	g, *g	g					g	g
LH1-120	g			g	g	p, g, *g				g	g	g	g
LH1-66.5	g, p			g, p	g, p	g, *g	g				g	g	g
LH1-2	g			g	g, p								g
BL5-92	g, p						g						
BL5-52							g			g			
BL1-155	g, p			g	g, p	g, *g	g		g	g		g	g
BL1-5	g					*g	g					g	g
BL3-272				g	g, p	g, *g, p	g		g			g	g
BL3-205				g, p	g, p	g, *g, p	g						
BL3-193				g, p	g, p	g, *g, p, *p	g		g			g	g
BL3-36	g, p			g	g, p	g, *g, p, *p	g, p	p	g				g
CP1-185	p			g, p	g, p	g, *g, p			g				g
CP1-92	g, p		p	g	g	g, *g	g						g
CP1-11				g	g	*g	g						g
GB1-3890				g	g	g, *g	g, p		g			g	g
GB1-4945	- - - - - - - - - - - - - - - - - - - no volcanic rock fragments documented by EMPA - - - - - - - - - - - - - - - - - - -												
GB1-5464				g			g						
GB1-6083				g		?*g		p					
GB1-8236	- - - - - - - - - - - - - - - - - - - no volcanic rock fragments documented by EMPA - - - - - - - - - - - - - - - - - - -												
GB1-9823				g	g, p								g
NAC1- 4195				g		g, *g	g				g		g
NAC1-4197				g	g	g	g					g	g
NAC1-4198				g			g					g	g

Table 5.8 Summary of feldspar clasts analyzed using electron microprobe analysis. An "x" indicates an unaltered clast. An "x" listed with an alternation mineral indicates both altered and unaltered clasts were identified.

Sample	Plagioclase	Alteration	K-Feldspar	Alteration	Albite	Alteration
BL2-176	x		x		x	sericite
LH1-182		albite		albite	x	laumontite
LH1-164	x		x			
LH1-120	x	albite	x		x	laumontite & calcite, sericite & calcite
LH1-66.5	x	calcite	x			
LH1-2	x					
BL5-92	x		x	albite	x	
BL5-52	x		x			
BL1-155	x	calcite		albite		
BL1-5	x				x	
BL3-272	x					
BL3-205	x				x	
BL3-193	x				x	
BL3-36	x		x	albite		
CP1-185	x					calcite
CP1-92	x	albite	x		x	illite, kaolinite, calcite
CP1-11	x		x		x	sericite, kaolinite
GB1-3890	x					
GB1-4945			x		x	sericite
GB1-5464			x	sericite	x	sericite, illite
GB1-6083			x	albite	x	sericite
GB1-8236			x		x	sericite, illite
GB1-9823			x		x	sericite
NAC1-4195	x		x		x	
NAC1-4197	x		x			sericite, illite
NAC1-4198	x		x	albite	x	Fe-K clay

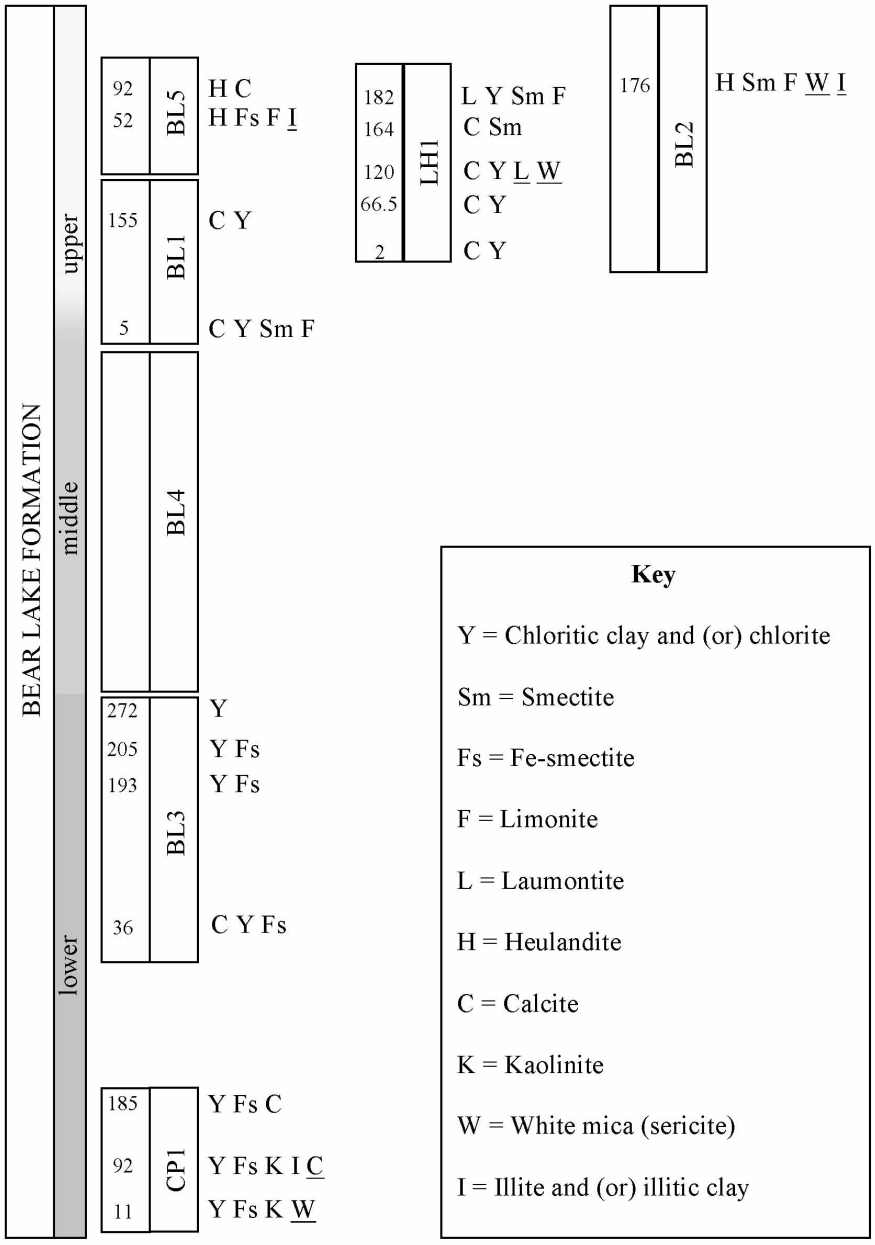

Fig. 5.2 Summary of pore-filling and replacement components of detrital minerals identified in outcrop samples using electron microprobe analysis. Underline indicates that the mineral is only present as a replacement component, and not a pore-filling component. This figure summarizes data from Table 5.5, Table 5.6, and Table 5.8. The measured sections are displayed in chronostratigraphic order (Decker et al., 2005; Finzel et al., 2005). The lower, middle, and upper designations are based on Decker et al. (2005).

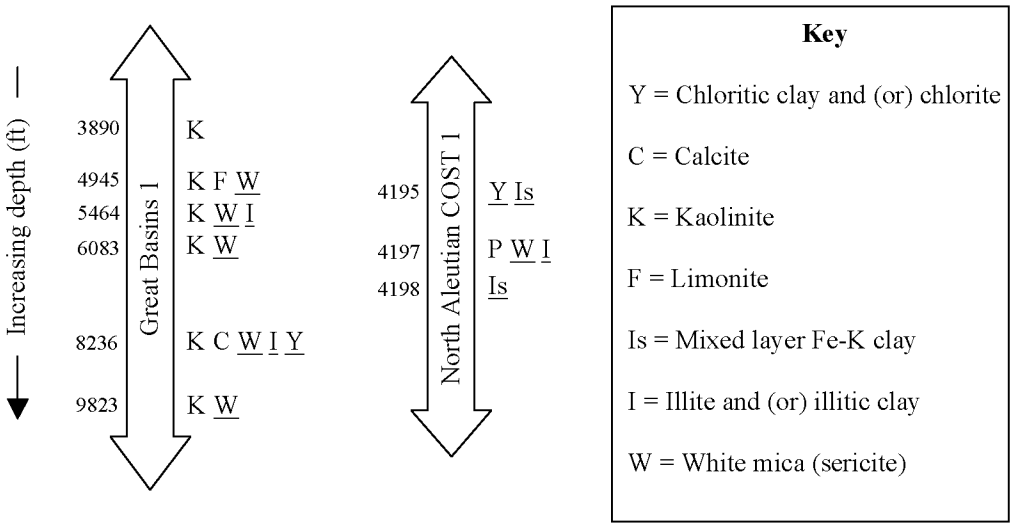

Fig. 5.3 Summary of pore-filling and replacement components of detrital minerals identified in well samples using electron microprobe analysis. Underline indicates that the mineral is only present as a replacement component, and not a pore-filling component. This figure summarizes data from Table 5.5, Table 5.6, and Table 5.8.

confirm identifications made using petrographic analysis (Chapter 4) and to report additional characteristics that I identified using EMPA. Summary diagrams of pore-filling, alteration, and replacement mineralogy for outcrop and well samples identified using point counting and EMPA illustrate the comparisons I make and characteristics that I report in this section (Fig. 4.2, Fig. 4.3, Fig. 5.2, and Fig. 5.3).

Petrographic identifications of zeolites are consistent with identifications made via EMPA. Heulandite is present in BL2-176, BL5-92, and BL5-52, whereas laumontite is present in LH1-182 and LH1-120. I documented no zeolites in BL1-155 using EMPA, but the amount of heulandite identified petrographically is small (Table 4.7).

The petrographer identified corrensite (mixed-layer smectite-chlorite) as a common pore-filling component. Chloritic clay identified using EMPA mgiht be mixed-layer smectite-chlorite (section 5.2.2). Identifications of smectite and corrensite made petrographically generally coincide with identifications of smectite, chloritic clay, and (or) chlorite using EMPA (for example, measured sections BL2, LH1, BL5, BL3, and CP1). Using EMPA, I documented smectite, chloritic clay, and chlorite in BL1, whereas the petrographer recorded no clay for samples from this measured section. Additionally, EMPA indicated biotite altered by chlorite and (or) chloritic clay in CP1, the Great Basins 1 well, and in the North Aleutian COST 1 well (Table 5.6). This was not noted by the petrographer. Both EMPA and petrography identified pore-filling kaolinite and kaolinite replacement in CP1 and the Great Basins 1 well (Table 4.9, Table 5.6, and Table 5.7). Additionally, EMPA indicated persistent alteration of feldspar clasts by sericite and (or) illite in the Great Basins 1 well (Table 5.8).

Identification of pore-filling calcite is consistent between the EMPA and petrographic methods (for example, LH1, BL5-92, BL1, BL3-36, CP1). Petrographic and EMPA data both show that calcite replacement of detrital clasts is common in samples with calcite cement (Table 4.8, Table 4.9, Table 5.5, Table 5.6, Table 5.7, and Table 5.8). Additionally, EMPA indicated calcite replacement of detrital hornblende in LH1-120, and minor pore-filling calcite in GB1-8236 (Table 5.6). Ferroan calcite (Table 4.8 and Table 4.9) was identified by the petrographer based on carbonate staining of thin sections. Weight percent FeO of calcite measured by EMPA ranges from 0.12% to 3.23%, confirming the identification.

Both methods indicated siderite in the Great Basins 1 well. Siderite identified using EMPA in GB1-3890 and GB1-6083 is Mg-rich and technically 'sideroplesite' (Table 5.5). The petrographer also documented siderite in CP1-185, which I did not document using EMPA. Limonite identified petrographically corresponds to limonite and (or) Fe-smectite identified using EMPA.

An important mineral I recognized using EMPA that was not distinguished petrographically is albite. EMPA indicated detrital albite clasts in samples from every measured section and both wells (Table 5.8). Albite is also a common replacement mineral in volcanic rock fragments from the Bear Lake Formation (Table 5.7). It replaces plagioclase phenocrysts and groundmass crystals.

5.3.2 Volcanic Rock Fragments

Appendix B contains descriptions of volcanic rock fragments analyzed using EMPA. Descriptions include identification of phenocryst and groundmass crystals, alteration and replacement minerals of phenocrysts and groundmass, and feldspar compositions of phenocrysts and groundmass. The felsic, intermediate, and mafic groundmass composition assignments in Appendix B are based on the averaged groundmass composition from EMPA.

5.3.2.1 Mineralogy and Alteration

Volcanic rock fragments that I analyzed using EMPA from the Bear Lake Formation display a range of textures (Fig. 5.4, Fig. 5.5, and Fig. 5.6) including porphyritic, trachytic, and mosaic (for example, granophyric). However, alteration of many volcanic clasts, principally by clay minerals, has obscured easily identifiable volcanic textures. Volcanic rock fragments with trachytic texture (flow-aligned feldspar) contain assemblages of plagioclase, albite, plagioclase and albite, K-feldspar and albite, or plagioclase and albite and K-feldspar. Volcanic rock fragments that I documented with mosaic texture contain groundmass quartz, K-feldspar, and albite.

Porphyritic volcanic rock fragments most commonly contain phenocrysts of plagioclase or albite. Zoned plagioclase phenocrysts also occur, and are present mainly in samples from BL3. K-feldspar phenocrysts are more rare: most commonly documented in sample BL1-155. A few hornblende phenocrysts occur in samples from measured sections and the Great Basins 1 well (GB1-3890). Pyroxene phenocrysts occur only in volcanic rock fragments from the North Aleutian COST 1 well. NAC1-4195

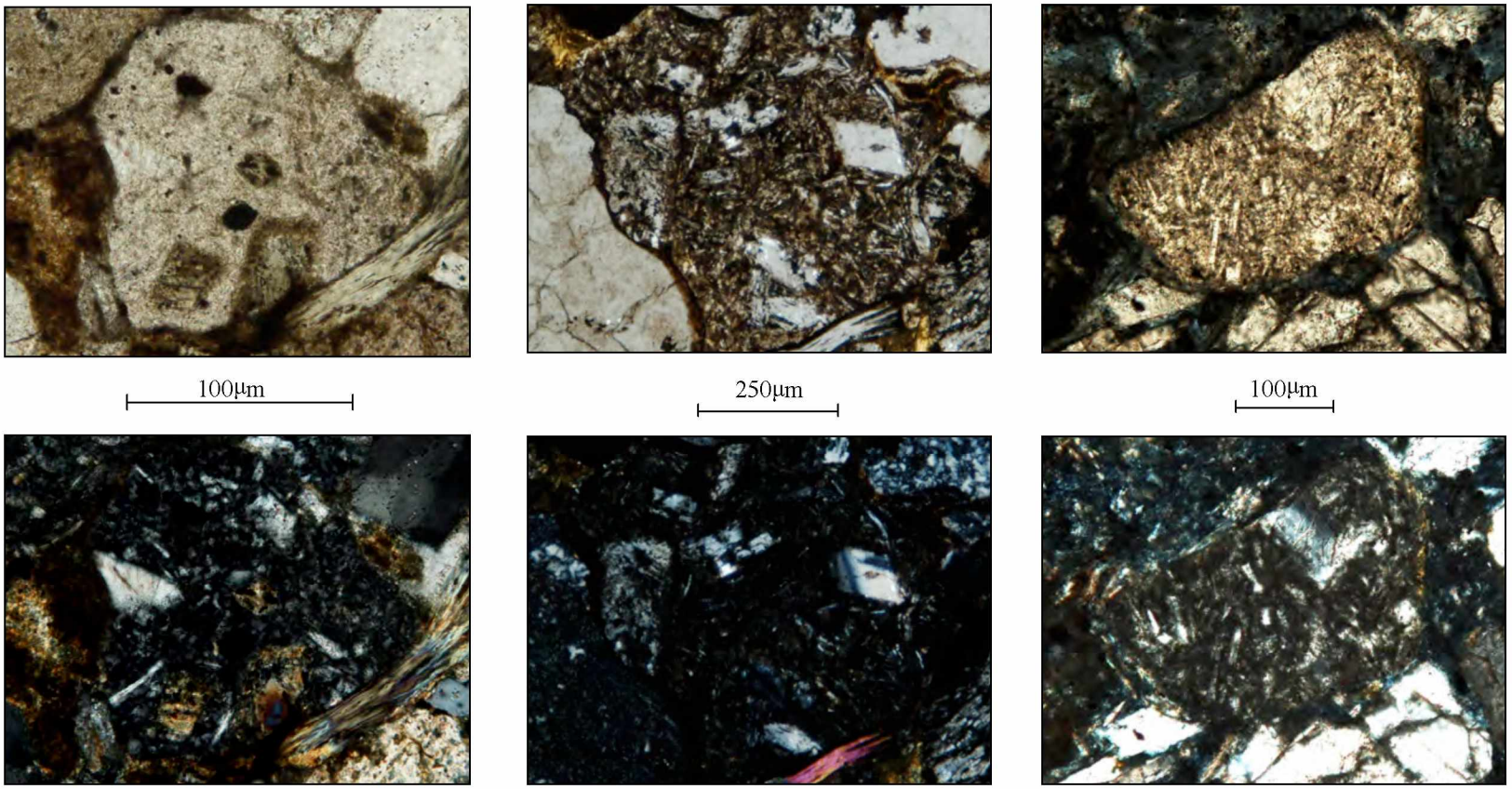

Fig. 5.4 Photomicrographs of volcanic rock fragments with porphyritic texture. Samples LH1-182, BL3-193, and NAC1-4197 (left to right). Plane polarized light (above) and crossed-polars (below).

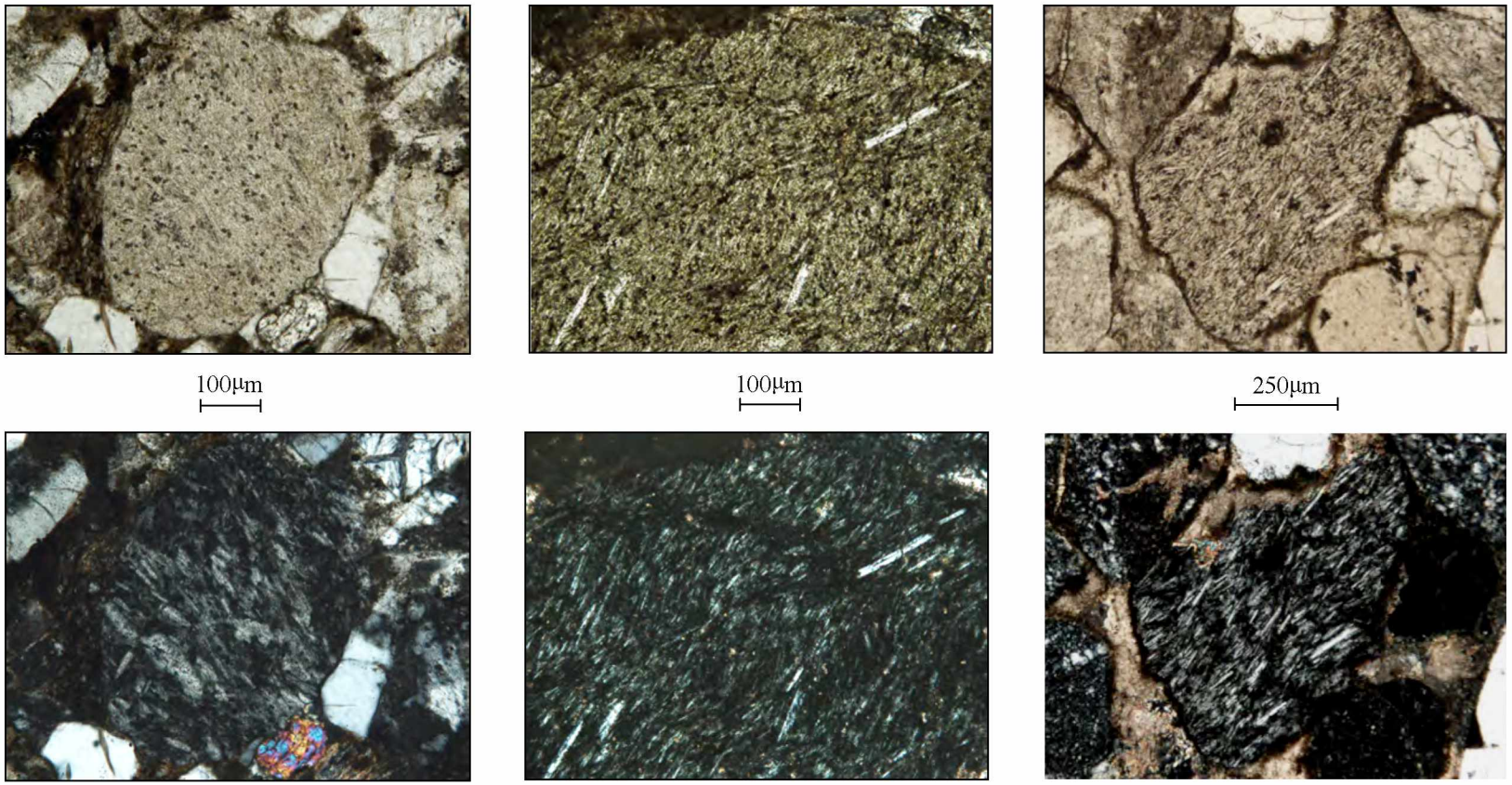

Fig. 5.5 Photomicrographs of volcanic rock fragments with trachytic texture. Samples LH1-182, CP1-185, and LH1-2 (left to right). Plane polarized light (above) and crossed-polars (below).

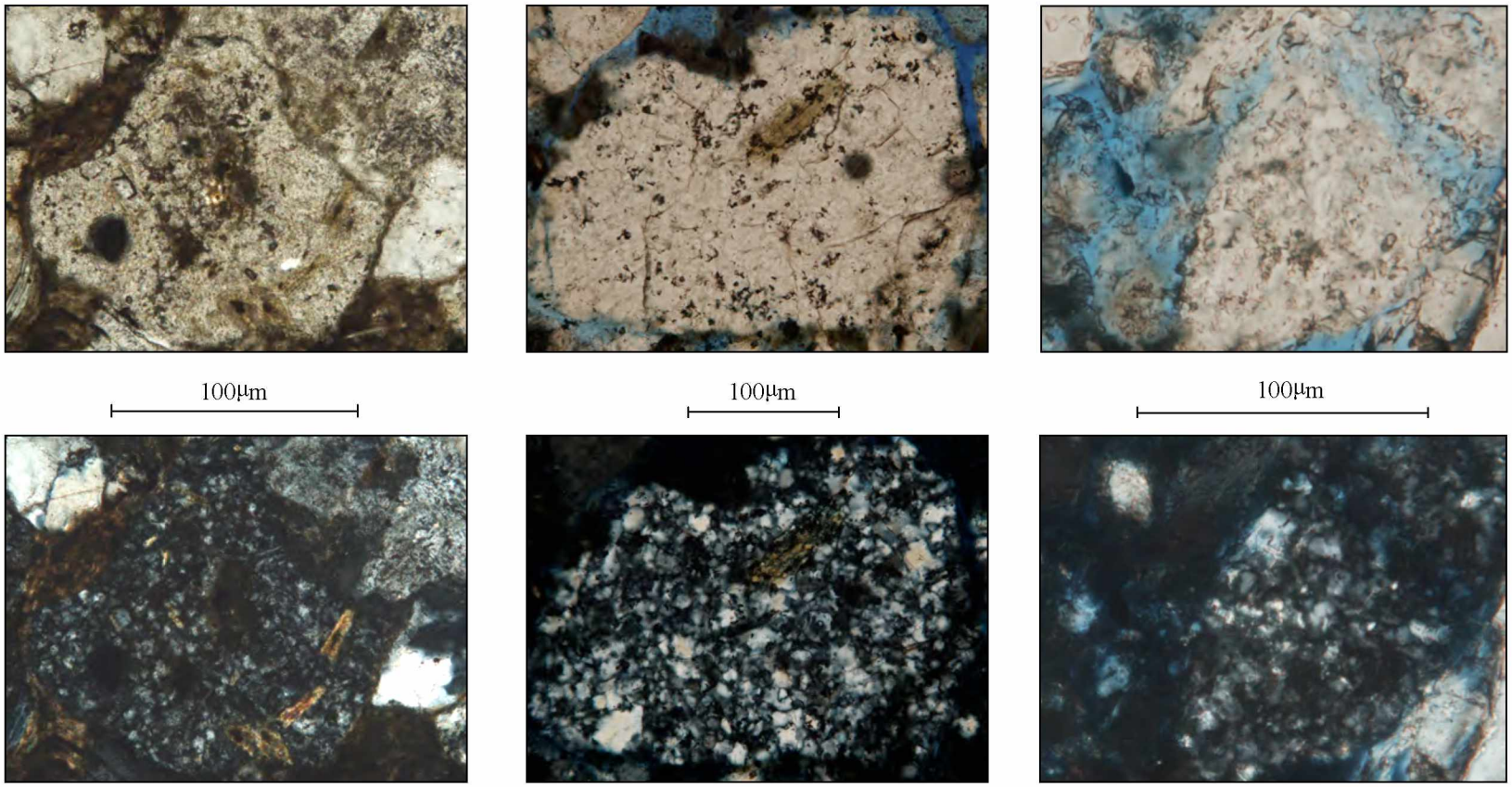

Fig. 5.6 Photomicrographs of volcanic rock fragments with mosaic textures. Samples LH1-182, GB1-9823, and GB1-5464 (left to right). Plane polarized light (above) and crossed-polars (below).

contains orthopyroxene, whereas NAC1-4197 contains clinopyroxene. The predominate alteration products of ferromagnesian minerals are chlorite and (or) chloritic clay. Remnants of the precursor minerals are rarely preserved, but in some instances I identified remnants of hornblende.

Calcite is a common replacement mineral in the volcanic rock fragments analyzed (Fig. 5.7). The severity of groundmass replacement ranges from minor replacement of microcrystalline feldspars to significant fine-grained replacement. In the most extreme case, complete replacement of groundmass has occurred (BL1-155). Calcite also commonly replaces plagioclase and albite phenocrysts.

Alteration and (or) replacement components of volcanic rock fragments are similar to pore-filling components in a given sample (Table 4.8, Table 5.5, and Table 5.7). Samples with volcanic rock fragments altered by clay (smectite, chloritic clay, and (or) chlorite) commonly contain pore-filling clays. Although EMPA indicated clay alteration of volcanic rock fragments in GB1-3890 (Table 5.7), pore-filling clay is not present in the Great Basins 1 well. However, the petrographer identified clasts of volcanic glass replaced by smectite (Table 4.9). Samples with volcanic rock fragments replaced by calcite contain pore-filling calcite. The same correlation exists for the zeolites, although zeolite alteration of volcanic rock fragments is not common. However, laumontite replaces phenocrysts in LH1-182 and a volcanic clast with relict perlitic texture in BL2-176 contains heulandite.

An exception to the correlation of volcanic alteration and replacement mineralogy with cement composition is the North Aleutian COST 1 well. Pore-filling smectite and chlorite are not present in this well, but both clays do occur as alteration minerals in volcanic rock fragments (Table 5.7). Also, EMPA indicated mixed-layer K-bearing clays as groundmass alteration in volcanic rock fragments from almost every sample analyzed (Table 5.7). However, K-bearing clay is rarely present outside of volcanic rock fragments (Table 5.5 and Table 5.6) except for illite alteration of feldspar clasts in samples from CP1, the Great Basins 1 well, and the North Aleutian COST 1 well (Table 5.8). Mixed-layer clays containing K are likely mixed-layer illite-smectite (section 5.2.2), which is a common alteration product of felsic volcanic glass (Gifkins et al., 2005).

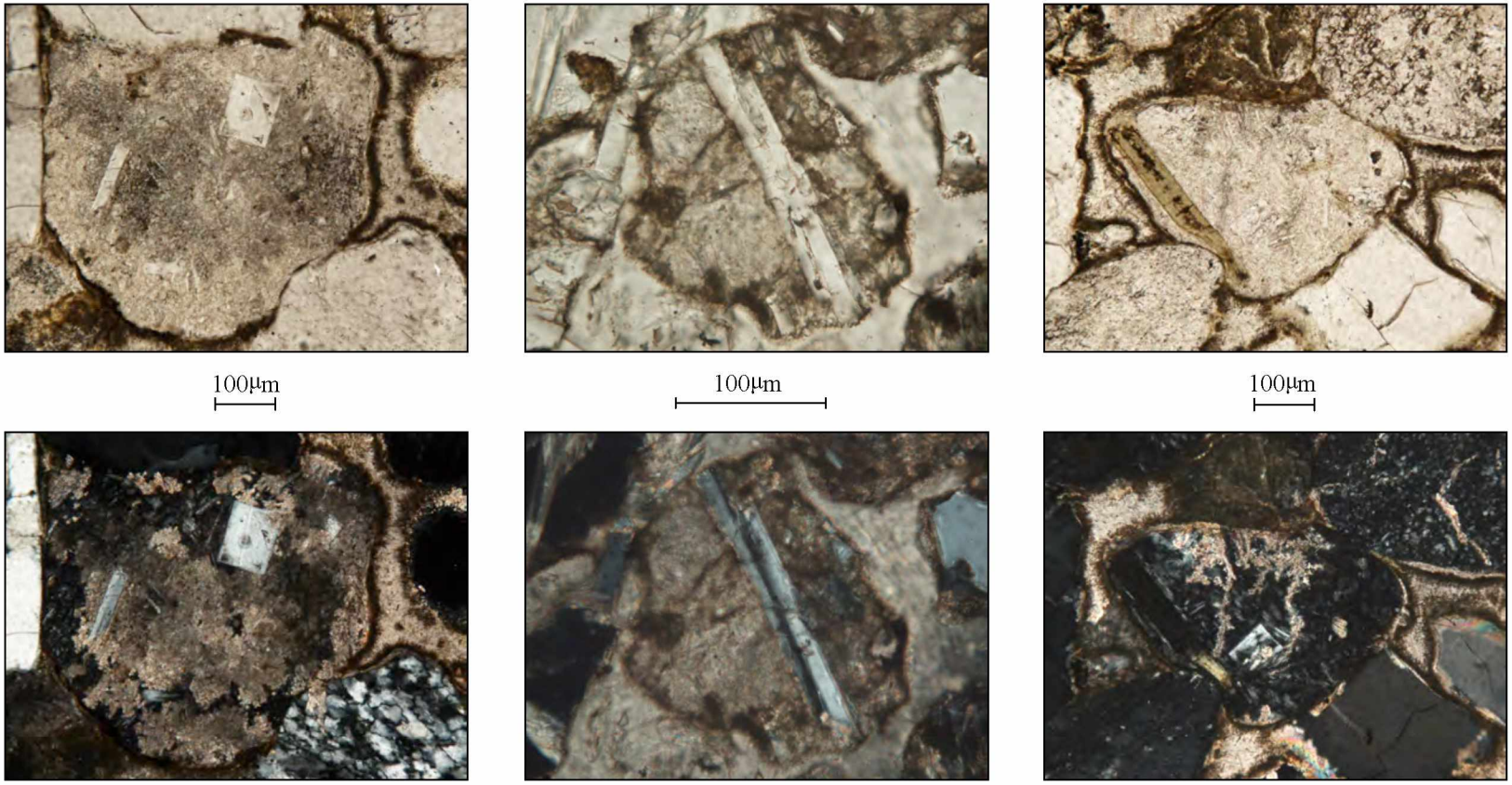

Fig. 5.7 Photomicrographs of volcanic rock fragments with calcite replacement. Samples LH1-2, BL1-155, and LH1-2 (left to right). Plane polarized light (above) and crossed-polars (below).

5.3.2.2 Composition

For each volcanic rock fragment that I analyzed, I averaged the chemical analyses that I obtained for multiple points within the groundmass. I plotted these averages on a total alkali-silica diagram (Fig. 5.8). It is important to be clear that these are *groundmass* averages and do not reflect whole-rock chemical compositions of the volcanic rock fragments (section 5.2.1). The total alkali-silica diagram shows that groundmass of volcanic rock fragments analyzed using EMPA is predominantly of felsic to intermediate composition (rhyolite to basaltic andesite; Fig. 5.8). The mafic groundmass analyses represent volcanic rock fragments altered by chlorite, chloritic clay, and (or) Fe-smectite. Some of the Bear Lake Formation volcanic rock fragments plot with high alkali content (as high as 10%). These data points generally represent averaging of microcrystalline K-feldspar or K-rich clay alteration with albite.

Mixed-layer clay and illitic clay are common groundmass alteration minerals present in the volcanic rock fragments with intermediate groundmass composition (andesite to basaltic andesite), although chloritic clay and chlorite also occur. Volcanic rock fragments with felsic groundmass compositions (rhyolite to dacite) typically contain quartz plus feldspar (K-feldspar ± plagioclase ± albite) groundmass crystals. Hornblende phenocrysts (and one possible orthopyroxene phenocryst) occur in volcanic rock fragments with felsic groundmass, whereas the few clinopyroxene phenocrysts I identified occur in volcanic rock fragments with intermediate groundmass. K-feldspar and quartz phenocrysts are most commonly associated with felsic groundmass, although I also identified them in volcanic rock fragments with intermediate groundmass.

The total alkali-silica diagram also shows data from Aleutian arc volcanoes (Fig. 5.8). Groundmass averages of volcanic rock fragments from the Bear Lake are somewhat comparable to the Aleutian arc data (Fig. 5.8). However, this comparison is between groundmass (Bear Lake Formation) and whole-rock (Aleutian arc) data. It is well established that for fresh volcanic rocks, the glassy groundmass is considerably more felsic (richer in Si, Na, and K) than is the composition of the entire rock. Further, increasing phenocryst crystallization results in increased SiO_2 and alkali (Na_2O+K_2O) content of the residual volcanic glass. Consequently the use of Bear Lake Formation volcanic rock fragment groundmass

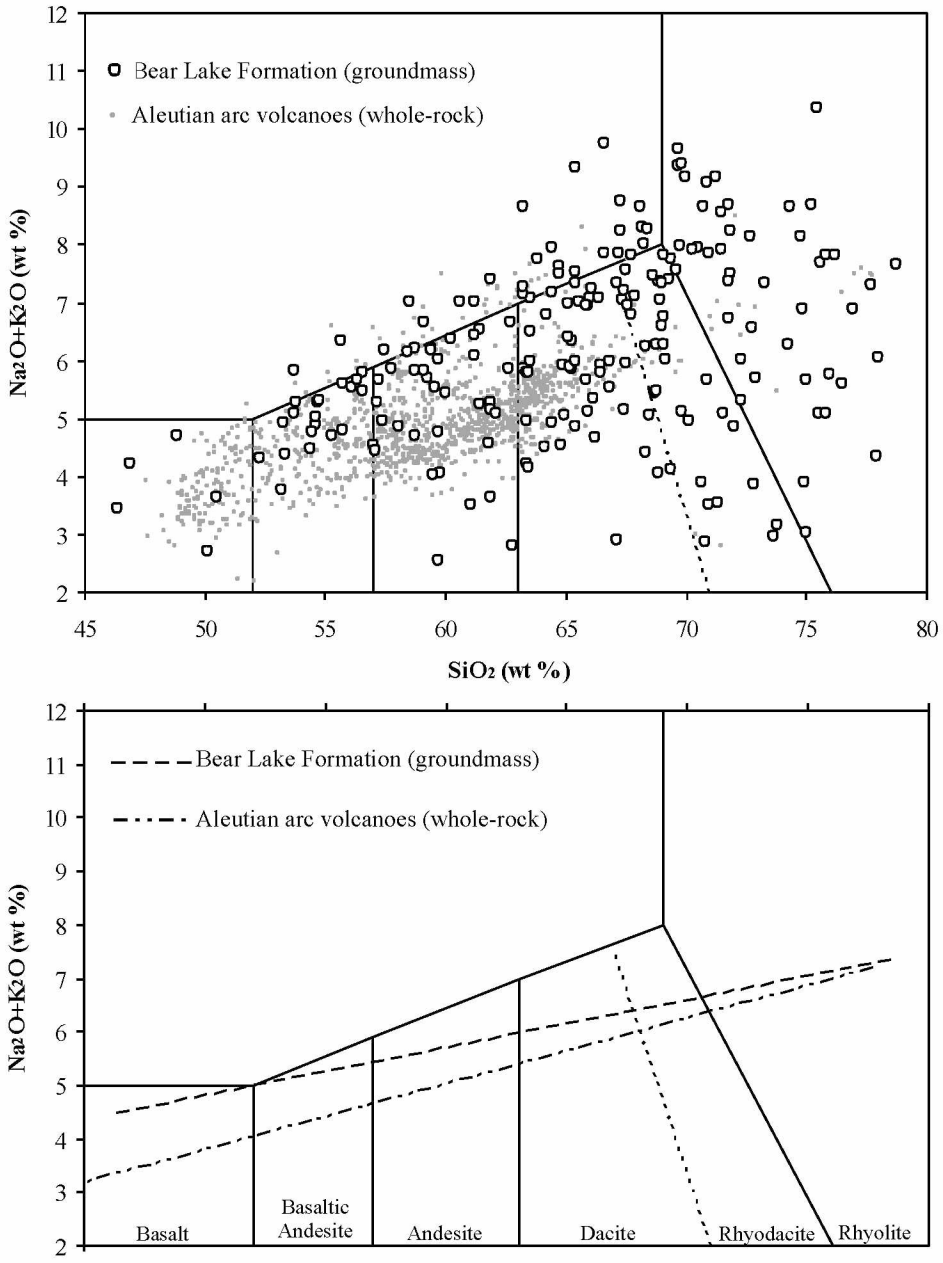

Fig. 5.8 Groundmass compositions of volcanic rock fragments from the Bear Lake Formation. The Bear Lake Formation groundmass compositions are based on averaged groundmass analyses for each volcanic rock fragment, obtained using electron microprobe analysis. The total alkali-silica diagrams also show whole-rock data from Aleutian arc volcanoes for comparison (provided by Christopher Nye, Alaska Volcano Observatory). The upper diagram shows data points and the lower diagram shows trendlines for each dataset.

data to approximate the major element composition of the original volcanic rock is intrinsically flawed. In order to correct for this effect I used groundmass abundance, glass composition, and whole rock composition data for young Aleutian volcanic rocks (Larsen et al., 2010 in press) and for experimental crystallization data from such rocks (Rader, 2010). Plotting phenocryst abundance versus difference between the glass composition and the whole rock composition (Fig. 5.9) shows considerable scatter, but is compatible with a simple linear relationship.

I used the trends of SiO_2 and alkalis versus phenocryst percentage (Fig. 5.9) to apply a correction to the groundmass averages of volcanic rock fragments from the Bear Lake Formation to better approximate the clast whole-rock compositions. I visually estimated the percentage of phenocrysts in each volcanic rock fragment plotted using standard estimation charts. For each averaged groundmass composition, I multiplied the phenocryst percentage by 0.34 (Fig. 5.9) and subtracted the result from the groundmass percent SiO_2. Similarly, I multiplied the phenocryst percentage by 0.06 (Fig. 5.9) and subtracted that from the groundmass percent alkali. These 'corrected' groundmass averages are my best estimate of whole-rock compositions for volcanic rock fragments from the Bear Lake Formation.

The largest error associated with this approach is from my estimates of the phenocryst abundance. This limitation is one reason why I did not try to average a whole-rock composition from the EMPA data (see section 5.2.1). Phenocryst representation of the parent rock is severely limited by the small grain size of the volcanic rock clasts (fine- to medium-grained sand). Many of the volcanic rock fragments have no phenocrysts and I estimated there to be 0% phenocrysts. Several volcanic rock fragments that I analyzed consist of one relatively large phenocryst in groundmass, and the phenocryst makes up more than 40% of the rock fragment. It is highly unlikely that these phenocryst percentage estimates accurately represent the phenocryst percentages of the parent rocks. On the other hand, estimating phenocryst abundance even in an entire thin section of a volcanic rock has significant errors, as indicated by replicate phenocryst abundance measurements from different thin sections of the same rock (Larsen et al., 2010 in press). Regardless, making some correction is clearly better than no correction, and the corrected values provide a closer estimate to the true whole-rock composition of volcanic rock fragment in the Bear Lake Formation than the groundmass compositions alone.

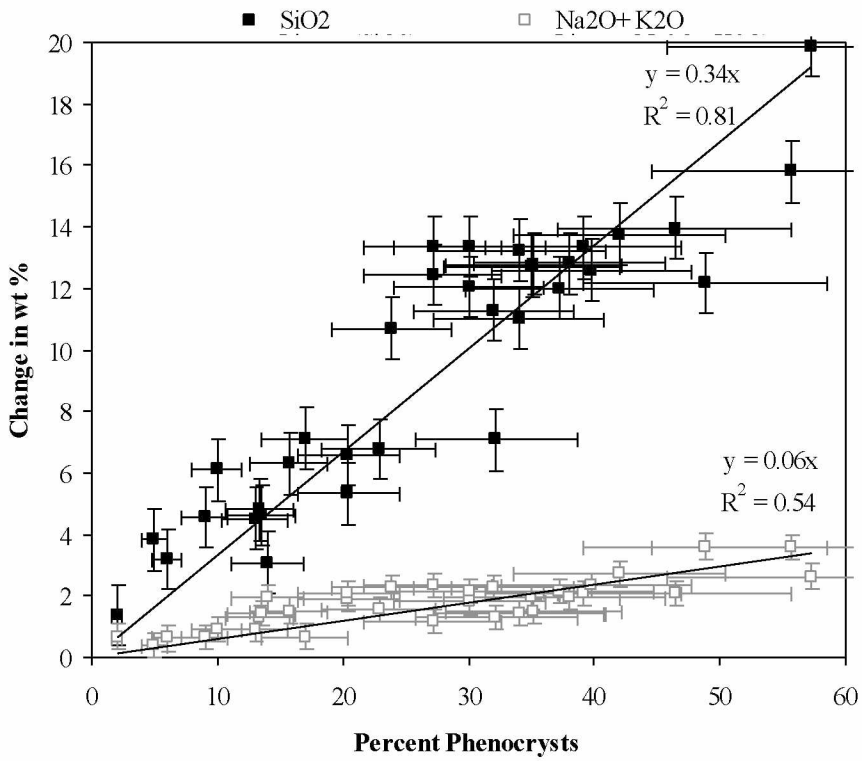

Fig. 5.9 Percent phenocrysts versus SiO_2 and Na_2O+K_2O. The y-axis represents the change in weight percent of SiO_2 and Na_2O+K_2O in volcanic glass from the whole-rock composition. Data are from Rader (2010) and Larsen et al. (2010 in press). Error bars represent typical errors (based on data reported by Rader, 2010 and Larsen et al., 2010 in press) of 1% for the change in SiO_2, 0.4% for the change in Na_2O+K_2O, and 20% of the phenocryst abundance for percent phenocrysts.

The corrected values shift the groundmass data for volcanic rock fragments in the Bear Lake Formation to lower values of weight percent SiO_2 and lower weight percent alkali (Fig. 5.10), as expected when comparing groundmass data to whole-rock data. The corrected values cluster in the andesite to dacite compositional range (Fig. 5.11), and are more comparable to the whole-rock Aleutian arc data (Fig. 5.8 and Fig. 5.11). The average of the entire Bear Lake Formation dataset also shifts from dacite to andesite when the correction is applied. In other words, a very large proportion of the volcanic rock fragments from the Bear Lake Formation are of intermediate composition.

Due to the alteration of volcanic clasts analyzed from the Bear Lake Formation, I plotted the relatively non-mobile elements Si and Ti as a secondary check of compositions indicated by the total alkali-silica plot. The weight percent SiO_2 versus TiO_2 diagram shows the averaged groundmass analyses for individual volcanic rock fragments from the Bear Lake Formation, and whole-rock data from Aleutian arc volcanoes (Fig. 5.12). The TiO_2 content of volcanic rock fragments from the Bear Lake Formation with felsic groundmass (rhyolite to dacite) corresponds fairly well to the high-SiO_2, low-TiO_2 trend of Aleutian arc rocks. Within intermediate compositions (andesite to basaltic andesite) the TiO_2 weight percent for many Bear Lake Formation volcanic clasts falls below that of Aleutian arc volcanic rocks. The discrepancy between TiO_2 content of groundmass in Bear Lake Formation volcanic clasts and of Aleutian arc rocks increases toward more mafic compositions (lower SiO_2). Even so, TiO_2 weight percent for many of the volcanic rock fragments from the Bear Lake Formation correspond to Aleutian arc rocks of mainly felsic to intermediate composition and show decreasing weight percents of TiO_2 with increasing weight percents of SiO_2.

Fig. 5.13 and Fig. 5.14 show plagioclase phenocryst compositions obtained using EMPA from outcrop and well samples. On these plots, I have illustrated generalized ranges of plagioclase composition for volcanic rock types. These approximate ranges are based on generalizations from literature of plagioclase phenocryst compositions for volcanic rock types, and from data presented for plagioclase of a given volcanic rock type (Brown, 1967; Marsh, 1976; Ewart, 1982; Marsh, 1982; Durant, 1989; McBirney, 1989; Tappen et al., 2009). Fig. 5.13 and Fig. 5.14 do not include albite phenocrysts (An < 10) identified

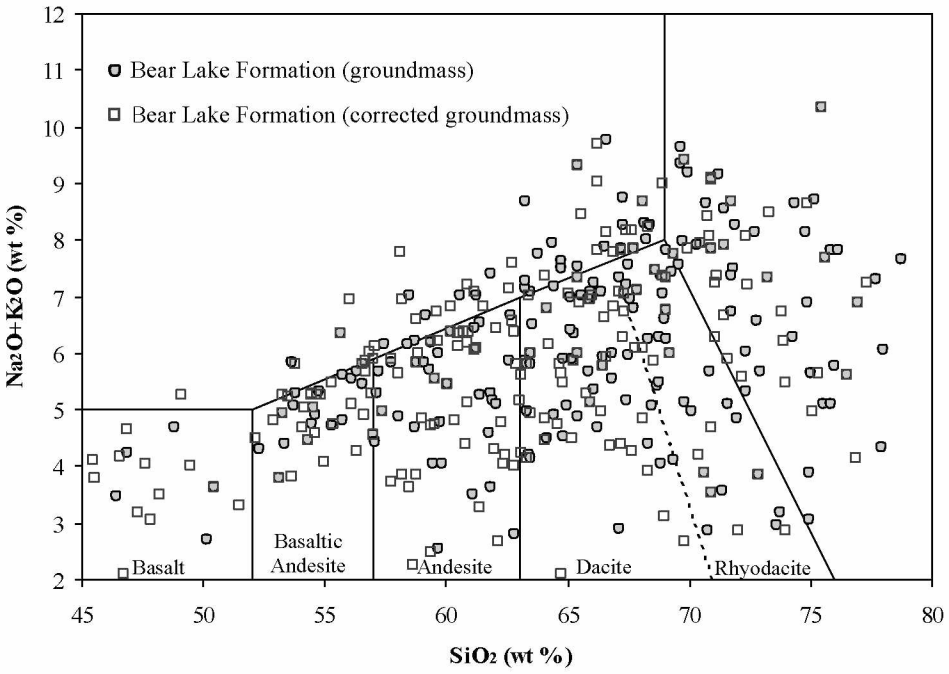

Fig. 5.10 Total alkali-silica diagram showing groundmass and corrected groundmass compositions. The Bear Lake Formation groundmass compositions are based on averaged groundmass analyses for each volcanic rock fragment, obtained using electron microprobe analysis. The corrected groundmass compositions are adjusted for the percentage of phenocrysts in each volcanic rock fragment (see section 5.3.2.2).

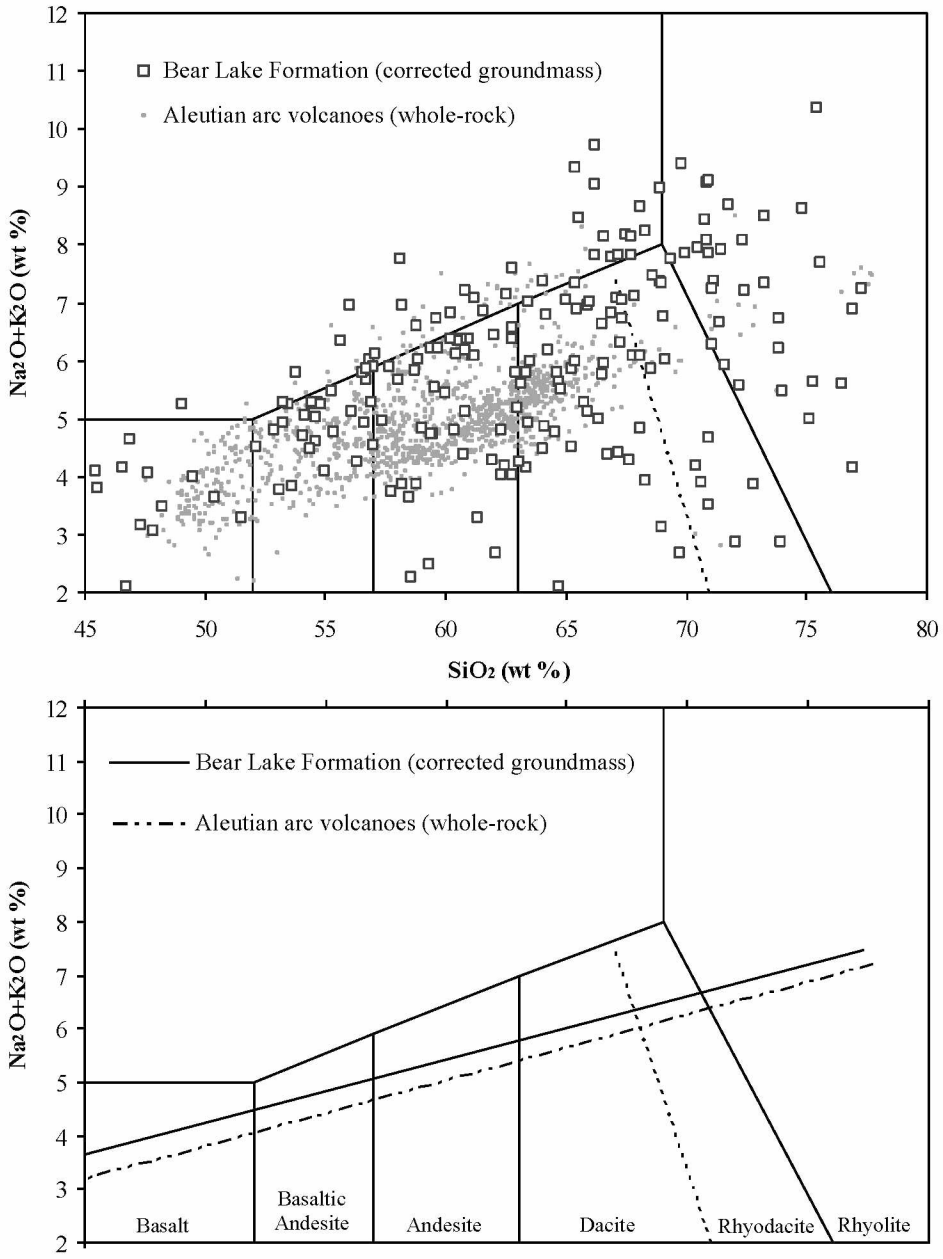

Fig. 5.11 Corrected groundmass compositions of volcanic rock fragments from the Bear Lake Formation. The Bear Lake Formation corrected groundmass compositions reflect adjustments of groundmass compositions based on averaged groundmass analyses for each volcanic rock fragment, obtained using electron microprobe analyses (see section 5.3.2.2). These total alkali-silica diagrams also show whole-rock data from Aleutian arc volcanoes for comparison (provided by Christopher Nye, Alaska Volcano Observatory). The upper diagram shows data points and the lower diagram shows trendlines for each dataset.

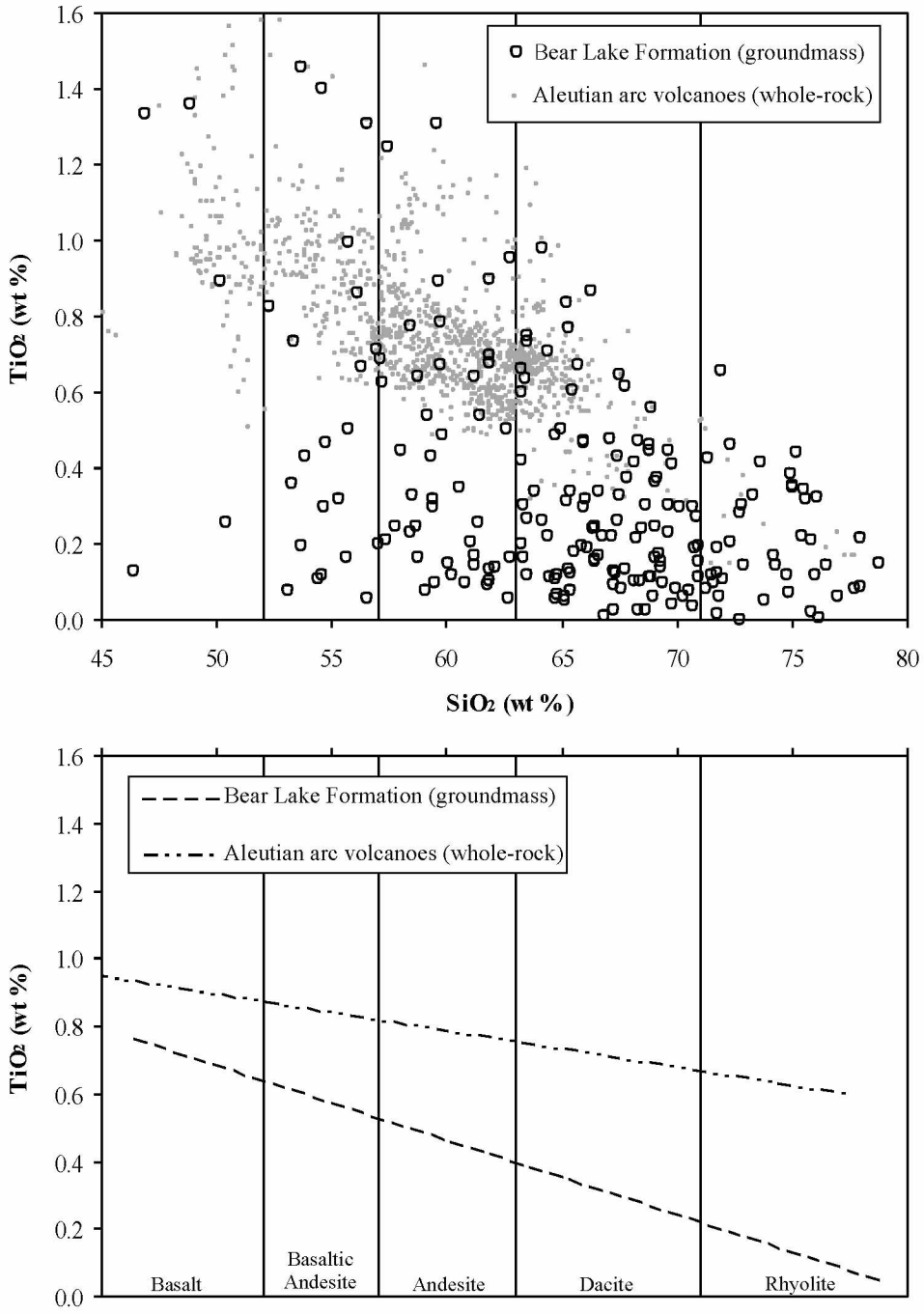

Fig. 5.12 Weight percent SiO_2 versus TiO_2 of groundmass in volcanic rock fragments from the Bear Lake Formation. The diagram also shows whole-rock data from Aleutian arc volcanoes for comparison (provided by Christopher Nye, Alaska Volcano Observatory). The upper diagram shows data points and the lower diagram shows trendlines for each dataset.

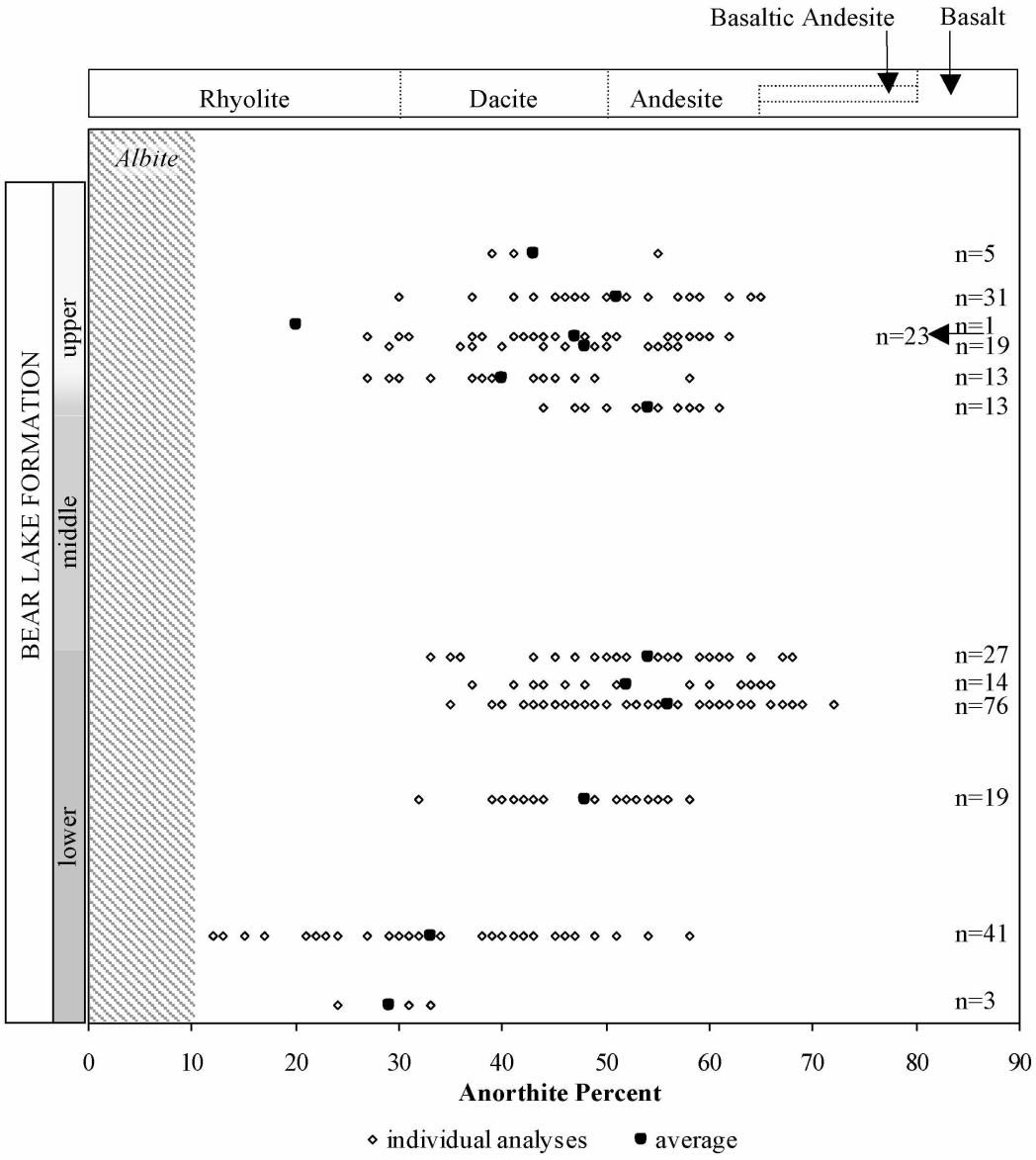

Fig. 5.13 Composition of plagioclase phenocrysts in volcanic rock fragments from Bear Lake Formation outcrop samples. Individual electron microprobe analyses of plagioclase phenocrysts are shown for samples from measured sections of the Bear Lake Formation. The average of analyses is also plotted for each sample, and the number (n) of analyses plotted for each sample is noted to the right. Generalized guidelines for plagioclase phenocryst compositions of volcanic rock types are illustrated above the plot and are approximations based on literature (Brown, 1967; Marsh, 1976; Ewart, 1982; Marsh, 1982; Durant, 1989; McBirney, 1989; Tappen et al., 2009).

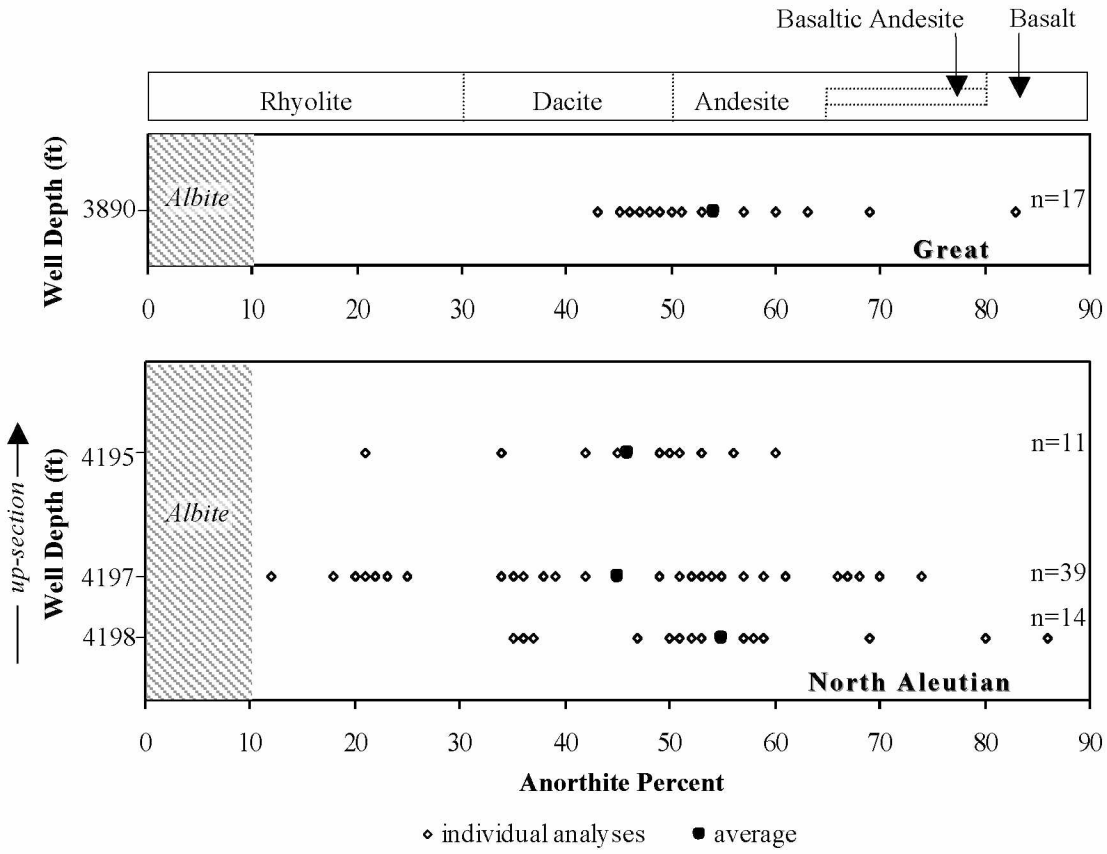

Fig. 5.14 Composition of plagioclase phenocrysts in volcanic rock fragments from Bear Lake Formation well samples. Individual electron microprobe analyses of plagioclase phenocrysts are shown for samples of the Bear Lake Formation from the Great Basins 1 and North Aleutian COST 1 wells. EMPA identified phenocrysts in only one sample from the Great Basins 1 well (GB1-3890). The average of analyses is also plotted for each sample, and the number (n) of analyses plotted for each sample is noted to the right. Generalized guidelines for plagioclase phenocryst compositions of volcanic rock types are illustrated above the plot and are approximations based on literature (Brown, 1967; Marsh, 1976; Ewart, 1982; Marsh, 1982; Durant, 1989; McBirney, 1989; Tappen et al., 2009).

using EMPA because their diagenetic origin precludes them from being a diagnostic indicator of volcanic rock type. These figures show that plagioclase phenocryst compositions in volcanic rock fragments from the Bear Lake Formation fall predominantly into the range expected for rocks of dacitic to andesitic composition. Two samples (NAC1-4197 and lower Bear Lake Formation outcrop sample CP1-185 with n=41) show a population of phenocrysts with lower anorthite content (An < 30). The well samples also show a minor population with high anorthite percentages (An > 70), requiring a basaltic origin.

5.3.3 Detrital Plagioclase Clasts

Diagrams similar to those illustrating plagioclase phenocryst compositions from volcanic rock fragments illustrate the composition of detrital plagioclase clasts obtained using EMPA (Fig. 5.15 and Fig. 5.16). These detrital plagioclase clasts may be of either volcanic or plutonic origin (Fig. 5.17). Therefore, I labeled the generalized ranges of anorthite percentage related to volcanic rock types shown in Fig. 5.15 and Fig. 5.16 as felsic (corresponding to rhyolite and dacite), intermediate (corresponding to andesite and basaltic andesite), and mafic (corresponding to basalt). Also, I included albite on this set of figures. Albite is common to both outcrop and well samples throughout the Bear Lake Formation (Fig. 5.15 and Fig. 5.16).

Detrital plagioclase in the Great Basins 1 well is almost exclusively albite with the exception of GB1-3890 (Fig. 5.16). Anorthite content of plagioclase clasts in this sample fall within the range associated with rocks of felsic composition. Composition of plagioclase clasts from samples of the North Aleutian COST 1 well also fall within the felsic range (Fig. 5.16). Anorthite percentages that correspond to an intermediate composition are mainly from zoned plagioclase in NAC1-4197. About one-quarter (5 out of 19) of the detrital plagioclase analyzed from the North Aleutian COST 1 well are compositionally zoned.

Detrital plagioclase clasts from outcrop samples have compositions that fall within the range associated with rocks of mainly felsic composition (Fig. 5.15). The range of anorthite content extends farther toward felsic compositions (An < 30) in samples from the upper Bear Lake Formation and lowermost Bear Lake Formation. Anorthite percentages at the higher end of the range (An > 30) are commonly from zoned plagioclase clasts. These zoned clasts are from measured sections BL3, BL1, and

Fig. 5.15 Composition of detrital plagioclase clasts from Bear Lake Formation outcrop samples. Individual electron microprobe analyses of plagioclase clasts (including albite) are shown for samples from measured sections of the Bear Lake Formation. The average of analyses is also plotted for each sample, and the number (n) of analyses plotted for each sample is noted to the right. Generalized compositional divisions relating to anorthite percentage are illustrated above the plot. These approximated guidelines are based on ranges of plagioclase phenocryst compositions for volcanic rock types found in literature (Brown, 1967; Marsh, 1976; Ewart, 1982; Marsh, 1982; Durant, 1989; McBirney, 1989; Tappen et al., 2009). These detrital plagioclase clasts may be of either volcanic or plutonic origin and so I labeled compositional divisions as felsic (corresponding to rhyolite and dacite), intermediate (corresponding to andesite and basaltic andesite), and mafic (corresponding to basalt).

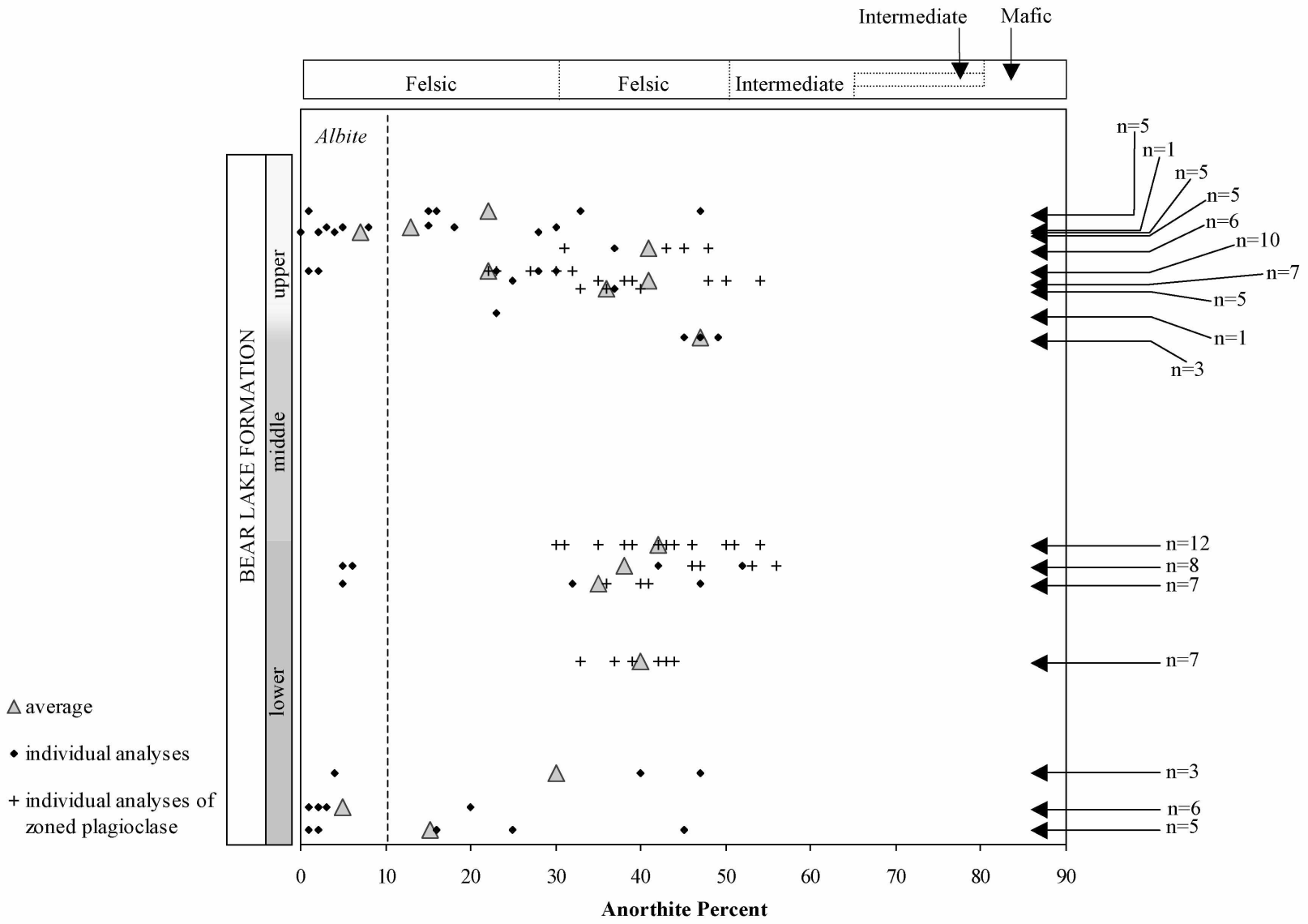
Intermediate
Mafic
Felsic
Felsic
Intermediate
Albite
BEAR LAKE FORMATION
upper
middle
lower
n=5
n=1
n=5
n=5
n=6
n=10
n=7
n=5
n=1
n=3
n=12
n=8
n=7
n=7
n=3
n=6
n=5
average
individual analyses
individual analyses of zoned plagioclase
0
10
20
30
40
50
60
70
80
90
Anorthite Percent

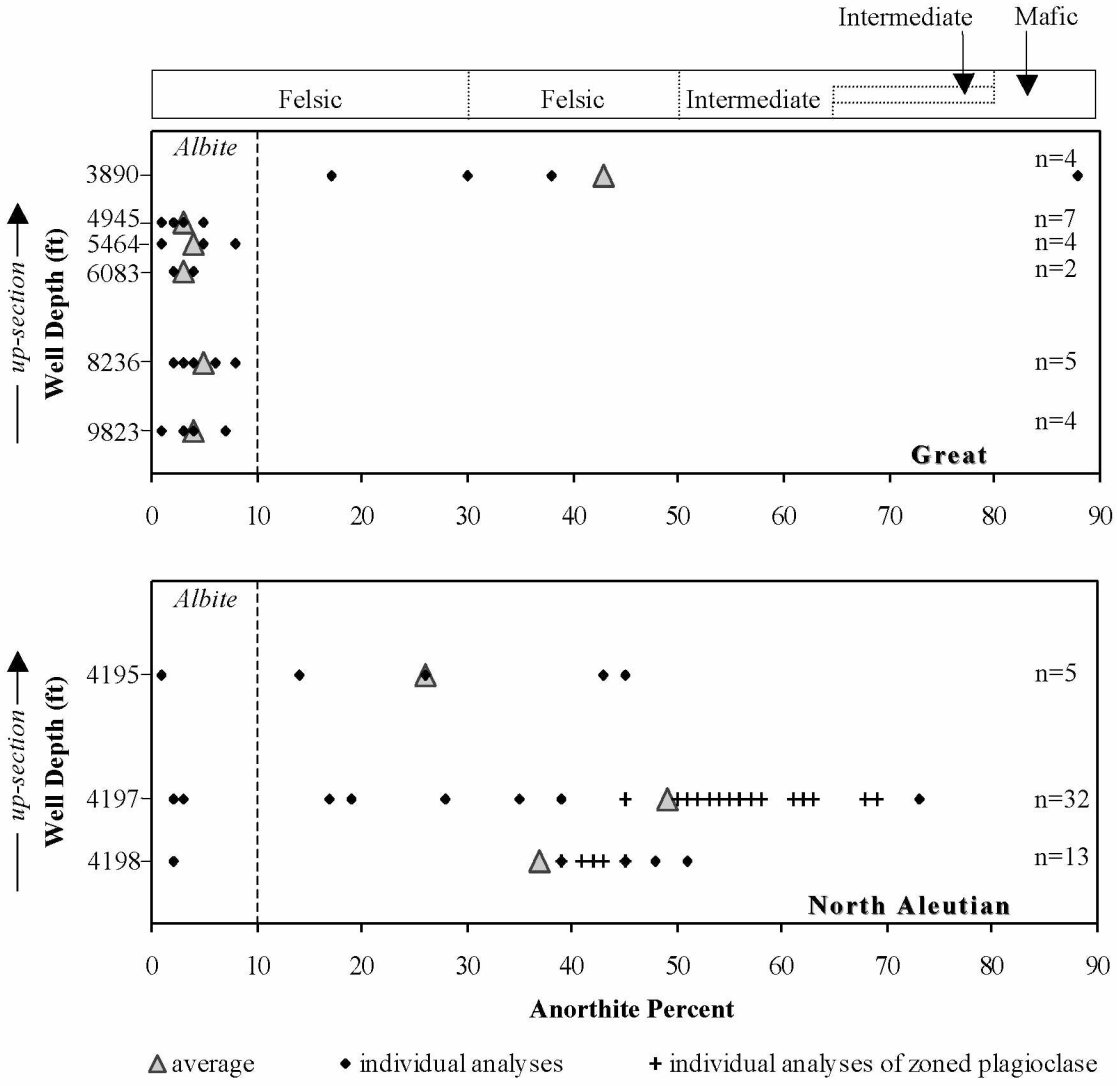

Fig. 5.16 Composition of detrital plagioclase clasts from Bear Lake Formation well samples. Individual electron microprobe analyses of plagioclase clasts (including albite) are shown for samples of the Bear Lake Formation from the Great Basins 1 and North Aleutian COST 1 wells. The average of analyses is also plotted for each sample, and the number (n) of analyses plotted for each sample is noted to the right. Generalized compositional divisions relating to anorthite percentage are illustrated above the plot. These approximated guidelines are based on ranges of plagioclase phenocryst compositions for volcanic rock types found in literature (Brown, 1967; Marsh, 1976; Ewart, 1982; Marsh, 1982; Durant, 1989; McBirney, 1989; Tappen et al., 2009).

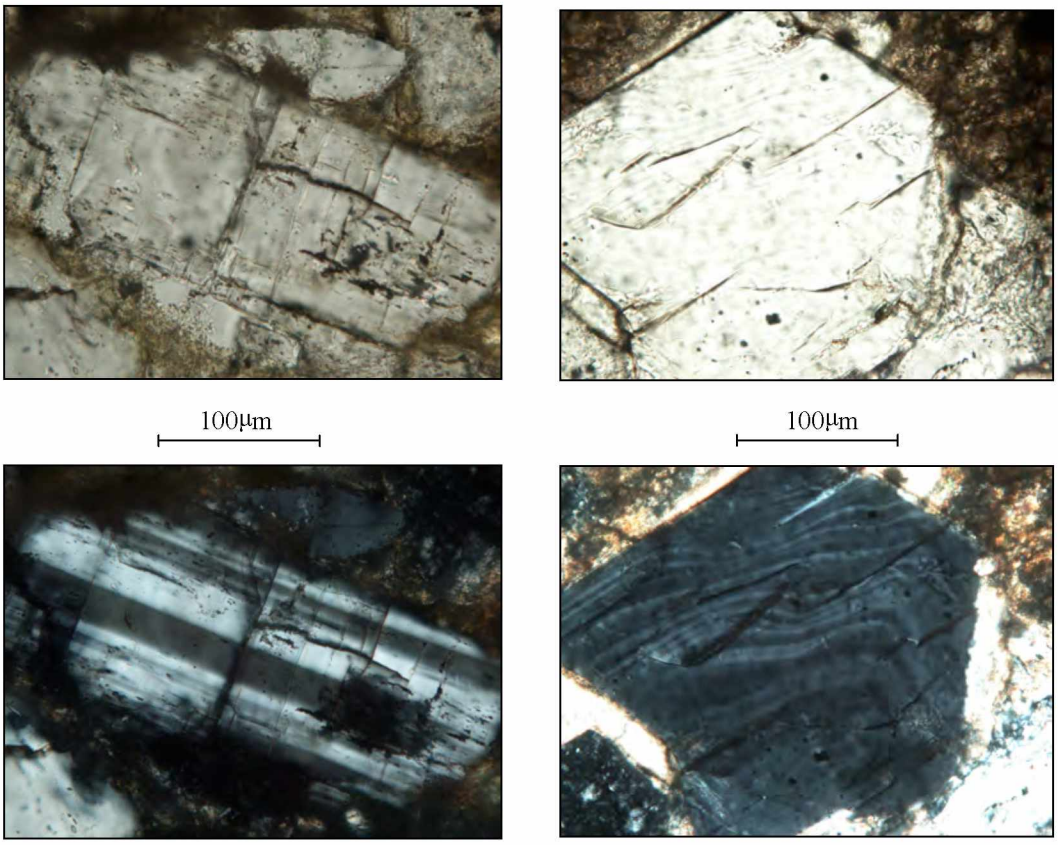

Fig. 5.17 Photomicrographs of detrital plagioclase clasts. The clast on the left (sample LH1-182) is twinned and the clast on the right is zoned (sample BL1-155). Plane polarized light (above) and crossed-polars (below).

LH1 (ascending stratigraphic height, see Fig. 2.2). Approximately half of the plagioclase clasts analyzed from BL3 are zoned (7 out of 12), one-third of those from BL1 are zoned (2 out of 6), and about one-thrid of those from LH1 are zoned (3 out of 6).

5.4 Discussion

5.4.1 Evaluation of Petrographic Identifications of Diagenetic Minerals

Petrographic examination indicated heulandite in sample BL1-155, but I was unable to confirm it using EMPA. This is also true for siderite in CP1-185. In both of these instances, the mineral is present in very minor amounts (0.3% heulandite and 0.7% siderite; Table 4.7). Overlooking the minerals during EMPA as a result of their low abundances is the likely reason I could not confirm them.

Petrographic identifications of corrensite and smectite are consistent with identifications of smectite, chloritic clay, and (or) chlorite made using EMPA. In a general sense, the identification of Fe-Mg clays is consistent between the two methods. Given that chloritic clay identified using EMPA may be mixed-layer smectite-chlorite (section 5.2.2), the consistent EMPA identification of corrensite (according to petrography) as smectite and chloritic clay is understandable. However, I am confident that clays I called chlorite using EMPA are truly chlorite and not a mixed-layer clay, since the compositions are very close to the chemical formula for chlorite (Table 5.4). Thus, most of the "corrensite" identified petrographically may be either mixed-layer smectite-chlorite or chlorite.

The largest inconsistency between diagenetic mineral identifications made petrographically and using EMPA lies in the recognition of albite. Albite was not identified petrographically, whereas I documented prolific albite using EMPA. Sodium cobaltinitrite staining of thin sections allowed identification of K-feldspar. However, this stain is not helpful in distinguishing albite from more calcic plagioclase. It is very common for albite to go unnoticed during petrographic study (Boggs, 2003).

An additional characteristic of feldspar identified using EMPA is sericite- and illite-altered detrital feldspar clasts in the Great Basins 1 well. Also, there is a conspicuous lack of plagioclase clasts is in the well (Table 5.8). The uniqueness of this detrital feldspar population compared to measured sections and the North Aleutian COST 1 well is notable. The absence of plagioclase is not likely related to provenance since I documented detrital plagioclase clasts using EMPA for all other samples. This suggests that the

feldspar clast compositions in the Great Basins 1 well reflect a diagenetic environment distinctive from the rest of the Bear Lake Formation (see Chapter 8).

5.4.2 Classification of Volcanic Rock Fragments

Data points for compositions of volcanic rock fragments from the Bear Lake Formation cluster in the same general pattern as those from Aleutian arc volcanoes and show predominantly felsic to intermediate compositions (Fig. 5.8 and Fig. 5.11). Corrected groundmass values provide a better comparison to the whole-rock Aleutian arc data and indicate that volcanic rock fragments in the Bear Lake Formation are predominately dacite and andesite (Fig. 5.11). The groundmass in Bear Lake Formation clasts also follow the TiO_2 versus SiO_2 trend of whole-rock data for Aleutian arc volcanoes (Fig. 5.12). However, it is clear that numerous volcanic rock fragments from the Bear Lake Formation scatter below the data shown for Aleutian arc volcanoes of intermediate compositions (andesite to basaltic andesite; Fig. 5.12). Comparing the trends of TiO_2 versus SiO_2 shows that the groundmass in volcanic rock fragments from the Bear Lake Formation falls below the Aleutian arc volcanoes across the entire compositional range (Fig. 5.12). I attribute these apparently low TiO_2 weight percents (with respect to corresponding weight percent SiO_2) to my analytical technique. Ti-oxide (rutile for example) is a common accessory component and replacement mineral in volcanic rocks (Gifkins et al., 2005). I found that obtaining realistic values for Ti content of groundmass in volcanic rock fragments is literally "hit or miss". If the electron beam hit rutile, then including that analytical point of very high TiO_2 in the groundmass average over-represents the actual proportion of TiO_2 present in the groundmass. In these cases I left out the TiO_2 when I averaged the groundmass analyses within each volcanic rock fragment. I conclude that this is what causes the low weight percents of TiO_2 with respect to weight percent SiO_2. The only way to get around this problem would be to drastically increase the number of analysis points per clast.

Plagioclase and albite are the most common phenocrysts present in volcanic rock fragments of the Bear Lake Formation. The common replacement of plagioclase by albite suggests that the albite replaced the original phenocrysts, and is not the primary composition. Plagioclase and albite phenocrysts in volcanic rock fragments of the Bear Lake Formation are associated with groundmass compositions ranging from felsic to mafic. K-feldspar and quartz are more rare, and most common in volcanic rock fragments

with felsic groundmass. The main ferromagnesian phenocryst is hornblende, but orthopyroxene and clinopyroxene are also present in a few volcanic rock fragments. The vast majority of ferromagnesian minerals are clay-altered and the original mineral is unidentifiable. These characteristics are all consistent with felsic to intermediate volcanic rock types (Table 2.1 in Gifkins et al., 2005).

Plagioclase phenocryst compositions in volcanic rock fragments from outcrop and well samples fall predominantly into the range expected for rocks of dacitic to andesitic composition. Two samples (NAC1-4197 and lower Bear Lake Formation outcrop sample CP1-185 with n=41) show a population of lath-shaped plagioclase phenocrysts with relatively lower anorthite content (An < 30) compared to other samples (Fig. 5.13 and Fig. 5.14). In the sample from the lower Bear Lake Formation the laths are sometimes associated with phenocrysts completely replaced by albite and (or) albite replacement of plagioclase. Groundmass plagioclase crystals in volcanic rock fragments that I analyzed from the Bear Lake Formation commonly have lower anorthite percentages than corresponding plagioclase phenocrysts. This suggests that the laths I considered as phenocrysts are probably late-growing crystals that crystallized after larger phenocrysts, resulting in a more sodic composition. The plagioclase phenocrysts associated with albite in volcanic rock fragments from the lower Bear Lake Formation sample likely show lower anorthite content as a result of mixed analysis of albite and plagioclase. Therefore, I do not think that the population of phenocrysts with An < 30 indicate more felsic (rhyolitic) provenance. My interpretation is consistent with the limited sources of rhyolite available on the Alaska Peninsula, mostly present as flows and domes on Unga Island (Wilson et al., 1999).

Each method of classification carries uncertainty from different sources of error. It is clear that the corrected groundmass values for volcanic rock fragments in the Bear Lake Formation provide a more satisfactory comparison to whole-rock compositions, but the challenge of estimating phenocryst percentages that accurately reflect the parent rock introduces a considerable uncertainty associated with this method. Measuring anorthite percent of plagioclase phenocrysts is a useful tool for classification of volcanic rock fragments, but the range of plagioclase compositions for different volcanic rock types makes classification problematic. For example, there is overlap in plagioclase compositions from dacite and andesite, and even basalt. Using relatively immobile elements, such as Si and Ti, provides a highly

questionable guide to classification of volcanic rock fragments due to limitations of the analytical procedure I employed. Nevertheless, it does illustrate the general trend of decreasing TiO_2 content with increasing SiO_2 that volcanic rocks show. Therefore, it is a useful tool for affirming a volcanic origin of the clasts (which is not always straightforward in thin section) when used in conjunction with other methods.

5.4.2.1 Potential Volcanic Provenance

The source of volcanic material in the Bear Lake Formation may be deposits of the Meshik Volcanics and, potentially, Late Miocene volcanism. Wilson (1985) noted that clasts from conglomerates of the Bear Lake Formation resemble rocks from the Meshik Volcanics. This is consistent with Burk's (1965) assertion that Paleogene volcanic rocks contributed sediment to mid-Miocene strata. Wisehart (1971) cites "locally derived volcanic debris" as a contributor to the Bear Lake Formation. The Meshik Volcanics and Late Miocene volcanic rocks are both exposed in the vicinity of the Bear Lake Formation near Port Moller (Fig. 5.18).

Late Miocene volcanic rocks exposed along the southeastern edge of the Alaska Peninsula have K-Ar ages ranging from 10.4 ± 0.49 to 6.1 ± 0.23 Ma (Fig. 5.18; Wilson et al., 1999). These rocks consist of hypabyssal and volcanic andesite and basalt flows (Detterman et al., 1996; Wilson et al., 1999). Detterman et al. (1996) describe late Tertiary volcanic rocks as containing phenocrysts of plagioclase, clinopyroxene, orthopyroxene, and hornblende with local alteration and silicification near plugs. They also note that the limited exposure of these rocks may be due to erosion associated with intense uplift during the Late Miocene and Pliocene, as well as glacial erosion during the Pleistocene. These rocks are too young to have sourced the lower Bear Lake Formation, although they could be contemporaneous with the upper Bear Lake Formation (Fig. 2.2). The intermediate to mafic composition of these rocks preclude them as a source for the felsic (~dacite) volcanic material that I identified in the Bear Lake Formation.

The Meshik Volcanics are Late Eocene to Early Oligocene volcanic deposits of the Meshik arc, extending from the southwestern end of the Alaska Peninsula northeast to the Ugashik Lakes area (Fig. 5.18; Wilson, 1985). Wilson (1985) describes the nature of volcanic rocks of the Meshik arc in

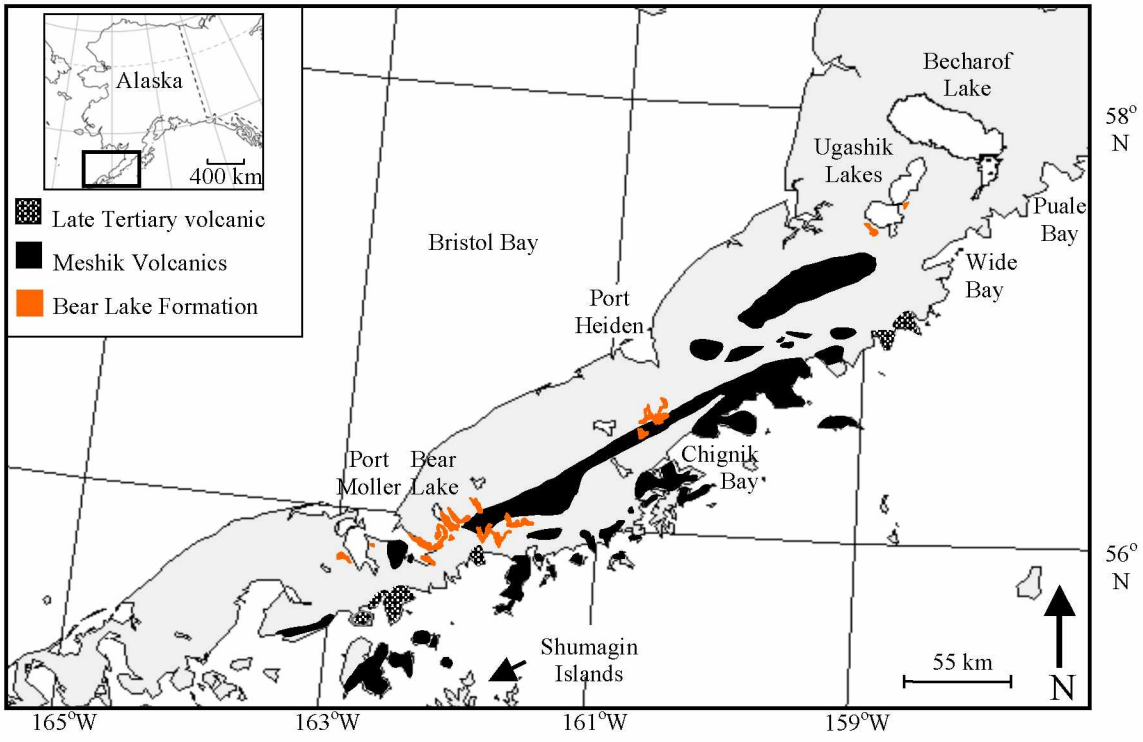

Fig. 5.18 Distribution of potential volcanic provenance units for the Bear Lake Formation. Exposures of late Tertiary volcanic rocks from Wilson et al. (1999). Exposures of Meshik Volcanics from (Wilson, 1985) and Wilson et al. (1999). Exposures of the Bear Lake Formation from Wilson et al. (1999) and Decker et al. (2008b).

detail. To summarize: Rocks of the Meshik arc include hypabyssal and volcanic rocks that range from dacite to basalt. Plagioclase phenocrysts are common, and often strongly zoned. The dominate mafic phenocryst is hornblende. Rocks sometimes contain other phenocrysts including quartz, orthopyroxene, and clinopyroxene. Groundmass is commonly composed of devitrified glass or fine-grained feldspar (sometimes flow-aligned). Some rocks contain chloritized or glassy groundmass.

Based on rock sample descriptions (Wilson, 1985; Wilson, F.H., written communication, 2007), groundmass of Meshik Volcanic rocks commonly contains fine-grained pyroxene (mostly clinopyroxene) and chlorite alteration of ferromagnesian minerals. Additionally, olivine is locally present in basalt.

The Meshik Volcanics are a much more likely source than the late Tertiary volcanic rocks, based on lithologic descriptions and unit ages. The Meshik Volcanics could have easily contributed volcanic rock fragments with the phenocryst and groundmass assemblages I identified using EMPA in the Bear Lake Formation (plagioclase, hornblende, and pyroxene phenocrysts; crystallized groundmass of quartz, plagioclase, and K-feldspar; clay alteration in groundmass; flow-aligned feldspar laths in groundmass). In general, ferromagnesian minerals in volcanic rocks are typically altered or replaced by chlorite and calcite (Gifkins et al., 2005). The fine grained calcite replacement of groundmass in some volcanic rock fragments from the Bear Lake Formation may reflect calcite replacement of fine-grained clinopyroxene common in the groundmass of Meshik Volcanic rocks. Chlorite-altered groundmass in volcanic clasts from the Bear Lake Formation may also reflect alteration of ferromagnesian minerals.

Dacite is conspicuously absent in the Meshik Volcanics in the Port Moller, Stepovak Bay, and Simeonof Island quadrangles; rather, the unit consists of andesite and basalt in these areas (Fig. 5.19; Wilson et al., 1994; Wilson, F.H., written communication, 2007). In the Chignik and Sutwik Island quadrangles, to the north (Fig. 5.19), dacitic rocks are common in the Meshik Volcanics (Wilson, 1980). Given that the volcanic rock fragments in the Bear Lake Formation are felsic to intermediate in composition, volcanic material in the Bear Lake Formation was probably sourced from the north. More specifically, the Meshik Volcanics are exposed to the northeast of Port Moller (Fig. 5.18).

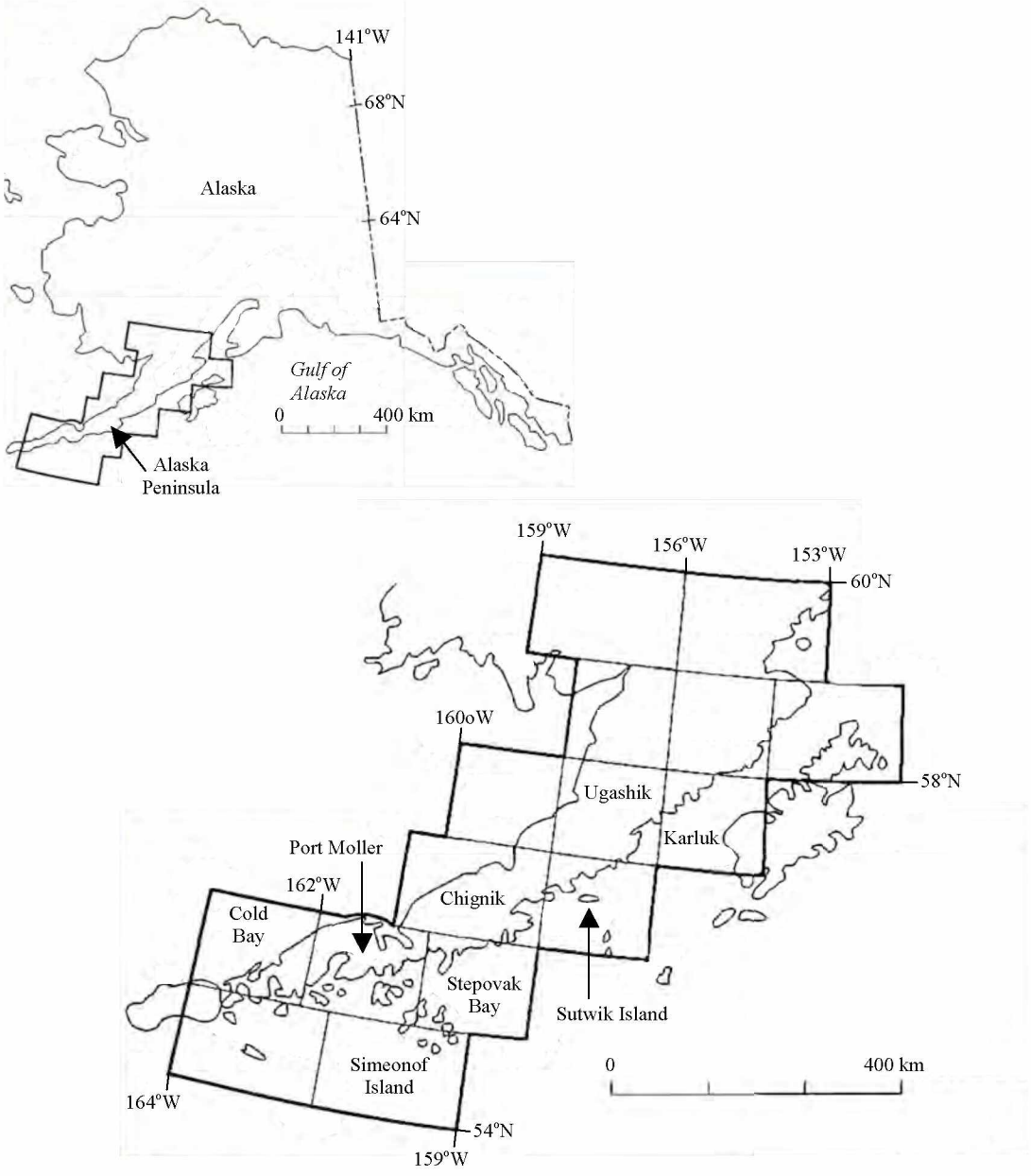

Fig. 5.19 Quadrangle location map of the Alaska Peninsula. Modified from Detterman et al. (1996)

5.4.3 Detrital Plagioclase Clast Provenance

The range of plagioclase compositions of detrital plagioclase clasts extends farther toward felsic compositions (An < 30) in samples from the upper Bear Lake Formation and lowermost Bear Lake Formation (Fig. 5.20). This population generally shows lower anorthite percentages than typical plagioclase phenocrysts in volcanic rock fragments from the Bear Lake Formation (Fig. 5.20). This separate population suggests that the low anorthite plagioclase clasts are not of volcanic origin, but rather were sourced originally from plutonic rocks. This interpretation is consistent with limited exposures of rhyolite on the Alaska Peninsula, mainly present on Unga Island (Wilson et al., 1999) and the prolific potential sources of recycled plutonic detritus in Mesozoic strata and the early Tertiary Tolstoi Formation. This latter unit was sourced from the Alaska-Aleutian Range batholith (Detterman et al., 1996). Considerable overlap between compositions of plagioclase clasts and phenocrysts does occur in the An > 30 range (Fig. 5.20). This suggests that volcanic rocks may have sourced detrital plagioclase, especially in the lower- to mid-lower Bear Lake Formation for which all detrital plagioclase clasts (non-albite) overlap with phenocrysts.

5.5 Conclusions

Petrographic identifications of diagenetic mineralogy are mostly supported by EMPA. Zeolites, calcite, kaolinite, and siderite were identified using both methods. I attribute minor disagreement in identification of zeolite and siderite to the low abundance of these minerals in samples for which discrepancies occur, allowing them to go unnoticed during EMPA. Discrepancies in identification of Fe-Mg clays (smectite, chlorite, and corrensite) suggest that "corrensite" as reported petrographically should not be strictly taken to mean mixed-layer smectite-chlorite, but also includes chlorite. I documented ubiquitous albite using EMPA, which the petrographer was not able to identify, but has important implications with regards to the diagenetic history of the Bear Lake Formation. Sericite- and illite-altered feldspar clasts in the Great Basins 1 well are accompanied by a lack of plagioclase clasts (Table 5.8), indicating a unique diagenetic environment relative to the other samples.

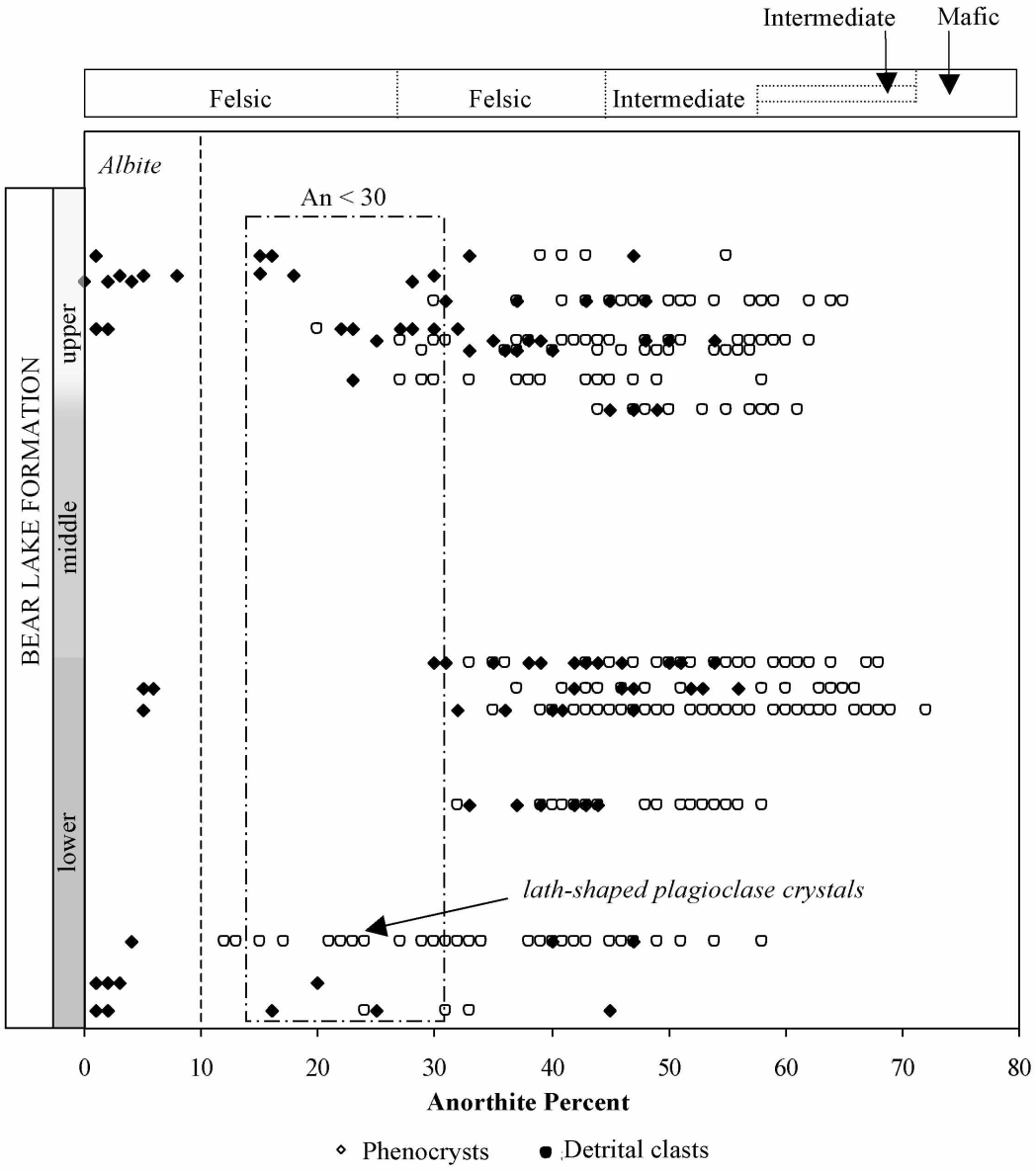

Fig. 5.20 Comparison of detrital and phenocryst plagioclase compositions. A population of detrital plagioclase clasts (enclosed in the box labeled An<30) has lower anorthite percentages than plagioclase phenocrysts in volcanic rock fragments from the Bear Lake Formation. The phenocrysts in the lower Bear Lake Formation that fall into the An < 30 range are lath-shaped plagioclase crystals, and sometimes associated with albite replacement (see section 5.4.2). This figure shows plagioclase compositions from Bear Lake Formation outcrop samples obtained using election microprobe analysis and combines data shown in Fig. 5.13 and Fig. 5.15.

The following factors indicate that volcanic rock fragments in the Bear Lake Formation range from mainly felsic to intermediate composition (dacitic to andesitic): groundmass compositions and corrected groundmass compositions, anorthite content of plagioclase phenocrysts, and the presence of plagioclase ± quartz, K-feldspar, hornblende, and pyroxene phenocrysts. Comparison of groundmass composition of volcanic rock fragments from the Bear Lake Formation to compositions of Aleutian arc volcanic rocks using total alkali-silica and weight percent TiO_2 versus SiO_2 diagrams indicates that the volcanic detritus in the Bear Lake Formation is consistent with volcanic rocks in an arc setting. Specifically, the volcanic clasts were likely derived from the Meshik Volcanics northeast of Port Moller.

Detrital plagioclase clast compositions suggest volcanic origin, since their anorthite contents overlap with those of plagioclase phenocrysts in volcanic rock fragments from the Bear Lake Formation. A granitic source contributed an additional plagioclase population to rocks of the upper Bear Lake Formation and lowermost lower Bear Lake Formation, characterized by more sodic plagioclase ($An < 30$). These clasts were originally derived from the Alaska-Aleutian Range batholith, and may be either primary or recycled through Mesozoic strata and the lower Tertiary Tolstoi Formation.

CHAPTER 6. GEOCHRONOLOGY

6.1 Introduction

It is commonly accepted that the Bear Lake Formation has a less volcanic-rich and more quartzose composition than other Tertiary formations on the Alaska Peninsula (with the exception of the Tolstoi Formation), and that this composition reflects derivation from recycling of Mesozoic sedimentary rocks (Burk, 1965; Lyle et al., 1979; Detterman et al., 1981; Wilson, 1985; Detterman, 1990; Detterman et al., 1996; Wilson et al., 1999). However, petrographic analyses completed as part of this study (see Chapter 4) and recent petrographic studies (Helmold and Brizzolara, 2005; Helmold et al., 2008) show that sandstones of the Bear Lake Formation contain volcanic rock fragments in varying abundances, composing 2% to 57% of the framework and anywhere from 10% to more than 90% of the lithic portion of the framework.

Radiometric dating is one tool that can be used to address provenance of this volcanic input, which has been largely ignored in the literature other than to comment on its relative scarcity. Due to the altered nature of volcanic rock fragments in samples that I used for this study, they are not suitable for $^{40}Ar/^{39}Ar$ dating. Biotite is a mineral commonly dated by the $^{40}Ar/^{39}Ar$ method and can be derived from igneous rocks, but as with the volcanic rock fragments, biotite is commonly altered. Instead, I used detrital hornblende grains due to their relative abundance and commonly unaltered state in selected samples from the upper Bear Lake Formation. Hornblende often provides more accurate $^{40}Ar/^{39}Ar$ date than minerals such as biotite due to hornblende's tight mineral structure which inhibits argon loss (McDougall and Harrison, 1999). Hornblende may be derived from either a volcanic or plutonic source, thereby providing radiometric dates of an igneous source rather than a strictly volcanic source.

6.2 Methods

I prepared hornblende mineral separates for $^{40}Ar/^{39}Ar$ analysis from samples LH1-182, LH1-164, and BL5-95 (Fig. 2.1 and Fig. 2.2). Evaluation of these samples in thin section indicated that they each contain sufficient hornblende to ensure that a large enough population could be obtained. I crushed the hand samples using a mortar and pestle and sieved the crushed material. The 60 to 100 mesh (250 to 150 μm) size fractions contained the most easily recognizable individual hornblende grains. I ultrasonically

cleaned and separated the 250 to 150 μm material using heavy liquids (sodium polytungstate). From the heaviest fraction, I used a hand magnet to separate out magnetic grains, and then handpicked hornblende grains under a binocular microscope. In picking grains, I looked for elongated grain shape and cleavage planes to recognize hornblende. I then submitted the handpicked hornblende grains to the Geochronology Laboratory at UAF. A summary of the analysis procedure provided by Paul Layer (analyst) is as follows:

> The monitor mineral MMhb-1 (Samson and Alexander, 1987) with an age of 513.9 Ma (Lanphere and Dalrymple, 2000) was used to monitor neutron flux (and calculate the irradiation parameter, J). The samples and standards were wrapped in aluminum foil and loaded into aluminum cans of 2.5 cm diameter and 6 cm height. The samples were irradiated in position 5c of the uranium enriched research reactor of McMaster University in Hamilton, Ontario, Canada for 20 megawatt-hours.
>
> Upon their return from the reactor, the samples (individual hornblende crystals) and monitors were loaded into 2 mm diameter holes in a copper tray that was then loaded in a ultra-high vacuum extraction line. The monitors and hornblende crystals were fused in single steps using a 6-watt argon-ion laser following the technique described in York et al. (1981), Layer et al. (1987), and Layer (2000). Argon purification was achieved using a liquid nitrogen cold trap and a SAES Zr-Al getter at 400°C. The samples were analyzed in a VG-3600 mass spectrometer at the Geophysical Institute, University of Alaska Fairbanks. The argon isotopes measured were corrected for system blank and mass discrimination, as well as calcium, potassium and chlorine interference reactions following procedures outlined in McDougall and Harrison (1999). System blanks generally were $2x10^{-16}$ mol ^{40}Ar and $2x10^{-18}$ mol ^{36}Ar which are 10 to 50 times smaller than fraction volumes. Mass discrimination was monitored by running both calibrated air shots and a zero-age glass sample. These measurements were made on a weekly to monthly basis to check for changes in mass discrimination.

6.3 Results

The Geochronology Laboratory analyzed multiple hornblende grains from each sample. They analyzed a total of 35 grains from sample BL5-95, 45 from LH1-182, and 39 from LH1-164. The filtered

data set (Table 6.1, Table, 6.2, Table 6.3, and Fig. 6.1) includes only those grains that I have interpreted to represent hornblende. There are 22 grains from sample BL5-95, 16 from LH1-182, and 19 from LH1-164.

I filtered the data based on groupings of grains that show different behavior related to three main parameters: atmospheric ^{40}Ar, ^{39}Ar release, and Ca/K. High values of atmospheric ^{40}Ar indicate alteration. Values of ^{39}Ar release can be related to both grain size and the amount of K present. In the case of this data set, generally, low ^{39}Ar release values appear to be related more to K content than grain size and I interpret them to represent either altered grains or non-hornblende grains with relatively low K. The grains that show low ^{39}Ar release also commonly have higher Ca/K ratios (Fig. 6.2), supporting my low K content interpretation. In addition, I do not expect grain size to be a major factor as I picked all the grains that were analyzed from the same sieve fraction, and therefore they should be similar in size (250-150 μm).

For sample BL5-95, the two most prominent groupings are related to atmospheric ^{40}Ar and ^{39}Ar release. Atmospheric ^{40}Ar shows two distinct groups (Fig. 6.3). The high group, greater than about 90% atmospheric ^{40}Ar, represents altered grains which I discarded. A discrete break appears in the ^{39}Ar release data around 0.02 (Fig. 6.4). All of the low ^{39}Ar release grains are altered (high atmospheric ^{40}Ar) except for two. I included one as a hornblende and considered the other a non-hornblende. The non-hornblende grain has both low ^{39}Ar release and higher Ca/K, indicating a lower K content, whereas the apparent hornblende's Ca/K ratio (17.4) groups more tightly to the lower range (Fig. 6.5). The low ^{39}Ar release paired with low Ca/K indicates that this hornblende grain may have been smaller than other hornblende grains, but of similar composition (^{39}Ar release related more to grain size than to K content for this grain). I discarded a total of 13 grains based on these parameters (Fig. 6.6).

For sample LH1-182, atmospheric ^{40}Ar is the only parameter that shows an identifiable grouping. Two groups separate around 80% atmospheric ^{40}Ar (Fig. 6.7). I discarded grains which fall into the high group, likely due to alteration. Three grains with atmospheric ^{40}Ar less than 80% have errors larger than their ages. I discarded two of these grains because their ^{39}Ar release values are low (0.0018 and 0.007; Fig. 6.8), apparently contributing to the large errors. The third grain has a Ca/K ratio (25.9) distinctly higher

Table 6.1 $^{40}Ar/^{39}Ar$ single grain fusion data for detrital hornblende grains from sample BL5-95. Weighted average of J from standards = 3.579e-03 ± 1.276e-05. Ages calculated using the constants of Steiger and Jaeger (1977).

$^{40}Ar/^{39}Ar$	±1 σ	$^{37}Ar/^{39}Ar$	±1 σ	$^{36}Ar/^{39}Ar$	±1 σ	% Atmospheric ^{40}Ar	Ca/K	±1 σ	$^{40*/39}K$	±1 σ	Age (Ma)	±1 σ
10.4	0.1	3.33	0.05	0.014	0.002	38.6	6.12	0.09	6.4	0.7	40.7	4.6
13.6	0.2	10.2	0.2	0.024	0.005	46.3	18.9	0.4	7.3	1.4	46.8	8.5
12.8	0.2	8.1	0.1	0.020	0.004	40.6	14.9	0.2	7.6	1.3	48.7	8.1
20.6	0.3	10.2	0.1	0.046	0.004	62.3	18.8	0.3	7.8	1.2	49.8	7.8
10.1	0.1	5.69	0.07	0.008	0.003	18.7	10.5	0.1	8.2	0.9	52.2	5.8
8.48	0.10	4.46	0.05	0.000	0.006	-4.0	8.20	0.10	8.8	1.7	56.0	10.5
12.4	0.1	6.32	0.06	0.013	0.001	26.0	11.7	0.1	9.2	0.4	58.5	2.7
13.6	0.1	5.34	0.04	0.012	0.002	23.6	9.83	0.08	10.4	0.6	66.1	3.7
15.4	0.2	6.8	0.1	0.018	0.002	31.3	12.5	0.2	10.6	0.6	67.4	3.6
17.0	0.2	7.3	0.1	0.019	0.002	30.3	13.5	0.2	11.9	0.6	75.4	3.9
23.8	0.2	6.36	0.06	0.016	0.002	18.2	11.7	0.1	19.5	0.6	121.9	3.5
26.7	0.3	6.44	0.07	0.023	0.003	23.3	11.9	0.1	20.5	1.0	127.8	5.9
26.3	0.3	9.4	0.1	0.021	0.005	20.5	17.4	0.3	21.0	1.4	130.7	8.6
28.5	0.3	7.74	0.08	0.024	0.003	22.2	14.3	0.2	22.2	1.0	138.1	6.0
31.7	0.4	11.2	0.1	0.035	0.003	29.9	20.7	0.3	22.4	1.1	139.2	6.4
27.6	0.3	6.00	0.06	0.013	0.002	12.6	11.0	0.1	24.2	0.6	149.7	3.8
29.2	0.3	5.11	0.06	0.013	0.002	11.9	9.4	0.1	25.8	0.8	159.3	4.6
29.5	0.3	8.63	0.08	0.011	0.003	8.7	15.9	0.1	27.0	0.8	166.6	4.9
30.9	0.3	4.51	0.05	0.012	0.002	10.7	8.30	0.09	27.7	0.6	170.4	3.6
31.3	0.3	4.28	0.04	0.012	0.002	9.9	7.88	0.08	28.2	0.6	173.6	3.6
32.3	0.3	5.04	0.05	0.013	0.002	11.0	9.28	0.10	28.8	0.8	177.2	4.6
32.4	0.2	3.09	0.03	0.005	0.001	3.4	5.68	0.05	31.4	0.4	191.9	2.2

Table 6.2 $^{40}Ar/^{39}Ar$ single grain fusion data for detrital hornblende grains from sample LH1-182. Weighted average of J from standards = 3.579e-03 ± 1.276e-05. Ages calculated using the constants of Steiger and Jaeger (1977).

$^{40}Ar/^{39}Ar$	±1 σ	$^{37}Ar/^{39}Ar$	±1 σ	$^{36}Ar/^{39}Ar$	±1 σ	% Atmospheric ^{40}Ar	Ca/K	±1 σ	$^{40*/39}K$	±1 σ	Age (Ma)	±1 σ
12.1	0.1	4.98	0.07	0.027	0.004	62.7	9.2	0.1	4.5	1.1	28.9	7.0
9.0	0.1	4.27	0.05	0.015	0.003	43.9	7.9	0.1	5.1	0.9	32.4	5.8
11.8	0.1	5.19	0.07	0.022	0.007	52.9	9.6	0.1	5.5	2.1	35.5	13.1
21.1	0.2	8.4	0.1	0.053	0.005	71.7	15.4	0.2	6.0	1.5	38.3	9.3
14.8	0.2	7.6	0.1	0.03	0.01	51.2	14.0	0.2	7.3	3.2	46.3	20.2
16.8	0.2	9.6	0.1	0.029	0.005	45.6	17.8	0.2	9.2	1.4	58.3	8.6
15.9	0.3	5.33	0.09	0.017	0.005	29.7	9.8	0.2	11.2	1.5	70.9	9.0
36.0	0.4	7.6	0.1	0.070	0.008	56.0	14.1	0.2	15.9	2.4	100.0	14.5
19.4	0.4	7.3	0.1	0.010	0.008	12.3	13.4	0.3	17.1	2.3	107.1	14.1
26.1	0.3	4.59	0.05	0.020	0.006	21.4	8.46	0.10	20.6	1.7	128.4	10.1
35.0	0.9	7.8	0.2	0.04	0.01	31.9	14.4	0.4	23.9	3.3	148.2	19.9
31.8	0.4	3.70	0.05	0.020	0.003	17.4	6.81	0.09	26.4	1.0	162.6	6.1
34.1	0.3	7.24	0.08	0.026	0.006	20.6	13.4	0.1	27.2	1.7	167.8	10.3
32.9	0.3	4.63	0.05	0.014	0.005	11.4	8.52	0.09	29.2	1.5	179.5	9.0
32.0	0.2	2.96	0.03	0.010	0.003	8.7	5.45	0.06	29.3	0.9	179.8	5.2
34.8	0.3	7.11	0.08	0.020	0.003	15.6	13.1	0.1	29.5	1.0	181.0	5.8

Table 6.3 $^{40}Ar/^{39}Ar$ single grain fusion data for detrital hornblende grains from sample LH1-164. Weighted average of J from standards = 3.579e-03 ± 1.276e-05. Ages calculated using the constants of Steiger and Jaeger (1977).

$^{40}Ar/^{39}Ar$	±1 σ	$^{37}Ar/^{39}Ar$	±1 σ	$^{36}Ar/^{39}Ar$	±1 σ	% Atmospheric ^{40}Ar	Ca/K	±1 σ	$^{40*/39}K$	±1 σ	Age (Ma)	±1 σ
9.6	0.2	10.1	0.3	0.026	0.005	70.3	18.6	0.5	2.9	1.6	18.4	10.4
5.98	0.09	10.2	0.2	0.009	0.005	29.0	18.9	0.3	4.3	1.4	27.3	8.7
17.1	0.3	1.33	0.03	0.040	0.004	68.9	2.44	0.05	5.3	1.2	34.0	7.8
7.9	0.2	7.6	0.2	0.011	0.002	32.6	14.1	0.3	5.3	0.7	34.0	4.4
11.9	0.1	8.64	0.08	0.017	0.002	37.6	16.0	0.2	7.4	0.7	47.4	4.4
12.1	0.2	3.46	0.05	0.016	0.003	36.4	6.37	0.09	7.7	1.0	49.1	6.3
12.1	0.2	7.3	0.1	0.014	0.002	29.3	13.5	0.2	8.6	0.5	54.6	3.0
12.5	0.1	5.42	0.07	0.012	0.005	24.0	10.0	0.1	9.5	1.3	60.6	8.4
12.7	0.1	5.79	0.07	0.012	0.003	23.9	10.7	0.1	9.7	1.0	61.5	6.5
12.1	0.1	4.90	0.07	0.008	0.002	16.8	9.0	0.1	10.1	0.5	63.8	3.0
16.3	0.2	7.7	0.1	0.015	0.006	24.0	14.3	0.2	12.4	1.8	78.4	11.0
28.1	0.5	7.9	0.2	0.025	0.004	23.7	14.6	0.3	21.5	1.3	134.0	7.5
28.2	0.3	7.43	0.07	0.016	0.002	15.0	13.7	0.1	24.0	0.7	148.9	3.9
28.0	0.3	7.30	0.08	0.013	0.002	12.1	13.5	0.2	24.7	0.7	153.1	4.1
30.3	0.3	5.04	0.07	0.016	0.006	14.5	9.3	0.1	25.9	1.8	160.2	10.4
30.4	0.4	6.00	0.09	0.015	0.004	12.9	11.1	0.2	26.6	1.3	163.9	7.8
32.9	0.5	3.58	0.06	0.013	0.002	11.0	6.6	0.1	29.4	0.8	180.3	4.4
32.4	0.5	5.88	0.09	0.010	0.004	8.0	10.8	0.2	30.0	1.2	183.8	7.2
37.2	0.5	8.8	0.1	0.021	0.002	15.1	16.3	0.2	31.7	0.6	194.0	3.5

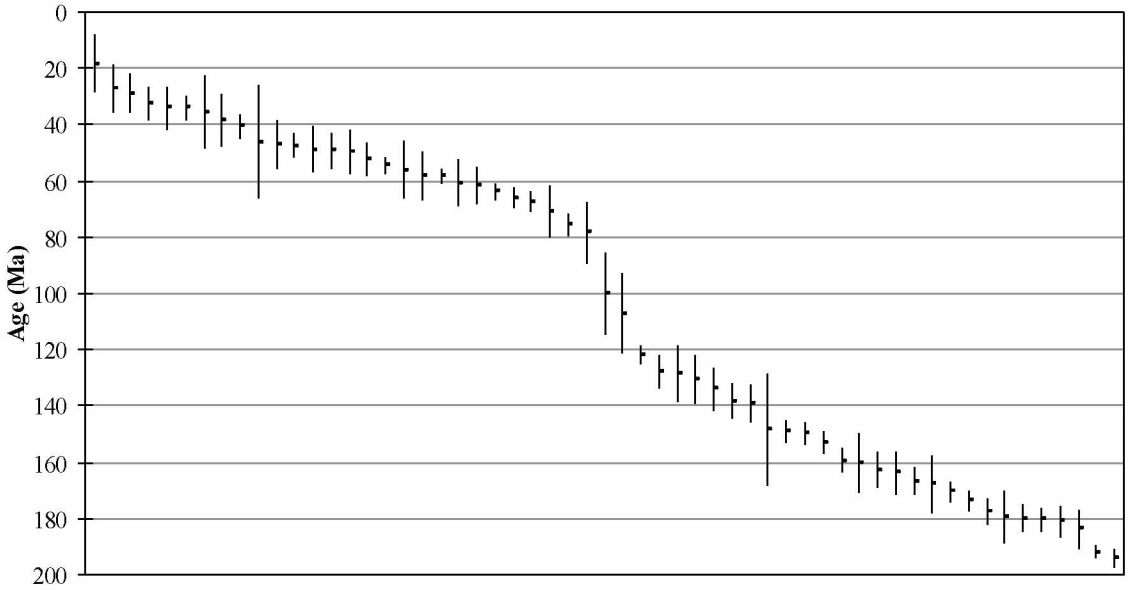

Fig. 6.1 $^{40}Ar/^{39}Ar$ ages of representative detrital hornblende grains from the Bear Lake Formation. This plot shows data for samples BL5-95, LH1-182, and LH1-164 with 1σ error bars. See Table 6.1, Table 6.2, and Table 6.3 for data.

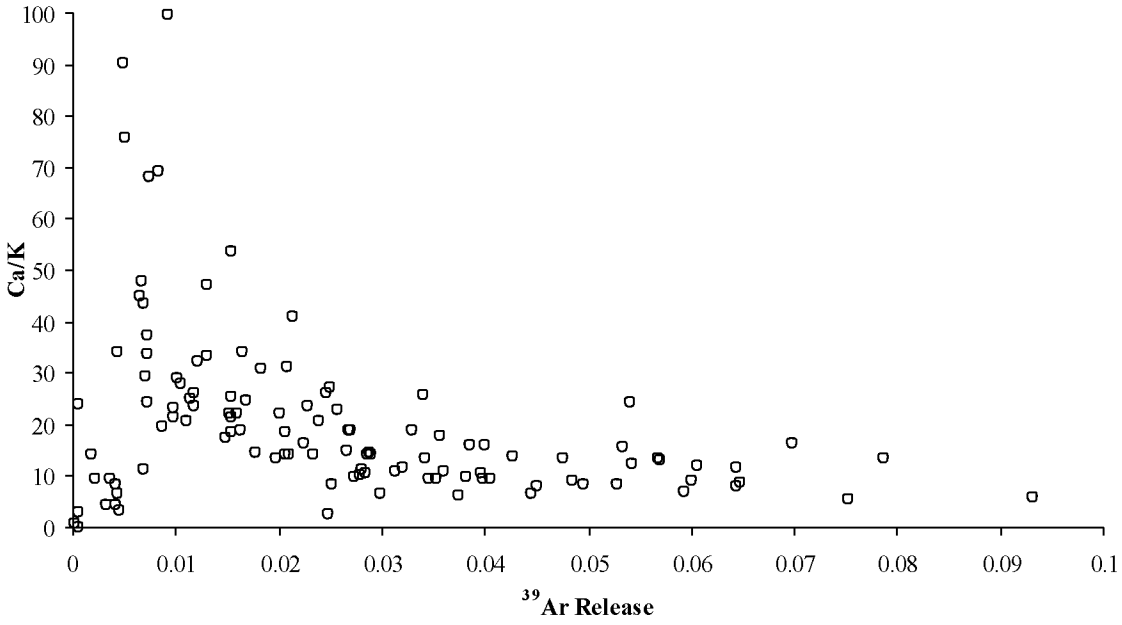

Fig. 6.2 ^{39}Ar release versus Ca/K plot for samples BL5-95, LH1-182, and LH1-164. Five additional points plot beyond the limits of the y-axis scale that I used for clarity. They plot at (0.0006, -0.2), (0.0009, 738), (0.0009, 1201), (0.0009, 1402), (0.0013, 504).

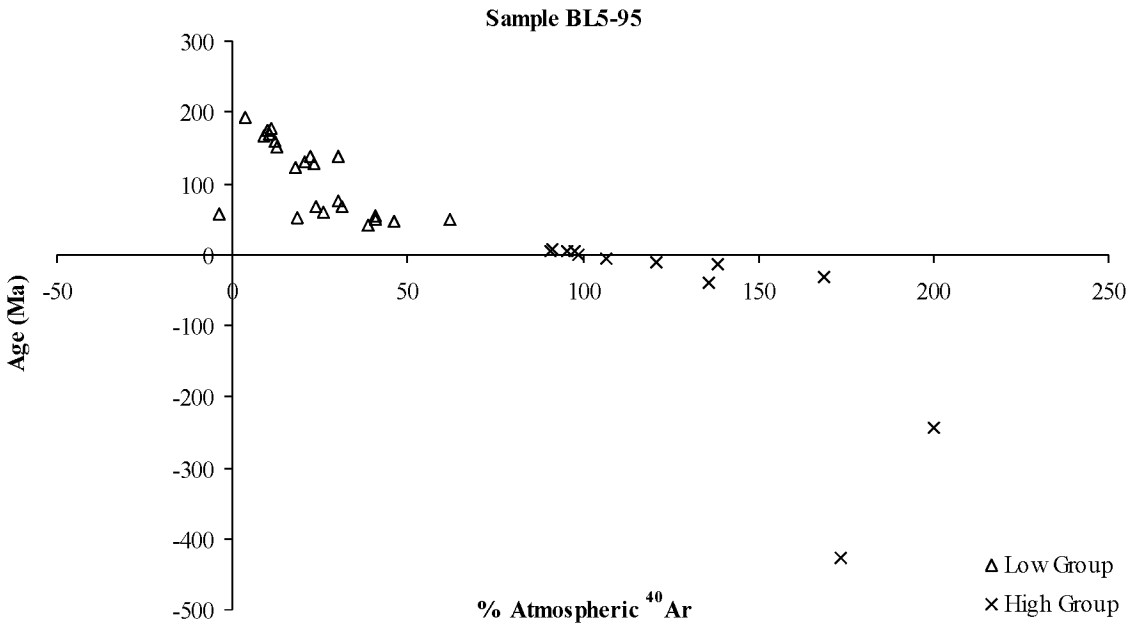

Fig. 6.3 Atmospheric ^{40}Ar versus calculated age plot for grains analyzed from sample BL5-95. See Table 6.1 for data.

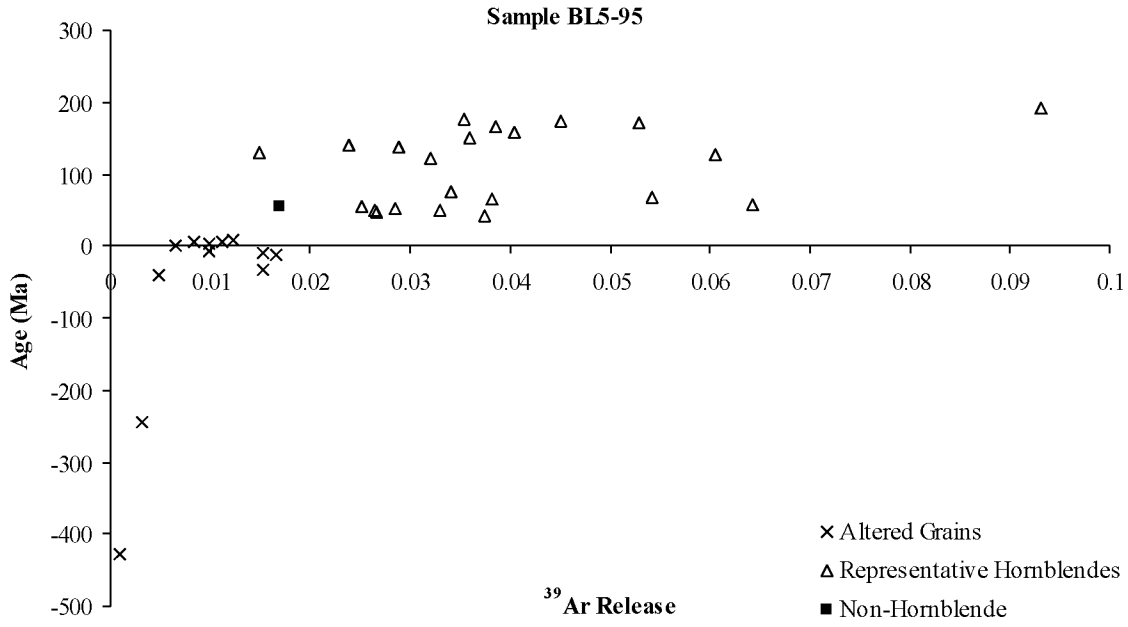

Fig. 6.4 ^{39}Ar release versus calculated age plot for grains analyzed from sample BL5-95.

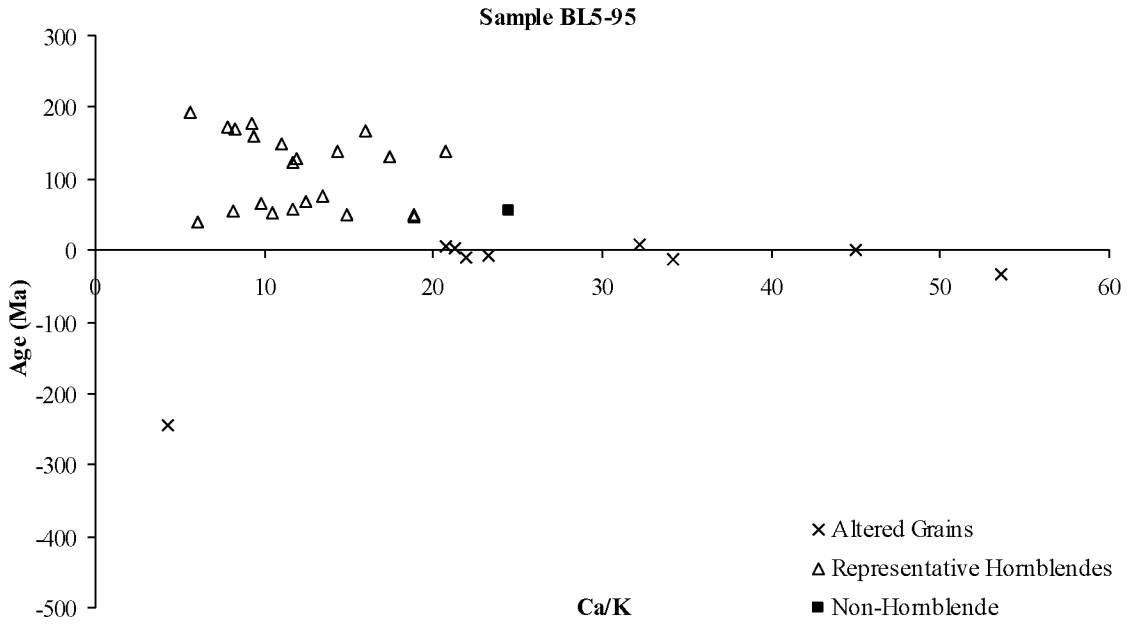

Fig. 6.5 Ca/K versus calculated age plot for grains analyzed from sample BL5-95. Three additional points plot beyond the limits of the scale that I used for clarity. They plot at (69, 6), (90, -41), and (738, -428). See Table 6.1 for data.

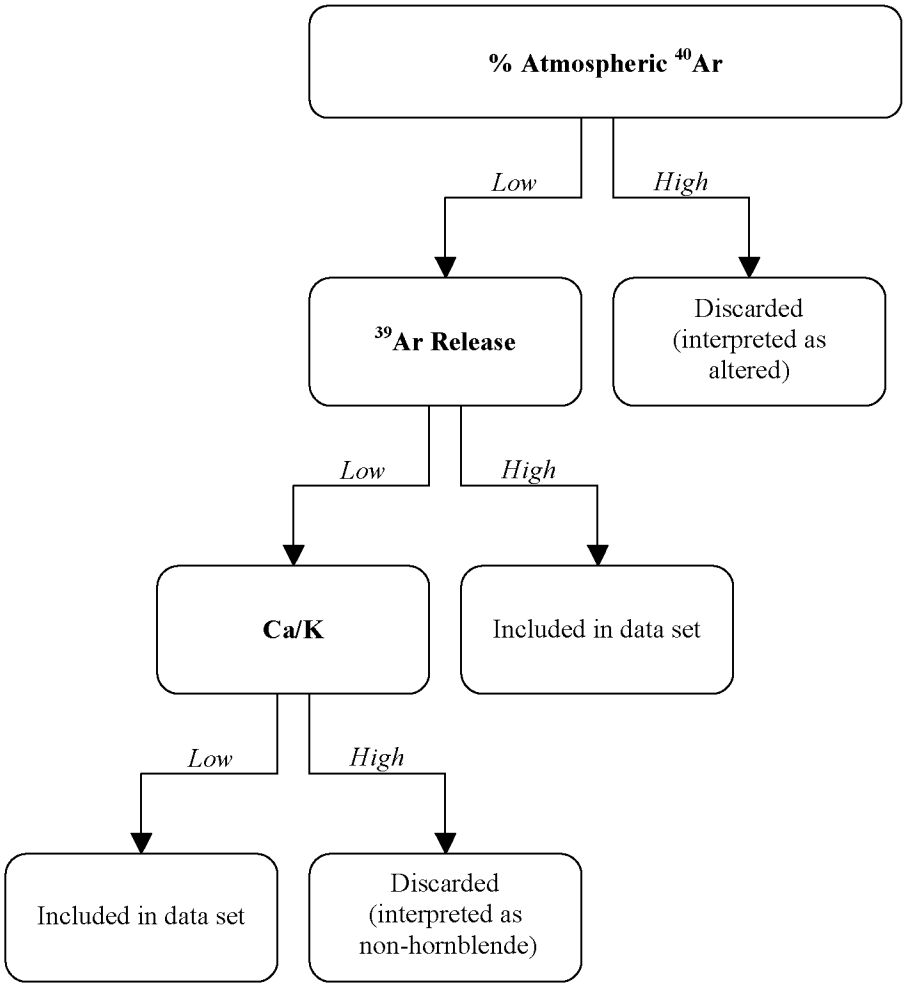

Fig. 6.6 Flowchart illustrating parameters used for filtering of $^{40}Ar/^{39}Ar$ data for sample BL5-95.

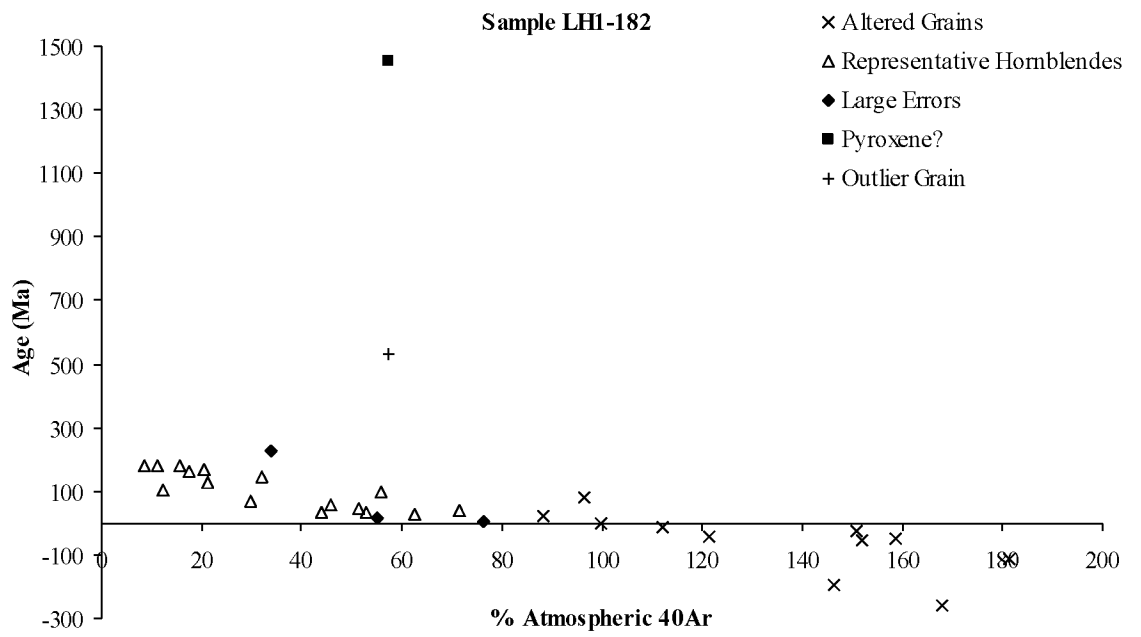

Fig. 6.7 Atmospheric ^{40}Ar versus calculated age plot for grains analyzed from sample LH1-182. Thirteen additional points plot beyond the limits of the scale that I used for clarity. They plot at (110, -9877), (208, -1413), (211, -57), (223, -68), (233, -280), (242, -66), (244, -743), (254, -3897), (300, -55), (315, -74), (370, -815), (417, -567), and (472, -1566). See Table 6.2 for data.

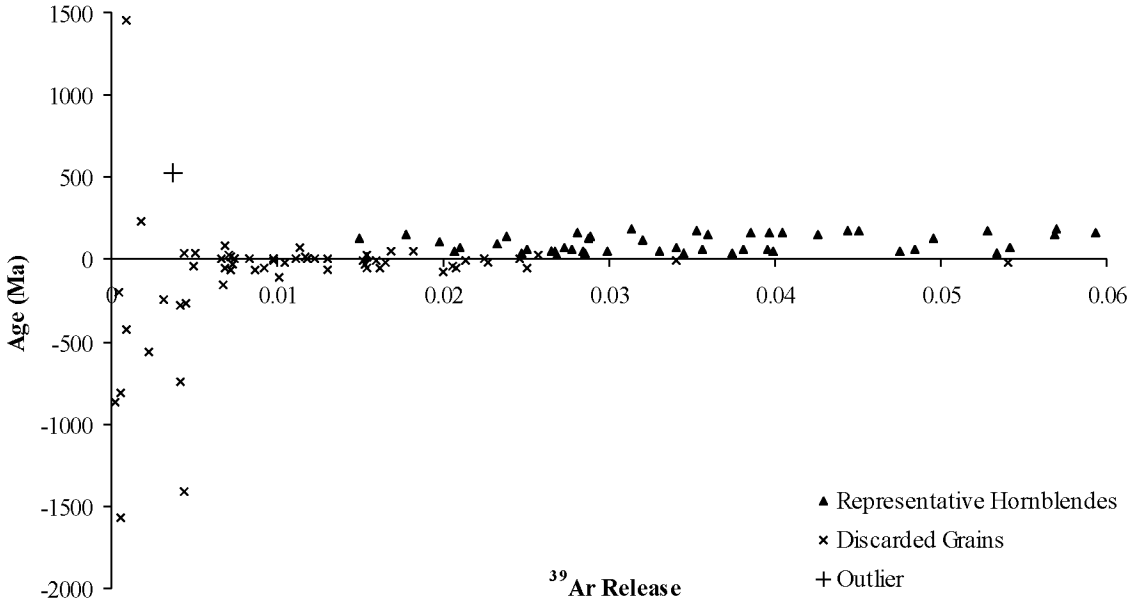

Fig. 6.8 ^{39}Ar release versus calculated age plot for samples BL5-95, LH1-182, and LH1-164. Several additional points plot beyond the limits of the scale that I used for clarity. All those that plot above 0.06 ^{39}Ar release are representative hornblendes.

than all hornblende grains (Table 6.2), indicating that it has a different composition and is considered a non-hornblende. I considered grains with low atmospheric ^{40}Ar and errors less than their ages to be hornblende, except for two. One is clearly a non-hornblende with very high Ca/K and low ^{39}Ar release (1201 and 0.0009 respectively), and is likely a pyroxene. The second grain appears to be an outlier. Its nature is unclear, but it is evident that this grain differs from all other hornblende grains in the entire dataset as indicated by its low ^{39}Ar release value and considerably older age (Fig. 6.8). It also has a much smaller Cl/K ratio. Following these criteria, I discarded a total of 29 grains (Fig. 6.9).

For sample LH1-164, the two most prominent groupings relate to atmospheric ^{40}Ar and Ca/K. Two groups separate around 75% atmospheric ^{40}Ar (Fig. 6.10). I discarded grains which fall into the high group due to alteration. The Ca/K plot shows a difference in the character of the grains with values greater than 20 (Fig. 6.11). Most are altered (high atmospheric ^{40}Ar) and three have large errors (almost as large as or larger than their ages). Groupings based on ^{39}Ar release are more ambiguous (Fig. 6.12). However, it is clear that the three grains with large errors have low ^{39}Ar release apparently causing the lack of precision. Three additional grains have Ca/K ratios greater than 20 (Fig. 6.11). They also have ^{39}Ar release values that fall in the lower range and are interpreted to be non-hornblendes (Fig. 6.12). Although their ^{39}Ar release values mingle with others that I considered hornblende, these three specifically have distinctly higher Ca/K, indicating that they have a different composition (lower K). The grains that I interpreted to be hornblende that "overlap" with discarded grains in the low end of ^{39}Ar release all have Ca/K ratios that group below 20 (Fig. 6.11 and Fig. 6.12). The combination of low ^{39}Ar release and low Ca/K (also seen in one hornblende grain from BL5-95) seems to indicate that these grains are smaller than the rest as opposed to being of a different composition (^{39}Ar release related more to grain size than to K content). Based on these parameters, I discarded a total of 20 grains (Fig. 6.13).

The filtered dataset includes a total of 57 grains that I considered to represent hornblende. Ages range from 18.4 ± 10.4 Ma to 194.0 ± 3.5 Ma (Early Miocene to Early Jurassic), with a noticeable separation around 100 Ma in the middle of the Cretaceous (Table 6.1, Table 6.2, Table 6.3, and Fig. 6.1).

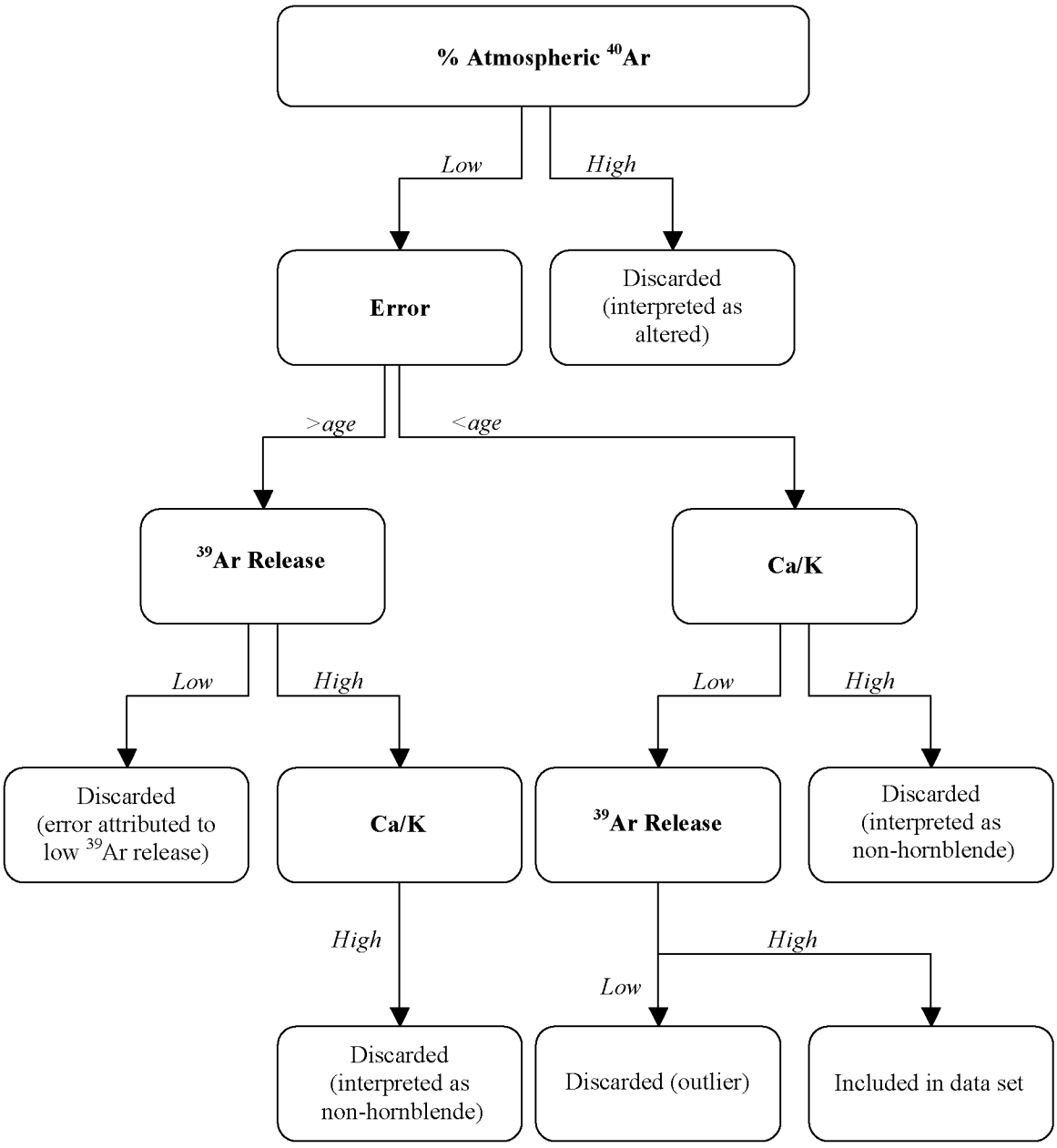

Fig. 6.9 Flowchart illustrating parameters used for filtering of $^{40}Ar/^{39}Ar$ data for sample LH1-182.

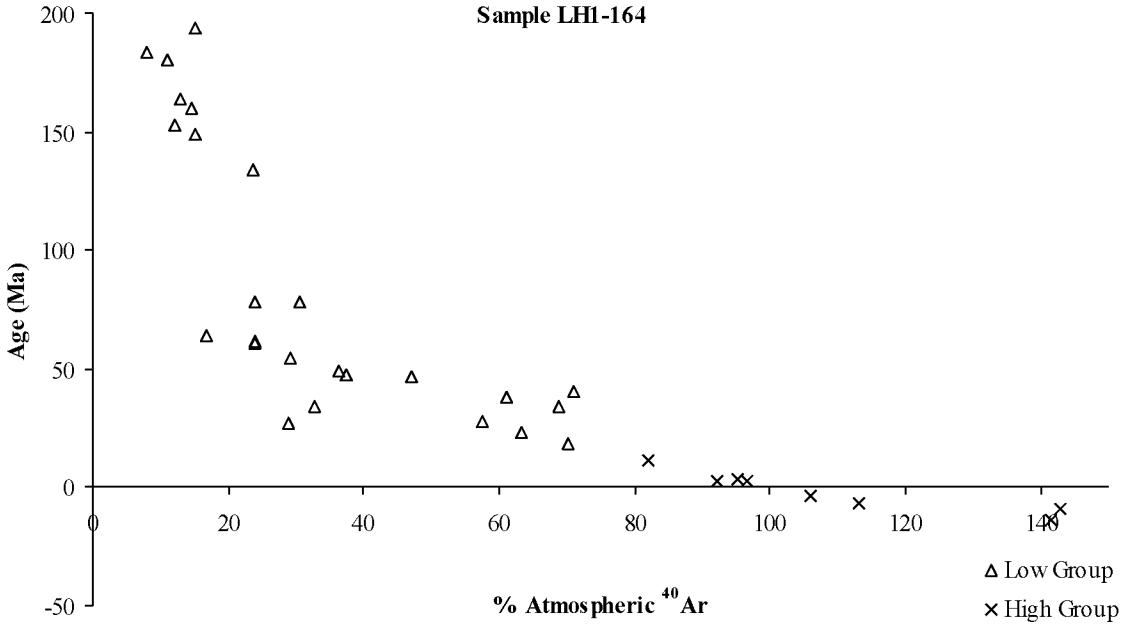

Fig. 6.10 Atmospheric ^{40}Ar versus calculated age plot for grains analyzed from sample LH1-164. Six additional points plot beyond the limits of the scale that I used for clarity. They plot at (176, -18), (192, -47), (193, -52), (236, -872), (260, -65), (438, -158). See Table 6.3 for data.

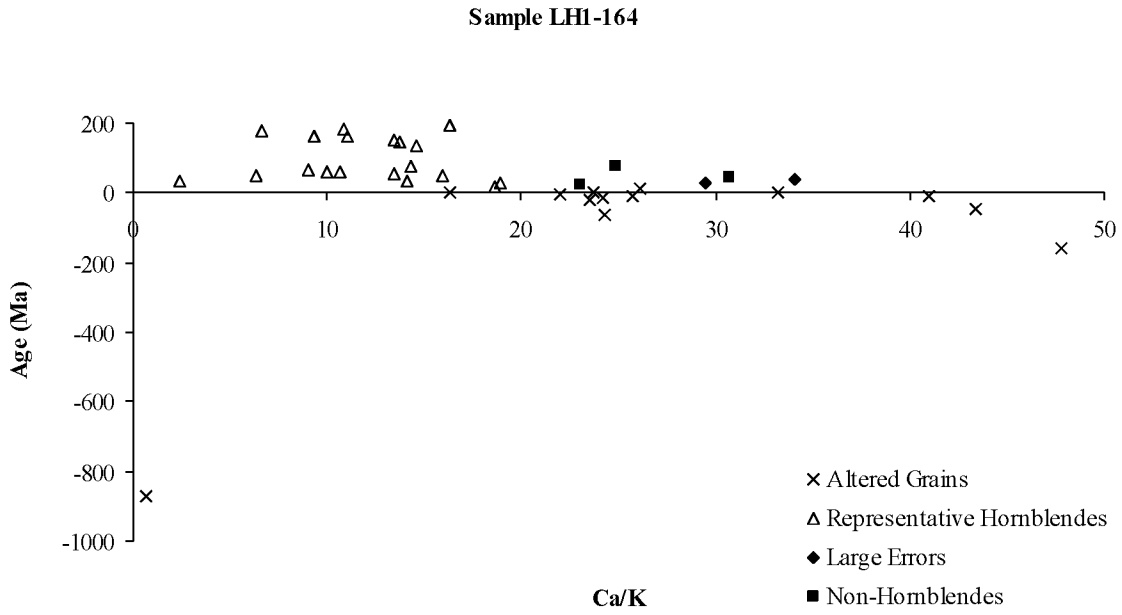

Fig. 6.11 Ca/K versus calculated age plot for grains analyzed from sample LH1-164. Two additional points plot beyond the limits of the scale that I used for clarity. They plot at (75, 38), which has a large error, and (100, -52). See Table 6.3 for data.

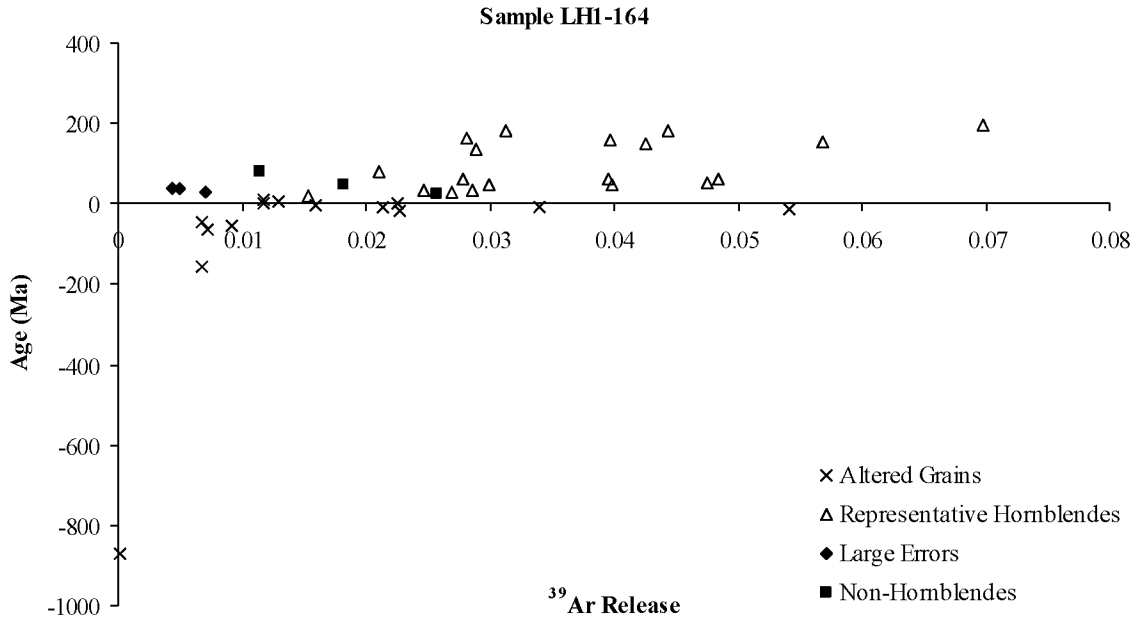

Fig. 6.12 ^{39}Ar release versus calculated age plot for sample LH1-164.

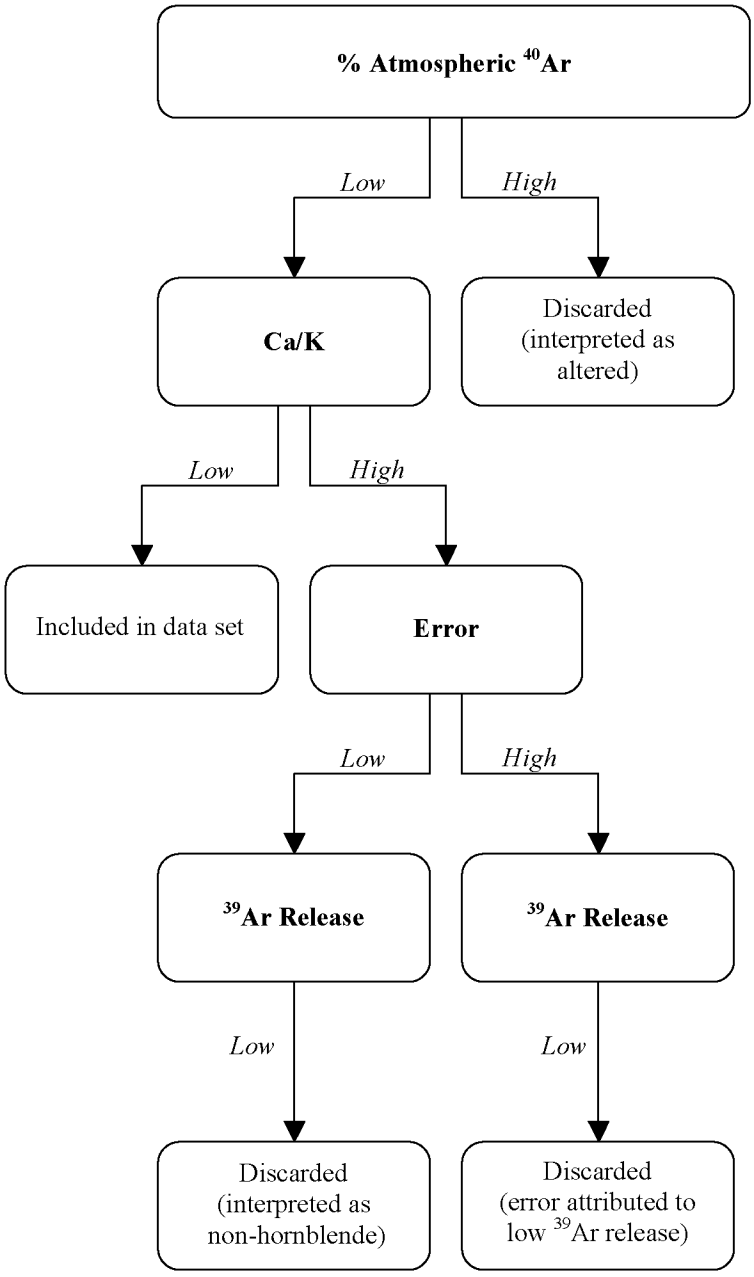

Fig. 6.13 Flowchart illustrating parameters used for filtering of $^{40}Ar/^{39}Ar$ data for sample LH1-164.

Probability histograms show four modes representing four distinct ages of source material: 1) Jurassic, 2) Early Cretaceous, 3) Paleocene to Early Eocene, and 4) Eocene to Oligocene (Fig. 6.14). I interpret the youngest age measured, 18.4 ± 10.4 Ma, to be a part of the Eocene to Oligocene range because it is the only Miocene age obtained and falls into the Eocene to Oligocene range within error.

Sample BL5-95 clearly lacks mode 4 and shows prominent peaks for the other three modes. Sample LH1-182 shows all four modes, although mode 3 is noticeably muted compared to the other two samples and mode 2 does not stand out appreciably. Sample LH1-164 shows all four modes, with mode 2 being the least prominent. Two data points for sample LH1-182 showing ages of 100.0 ± 14.5 Ma and 107.1 ± 14.1 Ma obscure mode 2.

6.3 Discussion

6.3.1 Potential Igneous Source Rocks on the Alaska Peninsula

Detrital hornblende grains from three samples of the upper Bear Lake Formation show a wide range of $^{40}Ar/^{39}Ar$ dates. I identified four modes within this range (Fig. 6.14), and the modes can be attributed to specific source units on the Alaska Peninsula in order to refine provenance interpretation for the Bear Lake Formation. Several possible primary sources of igneous rocks on the Alaska Peninsula correspond to the ages obtained for Bear Lake Formation hornblendes (Fig. 6.15). These potential sources include three intrusive episodes of the Alaska-Aleutian Range batholith, Shumagin batholith, volcanic and hypabyssal rocks of the Meshik arc (Fig. 6.15). Each of these units have been suggested as source material for the Bear Lake Formation (Burk, 1965; Wisehart, 1971; Nilsen, 1984; Wilson, 1985; Detterman, 1990; Detterman et al., 1996). Plutons exposed along the Pacific coast of the Alaska Peninsula are late Tertiary in age (Late Miocene to Pliocene), based on K-Ar radiometric dates (Wilson et al., 1981; Wilson and Shew, 1992; Detterman et al., 1996; Wilson et al., 1999). Previous authors who considered these intrusive rocks to be of middle Tertiary age (prior to availability of K-Ar dates) suggested that the coastal batholiths sourced granitic material found in the Bear Lake Formation (Burk, 1965; Wisehart, 1971; Lyle et al., 1979). The $^{40}Ar/^{39}Ar$ dates I obtained for detrital hornblende of the upper Bear Lake Formation show that these

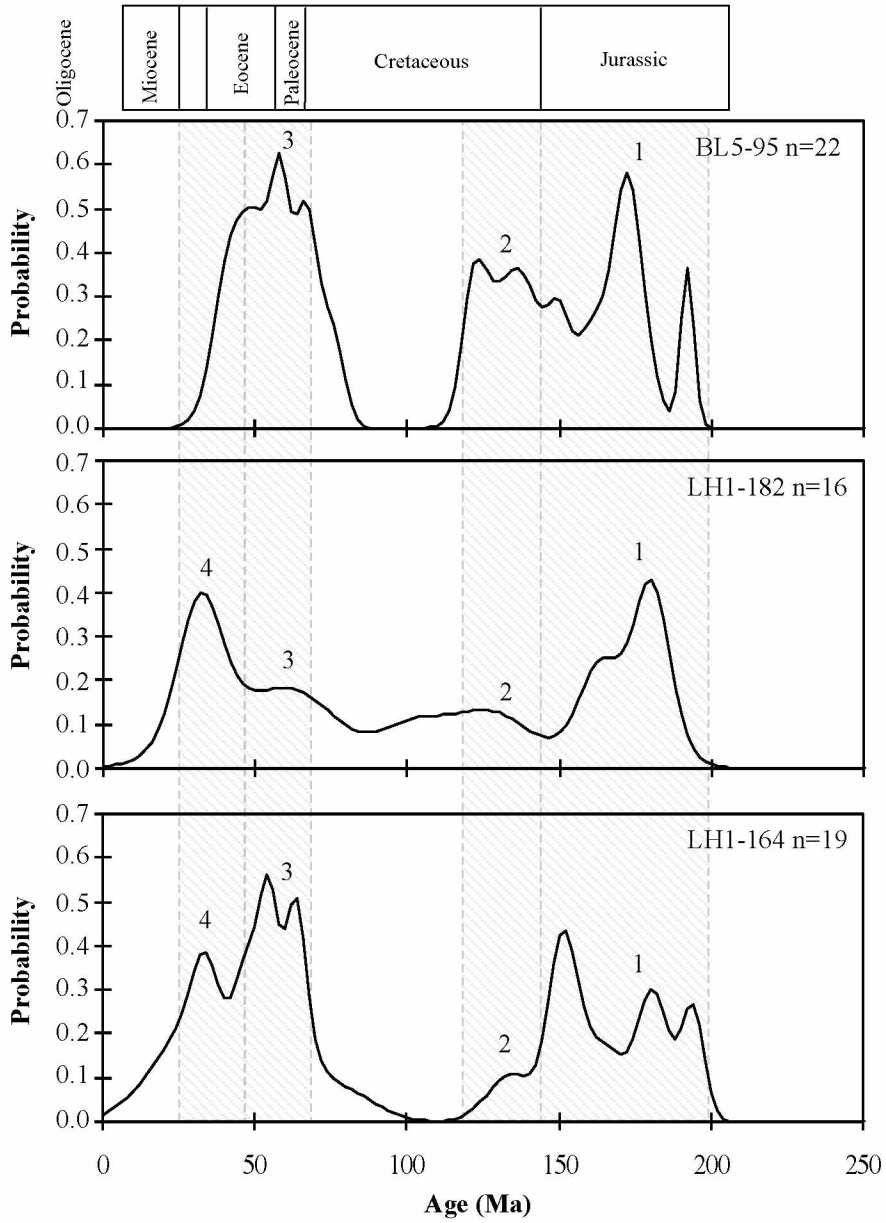

Fig. 6.14 Probability distribution of detrital hornblende ages. This figure shows $^{40}Ar/^{39}Ar$ age distribution for representative hornblende grains from samples BL5-95, LH1-182, and LH1-164 (Table 6.1, Table 6.2, and Table 6.3). Numbers 1 through 4 refer to modes discussed in text.

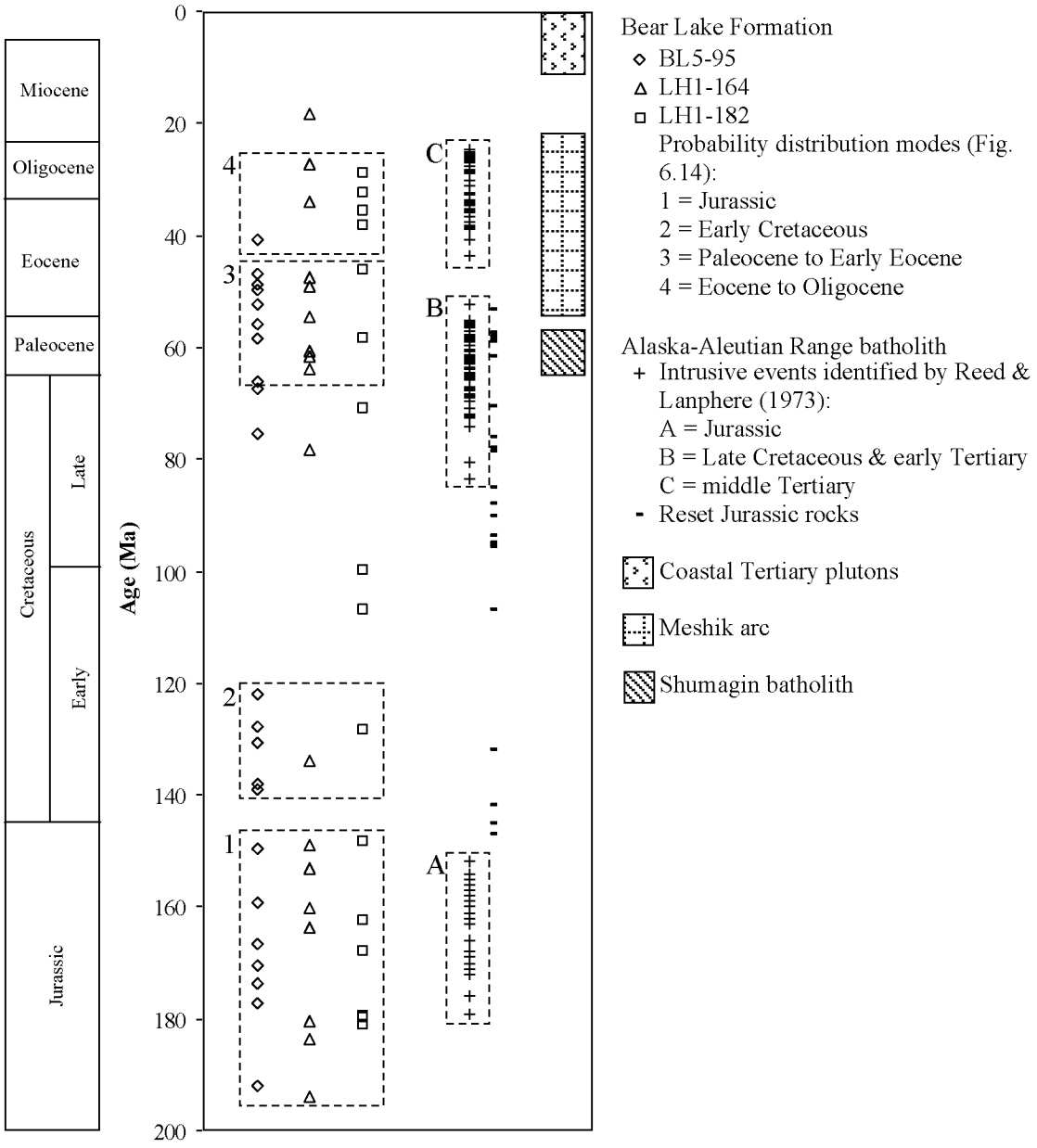

Fig. 6.15 Plot of ages for Bear Lake Formation hornblende and igneous rocks of the Alaska Peninsula. Alaska-Aleutian Range batholith ages represent K-Ar dates of mainly biotite and hornblende (Reed and Lanphere, 1973). Sources of the age ranges I plotted for other igneous rocks are as follows: Meshik arc (Wilson, 1985; Wilson et al., 1994); Shumagin batholith (Wilson et al., 1999); Coastal Tertiary plutons (Detterman et al., 1996; Wilson et al., 1999).

plutons are too young to have sourced any material dated in this study (Fig. 6.15). Other than these primary sources of igneous rocks, it is possible that the hornblende dated is second cycle and was eroded from Mesozoic sedimentary rocks which received first cycle plutonic input.

The Alaska-Aleutian Range batholith is exposed north of Becharof Lake, approximately 300 km northeast of Port Moller, and is primarily composed of hornblende-biotite granodiorite, with quartz diorite and granite locally present (Fig. 6.16; Detterman et al., 1996). The Jurassic intrusive rocks of the batholith (176 Ma to 156 Ma) form the majority of the southern exposure, whereas the Late Cretaceous and early Tertiary intrusive rocks (85 Ma to 58 Ma) are located in the northern part of the batholith (Reed and Lanphere, 1969; 1972; 1973; 1974). Given the batholith's distant location from the Port Moller area of the Alaska Peninsula it is likely that the plutonic rocks did not serve as a primary source of sediment for the Bear Lake Formation on the southwest end of the peninsula. The Jurassic intrusive rocks were the main source for the Late Jurassic Naknek Formation, which is widespread on the Alaska Peninsula and commonly contains accessory green hornblende, and granitic cobbles in conglomerate (McLean, 1979; Detterman et al., 1996; Wilson et al., 1999). Recycling of the Naknek and input from the batholith continued to be a source of later Mesozoic sedimentary units (Lankford and Magoon, 1977; Wilson, 1980; Detterman, 1990; Detterman et al., 1996; Wilson et al., 1999). Notably, composition of the Late Cretaceous Chignik Formation indicates erosion of a plutonic source as well as input from the Naknek Formation (Wilson, 1980; Detterman, 1990). The Chignik Formation also contains conglomerate clasts with granitic composition (Wilson et al., 1999) amenable to serve as a source for recycling of younger units such as the Bear Lake Formation.

The Shumagin batholith is exposed in the outer Shumagin Islands (Fig. 6.16; Burk, 1965; Moore, 1974a; b; Kienle and Turner, 1976; Wilson et al., 1999). These intrusive rocks are biotite-granodiorite and granite (Wilson et al., 1999) and consist of about 20% quartz, 50% plagioclase, 25% K-feldspar, and 5% biotite (Burk, 1965). Muscovite and biotite from granodiorite yield Paleocene K-Ar ages ranging from 65.6 ± 3.3 Ma to 57.4 ± 1.8 Ma (Burk, 1965; Moore, 1974a; Kienle and Turner, 1976; Wilson, 1980; Wilson et al., 1994; Wilson et al., 1999). Additionally, one zircon from a biotite-granodiorite yielded a

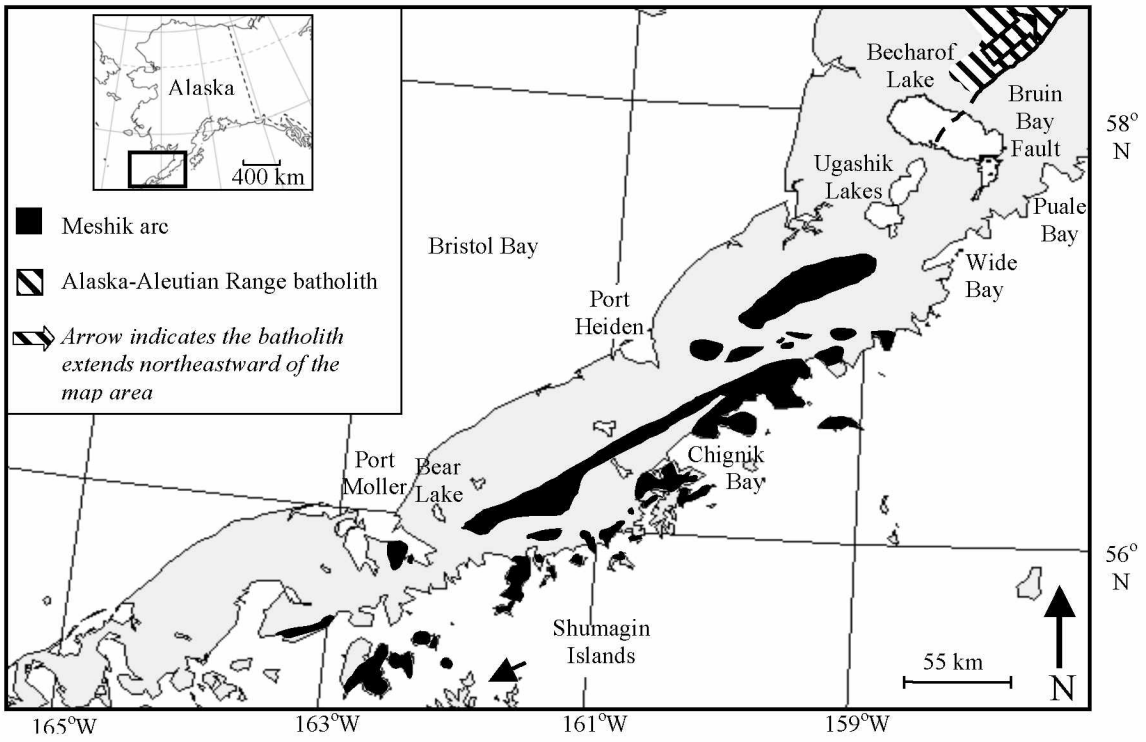

Fig. 6.16 Map showing generalized location of Meshik arc rocks and the Alaska-Aleutian Range batholith. Meshik arc rocks distribution is from Wilson (1985) and Wilson et al. (1999). Alaska-Aleutian Range batholith exposure is from Reed and Lanphere (1973).

$^{206}Pb/^{238}U$ date of 61.1 ± 0.3 Ma (Bradley et al., 2000). However, descriptions of the Shumagin intrusive rocks indicate an absence of hornblende (Grantz, 1963; Burk, 1965; Moore, 1974a; 1974b; Kienle and Turner, 1976; Wilson, 1980; Wilson et al., 1994; Detterman et al., 1996; Wilson et al., 1999; Wilson, F.H., personal communication, 2007). Therefore, the Shumagin batholith has to be ruled out as a contributor of hornblende to the Bear Lake Formation.

Volcanic and hypabyssal rocks of the Meshik arc (Meshik Volcanics) are Eocene to earliest Miocene with whole-rock, biotite, hornblende, and plagioclase K-Ar dates ranging from 54 Ma to 22 Ma (Wilson, 1980; Wilson et al., 1981; Wilson, 1985; Wilson et al., 1994). Exposures are present on the southwest end of the Alaska Peninsula in the vicinity of Port Moller and Bear Lake, extending northeast on the Pacific side of the peninsula as far as the Ugashik Lakes (Fig. 6.16; Wilson, 1985). The Meshik Volcanics include hornblende-bearing basalt to dacite, with hornblende being the dominant mafic phenocryst in basalts and andesites (Wilson, 1985).

6.3.2 Sources of Detrital Hornblende in the Upper Bear Lake Formation

6.3.2.1 Jurassic

Mode 1 identified on probability histograms of hornblende ages from the upper Bear Lake Formation indicates a Jurassic source (Fig. 6.14). This corresponds to the 176 Ma to 154 Ma Jurassic intrusive event of the Alaska-Aleutian Range batholith identified by (Fig. 6.15; Reed and Lanphere, 1969; 1972; 1973). However, as discussed above (section 6.3.1), the remote location of the batholith in relation to Port Moller suggests that the Jurassic source does not reflect primary erosion of the Alaska-Aleutian Range batholith. The Late Jurassic Naknek Formation is a much more likely source for mode 1. Additional input from the Chignik Formation is also a possibility, given that it was partially sourced from the Jurassic Naknek Formation as well as plutonic rocks of the Alaska-Aleutian Range batholith (Wilson, 1980; Detterman, 1990; Detterman et al., 1996). Therefore, I interpret mode 1 to represent recycling of Mesozoic sedimentary rocks, which were originally sourced directly from the Jurassic rocks of the Alaska-Aleutian Range batholith, and possible additional input from second cycle Naknek Formation (out of conglomerates of the Chignik Formation). Mode 1 is a prominent source in all three samples from the Bear

Lake Formation, indicating that this source was a consistent contributor during deposition of the upper Bear Lake Formation.

6.3.2.2 Early Cretaceous

Mode 2 identified on probability histograms of hornblende ages from the upper Bear Lake Formation indicates an Early Cretaceous source (Fig. 6.14). This age corresponds to the Jurassic plutonic rocks of the Alaska-Aleutian Range batholith whose ages have been reset by Cretaceous intrusions. Reed and Lanphere (1973) report ages of Jurassic rocks that have been reset by Tertiary and Cretaceous intrusive events, and hornblende ages from the Bear Lake Formation overlap with the reset Cretaceous ages (Fig. 6.15). As with the Jurassic source of mode 1, the remoteness of exposures of the Alaska-Aleutian Range batholith with respect to Port Moller (approximately 300 km) indicates that this Early Cretaceous source does not necessarily reflect primary erosion of the batholith. Again, a recycled source is more likely.

The Late Jurassic age of the Naknek Formation precludes it as a source for the Early Cretaceous hornblende of mode 2 (Fig. 6.14). Biotite from a granite cobble of the Chignik Formation has been dated as middle Cretaceous (89.9 Ma; Wilson, 1980; Wilson et al., 1981). This age falls into the range of Jurassic plutonic rocks of the Alaska-Aleutian Range batholith whose ages have been reset by Cretaceous intrusions (Fig. 6.15). Therefore, I interpret the Early Cretaceous source identified for the Bear Lake Formation (mode 2, Fig. 6.14) to represent recycling of material from the Chignik Formation, originally derived from Cretaceous-altered Jurassic plutonic rocks of the Alaska-Aleutian Range batholith. This mode is most prominent in sample BL5-95 and fairly subdued in both LH1-182 and LH1-164 (Fig. 6.15). Given the combined prominence of modes 1 and 2 in BL5-95, this sample appears to have received greater input from recycled Mesozoic formations than LH1-182 and LH1-164.

6.3.2.3 Paleocene to Early Eocene

Mode 3 identified on probability histograms of hornblende ages from the upper Bear Lake Formation indicates a Paleocene to Early Eocene source (Fig. 6.14). This corresponds to the Late Cretaceous and early Tertiary intrusive event of the Alaska-Aleutian Range batholith identified by Reed and Lanphere (1969; 1972; 1973), and to earliest rocks of the Meshik arc (Fig. 6.15). Mode 3 also overlaps

with the Paleocene Shumagin batholith (Fig. 6.15). However, the composition of the Shumagin batholith precludes it as source of hornblende, as discussed above (section 6.3.1).

There have been no Paleocene age determinations for rocks associated with the Meshik arc, and the Late Cretaceous and early Tertiary intrusive event of the Alaska-Aleutian Range batholith identified by Reed and Lanphere (1973) is not related to the Meshik arc (Wilson, 1980). The only plausible primary source for upper Bear Lake Formation Paleocene hornblende, and hornblende showing ages scattered in the Late Cretaceous (Fig. 6.15), are the Late Cretaceous early Tertiary plutonic rocks of the Alaska-Aleutian Range batholith. This intrusive event within the batholith is present in the northern area of the batholith, further north than the Jurassic rocks (Reed and Lanphere, 1969; 1972; 1973; 1974). Thus, they are even more remote to the Port Moller area than Jurassic exposures.

The Mesozoic sedimentary strata that are postulated to have sourced recycled detritus of the batholith (modes 1 and 2) are not viable sources of Paleocene age detritus. However, the Late Paleocene to Middle Eocene Tolstoi Formation contains detritus from both reworked Mesozoic sedimentary strata and the Alaska-Aleutian Range batholith (Detterman et al., 1996). Therefore, the Tolstoi Formation is a likely source for second cycle Paleocene detritus originally sourced from the Alaska-Aleutian Range batholith.

Mode 3 is most prominent in samples BL5-95 and LH1-164 (Fig. 6.14). This mode shows two peaks in these samples. The first peak is of Paleocene age and the second peak is of earliest Eocene age (Fig. 6.14). I interpret these two peaks to represent two separate sources. The Paleocene peak of mode 3 represents recycling of the Tolstoi Formation, originally sourced from Late Cretaceous and early Tertiary plutonic rocks of the Alaska-Aleutian Range batholith. The earliest Eocene peak of mode 3 represents erosion of early deposits of the Meshik arc.

6.3.2.4 Eocene to Oligocene

Mode 4 identified on probability histograms of hornblende ages from the upper Bear Lake Formation indicates an Eocene to Oligocene source (Fig. 6.14). This corresponds to both the middle Tertiary intrusive event of the Alaska-Aleutian Range batholith identified by Reed and Lanphere (1969; 1972; 1973) and to the Meshik arc (Fig. 6.15). Again, recycling of plutonic input is more likely than primary derivation due to the distance from Port Moller to the exposures of the Alaska-Aleutian Range

batholith. Volcanic activity associated with the Meshik arc in earliest Eocene through Oligocene time caused sedimentation to shift from a predominantly plutonic and Mesozoic recycled source to contemporaneous volcanic deposits, as indicated by the widespread Meshik Volcanics and the composition of the sedimentary volcaniclastic Stepovak and Unga formations (Detterman et al., 1996). Therefore, middle Tertiary rocks of the Alaska-Aleutian Range batholith were not incorporated into strata that could serve as a recycled source for the Bear Lake Formation southwest of the batholith. I interpret mode 4 to represent erosion of deposits of the Meshik arc. A histogram and age distribution plot of K-Ar dates of the Meshik arc presented by Wilson (1980) shows a peak around 35 Ma which corresponds very well with the peak of mode 4.

Mode 4 is prominent in samples LH1-182 and LH1-164, whereas only one sample from BL5-95 falls into this mode (Fig. 6.14 and Fig. 6.15). Interpreting mode 4 to represent input from a volcanic source indicates that the composition of LH1-182 and LH1-164 should be more volcanic-rich than sample BL5-95. Petrographic analysis reveals that samples from measured section LH1 are indeed more volcanic-rich than those from BL5. Volcanic rock fragments comprise an average of 17% and 8% of the framework for samples from LH1 and BL5 respectively (Table 4.5). The composition of these samples supports my interpretation of mode 4 as being representative of derivation from the Meshik arc.

6.4 Conclusions

Detrital hornblende ages from the upper Bear Lake Formation indicate that the formation was sourced from several different units of the Alaska Peninsula. $^{40}Ar/^{39}Ar$ dates obtained from 57 hornblende grains range from 18.4 ± 10.4 Ma to 194.0 ± 3.5 Ma (Early Miocene to Early Jurassic). Four modes representing sources of Jurassic, Early Cretaceous, Paleocene to Early Eocene, and Eocene to Oligocene age indicate derivation from two main sources: recycled Mesozoic sedimentary rocks originally sourced from the Alaska-Aleutian Range batholith, and deposits of the Meshik arc. The youngest age measured, 18.4 ± 10.4 Ma, is likely part of the Eocene to Oligocene mode because it is the only Miocene age obtained and falls into the Eocene to Oligocene mode within error.

The Jurassic mode (mode 1) represents plutonic detritus recycled from the Late Jurassic Naknek Formation, originally shed from Jurassic rocks of the Alaska-Aleutian Range batholith. Additional input

from conglomerates of the Late Cretaceous Chignik Formation, derived from recycling of the Naknek Formation, is possible. However, this requires a third cycle origin for hornblende grain which is unlikely. The Early Cretaceous mode (mode 2) represents recycling of plutonic clasts sourced from conglomerates of the Late Cretaceous Chignik Formation, originally shed from Jurassic rocks of the Alaska-Aleutian Range batholith whose ages have been reset by Late Cretaceous intrusions of the batholith. The Paleocene to Early Eocene mode (mode 3) represents two sources: recycling of the Tolstoi Formation containing detritus originally sourced from middle Tertiary rocks of the Alaska-Aleutian Range batholith, and earliest deposits of the Meshik arc. The Eocene to Oligocene mode (mode 4) represents erosion of the Meshik arc.

Prominence of modes 1, 2, and 3 in sample BL5-95 with a lack of mode 4 indicates that this sample predominantly reflects erosion of older sedimentary units – likely a combination of the Naknek, Chignik, and Tolstoi formations. Prominence of modes 1 and 4 in sample LH1-182 indicates input predominantly from recycling of the Naknek Formation as well as erosion of the Meshik arc. Prominence of modes 1, 3, and 4 in sample LH1-164 indicates input predominantly from recycling of the Naknek and Tolstoi formations as well as erosion of the Meshik arc.

Importantly, no Miocene source appears in the ages of the hornblende. A Miocene source would have indicated contemporaneous volcanic activity during deposition of the Bear Lake Formation. The absence of a Miocene mode supports previous interpretations by Wilson (1980), Nilsen (1984), Wilson (1985), and Detterman et al. (1996) that the Bear Lake Formation was deposited during a time of quiescence in volcanic activity on the Alaska Peninsula.

CHAPTER 7. PROVENANCE

The Alaska-Aleutian Range batholith served as a primary source for plutonic detritus incorporated into Mesozoic strata from Late Jurassic continuing into the Paleocene (Burk, 1965; Detterman et al., 1996; Wilson et al., 1999). During this time, Mesozoic sedimentary strata of the Chignik subterrane were also being uplifted and recycled, causing repeated recycling of input from the batholith (Wilson, 1980; Detterman et al., 1996; Wilson et al., 1999). Initiation of volcanic activity associated with the Meshik arc began during earliest Eocene time, shifting the source of sedimentation from predominantly plutonic and Mesozoic recycled sources to contemporaneous volcanic deposits as reflected by deposition of the Meshik Volcanics and Stepovak Formation (Wilson, 1985; Detterman, 1990; Detterman et al., 1996). Volcanic activity subsided by Middle Miocene deposition of the Bear Lake Formation, whose composition has been interpreted to reflect quiescence of arc activity on the Alaska Peninsula and derivation from plutonic and recycled Mesozoic strata (Wilson, 1980; 1985; Detterman, 1990; Detterman et al., 1996).

Investigation of sandstones from measured stratigraphic sections of the Bear Lake Formation near Port Moller, and from the North Aleutian COST 1 well and Great Basins 1 well (Fig. 2.1) provide several lines of evidence that point to both recycled plutonic, and volcanic source terrains for the Bear Lake Formation. Detailed petrographic analysis indicates compositional differences between the upper and lower Bear Lake Formations that reflect increased recycling of plutonic detritus from mainly Mesozoic sedimentary units (Naknek and Chignik formations), accompanied by decreased volcanic input up-section. The Meshik Volcanics are the most likely source of volcanic detritus, as volcanic clasts in the early Tertiary Tolstoi Formation are chloritized and other potential sources of volcanic input on the Alaska Peninsula are distant.

Electron microprobe analysis (EMPA) of volcanic rock fragments from the Bear Lake Formation also suggests derivation from the Meshik Volcanics (northeast of Port Moller) throughout deposition of the Bear Lake Formation. In addition, EMPA of detrital plagioclase clasts suggests a plutonic source which is most prominent in the upper Bear Lake Formation.

Geochronology of detrital hornblende from the upper Bear Lake Formation indicates recycling of Mesozoic and early Tertiary strata that were originally sourced from the Alaska-Aleutian Range batholith

(Naknek, Chignik, and Tolstoi formations). $^{40}Ar/^{39}Ar$ dates obtained from detrital hornblende also point to derivation from volcanic rocks of the Meshik arc.

All three methods reveal both recycled plutonic, and volcanic sources for the Bear Lake Formation throughout deposition. They also demonstrate that volcanic input from deposits of the Meshik arc was greater during deposition of the lower Bear Lake Formation, and that recycling of early Tertiary and Mesozoic strata was more prominent during deposition of the upper Bear Lake Formation. This pattern of incorporation of older sediments up-section indicates increased erosion of older units on the Alaska Peninsula (Fig. 7.1). However, input from the Meshik Volcanics and older sedimentary units throughout deposition suggests that these units were all exposed at the surface during erosion. Therefore, erosion of a simple layered stratigraphy (Fig. 1.2) does not fit the up-section compositional differences in the Bear Lake Formation. Alternatively, the source area must have been structurally deformed in order to expose all the source units (Fig. 7.2).

The source area likely consisted of Tertiary and Mesozoic strata exposed in eroded (and likely reverse-faulted) anticlines, similar to the structures currently exposed on the Alaska Peninsula to the northeast of Port Moller (see Wilson et al., 1999), and between Herendeen Bay and Port Moller (Decker et al., 2008b). Deep erosion of an anticline results in greater exposure of older rocks (Fig. 7.3A). This simplified model is one possible structural mechanism for deforming a stratigraphic succession that can explain the increased input of recycled rocks up-section in the Bear Lake Formation (Fig. 7.3B) by progressive, deeper erosion exposing older strata in the cores of anticlines.

The Great Basins 1 well is located in the Ugashik sub-basin, at the northeastern end of the greater Bristol Bay basin (Fig. 3.1; Decker et al., 2008a). Petrographic analysis shows that the base of the Bear Lake Formation in this well was derived from a primary plutonic source (see, for example, Fig. 4.14). The coarse-sand size at the base of the formation and high abundance of plutonic rock fragments accompanied by schist suggest that material was derived from rocks of the Iliamna subterrane which were exposed on the northern flank of the sub-basin (Fig. 7.4). Up-section in this well, the composition of the Bear Lake Formation reflects input from the same recycled source that fed the upper Bear Lake Formation near Port

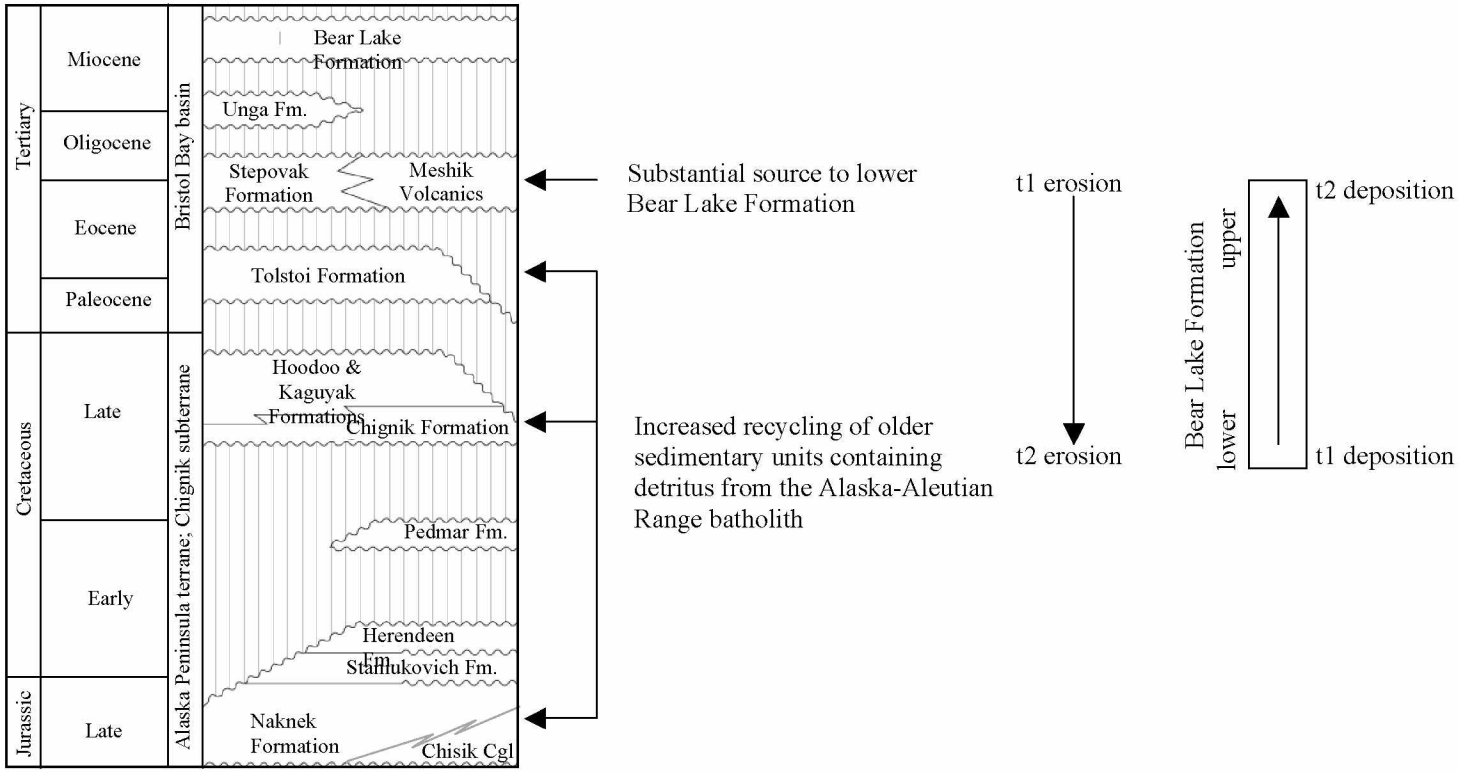

Fig. 7.1 Progressive erosion of older strata during deposition of the Bear Lake Formation. Time 1 (t1) indicates deposition of lower Bear Lake Formation and corresponding erosion of the Meshik arc. Time 2 (t2) indicates deposition of the upper Bear Lake Formation and corresponding erosion of coarser-grained early Tertiary and Mesozoic sedimentary units. Abbreviated stratigraphic column of the Alaska Peninsula modified from Reifenstuhl et al. (2004) and Decker et al. (2008a), after Detterman et al. (1996).

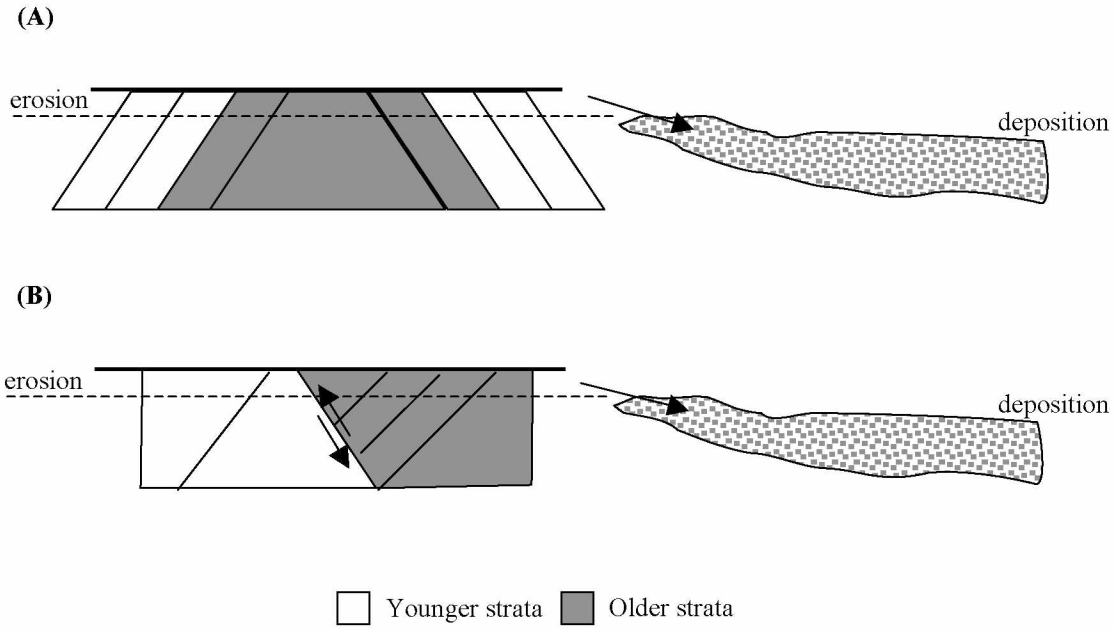

Fig. 7.2 Cartoons illustrating possible structural deformation of source area. (A) Erosion of an anticline exposes a mixture of source units. (B) A faulted stratigraphic succession exposes a mixture of source units during erosion and corresponding deposition.

Fig. 7.3 Simple model of erosion and corresponding deposition of the Bear Lake Formation. (A) Cartoon illustrating deeper erosion of an anticline resulting in greater exposure of older rocks. A greater amount of older rocks are eroded in the source area and deposited in the basin at time 2 (t2). (B) Abbreviated stratigraphic column of the Alaska Peninsula modified from Reifenstuhl et al. (2004) and Decker et al. (2008a), after Detterman et al. (1996). Annotations illustrate how erosion and corresponding deposition of specific source rocks relates to the cartoon presented above. Time 1 (t1) and time 2 (t2) notations correspond to t1 and t2 in above cartoon.

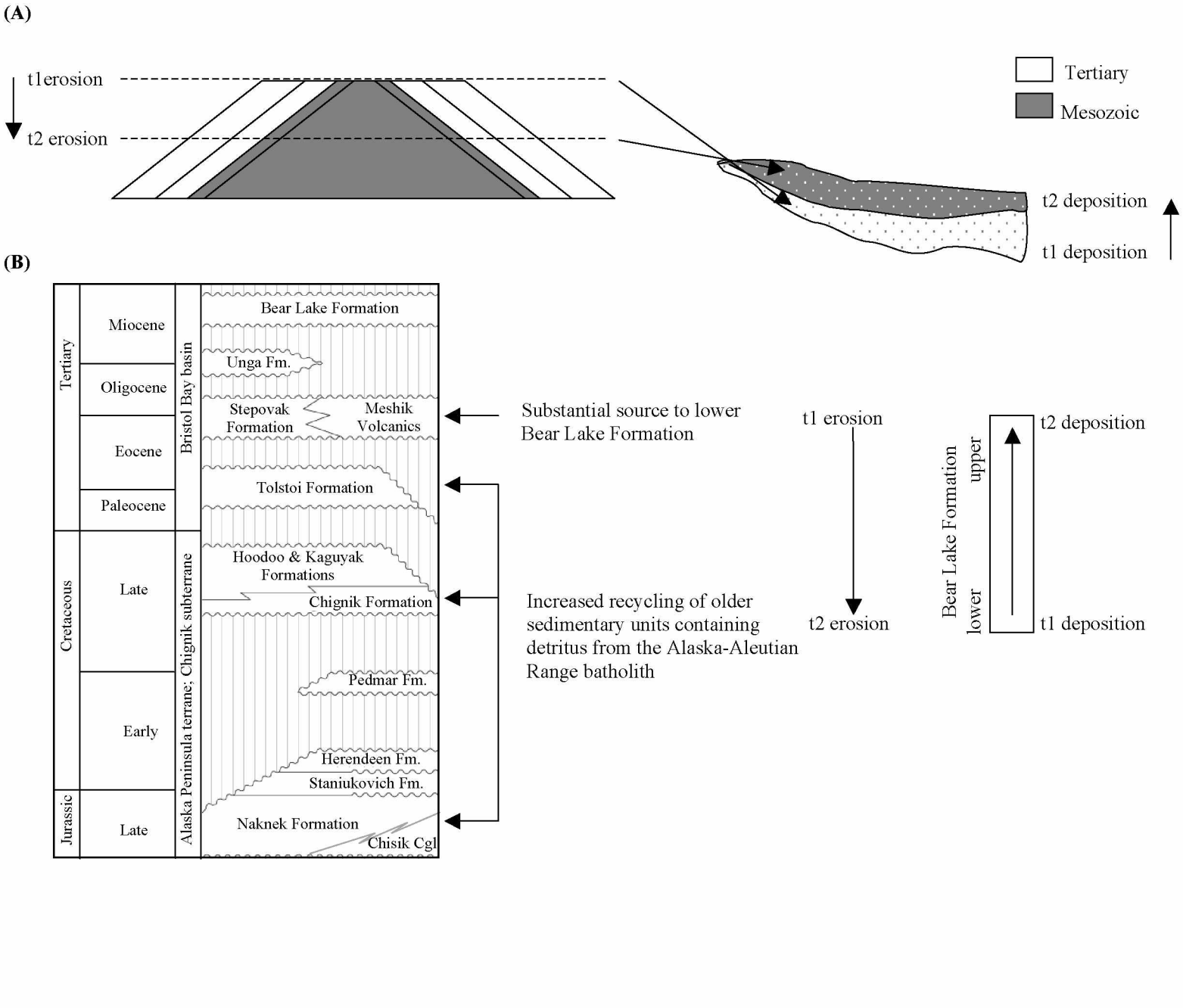
(A)
t1erosion
t2 erosion
Tertiary
Mesozoic
t2 deposition
t1 deposition
(B)
Tertiary
Cretaceous
Jurassic
Miocene
Oligocene
Eocene
Paleocene
Late
Early
Late
Bristol Bay basin
Alaska Peninsula terrane; Chignik subterrane
Bear Lake Formation
Unga Fm.
Stepovak Formation
Meshik Volcanics
Tolstoi Formation
Hoodoo & Kaguyak Formations
Chignik Formation
Pedmar Fm.
Herendeen Fm.
Staniukovich Fm.
Naknek Formation
Chisik Cgl
Substantial source to lower Bear Lake Formation
Increased recycling of older sedimentary units containing detritus from the Alaska-Aleutian Range batholith
t1 erosion
t2 erosion
Bear Lake Formation
upper
lower
t2 deposition
t1 deposition

Moller. Namely, recycled rocks from the Chisik Conglomerate Member of the Naknek Formation and the Chignik Formation. Recycled sediment was derived from the northeast or eastern flank of the basin where Mesozoic strata of the Chignik subterrane were uplifted relative to the sub-basin (Fig 7.4). Sediment was sourced primarily from the north (primary plutonic) or northeast (recycled), and volcanic rocks of the Meshik arc at the southern margin of the basin did not provide a substantial amount of volcanic input.

In conclusion, the Bear Lake Formation was sourced from recycling of the Naknek and Chignik formations, with additional input from recycling of the Tolstoi Formation in the upper Bear Lake Formation. Contribution from these sources account for the presence of chert and plutonic detritus (plutonic rock fragments, K-feldspar, quartz, detrital hornblende, and a population of plagioclase clasts with An < 30). This recycled source became more prominent during later deposition of the Bear Lake Formation. During early deposition, volcanic rocks of the Meshik arc provided a substantial amount of detritus to the Bear Lake Formation and continued to serve as a source throughout deposition, but became less prominent up-section. Geography of the Ugashik sub-basin provided a unique setting for deposition of the Bear Lake Formation on the northwestern end of the Alaska Peninsula. Proximity to exposures of the Alaska-Aleutian Range batholith directly to the north, and uplift relative to the basin associated with opening of the Ugashik sub-basin, allowed direct derivation from plutonic rocks and high grade metamorphic rocks of the Iliamna subterrane during early deposition of the Bear Lake Formation.

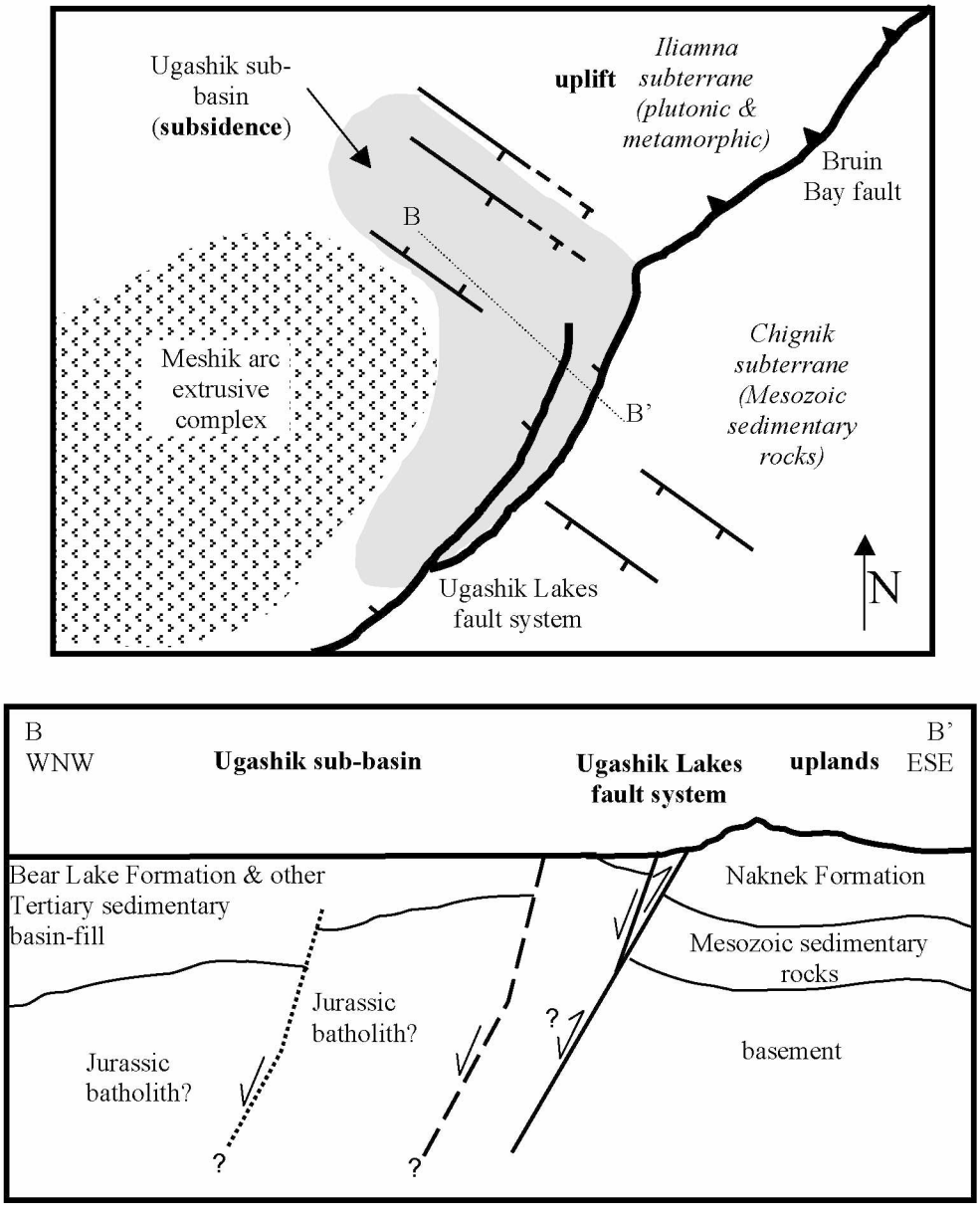

Fig, 7.4 Cartoon illustrating the fault-controlled Ugashik sub-basin. The cross section below the map is a conceptual model of the Ugashik sub-basin based on aeromagnetic anomaly patterns and is not to scale (Decker et al., 2008a). The Bear Lake Formation (and other Tertiary sedimentary units) in the Ugashik sub-basin lie beneath Quaternary sedimentary cover, and are not exposed at the surface (Decker et al., 2008a). Modified from Decker et al. (2008a). See Fig. 3.1 for regional context.

CHAPTER 8. DIAGENESIS

8.1 Introduction

Point count analysis and electron microprobe analysis indicate numerous diagenetic minerals in varying abundances (Fig. 8.1). The most diagnostic minerals identified in interpreting diagenetic conditions are zeolites (heulandite and laumontite), calcite, and kaolinite. Measured sections BL2, BL5, and the top of BL1 contain heulandite. The base of BL1 contains no zeolites. Calcite is prevalent in both samples analyzed from BL1. Measured section LH1 contains laumontite along with calcite. The Great Basins 1 well contains kaolinite, with no calcite or zeolites. Kaolinite in measured section CP1 decreases up-section as calcite increases. CP1 also contains no zeolites.

Thermal data available for the North Aleutian COST 1 well (Flett, 1988; Molenaar, 1996; Bergman et al., 2008), the Great Basins 1 well (McLean, 1977; Molenaar, 1996), and for measured sections CP1 and BL1 (Finzel et al., 2005) provide controls on the temperature ranges experienced by the Bear Lake Formation. This temperature control puts the documented diagenetic mineralogy into thermal context. It also allows for relative temperature estimates for measured sections with no available thermal maturation data by comparing the mineralogy with that of measured sections whose temperatures are constrained by vitrinite reflectance data.

8.2 Thermal maturity

Vitrinite reflectance values (R_o) reported for the North Aleutian COST 1 and Great Basins 1 wells show a simple progressive increase with depth (Fig. 8.2). The North Aleutian COST 1 well has an average geothermal gradient of 31°C/Km, and current temperatures are at or near maximum burial temperatures (Bergman et al., 2008). The two wells show very similar R_o values at a given depth, indicating that the geothermal gradient experienced in the Great Basins 1 well is similar to that of North Aleutian COST 1. Molenaar (1996) reported a range of geothermal gradients from 29.2°C/Km to 38.3°C/Km for wells of the Bristol Bay lowlands by, including North Aleutian COST 1 and Great Basins 1, which also suggests that the two wells have experienced similar temperatures.

Fig. 8.1 Summary of diagenetic mineralogy. The diagrams include all pore-filling, alteration, and replacement minerals identified by point count analysis and electron microprobe analysis. Underline indicates that the mineral is only present as an alteration product, and not a pore-filling component. Minerals are generally listed in order of decreasing abundance. (A) Great Basins 1 well. (B) North Aleutian COST 1 well. (C) Bear Lake Formation measured sections. The measured sections are displayed in chronostratigraphic order (Decker et al., 2005; Finzel et al., 2005; Decker et al., 2008a). The lower, middle, and upper designations are based on Decker et al. (2005).

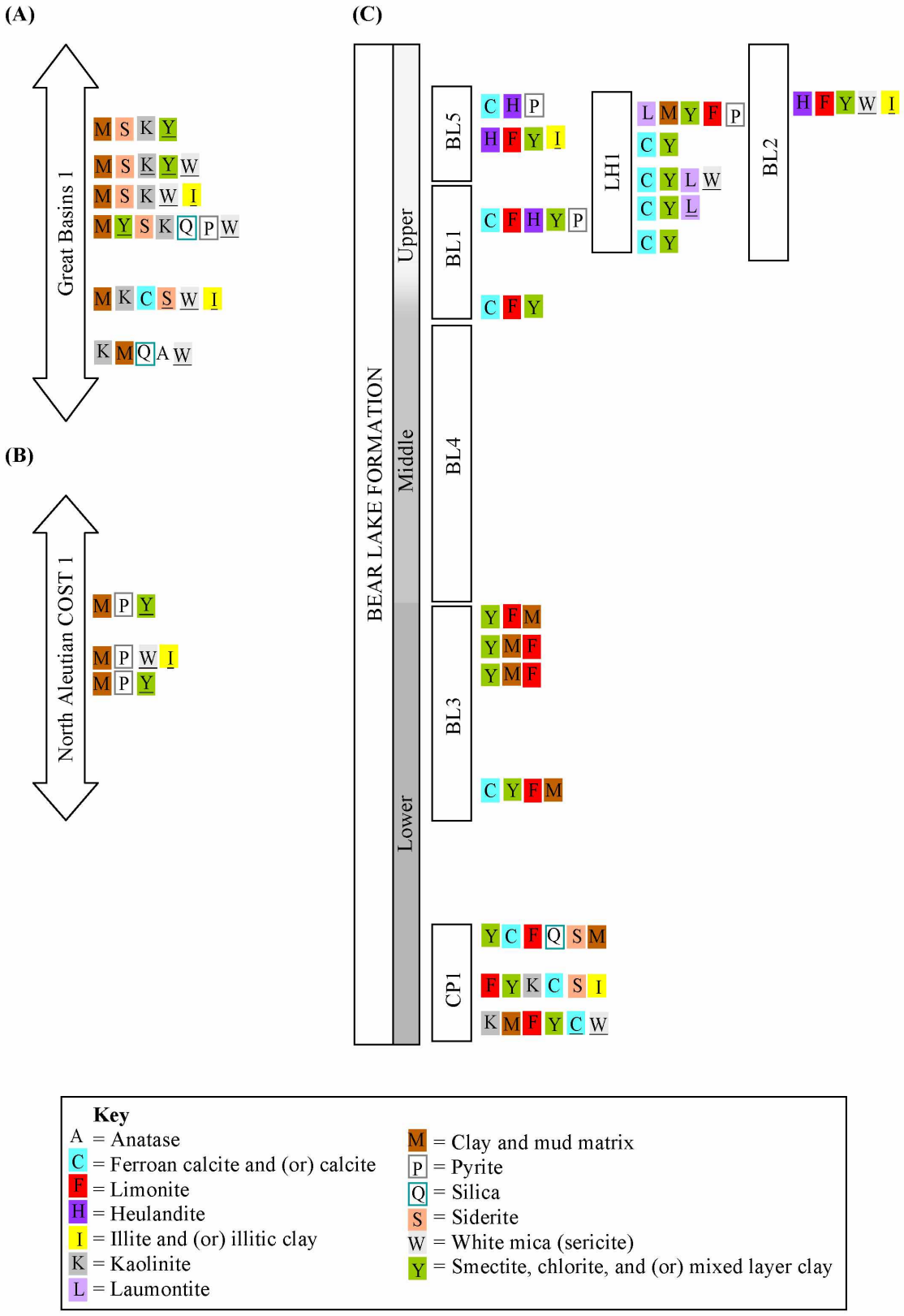
(A)
Great Basins 1
M S K Y
M S K Y W
M S K W I
M Y S K Q P W
M K C S W I
K M Q A W
(B)
North Aleutian COST 1
M P Y
M P W I
M P Y
(C)
BEAR LAKE FORMATION
Upper
Middle
Lower
BL5
C H P
H F Y I
BL1
C F H Y P
C F Y
BL4
BL3
Y F M
Y M F
Y M F
C Y F M
CP1
Y C F Q S M
F Y K C S I
K M F Y C W
LH1
L M Y F P
C Y
C Y L W
C Y L
C Y
BL2
H F Y W I
Key
A = Anatase
C = Ferroan calcite and (or) calcite
F = Limonite
H = Heulandite
I = Illite and (or) illitic clay
K = Kaolinite
L = Laumontite
M = Clay and mud matrix
P = Pyrite
Q = Silica
S = Siderite
W = White mica (sericite)
Y = Smectite, chlorite, and (or) mixed layer clay

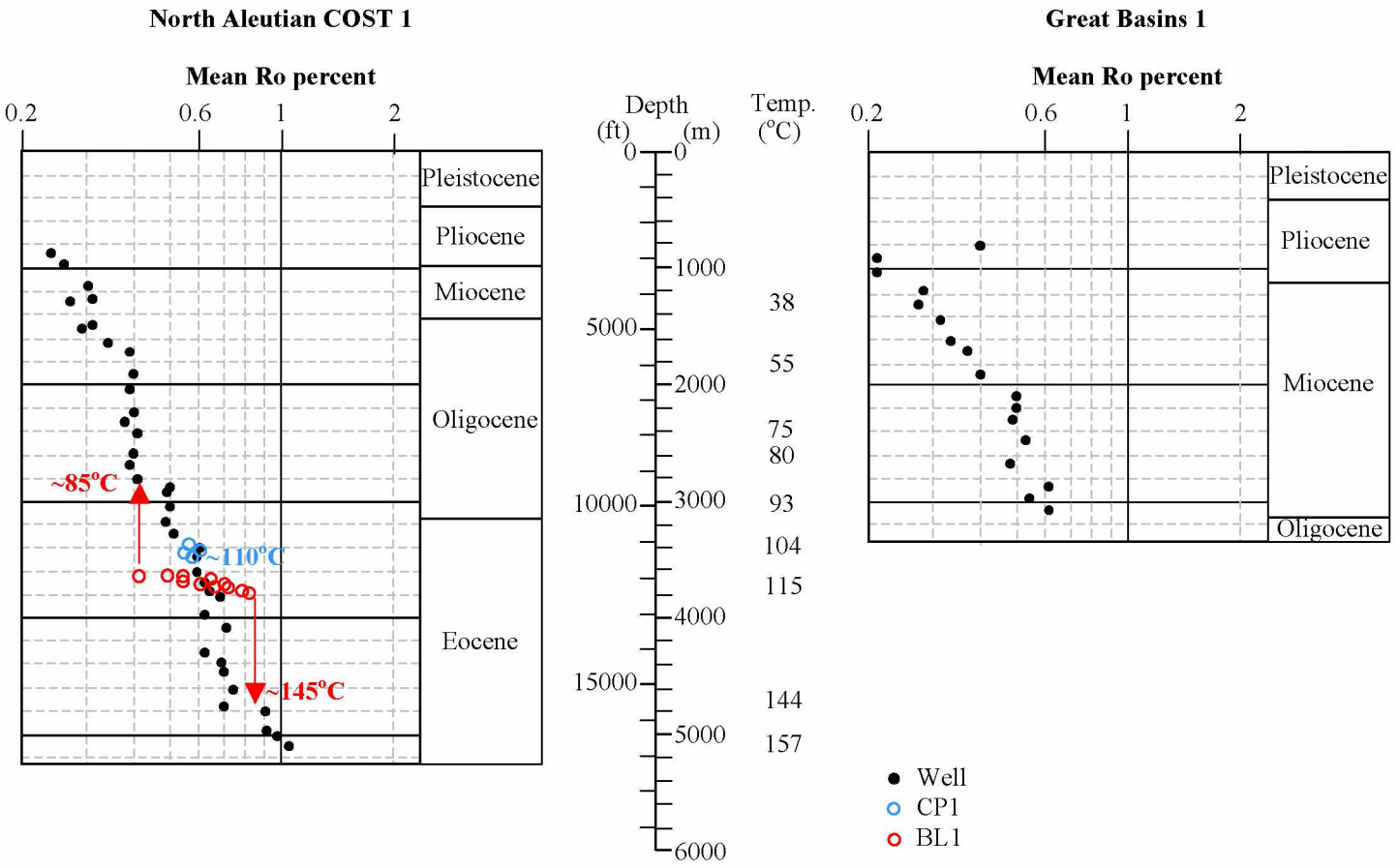

Fig. 8.2 Vitrinite reflectance (R_o) versus depth. Values from Bear Lake Formation (Miocene) measured sections CP1 and BL1 are plotted at a depth relative to the North Aleutian COST 1 R_o trend in order to illustrate estimated temperatures for the measured sections. Red arrows illustrate the estimated upper and lower temperature range for BL1 related to the R_o trend of the North Aleutian COST 1 well. Temperatures are from Bergman et al. (2008). Epoch boundaries are from Mickey et al. (2005). R_o values for the North Aleutian COST 1 well are from Flett (1988), values for the Great Basins 1 well are from McLean (1977), and values for CP1 and BL1 are from Finzel at al. (2005). Diagram modified from Molenaar (1996).

Although the "BL" measured sections are all located in the same geographic area (Fig. 2.1), they do not represent a continual, coherent section of the Bear Lake Formation (Fig. 2.2; sheet 2 in Decker et al., 2005). Structural complications present in the vicinity of the "BL" measured sections and of CP1 and LH1 (Wilson et al., 1995; Wilson et al., 1999; Decker et al., 2005) exclude the assumption of a consistent geothermal gradient between measured sections.

Vitrinite reflectance data indicate a significant geothermal gradient within measured section BL1. R_o values range from 0.41 near the top of the measured section to 0.83 near the base (Finzel et al., 2005). When compared to the trend of R_o versus depth observed in the North Aleutian COST 1 well, and corresponding temperatures, the temperatures experienced within BL1 (approximately 170 m) can be estimated to range from approximately 85°C near the top of the measured section to approximately 145°C near the base (Fig. 8.2). R_o values from CP1 show little variability, ranging from 0.54 to 0.6 (Finzel et al., 2005). This corresponds to an estimated temperature near 110°C when compared with the trend of the North Aleutian COST 1 well (Fig. 8.2). No thermal maturation data is available for measured sections LH1, BL2, BL3, and BL5.

In general, reported vitrinite reflectance values for a given sample represent an average of R_o values measured within the sample (Peters et al., 2005). An example given by Peters et al. (2005) shows an error of ±0.04 percent for a sample with 50 reflectance values. R_o measurements made for the North Aleutian COST 1 well showed good unimodal vitrinite reflectance histograms, and few significant problems interfered with evaluation of R_o data for this well (Flett, 1988). R_o averages for the Great Basins 1 well are based on approximately 40 measurements per sample, and show varying ranges of minimum and maximum measurements (McLean, 1977). Peters et al. (2005) also concisely discuss other factors that influence the accuracy of R_o values, including variation in kerogen type, sampling problems, and misidentification of vitrinite.

8.3 Mineral stability

8.3.1 Heulandite-Laumontite-Calcite

The two samples I studied from measured section BL1 represent opposite ends of the estimated temperature range of 85°C to 145°C, as determined from R_o values. The thermal gradient between BL1-

155 (near the top of the section) and BL1-5 (near the base) suggests that the presence of heulandite in BL1 may be temperature dependant. According to Neuhoff and Bird (2001), heulandite is stable relative to laumontite below 100°C (Fig. 8.3). This is consistent with the occurrence of heulandite in the upper portion of BL1, which has experienced temperatures less than 100°C, whereas heulandite is absent at the base of BL1, which has experienced temperatures greater than 100°C. Laumontite is expected to be present in measured section BL1 at some point below BL1-155 based on the thermal conditions. However, no laumontite is present in BL1-5, nor are higher temperature Ca-silicates (such as prehnite or wairakite). Instead, calcite is the lone diagenetic Ca-bearing mineral. This suggests that zeolite occurrence is not strictly temperature dependant, and that partial pressure of carbon dioxide (P_{CO2}) is an important factor. The influential role of P_{CO2} in the system is also indicated by the diagenetic mineralogy documented in LH1. Laumontite is present at the top of LH1 and becomes more limited down-section, whereas calcite becomes more prevalent and is accompanied by only minor laumontite (as replacement of albite clasts; Fig. 8.1C).

Zeolite stability is moderated by CO_2 abundance, where increased CO_2 inhibits Ca-zeolites relative to a calcite-kaolinite-quartz assemblage (Zen, 1961). The P_{CO2} required to favor kaolinite-calcite over laumontite decreases with lower temperatures (Ivanov and Gurevich, 1975; Sawaki et al., 1997). This relationship is illustrated in Fig. 8.4, and applies to isochemical systems (Zen, 1961). Replacement of clasts (such as volcanic rock fragments and hornblende) by calcite in LH1 and BL1 (Table 4.9, Table 5.6, and Table 5.7) indicates that the diagenetic system of the Bear Lake Formation was not isochemical for these measured sections. Rather, additional Ca was introduced to the system by fluid migration. Limited solubility of Al resulted in fluid chemistry rich in Ca relative to Al. Therefore, calcite precipitates whereas kaolinite can be absent at conditions where the calcite-kaolinite-quartz assemblage is stable. The documentation of laumontite coexisting with calcite (Fig. 8.1C) implies that conditions experienced by LH1 likely fall near equilibrium between laumontite and kaolinite-calcite stability. The apparent disappearance of zeolites in BL1 below BL1-155 implies that conditions in the lower part of BL1 reflect those of kaolinite-calcite stability.

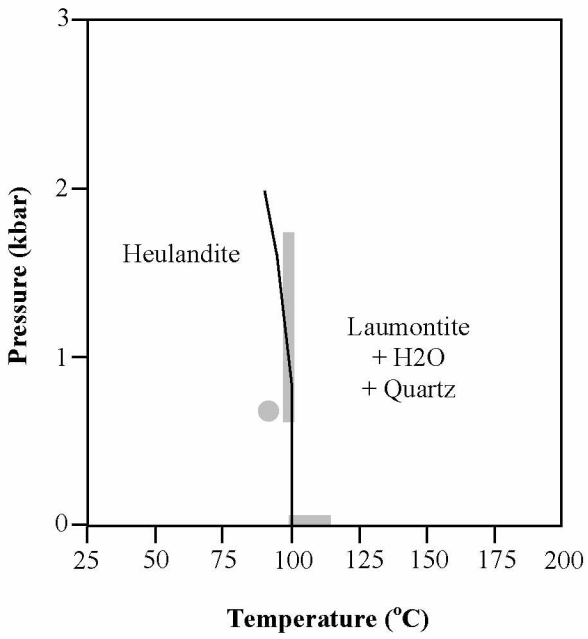

Fig. 8.3 Heulandite-Laumontite-Quartz stability diagram. Stability fields are based on experimental and geological observations of heulandite-laumontite coexistence. Geological observations are indicated by gray fields. Modified from Neuhoff and Bird (2001).

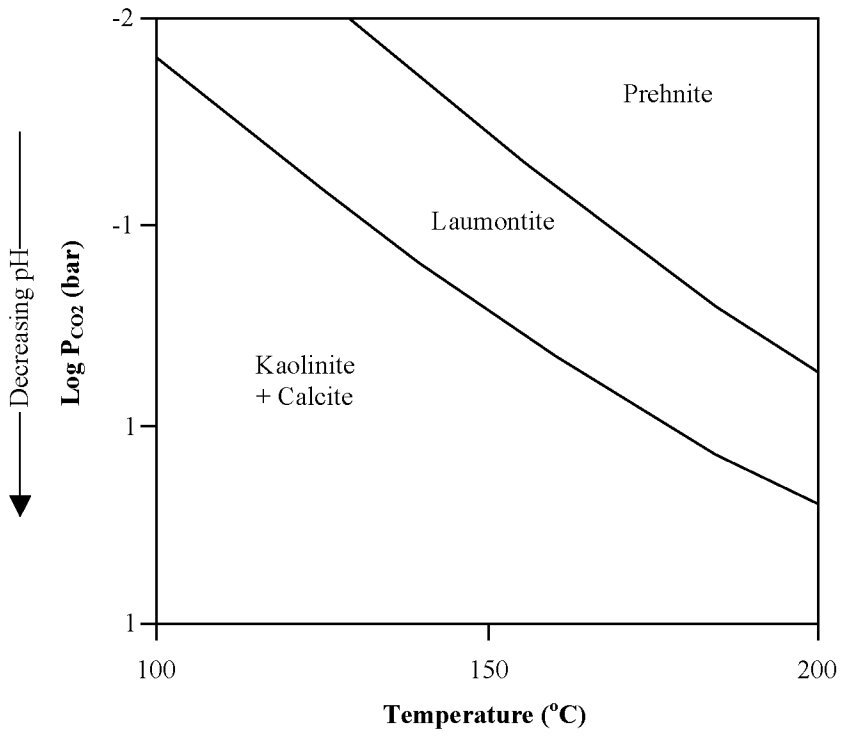

Fig. 8.4 Kaolinite-Laumontite-Prehnite stability related to P_{CO2} and temperature. Modified from Sawaki et al. (1997).

Although no thermal maturation data are available for BL5 and BL2, the occurrence of heulandite in both of these measured sections indicates that temperatures were similar to those experienced by the upper portion of BL1 which also contains heulandite. Additionally, the presence of laumontite in LH1 indicates that it has experienced temperatures greater than those seen by the upper portion of BL1 (and by BL5 and BL2). The temperature conditions of the lower portion of BL1 may have been similar to those experienced by LH1.

8.3.2 Kaolinite-Laumontite-Calcite

CP1 contains no zeolites although laumontite is stable at the estimated temperature for the measured section (around 110°C, based on R_o values). Instead, kaolinite and calcite are present (Fig. 8.1C). Additionally, albite clasts are altered to kaolinite and sericite (Table 5.8). The Great Basins 1 well has experienced a wider range in temperature. Assuming a comparable geothermal gradient to the North Aleutian COST 1 well, the estimated temperatures that the Bear Lake Formation has experienced in the Great Basins 1 well are approximately 38°C to 93°C (Fig. 8.2). The Great Basins 1 well contains kaolinte, but no calcite or zeolites (Fig. 8.1A). Both CP1 and the Great Basins 1 well contain K-feldspar and albite clasts (Table 5.8). X-ray fluorescence analysis by Rainer Newberry (Appendix C) of sample billets from the Great Basins 1 well and the measured sections shows a dramatically lower CaO content and a corresponding high Na_2O content for samples from the Great Basins 1 well, supporting the observed absence of Ca-bearing minerals and the presence of albite (Fig. 8.5). In CP1, kaolinite and sericite replace albite (Table 5.8). In the Great Basins 1 well, sericite replaces both K-feldspar and albite (Table 5.8).

Kaolinite and K-feldspar are not mutually stable and temperature is irrelevant with respect to equilibrium between the two minerals (Fig. 8.6). Conditions must be more acidic (lower pH) for kaolinite stability relative to K-feldspar (Fig. 8.6). Including Na as a variable in the system allows stability modeling of the occurrence of kaolinite, sericite (represented as muscovite), K-feldspar, and albite (Fig. 8.7). The rock system (represented by K-feldspar and albite clasts) is not in equilibrium with the fluid system (represented by pore-filling kaolinite). Interaction of the fluid system with the rock changes the fluid composition locally at sites of interaction. The fluid system is represented in Fig. 8.7 by "F" and the rock

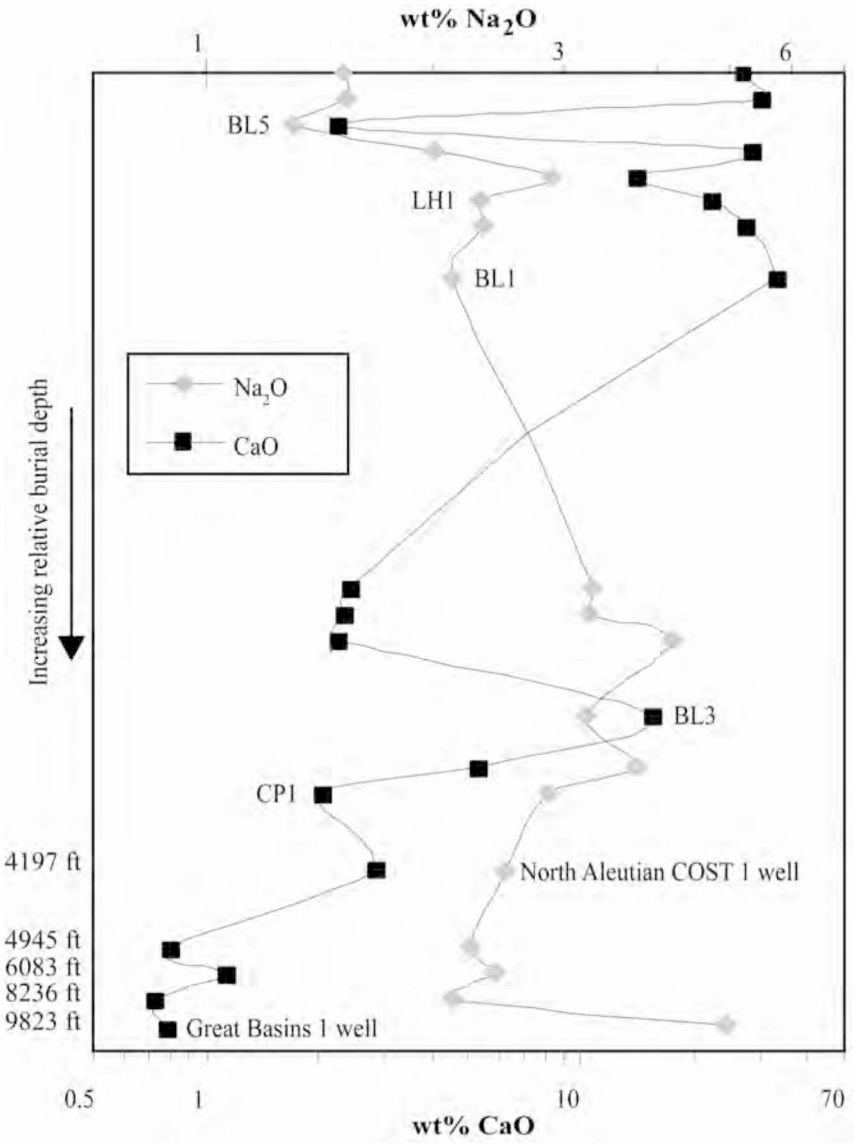

Fig. 8.5 Weight percent CaO and Na_2O versus burial depth in the Bear Lake Formation. Data obtained by XRF analysis of sample billets (Appendix C).

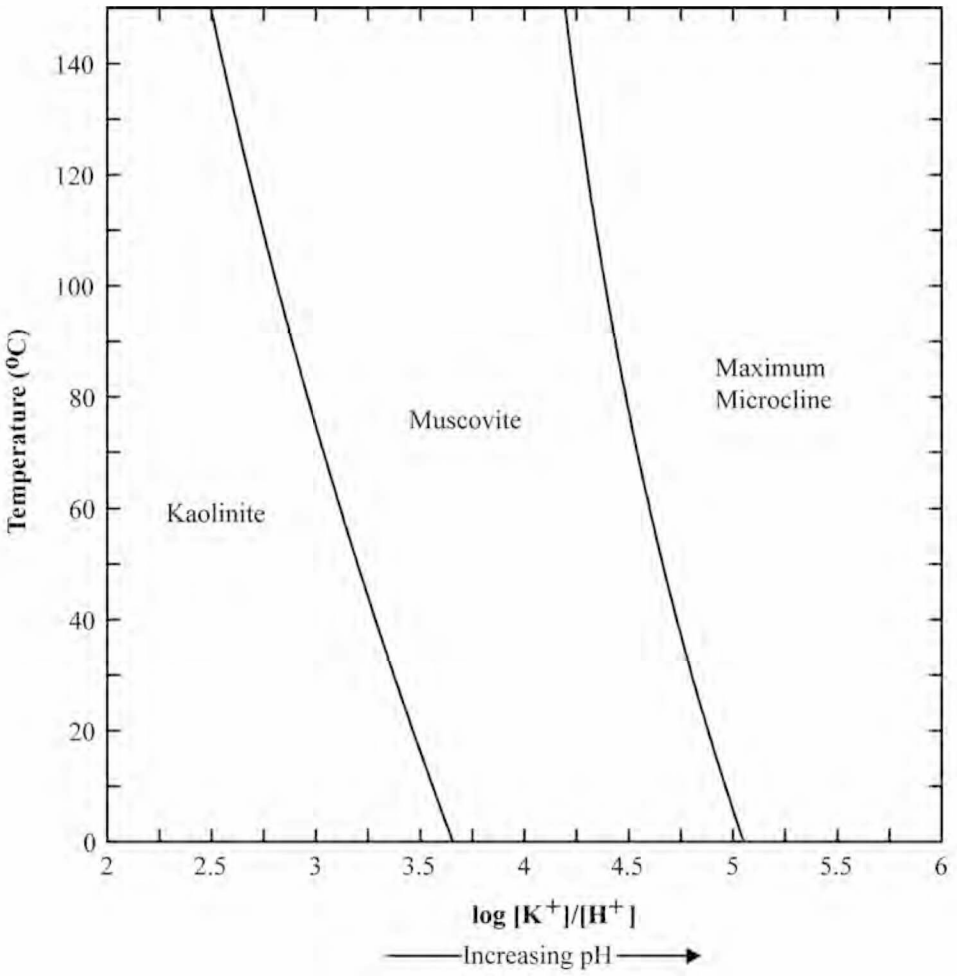

Fig. 8.6 Kaolinite-Muscovite-K-feldspar stability diagram. Modeled at pressure of 100 bars with quartz saturation. Modeled using Geochemist's Workbench.

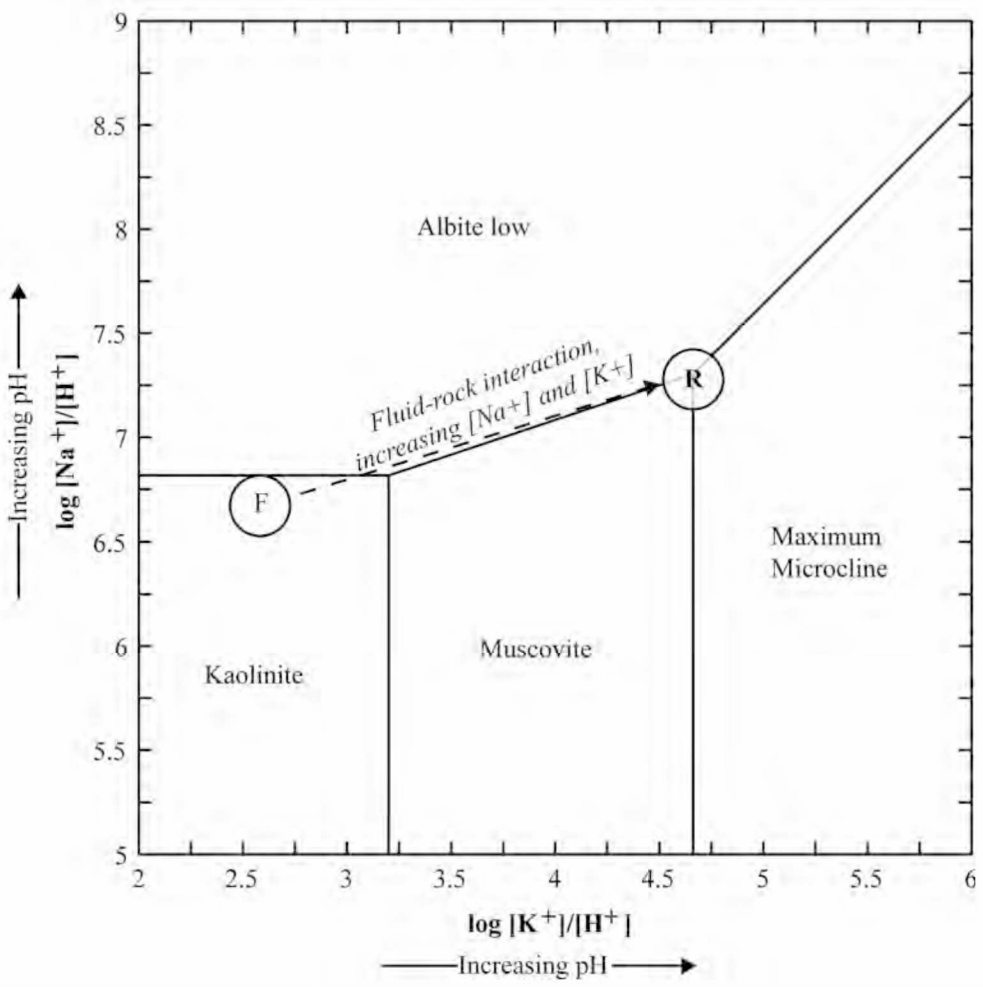

Fig. 8.7 Kaolinite-Muscovite-K-feldspar-Albite stability diagram. "F" indicates conditions of the fluid system and "R" indicates conditions of the rock system. The dashed arrow illustrates how the conditions change with fluid-rock interaction. Modeled at 50°C and 1 bar with quartz saturation. Paragonite theoretically has a small stability field, and its occurrence is rare. Therefore, it is suppressed in this model. Maximum microcline is the most stable alkali feldspar, but other forms of alkali feldspar are also stable under these conditions in the maximum microcline field. Modeled using Geochemist's Workbench.

system is represented by "R". The interaction of the fluid with K-feldspar and albite clasts increases the activities of K ([K+]) and Na ([Na+]) respectively, while the activity of H+ ([H+]) decreases. The conditions of the system change, resulting in stability of K-feldspar, albite, and muscovite. The mineralogy of CP1 and the Great Basins 1 well reflects this mineral assemblage by the presence of pore-filling kaolinite (at F in Fig. 8.7), and of both unaltered feldspars and alteration of the feldspars by sericite (at R in Fig. 8.7). The alteration of albite by kaolinite in CP1 is consistent with this model, and corresponds to equilibrium between kaolinite and albite.

The decrease in pH required for kaolinite stability is likely controlled by P_{CO2}. P_{CO2} affects pH as described by Eq. 1, where carbonic acid (H_2CO_3) equates with $CO_2 + H_2O$ (Faure, 1998).

(1) $CaCO_3 + H_2CO_3 \rightleftharpoons Ca^{2+} + 2HCO_3^-$
calcite *carbonic acid* *bicarbonate*

Increasing CO_2 in the system increases H_2CO_3, causing the pH to decrease and calcite to dissolve. Conversely, removing CO_2 decreases H_2CO_3 and pH rises. This can be graphically illustrated by relating Ca^{2+} concentration in solution to P_{CO2} and pH (Fig. 8.8). Calcite precipitates under the higher pH (lower P_{CO2}) conditions. Under lower pH (higher P_{CO2}) conditions calcite is soluble and kaolinite precipitates while Ca^{2+} remains in solution. The solubility of CO_2 in water is a function of pressure: higher pressure increases the amount of CO_2 dissolved in the fluid. Conversely, as pressure drops, CO_2 is released from fluid.

The inverse relationship between kaolinite and calcite in CP1 implies that the pH increases up-section as calcite becomes more prevalent relative to kaolinite. In the Great Basins 1 well the presence of kaolinite and absence of a Ca-bearing mineral phase is consistent with low pH conditions.

Notably, both CP1 and the Great Basins 1 well contain siderite (Fig. 8.1). Modeling the stability of Fe-bearing minerals in a system saturated with respect to kaolinite and quartz indicates that siderite is stable in higher P_{CO2} conditions when the oxidation state is below hematite stability (Fig. 8.9). This provides additional evidence for low pH in CP1 and the Great Basins 1 well.

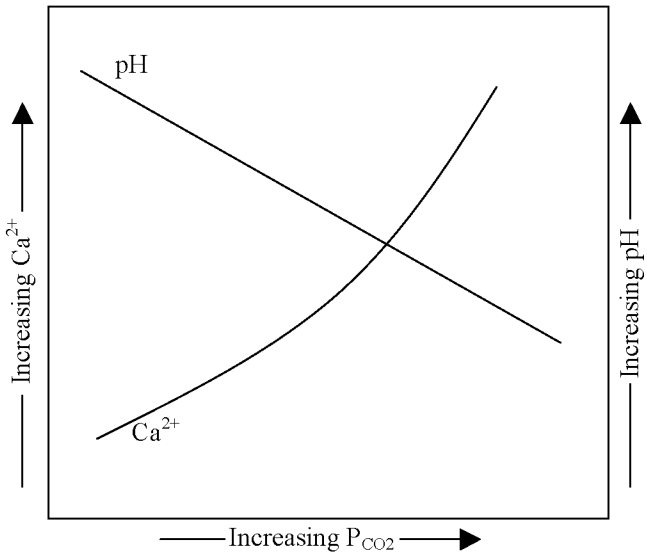

Fig. 8.8 Relationship of Ca^{2+} concentration in solution, P_{CO2}, and pH. Modified from Faure (1998).

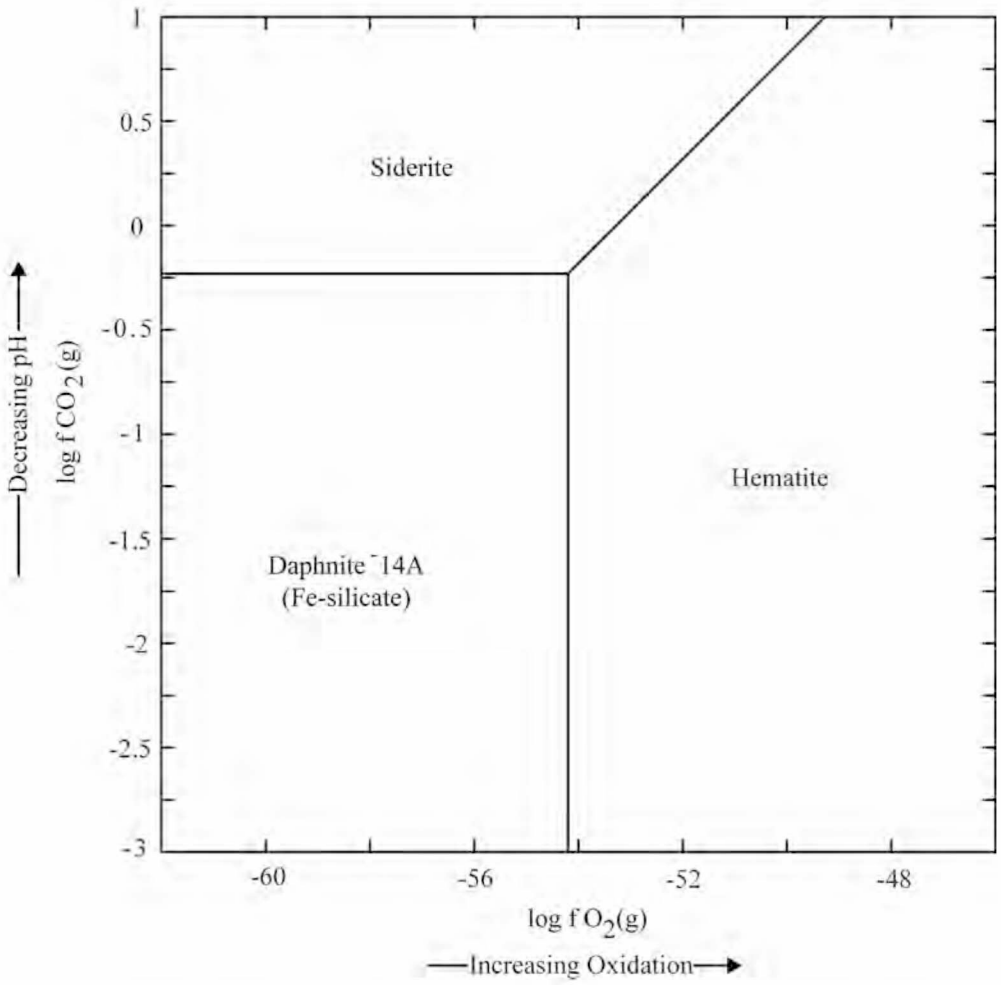

Fig. 8.9 Fe-bearing mineral stability diagram. Modeled at 100°C and 1 bar with kaolinite and quartz saturation. Modeled using Geochemist's Workbench

8.4 Summary and Conclusions

P_{CO2} is the most influential factor in the diagenetic system of the Bear Lake Formation, and is controlled by pressure. P_{CO2} is the variable which controls pH conditions related to the presence of kaolinite and calcite, and it controls zeolite stability relative to calcite. Fig. 8.10 summarizes this P_{CO2}-dependant, and thus pressure controlled, diagenetic system.

P_{CO2} effects on pH conditions experienced by the Bear Lake Formation in the Great Basins 1 well and CP1 controlled precipitation of kaolinite relative to calcite (Fig. 8.10 and Fig. 8.11). High P_{CO2} caused acidic conditions in the Great Basins 1 well. These conditions resulted in precipitation of kaolinite and the absence of calcite. Kaolinite in the Great Basins 1 well is in disequilibrium with albite and K-feldspar clasts, and alteration of the feldspar by sericite. Kaolinite and calcite in CP1 indicate more basic conditions up-section, moving from kaolinite to calcite stability. P_{CO2} decreases up-section, causing higher pH and precipitation of calcite.

Although temperature controls which zeolite minerals are present (heulandite versus laumontite), the presence of zeolite is controlled by P_{CO2}. In BL1 and LH1, P_{CO2} decreases up-section, allowing zeolite stability relative to calcite. LH1 experienced temperatures of at least 100°C as indicated by the presence of laumontite. R_o values indicate that BL1 experienced a temperature range from 85°C to 145°C. Heulandite present at the top of the section, and a substantial geothermal gradient, indicate that the heulandite-laumontite transition should be documented in BL1. The decrease in P_{CO2} down-section has obscured this zeolite transition, with P_{CO2} sufficiently high to precipitate calcite at the expense of zeolite.

The P_{CO2}-dependant mineral assemblages present in the Bear Lake Formation suggest that rocks of the upper Bear Lake Formation (calcite ± zeolite-bearing BL2, LH1, BL5, and BL1; Fig. 8.1C) experienced fluid migration under lower pressure conditions than rocks of the lower Bear Lake Formation (calcite ± kaolinite-bearing CP1; Fig. 8.1C). In the Great Basins 1 well, the mineral assemblage (kaolinite *minus* calcite and other Ca-bearing minerals; Fig. 8.1A) indicates that the Bear Lake Formation experienced fluid migration under higher pressure conditions than indicated for CP1. Geologic mapping of the Port Moller area (Wilson et al., 1995; Wilson et al., 1999; Decker et al., 2008b) shows that CP1 (Fig. 2.1) is located near a thrust-fault which juxtaposes the Jurassic Naknek Formation and the Miocene Bear Lake Formation.

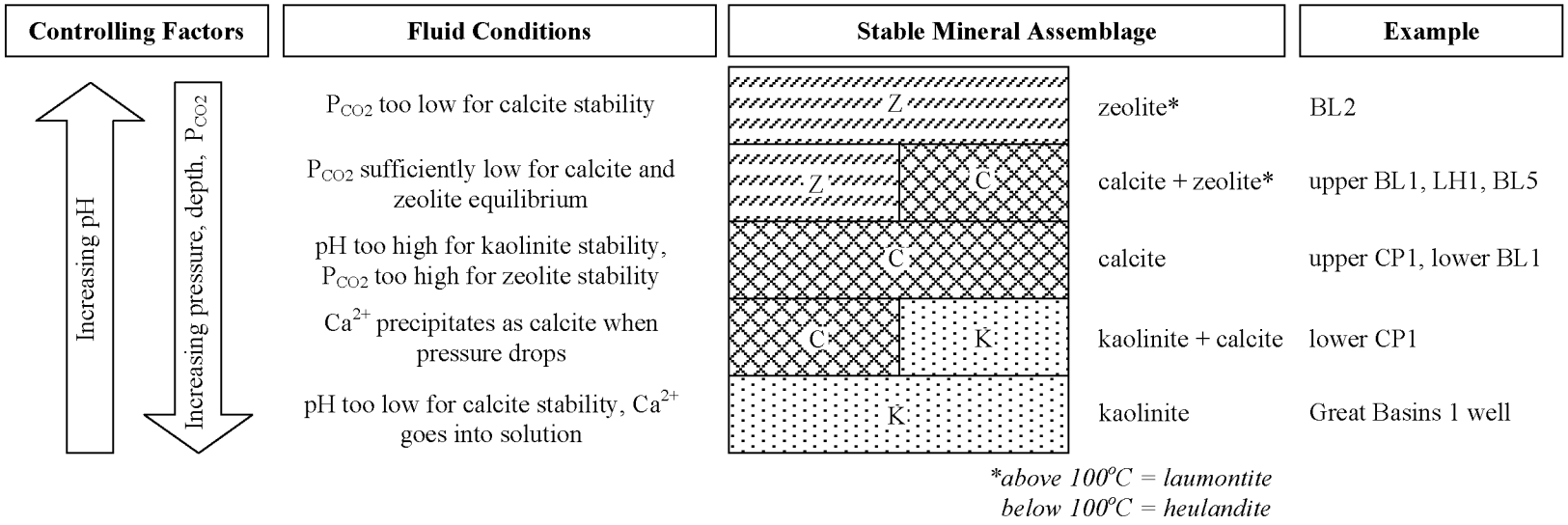

Fig. 8.10 Summary diagram of the pressure-dependant diagenetic system in the Bear Lake Formation.

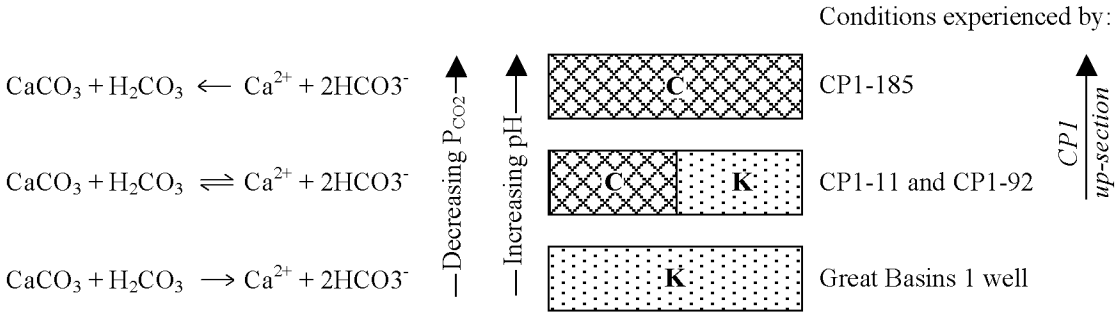

Fig. 811 Schematic illustration of P_{CO2} effects on precipitation of kaolinite versus calcite. K = kaolinite and C = calcite

Therefore, it is likely that pressure differences indicated by the diagenetic mineralogy of CP1 are a result of structural deformation, as opposed to a simple increase in pressure with stratigraphic depth. The over-thrusting at CP1, however, did not provide sufficiently deep burial (high pressure) at the time of fluid migration to result in kaolinite stability relative to calcite, as seen in the Great Basins 1 well.

Zeolite mineralogy documented in measured sections of the Bear Lake Formation can be used to draw comparisons of relative temperatures experienced by the different sections (Fig. 8.12). Heulandite-bearing measured sections (BL2, BL5, and upper BL1) have experienced similar temperatures (less than approximately 100°C), whereas laumontite-bearing LH1 has experienced higher temperatures (greater than approximately 100°C). In addition, thermal maturation data for CP1 indicates temperatures similar to those of lower BL1.

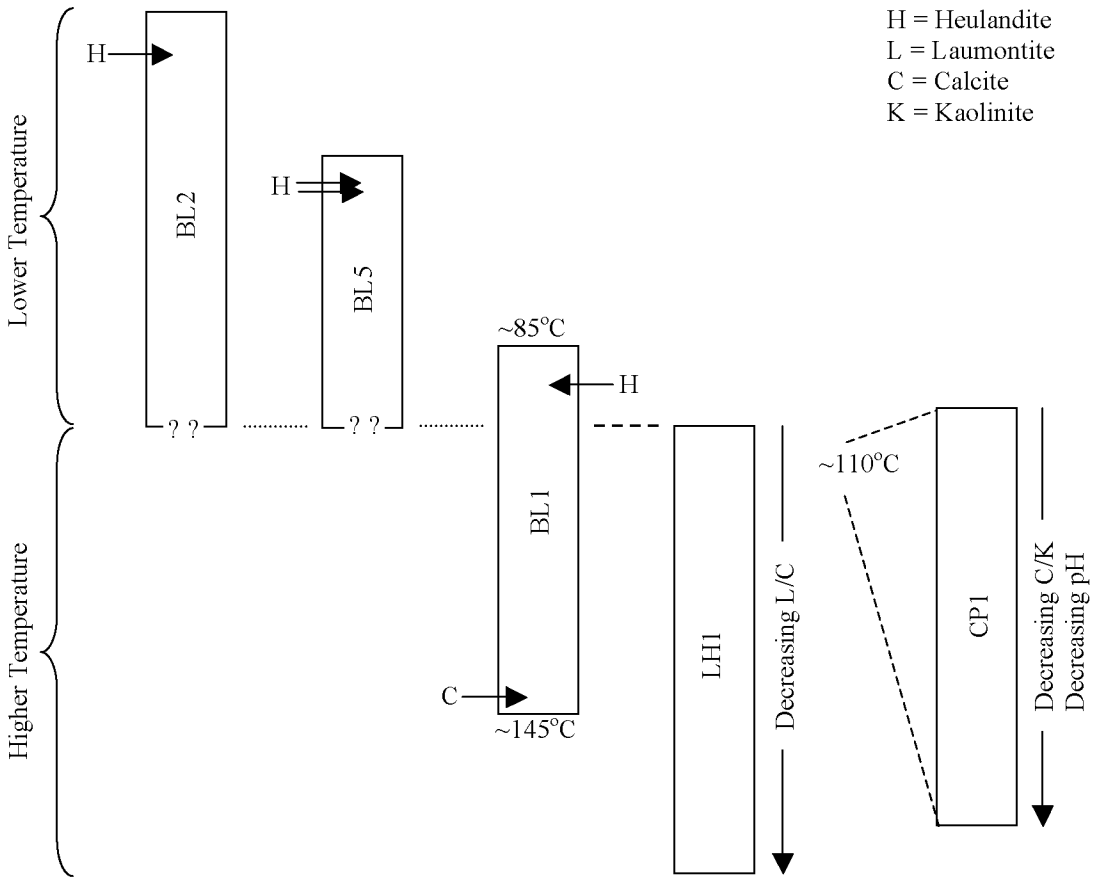

Fig. 8.12 Schematic representation of relative temperatures experienced by measured sections of the Bear Lake Formation. The height of each measured section is displayed proportionately to the total measured thickness.

CHAPTER 9. SUMMARY AND CONCLUSIONS

The Bear Lake Formation cannot simply be described as a quartz-rich, non-volcaniclastic unit derived from recycling of Mesozoic strata as several previous studies have indicated (for example, Burk, 1965; Wisehart, 1971; Lyle et al., 1979; Nilsen, 1984; Wilson, 1985; Detterman, 1990; Detterman et al., 1996; Wilson et al., 1999). Integration of traditional petrographic methods, electron microprobe analysis (EMPA), and $^{40}Ar/^{39}Ar$ dating of detrital grains indicates that the Bear Lake Formation was derived from a combination of volcanic, recycled strata, and locally plutonic provenance (lower part of the Great Basins 1 well).

Integration of these tools provided a much more detailed characterization of sandstone composition in the Bear Lake Formation than would have been possible using strictly traditional petrographic methods, with important implications for both provenance and diagenetic interpretations. Beyond the compositional abundances obtained from point count analysis that show compositional variation up-section, EMPA allowed more reliable identification of volcanic clast compositions and volcanic provenance, as well as insight into the origin of detrital plagioclase clasts. EMPA also allowed identification of diagenetically significant albite. $^{40}Ar/^{39}Ar$ ages of detrital hornblende grains show that multiple recycled sources and a volcanic source simultaneously provided detritus to the Bear Lake Formation, revealing the complicated nature of the source area. Combining multiple tools provides a more complete picture of sandstone composition, source units, diagenetic history, and source terrain. It also strengthens interpretations by providing multiple lines of evidence that point to similar conclusions.

In the Port Moller area, the lower Bear Lake Formation was predominately derived from the Meshik Volcanics northeast of Port Moller (Fig. 6.16), and the upper Bear Lake Formation was predominately derived from recycling of older sedimentary strata (Naknek, Chignik, and Tolstoi formations). However, input from a mixture of the Meshik Volcanics and recycled sediments occurred throughout deposition of the Bear Lake Formation. The erosion of a structurally deformed and juxtaposed stratigraphic succession would account for simultaneous exposure of all units that sourced the Bear Lake Formation. The source area likely consisted of Tertiary and Mesozoic strata exposed in eroded (and likely reverse-faulted) anticlines, similar to the structures currently exposed on the Alaska Peninsula to the

northeast of Port Moller (see Wilson et al., 1999), and between Herendeen Bay and Port Moller (Decker et al., 2008b). Erosion of an anticline results in greater exposure of older rocks (Fig. 7.3A), and this simplified model is one possible structural mechanism for deforming a stratigraphic succession that can explain the increased input of recycled rocks up-section in the Bear Lake Formation (Fig. 7.3B).

At the northeastern end of the greater Bristol Bay basin, in the Ugashik sub-basin (Fig. 3.1), the compositional changes up-section that occur in the Bear Lake Formation are different from those of the Port Moller area. In the Great Basins 1 well near the center of the sub-basin (Fig. 3.1), the base of the Bear Lake Formation was derived from plutonic and metamorphic rocks of the Iliamna subterrane which were exposed on the northern flank of the basin (Fig. 7.4). The composition of the Bear Lake Formation up-section reflects input from a recycled source, similar to rocks of the upper Bear Lake Formation. The recycled source terrain was located to the northeast or east of the sub-basin where the Chignik subterrane flanks the sub-basin (Fig. 7.4). Volcanic input was not substantial for the Bear Lake Formation at this location.

The Bear Lake Formation is less volcanic-rich than other Tertiary units on the Alaska Peninsula, but the volcanic detritus it contains has proven to be an important indicator of provenance. The volcanic clasts (and detrital hornblende grains) indicate derivation from the Meshik Volcanics northeast of Port Moller, and their decreasing abundance up-section indicates a shift of source units from mainly volcanic rocks to mainly recycled sedimentary units (Naknek, Chignik, and Tolstoi formations).

The decrease in volcanic clasts coupled with an increase of quartzose components up-section (see, for example, Fig. 4.15C) is important with regard to reservoir quality of the Bear Lake Formation. The average volcanic component of the lower Bear Lake Formation (33% of the framework) is twice that of the upper Bear Lake Formation (15% of the framework). Conversely, the average quartzose component (Q+ as defined in Table 4.2) of the lower Bear Lake Formation (27% of the framework) is about half that of the upper Bear Lake Formation (50% of the framework). As a result, the reservoir quality likely increases up-section, as the rock composition becomes more quartz-rich, and less volcaniclastic in the upper Bear Lake Formation.

In addition to changes in framework composition, the Bear Lake Formation shows significant variation in diagenetic mineralogy (Fig. 8.1). Three main factors influenced the diagenetic conditions experienced by the Bear Lake Formation: temperature, partial pressure of carbon dioxide (P_{CO2}), and pH. Temperature controls zeolite mineralogy (heulandite versus laumontite), whereas P_{CO2} controls whether zeolite or calcite (commonly plus albite) precipitate. P_{CO2}, which increases with pressure, also controls the pH, and thus caused kaolinite precipitation at high P_{CO2}. As a result, temperature was most influential in the upper Bear Lake Formation, where heulandite and laumontite are present. P_{CO2} was sufficiently low that zeolites are stable relative to calcite. Increased P_{CO2} down-section in the Bear Lake Formation resulted in an absence of zeolites in favor of calcite (for example, lower BL1, Fig. 8.1C). Even greater P_{CO2} caused low pH conditions in lower CP1 and the Great Basins 1 well, which contain kaolinite. Additionally, the Great Basins 1 well lacks calcite (and Ca-bearing minerals; Fig. 8.1A).

The presence of mineral assemblages that are dependant on P_{CO2} conditions suggests that rocks of the upper Bear Lake Formation have experienced fluid migration at lower pressures than those of the lower Bear Lake Formation (CP1), and still lower pressures than the Great Basins 1 well. The sandstones of the upper Bear Lake Formation have pore spaces filled with zeolite and (or) calcite, and the lower Bear Lake Formation at CP1 contains pore-filling calcite ± kaolinite (Fig. 8.1C). Pressure differences between the upper and lower Bear Lake Formation are not related to stratigraphic depth, but to structural deformation that placed Mesozoic strata overtop the Bear Lake Formation at CP1 west of Herendeen Bay (see Wilson et al., 1995; Wilson et al., 1999; Decker et al., 2008b). However, the presence of calcite in CP1 indicates that the pressure during fluid migration was less than that experienced by the Great Basins 1 well. The over-thrusting at CP1 apparently did not provide sufficiently deep burial (high pressure) at the time of fluid migration to result in kaolinite stability relative to calcite. Sandstones of the Great Basins 1 well contain pore-filling kaolinite minus calcite, with greatly increased open pore space due to low pH (high P_{CO2} and high pressure).

Petrographic comparison of samples used in this study indicates that porosity is greater in the well samples than in samples from outcrops near Port Moller (Fig. 1.3 and Fig. 9.1). The diagenetic mineralogy

Fig. 9.1 Diagenetic variation of the Bear Lake Formation. Photomicrographs of samples from outcrops in the Port Moller (samples BL5-52, LH1-2, BL1-155, left to right) area compared to the North Aleutian COST 1 well (sample NAC1-4195) and Great Basins 1 well (sample GB1-3890) illustrate greater porosity in the well samples as indicated by blue-dyed epoxy. Well locations from Detterman (Detterman, 1990). Outcrop exposures of the Bear Lake Formation from Wilson et al. (1999) and Decker et al. (2008b).

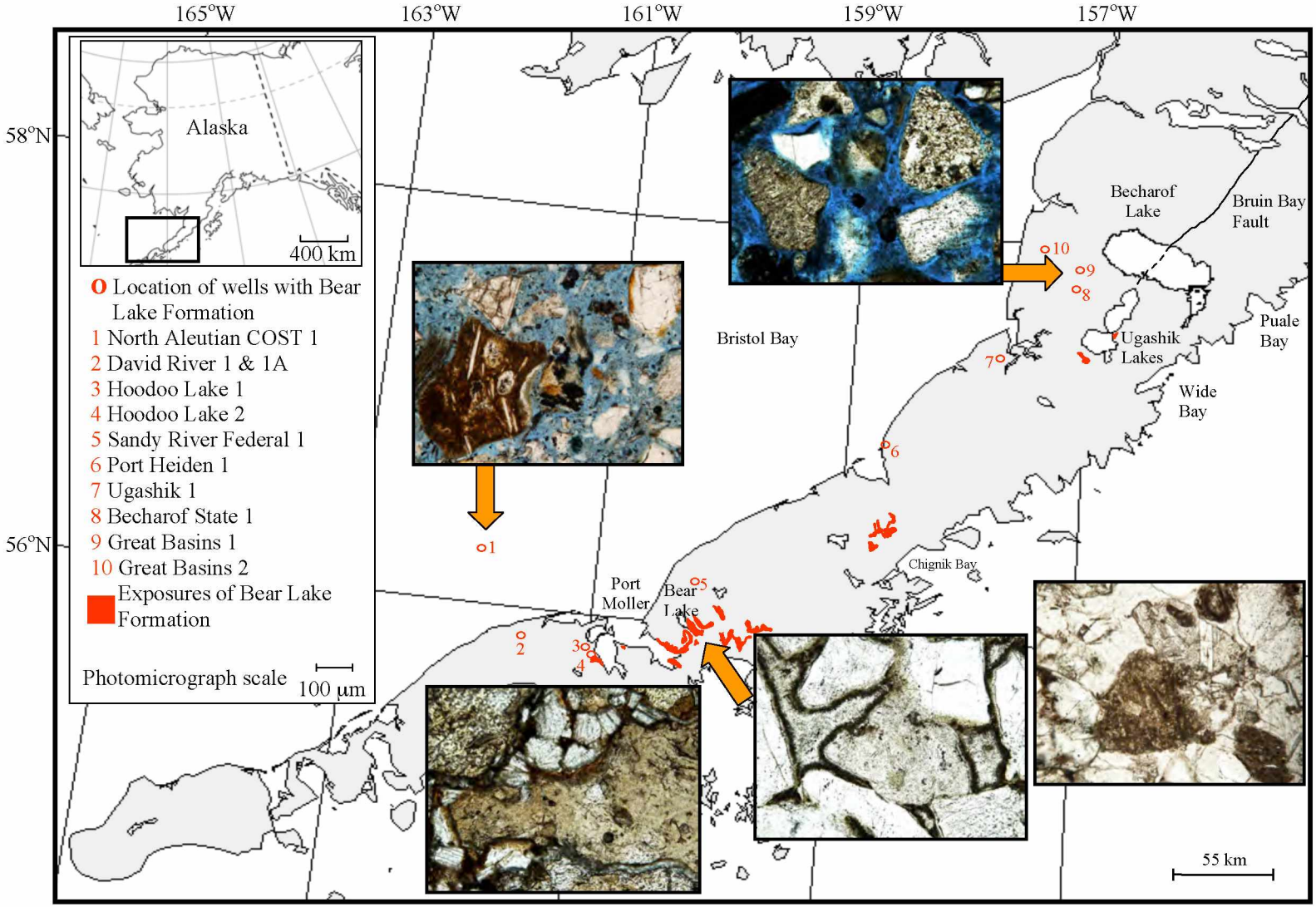
165°W
163°W
161°W
159°W
157°W
58°N
56°N
Alaska
400 km
O Location of wells with Bear Lake Formation
1 North Aleutian COST 1
2 David River 1 & 1A
3 Hoodoo Lake 1
4 Hoodoo Lake 2
5 Sandy River Federal 1
6 Port Heiden 1
7 Ugashik 1
8 Becharof State 1
9 Great Basins 1
10 Great Basins 2
Exposures of Bear Lake Formation
Photomicrograph scale
100 µm
Bristol Bay
Becharof Lake
Bruin Bay Fault
Puale Bay
Ugashik Lakes
Wide Bay
Chignik Bay
Port Moller
Bear Lake
55 km

in the Bear Lake Formation changes as a function of pressure, and specifically as a result of P_{CO2}. Rocks that experienced fluid-migration at high pressure contain kaolinite, and Ca-bearing minerals are replaced (for example, plagioclase is replaced by albite). The Ca then goes into solution. As the fluid rises to shallower depths and lower pressures, P_{CO2} decreases and the Ca precipitates as pore-filling calcite. At shallower depths, following calcite precipitation, P_{CO2} is sufficiently low to allow Ca-zeolite formation. At temperatures above 100°C laumontite forms, and at temperatures below 100°C heulandite forms. XRF data (Appendix C) confirm the increase of Ca-bearing minerals with decreasing pressure (shallower burial), and albite replacement of Ca-bearing minerals at high pressure (deeper burial), showing a decrease in weight percent CaO and increase in Na2O at greater burial depths (Fig. 8.5). The influence of pressure on the diagenetic system (Fig. 8.10) has important implications with respect to the distribution of reservoir quality within the Bear Lake Formation.

Rocks that experienced fluid-migration at high pressure should have greater porosity, as in the Great Basins 1 well (Fig. 4.13B and Fig. 9.1). Rocks that experienced fluid-migration at low pressure should have pore space filled with calcite and (or) zeolites, as in most samples from the measured sections (Fig. 8.1C and Fig. 9.1). Therefore, reservoir quality is likely to be greater in rocks that experienced fluid-migration at high pressure. These higher-quality conditions are present in subsurface strata of the Bear Lake Formation along the northwestern coast of the Alaska Peninsula between Port Moller and Becharof Lake (for example, wells 5 to 10 in Fig. 9.1). The Bear Lake Formation in these wells occurs at depths comparable to the 3,700 ft to 10,320 ft of burial in the Great Basins 1 well (as indicated by depths of Miocene intervals on well correlations by Mickey et al., 2005). Reservoir quality is likely to be degraded where the Bear Lake Formation has experienced fluid-migration at lower pressures (shallower depths). These lower-quality conditions are present in the Bear Lake Formation at the basin margin on the southwest end of the Alaska Peninsula, near Herendeen Bay and Port Moller.

The quartz-rich and relatively volcanic-poor framework composition of the upper Bear Lake Formation (see, for example, Fig. 4.15C) suggests that it has better reservoir quality than the lower Bear Lake Formation. However, the upper Bear Lake Formation in the Port Moller area experienced fluid migration at low pressures resulting in pore-filling calcite and (or) zeolite, and this negatively affected

reservoir quality. Optimal reservoir quality within the Bear Lake Formation is likely to be in the upper part of the formation along the northwestern coast of the Alaska Peninsula (and deeper in the basin), and in the Ugashik sub-basin, where sandstone composition is presumably more quartz-rich, has fewer volcanic clasts, and has experienced fluid migration under higher pressures.

Future studies that would be beneficial to further test these conclusions include:

1) Petrographic analysis of the middle Bear Lake Formation (measured section BL4; Fig. 2.2). This part of the formation is likely to be cemented by calcite and (or) non-kaolinite clay, and to have framework compositions that show a transition between the predominately volcanic-derived lower Bear Lake Formation, and the predominately recycled upper Bear Lake Formation.

2) Petrographic analysis of the Bear Lake Formation in wells on the northwestern coast of the Alaska Peninsula (Fig. 9.1). The Ugashik sub-basin provided a unique setting for deposition of the Bear Lake Formation at the northeast end of the greater Bristol Bay basin (Fig. 3.1). Therefore, the compositional differences observed between the lower and upper Bear Lake Formation near Port Moller are not present in the Great Basins 1 well. The compositional differences are, however, likely present outside of the sub-basin (wells 2 to 7 in Fig. 9.1). The Bear Lake Formation in wells between Port Moller and Becharof Lake (wells 5 to 10 in Fig. 9.2) probably contain minimal calcite cement due to their comparatively deep burial.

3) Porosity and permeability evaluation of the Bear Lake Formation in measured section samples, wells west of Port Moller (wells 2 to 4 in Fig. 9.1), and wells on the northwestern coast of the Alaska Peninsula between Port Moller and Becharof Lake (wells 5 to 10 in Fig. 9.1). Porosity and permeability are likely lower at the onshore, southwestern end of the basin due to more shallow burial depths and resulting lower pressure during fluid migration (low P_{CO2}). In wells to the northeast, porosity and permeability are likely to be greater due to greater burial depths and resulting higher pressure during fluid migration (high P_{CO2}), and to increase up-section as the abundance of volcanic clasts decreases. Porosity and permeability data are available for several of these wells (1, 5, 6, 8, and 9 in Fig. 9.1) and for samples from measured

sections LH1 and CP1 (Helmold et al., 2008). However, porosity and permeability data for wells west of Port Moller (wells 2 to 4 in Fig. 9.1) and for samples from the other measured sections (BL2, BL5, BL1, and BL3) are needed to evaluate porosity and permeability distribution in relation to compositional differences and varying diagenetic conditions in the Bear Lake Formation.

REFERENCES CITED

Abbot, P.L., and Peterson, G.L., 1978, Effects of abrasion durability on conglomerate clast populations: examples from Cretaceous and Eocene conglomerates of the San Diego area, California: Journal of Sedimentary Petrology, v. 48, p. 31-42.

Bergman, S.C., Murphy, J.M., and Kelley, S., 2008, Fission track geochronology of the North Aleutian COST #1 Well (OCS-8218), Bristol Bay Basin, Alaska, *in* Reifenstuhl, R.R., and Decker, P.L., eds., Bristol Bay - Alaska Peninsula region, overview of 2004-2007 geologic research: Alaska Division of Geological and Geophysical Surveys Report of Investigation 2008-1J, p. 177-206.

Blodgett, R.B., Finzel, E.S., Reifenstuhl, R.R., Clautice, K.H., Ridgway, K.D., and Gillis, R.J., 2008, Jurassic through Pliocene age megafossil samples collected in 2005 by the Alaska Divison of Geological and Geophysical Surveys from the Bristol Bay–Port Moller area, Alaska Peninsula: Alaska Division of Geological and Geophysical Surveys Preliminary Interpretive Report 2008-2, 12 p.

Boggs, S., Jr., 2003, Petrology of sedimentary rocks, reprint: New Jersey, The Blackburn Press, 707 p.

Boles, J.R., and Coombs, D.S., 1975, Mineral reactions in zeolitic Triassic tuff, Hokonui Hills, New Zealand: Geological Society of America Bulletin, v. 86, p. 163-173.

Bolger, G.W., and Reifenstuhl, R.R., 2008, Mercury injection capillary pressure and reservoir seal capacity of 26 outcrop samples, Miocene to Triassic Age, *in* Reifenstuhl, R.R., and Decker, P.L., eds., Bristol Bay-Alaska Peninsula region, overview of 2004-2007 geologic research: Alaska Division of Geological and Geophysical Surveys Report of Investigation 2008-1D, p. 69-78.

Bradley, D.C., Parrish, R., Clendenen, W., Lux, D., Layer, P.W., Heizler, M., and Donley, D.T., 2000, New geochronological evidence for the timing of early Tertiary ridge subduction in Southern Alaska, *in* Kelley, K.D., and Gough, L.P., eds., Geologic studies in Alaska by the U. S. Geological Survey, 1998: U.S. Geological Survey Professional Paper 1615, p. 5-21.

Brockway, R.G., Alexander, B., Day, P.D., Lyle, W.M., Hiles, R., Decker, W.M., Polski, W., and Reed, B.L., 1975, Bristol Bay region, stratigraphic correlation section, southwest Alaska: Anchorage, Alaska Geological Society, 1 sheet.

Brown, G.M., 1967, Mineralogy of basaltic rocks, *in* Hess, H.H., and Poldervaart, A., eds., Basalts: The Poldervaart treatise on rocks of basaltic composition, Volume 1: New York, Interscience Publishers, p. 103-162.

Burk, C.A., 1965, Geology of the Alaska Peninsula - island arc and continental margin (part 1): Geological Society of America Memoir 99, 250 p.

Decker, J., 1985, Sandstone modal anlaysis procedure: Alaska Division of Geological and Geophysical Surveys Public-data File 85-3, 38 p.

Decker, J., and Helmold, K.P., 1985, The effect of grain size on detrital modes: a test of the Gazzi-Dickinson point-counting method - discussion: Journal of Sedimentary Petrology, v. 55, p. 618-620.

Decker, P.L., 2008, Mesozoic and Cenozoic source rock-characteristics, Puale Bay outcrops and North Aleutian Shelf COST #1 Well, *in* Reifenstuhl, R.R., and Decker, P.L., eds., Bristol Bay-Alaska

Peninsula region, overview of 2004-2007 geologic research: Alaska Division of Geological and Geophysical Surveys Report of Investigation 2008-1B, p. 11-33.

Decker, P.L., Finzel, E.S., Ridgway, K.D., Reifenstuhl, R.R., and Blodgett, R.B., 2005, Preliminary summary of the 2005 field season: Port Moller, Herendeen Bay, and Dillingham areas, Bristol Bay Basin, Alaska Peninsula: Alaska Division of Geological and Geophysical Surveys Preliminary Interpretive Report 2005-7, 55 p., 2 sheets.

Decker, P.L., Reifenstuhl, R.R., Finzel, E.S., and Helmold, K.P., 2006, Play concepts for reopening the Bristol Bay basin; Tertiary and Mesozoic petroleum systems of the Alaska Peninsula [abs]: American Association of Petroleum Geologists Bulletin, v. 90, Program Abstracts (digital).

Decker, P.L., Reifenstuhl, R.R., and Gillis, R.J., 2008a, Structural linkage of major tectonic elements in the Ugashik-Becharof Lakes region, northeastern Alaska Peninsula, *in* Reifenstuhl, R.R., and Decker, P.L., eds., Bristol Bay - Alaska Peninsula region, overview of 2004-2007 geologic research: Alaska Division of Geological and Geophysical Surveys Report of Investigation 2008-1F, p. 85-103, 1 sheet.

Decker, P.L., Reifenstuhl, R.R., Gillis, R.J., and Loveland, A., 2008b, Revised geologic map and structural model of the Staniukovich Peninsula-Herendeen Bay area, *in* Reifenstuhl, R.R., and Decker, P.L., eds., Bristol Bay-Alaska Peninsula region, overview of 2004-2007 geologic research: Alaska Division of Geological and Geophysical Surveys Report of Investigation 2008-1I, p. 161-176, 2 sheets, scale 1:50,000.

Deer, W.A., Howie, R.A., and Zussmzn, J., 1992, An introduction to the rock-forming minerals - 2nd edition: Harlow, Prentice Hall, 696 p.

Detterman, R.L., 1990, Stratigraphic correlation and interpretation of exploratory wells, Alaska Peninsula: U.S. Geological Survey Open-File Report 90-279, 51 p.

Detterman, R.L., Case, J.E., Miller, J.W., Wilson, F.H., and Yount, M.E., 1996, Stratigraphic framework of the Alaska Peninsula: U.S. Geological Survey Bulletin 1969-A, 74 p.

Detterman, R.L., Case, J.E., Wilson, F.H., and Yount, M.E., 1987, Geologic map of the Ugashik, Bristol Bay, and western part of Karlik quadrangles, Alaska: U.S. Geological Survey Miscellaneous Investigations Series Map 1685, 1 plate, scale 1:250,000.

Detterman, R.L., and Hartsock, J.K., 1966, Geology fo the Iniskin-Tuxedni region, Alaska: U.S. Geological Survey Professional Paper 512, 78 p., 6 plates, scale 1:63,000.

Detterman, R.L., Hudson, T., Plafker, G., Tysdal, R.G., and Hoare, J.M., 1976, Reconnaissance geologic map along Bruin Bay and Lake Clark faults in Kenai and Tyonek quadrangles, Alaska: U.S. Geological Survey Open-File Report 76-477, 4 p., 1 sheet, scale 1:250,000.

Detterman, R.L., Miller, T.P., Yount, M.E., and Wilson, F.H., 1981, Geologic map of the Chignik and Sutwik Island quadrangles, Alaska: U.S. Geological Survey Miscellaneous Investigations 1229, 1 sheet, scale 1:250,000.

Detterman, R.L., and Reed, B.L., 1980, Stratigraphy, structure, and economic geology of the Iliamna Quadrangle, Alaska: U.S. Geological Survey Bulletin 1368-B, 86 p., 1 plate, scale 1:250,000.

Dickinson, W.R., 1970, Interpreting detrital modes of graywacke and arkose: Journal of Sedimentary Petrology, v. 40, p. 695-707.

—, 1985, Interpreting provenance relations from detrital modes of sandstones, *in* Zuffa, G.G., ed., Provenance of arenites: Dordrecht, D. Reidel Publishing Company, p. 333-362.

Dickinson, W.R., Beard, L.S., Brakenridge, G.R., Erjavec, J.L., Ferguson, R.C., Inman, K.F., Knepp, R.A., Lindberg, F.A., and Ryberg, P.T., 1983, Provenance of North American Phanerozoic sandstones in relation to tectonic setting: Geological Society of America Bulletin, v. 94, p. 222-235.

Dickinson, W.R., and Rich, E.I., 1972, Petrologic intervals and petrofacies in the Great Valley Sequence, Sacremento Valley, California: Geological Society of America Bulletin, v. 83, p. 3007-3024.

Dickinson, W.R., and Suczek, C.A., 1979, Plate tectonics and sandstone compositions: The American Association of Petroleum Geologists Bulletin, v. 63, p. 2164-2182.

Durant, G.P., 1989, Rhyolite, *in* Bowes, D.R., ed., The encyclopedia of igneous and metamorphic petrology: New York, Van Nostrand Reinhold, p. 512-513.

Ewart, A., 1982, The mineralogy and petrology of Tertiary-Recent orogenic volcanic rocks: with special reference to the andesitic-basaltic compositional range, *in* Thorpe, R.S., ed., Andesites: orogenic andesites and related rocks: Chichester, John Wiley & Sons, p. 25-95.

Faure, G., 1998, Principles and applications of geochemistry: Upper Saddle River, Prentice Hall, 600 p.

Finzel, E.S., Reifenstuhl, R.R., Decker, P.L., and Ridgway, K.D., 2005, Sedimentology, stratigraphy, and hydrocarbon reservoir-source rock potential, using surface and subsurface data, of Tertiary and Mesozoic strata, Bristol Bay Basin and Alaska Peninsula: Alaska Division of Geological and Geophysical Surveys Preliminary Interpretive Report 2005-4, 69 p.

Flett, T.O., 1988, Organic geochemistry, *in* Turner, R.F., ed., Geological and operational summary, North Aleutian Shelf COST No. 1 well, Bering Sea, Alaska: Minerals Management Service OCS Report MMS 88-0089, p. 184-202.

Gifkins, C., Herrmann, W., and Large, R., 2005, Altered volcanic rocks: a guide to description and interpretation: Hobart, Centre for Ore Deposit Research, 275 p.

Graham, S.A., Ingersoll, R.V., and Dickinson, W.R., 1976, Common provenance for lithic grains in Carboniferous sandstones from Ouachita Mountains and Black Warrior Basin: Journal of Sedimentary Petrology, v. 46, p. 620-632.

Grantz, A., 1963, Aerial reconnaissance of the outer Shumagin Islands, Alaska, *in* U.S. Geological Survey Staff, Geological survey research 1963, Short papers in geology, hydrology, Articles 1-59: U.S. Geological Survey Professional Paper 475-B, p. B106-B109.

Hartbauer, C., 2008, Bear Lake Formation microprobe data, *in* Reifenstuhl, R.R., and Decker, P.L., eds., Bristol Bay - Alaska Peninsula region, overview of 2004-2007 geologic research: Alaska Division of Geological and Geophysical Surveys Report of Investigation 2008-1E, p. 79-83.

Helmold, K.P., and Brizzolara, D.W., 2005, Reservoir quality of Tertiary sandstones from Bristol Bay basin, Alaska Peninsula: preliminary report: Alaska Division of Oil and Gas 32 p.

Helmold, K.P., Brizzolara, D.W., and Reifenstuhl, R.R., 2008, Reservoir quality of 84 Tertiary sandstones from three exploratory wells, Bristol Bay basin, Alaska Peninsula, *in* Reifenstuhl, R.R., and Decker, P.L., eds., Bristol Bay - Alaska Peninsula region, overview of 2004-2007 geologic research: Alaska Division of Geological and Geophysical Surveys Report of Investigation 2008-1C, p. 35-67.

Hicks, S.A., Jensen, K.K., and Newberry, R.J., 2003, 'Slab' XRF, a quick and not-so-dirty method for estimating compositions of fine-grained rocks [abs]: Alaska Geological Society Geology Symposium 2003 - Abstracts and program, p. 38.

Ingersoll, R.V., 1978, Petrofacies and petrologic evolution of the Late Cretaceous fore-arc basin, northern and central California: Journal of Geology, v. 86, p. 335-352.

—, 1983, Petrofacies and provenance of late Mesozoic forearc basin, northern and central California: American Association of Petroleum Geologists Bulletin, v. 67, p. 1125-1142.

Ingersoll, R.V., Bullard, T.F., Ford, R.L., Grimm, J.P., Pickle, J.D., and Sares, S.W., 1984, The effect of grain size on detrital modes: a test of the Gazzi-Dickinson point-counting method: Journal of Sedimentary Petrology, v. 54, p. 103-116.

Ingersoll, R.V., Bullard, T.F., Ford, R.L., and Pickle, J.D., 1985, The effect of grain size on detrital modes: a test of the Gazzi-Dickinson point-counting method - reply to discussion of John Decker and Kenneth P. Helmold: Journal of Sedimentary Petrology, v. 55, p. 620-621.

Ivanov, I.P., and Gurevich, L.P., 1975, Experimental sutdy of T-XCO2 boundaries of metamorphic zeolite facies: Contributions to Mineralogy and Petrology, v. 53, p. 55-60.

Kienle, J., and Turner, D.L., 1976, The Shumagin-Kodiak Batholith - A Paleocene magmatic arc?: Alaska Division of Geological and Geophysical Surveys Geologic Report 51C, p. 9-11.

Kirschner, C.E., 1988, Map showing sedimentary basins of offshore and continental shelf areas, Alaska: U.S. Geological Survey Miscellaneous Investigations Series 1873, 1 plate, scale 1:2,500,000.

Lankford, S.M., and Magoon, L.B., 1977, Petrography of hte Upper Juassic through Oligocene sandstones in the Cape Douglas-Kamishak Hills area, lower Cook Inlet, *in* Johnson, K.M., ed., The United States Geological Survey in Alaska: accomplishments during 1977, U.S. Geological Survey Circular 772-B, p. B60-B62.

Lanphere, M.A., and Dalrymple, G.B., 2000, First-principles calibration of 38Ar tracers: implications for the ages of 40Ar/39Ar fluence monitors: U.S. Geological Survey Professional Paper 1621, 10 p.

Larsen, J.F., Nye, C.J., Coombs, M.L., Tilman, M., Izbekov, P., and Cameron, C., 2010 in press, Petrology and Geochemistry of the 2006 Eruption of Augustine Volcano, *in* Power, J.A., Coombs, M.L., and Freymueller, J.T., eds., The 2006 Eruption of Augustine Volcano, Alaska: U.S. Geological Survey Professional Paper 1769, p. unknown.

Layer, P.W., 2000, Argon-40/argon-39 age of the El'gygytgyn impact event, Chukotka, Russia: Meteroitics and Planatary Science, v. 35, p. 591-599.

Layer, P.W., Hall, C.M., and York, D., 1987, The derivation of 40Ar/39Ar age spectra of single grains of hornblende and biotite by laser step heating: Geophyscial Research Letters, v. 14, p. 757-760.

Loveland, A.M., Reifenstuhl, R.R., Gillis, R.J., and Decker, P.L., 2007, Outcrop sample results from mercury injection capillary pressure analyses, Bristol Bay, Alaska Peninsula: Alaska Division of Geological and Geophysical Surveys Raw Data File 2007-3, 11 p.

Lyle, W.M., Morehouse, J.A., Palmer, I.F., Jr., and Bolm, J.G., 1979, Tertiary formations and associated Mesozoic rocks in the Alaska Peninsula area, Alaska, and their petroleum-reservoir and source-rock potential: Alaska Division of Geological and Geophysical Surveys Geologic Report 62, 69 p.

Mack, G.H., 1984, Exceptions to the relationship between plate tectonics and sandstone composition: Journal of Sedimentary Petrology, v. 54, p. 212-220.

Mancini, E.A., 1978, Upper Cretaceous arc-trench gap sedimentation on the Alaska Peninsula: Geology, v. 6, p. 437-439.

Marincovich, L., Jr, 1983, Molluscan paleontology, paleoecology, and North Pacific correlations of the Miocene Tachilni Formation, Alaska Peninsula, Alaska: Bulletins of American Paleontology, v. 84, p. 59-155.

Marlow, M.S., Cooper, A.K., and Fisher, M.A., 1994, Geology of the eastern Bering Sea continental shelf, *in* Plafker, G., and Berg, H.C., eds., The Geology of Alaska: Boulder, Geological Society of America, The Geology of North America, v. G-1, p. 271-284.

Marsh, B.D., 1976, Some Aleutian andesites: their nature and source: Journal of Geology, v. 84, p. 27-45.

—, 1982, The Aleutians, *in* Thorpe, R.S., ed., Andesites: orogenic andesites and related rocks: Chichester, John Wiley & Sons, p. 99-114.

McBirney, A.R., 1989, Andesite and dacite, *in* Bowes, D.R., ed., The encyclopedia of igneous and metamorphic petrology: New York, Van Nostrand Reinhold, p. 18-22.

McDougall, I., and Harrison, T.M., 1999, Geochronology and Thermochronology by the 40Ar/39Ar method - 2nd edition: New York, Oxford University Press, 269 p.

McLean, H., 1977, Organic geochemistry, lithology, and paleontology of Tertiary and Mesozoic rocks from wells on the Alaska Peninsula: U.S. Geological Survey Open-File Report 77-813, 63 p.

—, 1979, Sandstone petrology: Upper Jurassic Naknek Formation of the Alaska Peninsula and coeval rocks on the Bering shelf: Journal of Sedimentary Petrology, v. 49, p. 1263-1268.

Mickey, M.B., Haga, H., Boettcher, R.S., and Kling, S.A., 2005, Northwestern Alaska Peninsula - Bristol Bay basin biostratigraphy study: Micropaleo Consultants Job No. 25-104: Alaska Division of Oil and Gas online publication http://www.dog.dnr.state.ak.us/oil/products/publications/akpeninsula/biostrat.htm, 287 p.

Molenaar, C.M., 1996, Thermal-maturity patterns and geothermal gradients on the Alaska Peninsula, *in* Johnsson, M.J., and Howell, D.G., eds., Thermal evolution of sedimentary basins in Alaska: U.S. Geological Survey Bulletin 2142, p. 11-19.

Moore, J.C., 1974a, Geologic and structural map of part of the outer Shumagin Islands, southwestern Alaska: U.S. Geological Survey Miscellaneous Investigations 815, 1 sheet, scale 1:63,360.

—, 1974b, Geologic and structural map of the Sanak Islands, southwestern Alaska: U.S. Geological Survey Miscellaneous Investigations 817, 1 sheet, scale 1:63,360.

Nesse, W.D., 1991, Introduction to optical mineralogy - 2nd edition: New York, Oxford University Press, 335 p.

Neuhoff, P.S., and Bird, D.K., 2001, Partial dehydration of laumontite: thermodynamic constraints and petrogenetic implications: Mineralogical Magazine, v. 65, p. 59-70.

Nilsen, T.H., 1984, Miocene back-arc tidal deposits of the Bear Lake Formation, Alaska Peninsula, *in* Reed, K.M., and Bartsch-Winkler, S., eds., The United States Geological Survey in Alaska - accomplishments during 1982: U.S. Geological Survey Circular 939, p. 85-88.

Peters, K.E., Walters, C.C., and Moldowan, J.M., 2005, The biomarker guide, volume 1: biomarkers and isotopes in the environment and human history - 2nd edition: Cambridge, Cambridge University Press.

Rader, E., 2010, Mineral stability in H2O undersaturated magmas: experiments on basaltic andesite from Westdahl Volcano [M.S. thesis]: Fairbanks, University of Alaska, unknown p.

Reed, B.L., and Lanphere, M.A., 1969, Age and chemistry of Mesozoic and Tertiary plutonic rocks in south-central Alaska: Geological Society of America Bulletin, v. 80, p. 23-44.

—, 1972, Generalized geologic map of the Alaska-Aleutian Range batholith showing potassium-argon ages of the plutonic rocks: U.S. Geological Survey Miscellaneous Field Studies 372, 2 sheets.

—, 1973, Alaska-Aleutian Range Batholith: geochronology, chemistry, and relation to circum-Pacific plutonism: Geological Society of America Bulletin, v. 84, p. 2583-2610.

—, 1974, Chemical variations across the Alaska-Aletuian range batholith: U.S. Geological Survey Journal of Research, v. 2, p. 343-352.

Reifenstuhl, R.R., and Decker, P.L., eds., 2008, Bristol Bay-Alaska Peninsula region, overview of 2004-2007 geologic research: Alaska Division of Geological and Geophysical Surveys Report of Investigation 2008-1, 223 p., 3 sheets, scale 1:50,000.

Reifenstuhl, R.R., Shafer, D.C., Ryherd, T.J., Brizzolara, D.W., and Blodgett, R.B., 2004, Summary of May 25-June 4, 2004, field notes and samples, Puale Bay and Wide Bay areas, Alaska Peninsula: Alaska Division of Geological and Geophysical Surveys Raw Data File 2004-3, 16 p.

Samson, S.D., and Alexander, E.C., 1987, Calibration of the interlaboratory 40Ar/39Ar dating standard, MMhb-1: Chemical Geology, v. 66, p. 27-34.

Sawaki, T., Sasada, M., Sasaki, M., and Goko, K., 1997, Fluid inclusion study of the Kirishima geothermal system, Japan: Geothermics, v. 26, p. 305-327.

Sherwood, K.W., Larson, J.A., Comer, C.D., Craig, J.D., and Reitmeier, C., 2006, North Aleutian basin OCS planning area assessment of undiscovered technically-recoverable oil and gas: U.S. Minerals Management Service Alaska OCS Region report, 138 p., 4 plates.

Steiger, R.H., and Jaeger, E., 1977, Subcommission on geochronology: convention on the use of decay constants in geo and cosmochronology: Earth and Planetary Science Letters, v. 36, p. 359-362.

Suttner, L.J., and Basu, A., 1985, The effect of grain size on detrital modes: a test of the Gazzi-Dickinson point-counting method - discussion: Journal of Sedimentary Petrology, v. 55, p. 616-617.

Tappen, C.M., Webster, J.D., Mandeville, C.W., and Roderick, D., 2009, Petrology and geochemistry of ca. 2100–1000 a.B.P. magmas of Augustine volcano, Alaska, based on analysis of prehistoric pumiceous tephra: Journal of Volcanology and Geothermal Research, v. 183, p. 42-62.

Turner, R.F., McCarthy, C.M., Lynch, M.B., Hoose, P.J., Martin, G.C., Larson, J.A., Flett, T.O., Sherwood, K.W., and Adams, A.J., 1988, Geological and operation summary, North Aleutian Shelf COST No. 1 well, Bering Sea, Alaska: Minerals Management Service OCS Report MMS 88-0089, 256 p.

Van der Plas, L., and Tobi, A.C., 1965, A chart for judging the reliability of point counting results: American Journal of Science, v. 263, p. 87-90.

Walker, K.T., McGeary, S.E., and Klemperer, S.L., 2003, Tectonic evolution of the Bristol Bay basin, southeast Bering Sea: constraints from seismic reflection and potential field data: Tectonics, v. 22, p. 4-1-4-19.

Wilson, F.H., 1980, Late Mesozoic and Cenozoic tectonics and the age of porphyry copper prospects; Chignik and Sutwik Island quadrangles, Alaska Peninsula: U.S. Geological Survey Open-File Report 80-543, 94 p., 5 sheets, scale 1:250,000.

—, 1985, The Meshik arc - an Eocene to earliest Miocene magmatic arc on the Alaska Peninsula: Alaska Division of Geological and Geophysical Surveys Professional Report 88, 14 p.

Wilson, F.H., Detterman, R.L., and DuBois, G.D., 1999, Digital data for the geologic framework of the Alaska Peninsula, Southwest Alaska, and the Alaska Peninsula Terrane: U.S. Geological Survey Open-File Report 99-317, 41 p., 1 plate, scale 1:500,000. Wilson, F.H., Gaum, W.C., and Herzon, P.L., 1981, Map and tables showing geochronology and whole-rock geochemistry of the Chignik and Sutwik Island quadrangles, Alaska: U.S. Geological Survey Miscellaneous Field Studies Map 1053-M, 3 sheets, scale 1:250,000.

Wilson, F.H., Miller, J.W., and Case, J.E., 1995, Geologic map of the Port Moller, Stepovak Bay, and Simeonof Island quadrangles, Alaska Peninsula, Alaska: U.S. Geological Survey Miscellaneous Investigations 2272, 2 sheets, scale 1:250,000.

Wilson, F.H., and Shew, N., 1992, Map and tables showing geochronology and whole-rock geochemistry of selected samples, Ugashik and part of Karluk quadrangles, Alaska: U.S. Geological Survey Miscellaneous Field Studies Map 1539-E, scale 1 :250,000.

Wilson, F.H., Shew, N., DuBois, G.D., and Bie, S.W., 1994, Sample locality map and analytical data for potassium-argon ages in the Port Moller, Stepovak Bay, and Simeonof Island quadrangles, Alaska Peninsula: U.S. Geological Survey Miscellaneous Field Studies 2155-E, 18 p., 1 sheet, scale 1:250,000.

Wisehart, R.M., 1971, Paleoenvironmental analysis of the Bear Lake Formation, Alaska Peninsula, Alaska [M.S. thesis]: Los Angeles, University of California, 112 p.

Worrall, D.M., 1991, Tectonic history of the Bering Sea and the evolution of Tertiary strike-slip basins of the Bering Shelf: Geological Society of America Special Paper 257, 120 p., 1 sheet, 4 plates, scale 1:2,500,000.

York, D., Hall, C.M., Yanase, Y., Hanes, J.A., and Kenyon, W.J., 1981, 40Ar/39Ar dating of terrestrial minerals with a continuous laser: Geophyscial Research Letters, v. 8, p. 1136-1138.

Zen, E., 1961, The zeolite facies: an interpretation: American Journal of Science, v. 259, p. 401-409.

APPENDIX A

BEAR LAKE FORMATION BIBLIOGRAPHY

I have compiled selected references pertaining to the Bear Lake Formation in this bibliography. It is meant only to be a helpful resource and does not represent a complete list of all publications related to the Bear Lake Formation. It is important to note two key points when reviewing literature of the Bear Lake Formation:

1) As discussed by Finzel et al. (2005, p. 45), recent biostratigraphic results (Mickey et al., 2005) provide the basis for current formation picks in the subsurface, which disagree with previous lithologic-based interpretations (for example, Brockway et al., 1975; McLean, 1977; Detterman, 1990).

2) Prior to work presented by Detterman et al. (1996), the Unga Conglomerate was considered to be the basal member of the Bear Lake Formation. As currently defined, the Unga Formation is a formation separate from the Bear Lake Formation with exposures restricted to Unga Island, Ukolnoi Island, Wosnesenski Island, and the southern shore of the Alaska Peninsula near Unga Strait (Fig. A-1; Detterman et al., 1996; Wilson et al., 1999). This key point is especially important as related to biostratigraphy reported by Marincovish and Kase (1986) and Marincovich (1988). Detterman et al. (1996, p. 51, 56-57) indicate that these two publications report on what is now considered to be the Unga Formation, and not the Bear Lake Formation.

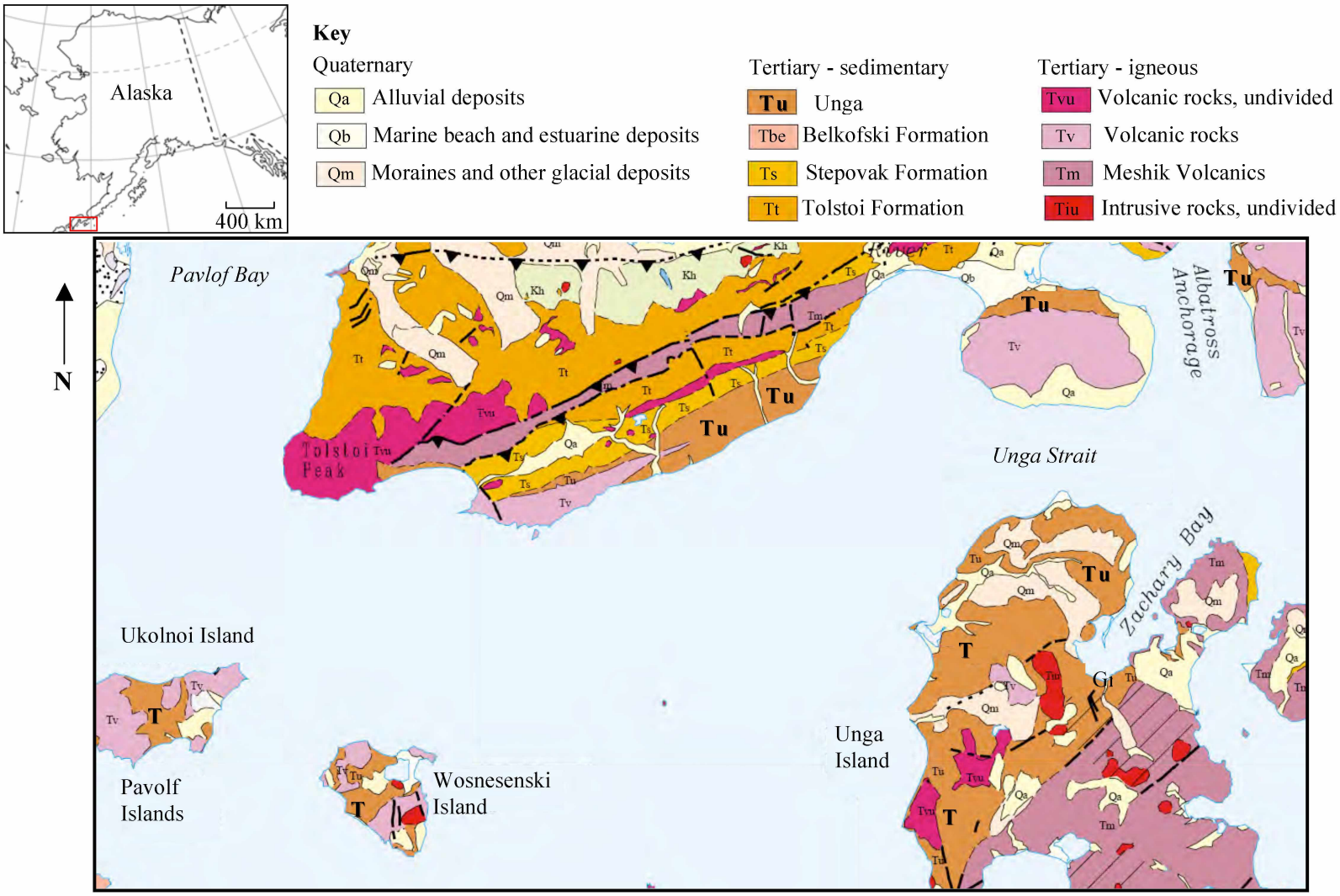

Fig. A-1 Outcrop exposure of the Unga Formation. Modified from Wilson et al. (1999). The Bear Lake Formation crops out to the north of the map area (Fig. 3.3).

Bibliography

Alaska Division of Oil and Gas, 2004, Alaska Peninsula areawide oil and gas leae sale and Bristol Bay basin exploration license area, information and data compilation: Alaska Division of Oil and Gas Alaska Peninsula oil and gas resource series, 3 volume CD-ROM.

Atwood, W.W., 1911, Geology and mineral resources of parts of the Alaska Peninsula: U.S. Geological Survey Bulletin 467, 137 p.

Bergman, S.C., Murphy, J.M., and Kelley, S., 2008, Fission track geochronology of the North Aleutian COST #1 Well (OCS-8218), Bristol Bay Basin, Alaska, *in* Reifenstuhl, R.R., and Decker, P.L., eds., Bristol Bay - Alaska Peninsula region, overview of 2004-2007 geologic research: Alaska Division of Geological and Geophysical Surveys Report of Investigation 2008-1J, p. 177-206.

Blodgett, R.B., Finzel, E.S., Reifenstuhl, R.R., Clautice, K.H., Ridgway, K.D., and Gillis, R.J., 2008, Jurassic through Pliocene age megafossil samples collected in 2005 by the Alaska Divison of Geological and Geophysical Surveys from the Bristol Bay–Port Moller area, Alaska Peninsula: Alaska Division of Geological and Geophysical Surveys Preliminary Interpretive Report 2008-2, 12 p.

Bolger, G.W., and Reifenstuhl, R.R., 2008, Mercury injection capillary pressure and reservoir seal capacity of 26 outcrop samples, Miocene to Triassic Age, *in* Reifenstuhl, R.R., and Decker, P.L., eds., Bristol Bay-Alaska Peninsula region, overview of 2004-2007 geologic research: Alaska Division of Geological and Geophysical Surveys Report of Investigation 2008-1D, p. 69-78.

Brockway, R.G., Alexander, B., Day, P.D., Lyle, W.M., Hiles, R., Decker, W.M., Polski, W., and Reed, B.L., 1975, Bristol Bay region, stratigraphic correlation section, southwest Alaska: Anchorage, Alaska Geological Society, 1 sheet.

Burk, C.A., 1965, Geology of the Alaska Peninsula - island arc and continental margin (part 1): Geological Society of America Memoir 99, 250 p.

Decker, P.L., 2008, Mesozoic and Cenozoic source rock-characteristics, Puale Bay outcrops and North Aleutian Shelf COST #1 Well, *in* Reifenstuhl, R.R., and Decker, P.L., eds., Bristol Bay-Alaska Peninsula region, overview of 2004-2007 geologic research: Alaska Division of Geological and Geophysical Surveys Report of Investigation 2008-1B, p. 11-33.

Decker, P.L., Finzel, E.S., Ridgway, K.D., Reifenstuhl, R.R., and Blodgett, R.B., 2005, Preliminary summary of the 2005 field season: Port Moller, Herendeen Bay, and Dillingham areas, Bristol Bay Basin, Alaska Peninsula: Alaska Division of Geological and Geophysical Surveys Preliminary Interpretive Report 2005-7, 55 p., 2 sheets.

Decker, P.L., Reifenstuhl, R.R., Finzel, E.S., and Helmold, K.P., 2006, Play concepts for reopening the Bristol Bay basin; Tertiary and Mesozoic petroleum systems of the Alaska Peninsula [abs]: American Association of Petroleum Geologists Bulletin, v. 90, Program Abstracts (digital).

Decker, P.L., Reifenstuhl, R.R., and Gillis, R.J., 2008a, Structural linkage of major tectonic elements in the Ugashik-Becharof Lakes region, northeastern Alaska Peninsula, *in* Reifenstuhl, R.R., and Decker, P.L., eds., Bristol Bay - Alaska Peninsula region, overview of 2004-2007 geologic research: Alaska Division of Geological and Geophysical Surveys Report of Investigation 2008-1F, p. 85-103, 1 sheet.

Decker, P.L., Reifenstuhl, R.R., Gillis, R.J., and Loveland, A., 2008b, Revised geologic map and structural model of the Staniukovich Peninsula-Herendeen Bay area, *in* Reifenstuhl, R.R., and Decker, P.L., eds., Bristol Bay-Alaska Peninsula region, overview of 2004-2007 geologic research: Alaska Division of Geological and Geophysical Surveys Report of Investigation 2008-1I, p. 161-176, 2 sheets, scale 1:50,000.

Detterman, R.L., 1990, Stratigraphic correlation and interpretation of exploratory wells, Alaska Peninsula: U.S. Geological Survey Open-File Report 90-279, 51 p.

Detterman, R.L., Case, J.E., Miller, J.W., Wilson, F.H., and Yount, M.E., 1996, Stratigraphic framework of the Alaska Peninsula: U.S. Geological Survey Bulletin 1969-A, 74 p.

Detterman, R.L., Case, J.E., Wilson, F.H., and Yount, M.E., 1987, Geologic map of the Ugashik, Bristol Bay, and western part of Karlik quadrangles, Alaska: U.S. Geological Survey Miscellaneous Investigations Series Map 1685, 1 plate, scale 1:250,000.

Detterman, R.L., Miller, T.P., Yount, M.E., and Wilson, F.H., 1981, Geologic map of the Chignik and Sutwik Island quadrangles, Alaska: U.S. Geological Survey Miscellaneous Investigations 1229, 1 sheet, scale 1:250,000.

Finzel, E.S., Reifenstuhl, R.R., Decker, P.L., and Ridgway, K.D., 2005a, Sedimentology, stratigraphy, and hydrocarbon reservoir-source rock potential, using surface and subsurface data, of Tertiary and Mesozoic strata, Bristol Bay Basin and Alaska Peninsula: Alaska Division of Geological and Geophysical Surveys Preliminary Interpretive Report 2005-4, 69 p.

Finzel, E.S., Ridgway, K.D., Decker, P.L., and Reifenstuhl, R.R., 2005b, Reservoir characterization of the Bear Lake and Milky River Formations, Bristol Bay basin, Alaska Peninsula [abs]: Geological Society of America Abstracts with Programs, v. 37, p. 96.

Finzel, E.S., Ridgway, K.D., Reifenstuhl, R.R., Blodgett, R.B., White, J.M., and Decker, P.L., 2009, Stratigraphic framework and estuarine depositional environments of the Miocene Bear Lake Formation, Bristol Bay Basin, Alaska; onshore equivalents to potential reservoir strata in a frontier gas-rich basin: AAPG Bulletin, v. 93, p. 379-405.

Hartbauer, C., 2008, Bear Lake Formation microprobe data, *in* Reifenstuhl, R.R., and Decker, P.L., eds., Bristol Bay - Alaska Peninsula region, overview of 2004-2007 geologic research: Alaska Division of Geological and Geophysical Surveys Report of Investigation 2008-1E, p. 79-83.

Helmold, K.P., and Brizzolara, D.W., 2005, Reservoir quality of Tertiary sandstones from Bristol Bay basin, Alaska Peninsula: preliminary report: Alaska Division of Oil and Gas 32 p.

Helmold, K.P., Brizzolara, D.W., and Reifenstuhl, R.R., 2008, Reservoir quality of 84 Tertiary sandstones from three exploratory wells, Bristol Bay basin, Alaska Peninsula, *in* Reifenstuhl, R.R., and Decker, P.L., eds., Bristol Bay - Alaska Peninsula region, overview of 2004-2007 geologic research: Alaska Division of Geological and Geophysical Surveys Report of Investigation 2008-1C, p. 35-67.

Loveland, A.M., Reifenstuhl, R.R., Gillis, R.J., and Decker, P.L., 2007, Outcrop sample results from mercury injection capillary pressure analyses, Bristol Bay, Alaska Peninsula: Alaska Division of Geological and Geophysical Surveys Raw Data File 2007-3, 11 p.

Lyle, W.M., Morehouse, J.A., Palmer, I.F., Jr., and Bolm, J.G., 1979, Tertiary formations and associated Mesozoic rocks in the Alaska Peninsula area, Alaska, and their petroleum-reservoir and source-rock potential: Alaska Division of Geological and Geophysical Surveys Geologic Report 62, 69 p.

Marincovich, L., Jr, 1983, Molluscan paleontology, paleoecology, and North Pacific correlations of the Miocene Tachilni Formation, Alaska Peninsula, Alaska: Bulletins of American Paleontology, v. 84, p. 59-155.

—, 1988, Miocene mollusks from the lower part of the Bear Lake Formation on Ukolnoi Island, Alaska Peninsula, Alaska: Contributions in Science, v. 397, p. 1-20.

Marincovich, L., Jr, and Kase, T., 1986, An occurance of *Turritella (Hataiella) sagai* in Alaska - implications for the age of the Bear Lake Formation: Bulletin of the National Science Museum, Tokyo, v. 12, p. 61-66.

Marincovich, L., Jr, and McCoy, S., Jr, 1984, An overview of Paleogene molluscan biostratigraphy and paleoecology of the Gulf of Alaska region: Palaeogeography, Palaeoclimatology, Palaeoecology, v. 47, p. 91-103.

Marincovich, L., Jr, and Powell, C.L., II, 1989, Preliminary Tertiary molluscan biostratigraphy of the Alaskan Peninsula, southwestern Alaska: U.S Geological Survey Open-File Report 89-674, 2 sheets.

McLean, H., 1977, Organic geochemistry, lithology, and paleontology of Tertiary and Mesozoic rocks from wells on the Alaska Peninsula: U.S. Geological Survey Open-File Report 77-813, 63 p.

Mickey, M.B., Haga, H., Boettcher, R.S., and Kling, S.A., 2005, Northwestern Alaska Peninsula - Bristol Bay basin biostratigraphy study: Micropaleo Consultants Job No. 25-104: Alaska Division of Oil and Gas online publication http://www.dog.dnr.state.ak.us/oil/products/publications/akpeninsula/biostrat.htm, 287 p.

Molenaar, C.M., 1996, Thermal-maturity patterns and geothermal gradients on the Alaska Peninsula, *in* Johnsson, M.J., and Howell, D.G., eds., Thermal evolution of sedimentary basins in Alaska: U.S. Geological Survey Bulletin 2142, p. 11-19.

Nilsen, T.H., 1984, Miocene back-arc tidal deposits of the Bear Lake Formation, Alaska Peninsula, *in* Reed, K.M., and Bartsch-Winkler, S., eds., The United States Geological Survey in Alaska - accomplishments during 1982: U.S. Geological Survey Circular 939, p. 85-88.

—, 1985, Sedimentology of tidally deposited Miocene Bear Lake Formation, Alaskan Peninsula: AAPG Bulletin, v. 69, p. 673.

Reifenstuhl, R.R., and Finzel, E.S., 2005, Bristol Bay, frontier basin, Alaska Peninsula: hydrocarbon resources, petroleum reservoir characterization, and source potential: Geological Society of America Abstracts with Programs, v. 37, p. 96.

Reifenstuhl, R.R., Shafer, D.C., Ryherd, T.J., Brizzolara, D.W., and Blodgett, R.B., 2004, Summary of May 25-June 4, 2004, field notes and samples, Puale Bay and Wide Bay areas, Alaska Peninsula: Alaska Division of Geological and Geophysical Surveys Raw Data File 2004-3, 16 p.

Sherwood, K.W., Larson, J.A., Comer, C.D., Craig, J.D., and Reitmeier, C., 2006, North Aleutian basin OCS planning area assessment of undiscovered technically-recoverable oil and gas: U.S. Minerals Management Service Alaska OCS Region report, 138 p., 4 plates.

Turner, R.F., McCarthy, C.M., Lynch, M.B., Hoose, P.J., Martin, G.C., Larson, J.A., Flett, T.O., Sherwood, K.W., and Adams, A.J., 1988, Geological and operation summary, North Aleutian Shelf COST No. 1 well, Bering Sea, Alaska: Minerals Management Service OCS Report MMS 88-0089, 256 p.

Wilson, F.H., 1980, Late Mesozoic and Cenozoic tectonics and the age of porphyry copper prospects; Chignik and Sutwik Island quadrangles, Alaska Peninsula: U.S. Geological Survey Open-File Report 80-543, 94 p., 5 sheets, scale 1:250,000.

—, 1985, The Meshik Arc - an Eocene to earliest Miocene magmatic arc on the Alaska Peninsula: Alaska Division of Geological and Geophysical Surveys Professional Report 88, 14 p.

Wilson, F.H., Detterman, R.L., and DuBois, G.D., 1999, Digital data for the geologic framework of the Alaska Peninsula, Southwest Alaska, and the Alaska Peninsula Terrane: U.S. Geological Survey Open-File Report 99-317, 41 p., 1 plate, scale 1:500,000.

Wilson, F.H., Detterman, R.L., and Harris, E.E., 1991, Generalized geologic map of the Port Moller, Stepovak Bay, and Simeonof Island quadrangles, Alaska Peninsula, Alaska: U.S. Geological Survey Miscellaneous Field Studies 2155-A, 1 sheet, scale 1:250,000.

Wilson, F.H., Miller, J.W., and Case, J.E., 1995, Geologic map of the Port Moller, Stepovak Bay, and Simeonof Island quadrangles, Alaska Peninsula, Alaska: U.S. Geological Survey Miscellaneous Investigations 2272, 2 sheets, scale 1:250,000.

Wilson, F.H., Shew, N., DuBois, G.D., and Bie, S.W., 1994, Sample locality map and analytical data for potassium-argon ages in the Port Moller, Stepovak Bay, and Simeonof Island quadrangles, Alaska Peninsula: U.S. Geological Survey Miscellaneous Field Studies 2155-E, 18 p., 1 sheet, scale 1:250,000.

Wisehart, R.M., 1971, Paleoenvironmental analysis of the Bear Lake Formation, Alaska Peninsula, Alaska [M.S. thesis]: Los Angeles, University of California, 112 p.

APPENDIX B

DESCRIPTION OF VOLCANIC ROCK FRAGMENTS IN SANDSTONES OF THE BEAR LAKE FORMATION

Table B-1 presents descriptions of volcanic rock fragments analyzed using electron microprobe analysis. The term "phenocryst" refers to any discreetly identifiable crystal with euhedral or subeuhedral shape. The term "lath" specifies when an analysis was performed on a relatively small lath-shaped feldspar crystal, typically a few microns across on the short-axis. Alteration of groundmass by "fine-grained siliceous material" refers to dark (usually brownish) non-crystalline material with high weight percent SiO_2 (commonly greater than about 85 wt. %).

The symbol "(?)" indicates that either the analysis has a low analytical total or that the analysis is interpreted to represent a combination of multiple minerals. In the second instance, the mineral(s) reported is a reasonable interpretation of the mineral or combination of minerals present based on the chemistry. For example, the groundmass crystals listed for one volcanic rock fragment from sample LH1-66.5 are quartz(?), K-feldspar(?), and albite(?). This indicates that analyses of the groundmass in the volcanic rock fragment represent a combination of minerals interpreted to be quartz, K-feldspar, and albite.

Compositional information for feldspar is given in the form of end-member percentages. Anorthite percentages ($An_{\#}$) are reported for plagioclase and albite ($An_{\#}$ = 100*Ca/(Ca+Na) using atomic percentages). Orthoclase percentages ($Or_{\#}$) are reported for K-feldspar ($Or_{\#}$ = 100*K/(K+Na) using atomic percentages). The values reported for zoned plagioclase do not necessarily represent the compositional range from rim to core, but merely the range of points analyzed within the crystal. For some zoned plagioclase phenocrysts only one point within the crystal was analyzed and the zoning was identified petrographically.

In some cases no feldpsar composition is given and the crystal is simply listed as either plagioclase, albite, or K-feldspar. This indicates that no $An_{\#}$ or $Or_{\#}$ could be calculated. One reason for this is that the analytical total may be too low for a reliable enough calculation (for example, the analytical total is less than about 85%). The second reason that no composition was calculated is that the attempted analysis of a single crystal actually included a combination of minerals (for example, phenocryst +

groundmass or two groundmass crystals instead of one). Despite either the low analytical total or the analysis representing a combination of minerals, I am confident that the mineral reported in the table is present in the volcanic rock fragment. K-feldspar reported with no $Or_{\#}$ likely have potassium end-member compositions (high $Or_{\#}$).

The felsic (rhyolite to dacite), intermediate (andesite to basaltic andesite), and mafic (basalt) groundmass composition assignments are based on the groundmass mineralogy and the average chemical composition of multiple analyses of groundmass in each volcanic rock fragment.

Table B-1 Description of volcanic rock fragments analyzed by electron microprobe analysis.

Sample	Phenocrysts	Phenocryst Alteration/ Replacement	Groundmass Crystals	Groundmass Alteration	Groundmass Composition	Comments
BL2-176			quartz, K-feldspar (Or_{85}), heulandite	illitic clay, smectite, mixed-layer K-Ca clay	felsic	relict perlite
BL2-176	albite (An_{6-9})			Fe-smectite, Ti-oxide	intermediate	
BL2-176	albite (An_0)		quartz, K-feldspar, albite (An_{0-1})	mixed-layer Fe-K clay, mixed-layer K-Na clay	felsic	
BL2-176		mixed-layer Fe-K clay, chloritic clay	quartz, K-feldspar, albite	illitic clay, Ti-oxide	felsic	
BL2-176	albite (An_{7-11})			chloritic(?) clay, Ti-oxide	intermediate	highly altered, possibly plutonic
LH1-182			K-feldspar (Or_{80-87}), albite (An_2)		felsic	
LH1-182	feldspar	chloritic clay, sphene	quartz, K-feldspar (Or_{97}), albite (An_2)		felsic	
LH1-182			K-feldspar (Or_{88-90}), albite (An_1& An_2)		felsic	
LH1-182			quartz, K-feldspar, albite (An_1)		felsic	
LH1-182			quartz, albite (An_2 & An_3)		felsic	
LH1-182		chlorite, chloritic clay	albite (An_{1-4})	Na-smectite	felsic	
LH1-182		laumontite, chloritic clay	quartz, K-feldspar, albite (An_2)	illitic clay	felsic	
LH1-182	hornblende, Fe-oxide	laumontite	quartz(?), K-feldspar (Or_{82} & Or_{85}), albite (An_2 & An_3)		felsic	
LH1-182			quartz, K-feldspar (Or_{97}), albite (An_2)		felsic	

Table B-1 continued

Sample	Phenocrysts	Phenocryst Alteration/ Replacement	Groundmass Crystals	Groundmass Alteration	Groundmass Composition	Comments
LH1-182		laumontite	K-feldspar and albite (An_2)		felsic	
LH1-164	plagioclase (An_{46-50}), K-feldspar (Or_{71} & Or_{88})		apatite	illitic clay, Fe-smectite, mixed-layer Fe-K clay, mixed-layer Na-K clay, chloritic clay, fine-grained calcite	intermediate	
LH1-164	plagioclase (An_{37-62}), albite (An_8)		K-feldspar (Or_{84} & Or_{87})	chlorite, illitic clay, Fe-oxide, Fe-smectite	intermediate	
LH1-164			plagioclase (An_{12-18}), albite (An_6)	chloritic clay, chlorite	intermediate	
LH1-164	plagioclase (An_{30})		K-feldspar (Or_{91} & Or_{92})	chloritic clay, chlorite	felsic	
LH1-164	plagioclase (An_{65})			mixed-layer Fe-K clay, Ti-oxide	intermediate	
LH1-164	plagioclase (An_{50})		quartz, plagioclase (An_{34}), K-feldspar (Or_{70})		felsic	
LH1-164	plagioclase (An_{45-57})			chloritic(?) clay		
LH1-164	quartz		K-feldspar (Or_{85})		felsic	
LH1-164	plagioclase (An_{45-59})		K-feldspar (Or_{73} & Or_{75})	chloritic clay, smectite, Na-smectite, mixed-layer Fe-K clay	intermediate	
LH1-164	plagioclase (An_{50})	calcite		calcite, Na-smectite, Fe-smectite, illitic clay	intermediate	
LH1-164			quartz, K-feldspar (Or_{83}),	illitic clay	felsic	
LH1-164	plagioclase (An_{43-52})	chloritic clay		chloritic clay	intermediate	

Table B-1 continued

Sample	Phenocrysts	Phenocryst Alteration/ Replacement	Groundmass Crystals	Groundmass Alteration	Groundmass Composition	Comments
LH1-164	plagioclase (An_{50-64})			chloritic clay	mafic	
LH1-164	plagioclase (An_{41-54})			smectite, Ti-oxide	felsic	
LH1-120			quartz, K-feldspar, albite		felsic	
LH1-120			quartz, K-feldspar (Or_{86}), albite		felsic	
LH1-120	albite (An_4)	chlorite	quartz, albite	Fe-oxide	felsic	
LH1-120			quartz, albite	smectite(?)	felsic	
LH1-120	albite		quartz, K-feldspar, albite (An_4)	Fe-oxide, Ti-oxide	felsic	
LH1-120			K-feldspar (Or_{83} & Or_{97}), albite (An_4)	calcite	felsic	
LH1-120			quartz, K-feldspar, albite (An_{10})	Fe-smectite	felsic	
LH1-120			quartz, K-feldspar (Or_{85}), albite (An_4)	chloritic clay	felsic	flow-aligned laths present
LH1-120	albite (An_7)	Fe-smectite	quartz, K-feldspar (Or_{80}), albite (An_4)		felsic	
LH1-120			quartz, K-feldspar, albite (An_4)	Fe-oxide, Ti-oxide, calcite	felsic	
LH1-120	plagioclase (An_{20})		quartz, K-feldspar, albite (An_{3-4})		felsic	
LH1-120			plagioclase (An_{11-23})	chlorite, minor calcite, sphene, ilmenite	felsic	
LH1-120	albite (An_3)		quartz, K-feldspar	sphene, ilmenite(?), Fe-smectite, chloritic clay	felsic	
LH1-66.5	plagioclase (An_{40} & An_{46})	chloritic clay	plagioclase (An_{28} & An_{33})	Fe-smectite, Ti-oxide	felsic	

Table B-1 continued

Sample	Phenocrysts	Phenocryst Alteration/ Replacement	Groundmass Crystals	Groundmass Alteration	Groundmass Composition	Comments
LH1-66.5	zoned plagioclase (An_{29})		quartz(?), K-feldspar(?), albite (?)	Ti-oxide	felsic	
LH1-66.5	albite (An_0)		quartz, feldspar laths	chlorite, chloritic clay, mixed-layer Fe-K clay, Ti-oxide, Fe-oxide	intermediate	
LH1-66.5	plagioclase (An_{50-56})		albite (An_{11})	Fe-smectite, calcite	intermediate	
LH1-66.5	plagioclase (An_{49})		quartz	smectite, chloritic clay, calcite, Ti-oxide	intermediate	
LH1-66.5	plagioclase (An_{44}) lath			calcite	intermediate	
LH1-66.5	plagioclase (An_{44-55})		quartz	chlorite, calcite	intermediate	
LH1-66.5	plagioclase	calcite altered plagioclase	quartz, plagioclase(?)	calcite, Ti-oxide	felsic	
LH1-66.5	plagioclase (An_{46} & An_{57})	albite (An_3) altered plagioclase (An_{56})	K-feldspar, albite (An_3)	calcite, chloritic clay	felsic	flow-aligned laths present in groundmass
LH1-66.5			plagioclase (An_{34-50})	chloritic clay, mixed-layer Na-K clay, ilmenite(?)	intermediate	groundmass consists of flow-aligned laths
LH1-66.5	plagioclase (An_{36} & An_{37}), zoned plagioclase (An_{48-57})		plagioclase laths (An_{20} & An_{22})	Fe-oxide, minor calcite, smectite(?)	felsic	
LH1-66.5	albite (An_4)	calcite altered albite (An_5)		Ti-oxide, Fe-Smectite	intermediate	
LH1-66.5			K-feldspar (Or_{96-98})	Fe-smectite, chloritic clay	intermediate	Fe-K clay, chloritic clay, calcite filled vesicles
LH1-2	albite (An_1)		K-feldspar (Or_{92})	significant fine-grained calcite alteration	felsic	

Table B-1 contintued

Sample	Phenocrysts	Phenocryst Alteration/ Replacement	Groundmass Crystals	Groundmass Alteration	Groundmass Composition	Comments
LH1-2	albite (An_6)		quartz, albite (An_3)	chloritic(?) clay, Ti-oxide	felsic	flow-aligned laths present
LH1-2	plagioclase (An_{39-49})		plagioclase (An_{29} & An_{32})	chloritic clay, calcite	felsic	
LH1-2	quartz, plagioclase (An_{27-30}), K-feldspar (Or_{75} & Or_{90})		quartz, K-feldspar		felsic	
LH1-2	feldspar	Fe-smectite	plagioclase (An_{33}), K-feldspar(?)	calcite	felsic	
LH1-2	plagioclase (An_{37} & An_{33}), zoned plagioclase (An_{38} & An_{45})		quartz, albite (An_4)	chloritic clay, significant fine-grained calcite	felsic	
BL5-92		calcite altered plagioclase (An_{43} & An_{55})		mixed-layer Fe-K clay, illitic clay, and calcite	intermediate	
BL5-92	plagioclase (An_{39-41})		plagioclase (An_{46})	mixed-layer Fe-K clay	intermediate	
BL5-52	albite (An_{1-6})		plagioclase (An_{15})	illitic clay, sphene		
BL5-52				illitic clay, mixed-layer K-Na clay		possible volcanic rock fragment; spherical features present may be filled vesicles
BL1-155	plagioclase (An_{45} & An_{48}), K-feldspar (Or_{50})		quartz, K-feldspar, albite		felsic	
BL1-155	quartz, albite (An_2)			calcite, sphene		
BL1-155	plagioclase (An_{27-50})		plagioclase (An_{41})	minor calcite	felsic	
BL1-155	quartz, plagioclase (An_{30} & An_{37})		plagioclase (An_{34}), K-feldspar(?)		felsic	

Table B-1 continued

Sample	Phenocrysts	Phenocryst Alteration/ Replacement	Groundmass Crystals	Groundmass Alteration	Groundmass Composition	Comments
BL1-155			K-feldspar (Or_{73-93})	fine-grained silicious material	felsic	
BL1-155	plagioclase (An_{51})	calcite	plagioclase(?), K-feldspar(?)	smectite, mixed-layer Ca-K clay, pyrite	felsic	
BL1-155	plagioclase (An_{51})	chloritic clay	plagioclase (An_{50})	chlorite		
BL1-155			quartz, plagioclase (An_{16})	smectite	felsic	
BL1-155	plagioclase (An_{42}), K-feldspar (Or_{82})		plagioclase (An_{34} & An_{55}), K-feldspar(?)		felsic	
BL1-155			plagioclase (An_{44-53})	minor calcite	felsic	
BL1-155			plagioclase (An_{40} & An_{47})	illitic clay, mixed-layer K-Na clay, fine-grained silicious material	felsic	
BL1-155	plagioclase (An_{41}), K-feldspar (Or_{71}) lath, hornblende (Mg_{69})		K-feldspar (Or_{62-67})	Ti-oxide	felsic	laths present in groundmass
BL1-155	plagioclase (An_{44} & An_{56})		plagioclase (An_{37} & An_{41})	Ti-oxide, Fe-oxide	felsic	
BL1-155				Fe-smectite , Na-Smectite	felsic	
BL1-155			quartz, apatite	illitic clay	felsic	
BL1-155	K-feldspar (Or_{20}?)	altered ferromagnesian phenocryst	plagioclase (An_{33})		felsic	
BL1-155	plagioclase (An_{57})			groundmass has been replaced by calcite		
BL1-155	plagioclase (An_{58} & An_{60})			groundmass has been replaced by calcite		
BL1-155	plagioclase (An_{59})	calcite	plagioclase (An_{35})	significant fine-grained calcite		

Table B-1 continued

Sample	Phenocrysts	Phenocryst Alteration/ Replacement	Groundmass Crystals	Groundmass Alteration	Groundmass Composition	Comments
BL1-155	plagioclase (An_{31-62})		quartz	significant fine-grained calcite		
BL1-5	plagioclase (An_{48-61})		plagioclase(?), K-feldspar(?), apatite	Ti-oxide, Fe-oxide	felsic	
BL1-5	plagioclase (An_{44-59})			smectite, mixed-layer K-Ca clay, calcite, Ti-oxide	intermediate	
BL1-5	albite (An_4)			mixed-layer K-Ca clay	felsic	
BL1-5	plagioclase (An_{50} & An_{57})		plagioclase (An_{32})	calcite	felsic	
BL1-5	albite (An_{2-5})		quartz	Na-smectite, Ti-oxide	felsic	
BL1-5	plagioclase (An_{58}), K-feldspar (Or_{72}) lath		quartz, K-feldspar (Or_{55})	calcite	felsic	
BL1-5			plagioclase (An_{45-49})	mixed-layer K-Na clay	intermediate	
BL1-5	plagioclase (An_{38-57})		plagioclase (An_{33}), K-feldspar (Or_{65})	mixed-layer Fe-K clay, calcite	felsic	
BL1-5			quartz, plagioclase (An_{46}), K-feldspar (Or_{80})		felsic	
BL1-5			quartz	smectite, illitic clay	felsic	
BL3-272	plagioclase (An_{57-74})		plagioclase (An_{37} & An_{40})	Fe-smectite	intermediate	
BL3-272	plagioclase (An_{55-67}), albite (An_5)			Na-smectite, Fe-smectite, chloritic clay	intermediate	
BL3-272	plagioclase (An_{51} & An_{54})		quartz, K-feldspar, albite	Fe-smectite	felsic	

Table B-1 continued

Sample	Phenocrysts	Phenocryst Alteration/ Replacement	Groundmass Crystals	Groundmass Alteration	Groundmass Composition	Comments
BL3-272	plagioclase (An_{67} & An_{68})		plagioclase (An_{38}), K-feldspar(?)	Fe-smectite, fine-grained silicious material	felsic	
BL3-272	plagioclase (An_{59} & An_{61})		plagioclase (An_{38})		felsic	
BL3-272	plagioclase (An_{56})		plagioclase, K-feldspar	Ti-oxide, Fe-smectite	felsic	
BL3-272	plagioclase (An_{52}), zoned feldspar	chloritic clay, Fe-smectite	K-feldspar, albite		felsic	
BL3-272	plagioclase (An_{36-61}) including zoned phenocryst (An_{52-61})		feldspar	Fe-smectite, fine-grained silicious material	felsic	
BL3-272			quartz, K-feldspar, albite	mixed-layer Fe-K clay	felsic	
BL3-272			quartz, plagioclase (An_{24})	chloritic clay	felsic	
BL3-272	zoned plagioclase (An_{49} & An_{62})		plagioclase(?)	smectite(?), Ti-oxide	felsic	
BL3-272	with plagioclase (An_{47} & An_{49}), albite (An_4 & An_7)			Fe-smectite		
BL3-272	plagioclase (An_{33} & An_{35}), albite (An_3)		K-feldspar, albite (An_3)		felsic	
BL3-205	plagioclase (An_{41})	Fe-smectite	plagioclase (An_{37} & An_{46})	chlorite	intermediate	
BL3-205	plagioclase (An_{60})	albite altered plagioclase (An_{66})		Na-smectite, Fe-smectite	intermediate	
BL3-205			K-feldspar(?), albite (An_6)	Fe-smectite	felsic	
BL3-205	plagioclase (An_{37-51})		quartz	mixed-layer K-Na clay	felsic	

Table B-1 continued

Sample	Phenocrysts	Phenocryst Alteration/ Replacement	Groundmass Crystals	Groundmass Alteration	Groundmass Composition	Comments
BL3-205	plagioclase (An_{43} & An_{49})		quartz, K-feldspar (Or_{81})		felsic	
BL3-205	plagioclase (An_{44} & An_{48})		quartz, K-feldspar, albite(?)	mixed-layer Fe-K clay, mixed-layer K-Na clay	felsic	
BL3-205		chloritic clay	quartz, plagioclase (An_{32} & An_{46}), K-feldspar (Or_{90})		felsic	
BL3-205	plagioclase (An_{58-65})		quartz	illitic clay, mixed-layer K-Ca clay	intermediate	
BL3-205			quartz, K-feldspar(?), albite(?)		felsic	
BL3-205	plagioclase (An_{64})		plagioclase (An_{45} & An_{48}), apatite		intermediate	
BL3-205			quartz, K-feldspar, albite(?)		felsic	
BL3-193	plagioclase (An_{39-52})		albite (An2)	Ti-oxide	felsic	
BL3-193	albite laths (An_1)		quartz(?), K-feldspar(?), albite(?)	illitic clay	felsic	flow-aligned laths present
BL3-193	plagioclase (An_{55-67}), albite (An_{3-6})		quartz, plagioclase (An_{40})		felsic	
BL3-193	plagioclase (An_{35-61}), albite (An_3 & An_4)		quartz, plagioclase (An_{49}), albite	smectite, Fe-smectite, mixed-layer Fe-K clay	intermediate	
BL3-193	plagioclase (An_{54-61})		plagioclase (An_{24-34}), K-feldspar(?), albite(?)		felsic	
BL3-193	plagioclase (An_{49-56}), albite (An_1)		quartz, plagioclase (An_{32}), albite(?)	chloritic clay	felsic	

Table B-1 continued

Sample	Phenocrysts	Phenocryst Alteration/ Replacement	Groundmass Crystals	Groundmass Alteration	Groundmass Composition	Comments
BL3-193	plagioclase (An_{44-68})	chloritic clay	quartz, K-feldspar, albite (An7)	smectite(?)	felsic	one of the chloritic clay altered phenocrysts is likely altered hornblende
BL3-193	plagioclase (An_{42})	chlorite, chloritic clay	quartz, plagioclase (An_{25}), albite (An_{10})		felsic	
BL3-193	plagioclase (An_{60} & An_{69})		quartz	mixed-layer K-Na clay, fine-grained silicious material	felsic	
BL3-193	plagioclase (An_{63}), albite (An_{1})			smectite, chlorite, chloritic clay, Fe-oxide, fine-grained silicious material	intermediate	
BL3-193	plagioclase (An_{57} & An_{60})		quartz, plagioclase (An_{47})	smectite	felsic	
BL3-193	plagioclase (An_{48-72}), including zoned phenocryst (An_{59-66})		quartz, plagioclase (An_{50})	fine-grained silicious material, smectite	felsic	
BL3-193	albite (An_{5})	albite altered zoned plagioclase (An_{46-67}), Fe-smectite, smectite	quartz, albite(?), and K-feldspar (Or_{79})		felsic	
BL3-193	plagioclase (An_{49-61}), albite (An_{1})	chlorite	quartz, albite (An_{9})		felsic	
BL3-193	plagioclase (An_{47-60})		quartz, plagioclase, and K-feldspar (Or_{81})		felsic	
BL3-193	plagioclase (An_{41-62})			Ca-smectite, fine-grained silicious material	felsic	

Table B-1 continued

Sample	Phenocrysts	Phenocryst Alteration/ Replacement	Groundmass Crystals	Groundmass Alteration	Groundmass Composition	Comments
BL3-193	plagioclase (An_{47-69})	chloritic clay	quartz, K-feldspar (Or_{77}), albite (An_9)		felsic	
BL3-193	plagioclase (An_{54}), albite (An_5)		quartz, albite (An_{10}), apatite	Na-smectite, Fe-smectite, Ti-oxide, chloritic clay	felsic	
BL3-193	plagioclase (An_{53}) & zoned plagioclase (An_{55-61})		quartz, K-feldspar, albite (An_{3-7})	Fe-oxide	felsic	
BL3-36		calcite replaced feldspar lath	plagioclase (An_{37}), albite (An_0)	chloritic clay	intermediate	
BL3-36	plagioclase (An_{44} & An_{51}), albite (An_4 & An_9)		plagioclase(?), apatite	Na-smectite, Fe-smectite, Ti-oxide	intermediate	
BL3-36	plagioclase (An_{40-48})	clay (Fe-smectite?)	plagioclase laths	Fe-smectite	intermediate	
BL3-36	plagioclase (An_{52})		plagioclase (An_{45}), albite	mixed-layer Fe-K clay, Na-smectite, chloritic clay	intermediate	
BL3-36			plagioclase (An_{32}), albite (An_6)	mixed-layer K-Ca clay, Ti-oxide, calcite	intermediate	
BL3-36	plagioclase (An_{53-56})	calcite, chloritic clay, chlorite	albite (An_7)	chloritic clay, Ti-oxide	mafic	one of the altered phenocrysts is calcite altered albite
BL3-36	plagioclase (An_{58})	Na-smectite	plagioclase (An_{51})	mixed-layer Fe-K clay	intermediate	
BL3-36	albite (An_6)	chlorite	plagioclase (An_{13}), albite (An_6)	fine-grained silicious material	felsic	
BL3-36	plagioclase (An_{39-41})		quartz, plagioclase (An_{12} & An_{14}), albite	Fe-smectite	felsic	

Table B-1 continued

Sample	Phenocrysts	Phenocryst Alteration/ Replacement	Groundmass Crystals	Groundmass Alteration	Groundmass Composition	Comments
BL3-36	plagioclase (An_{32-58})	chlorite, calcite	quartz, albite (An_{10}), apatite	chloritic clay, mixed-layer Fe-K clay, Ti-oxide	intermediate	
BL3-36	albite (An_8)	chlorite	plagioclase (An_{36})	chloritic clay, Ti-oxide	intermediate	
BL3-36	plagioclase (An_{55})	calcite, illitic, mixed-layer Fe-K clay, chloritic clay	quartz, plagioclase(?),	chlorite(?), Ti-oxide	felsic	calcite & chloritic clay alter a plagioclase (An_{44}) phenocryst
BL3-36	plagioclase		plagioclase	chloritic clay, Na-smectite	intermediate	
BL3-36			plagioclase (An_{50} & An_{51})	Fe-smectite, chloritic clay	mafic	
BL3-36			plagioclase (An_{52})	chlorite, chloritic clay	mafic	
BL3-36	albite (An_3)		albite (An_2)	chloritic clay, chlorite, calcite, mixed-layer Fe-K clay	intermediate	
BL3-36	plagioclase (An_{42} & An_{49})		quartz, plagioclase (An_{42})	Ti-oxide, minor calcite	felsic	
BL3-36			plagioclase (An_{49})	chloritic clay, fine-grained silicious material, significant fine-grained calcite	intermediate	
BL3-36	plagioclase (An_{20})	calcite altered plagioclase (An_{52}), Fe-smectite	apatite	fine-grained silicious material, Ti-oxide	felsic	
CP1-185	plagioclase (An_{43-51})	calcite	plagioclase (An_{26-27}), apatite	chlorite, smectite(?)	felsic	

Table B-1 continued

Sample	Phenocrysts	Phenocryst Alteration/ Replacement	Groundmass Crystals	Groundmass Alteration	Groundmass Composition	Comments
CP1-185		chlorite	plagioclase (An_{12-32}), albite (An_8)	Na-smectite	felsic	groundmass consists of flow-aligned laths
CP1-185	plagioclase (An_{13-21})	chlorite	plagioclase (An_{17-28})	Na-smectite, Fe-smectite	felsic	
CP1-185			quartz, plagioclase (An_{38})	Na-smectite, Ti-oxide	felsic	
CP1-185	plagioclase (An_{29-51}), albite (An_{4-9})		quartz	Na-smectite, chlorite, Ti-oxide	felsic	
CP1-185	plagioclase (An_{12}), albite (An_{1-7})		quartz, plagioclase (An_{28})	Ti-oxide	felsic	
CP1-185	plagioclase (An_{32} & An_{39})		plagioclase (An_{16-28})	chlorite, chloritic clay	intermediate	
CP1-185	plagioclase laths (An_{22-38})	calcite	plagioclase (An_{23}), apatite	chlorite	intermediate	groundmass consists of flow-aligned laths
CP1-185	plagioclase (An_{12-31}), albite (An_{2-7})	calcite	quartz	clay (smectite?), Ti-oxide	felsic	some of the phenocrysts are laths
CP1-185	plagioclase (An_{21-34})		albite (An_2), apatite	chlorite, Na-smectite	intermediate	
CP1-185	albite (An_6) & plagioclase (An_{22}) laths		plagioclase (An_{22}), albite (An_4 & An_8)	smectite(?)	felsic	
CP1-185			albite (An_2 & An_3), apatite	chloritic clay	intermediate	

Table B-1 continued

Sample	Phenocrysts	Phenocryst Alteration/ Replacement	Groundmass Crystals	Groundmass Alteration	Groundmass Composition	Comments
CP1-185	albite (An_4)	calcite altered albite (An_8) & plagioclase (An_{33}& An_{42}), albite (An_2) altered plagioclase (An_{23})	quartz	Ti-oxide	felsic	
CP1-185		calcite, Fe-smectite	quartz, plagioclase (An_{27}), albite (An_3)	chloritic clay, fine-grained silicious material, Ti-oxide	felsic	chlorite-filled amygdule(s)
CP1-185	albite (An_{2-9})	calcite altered plagioclase (An_{32})	albite (An_9)	Na-smectite, Fe-smectite	intermediate	chlorite-filled amygdule(s)
CP1-185		albite (An_5) altered plagioclase (An_{24}) lath	albite(?), apatite	chloritic clay, Ti-oxide	intermediate	groundmass consists of flow-aligned laths
CP1-185		calcite, chloritic clay		chloritic clay, Ti-oxide	intermediate	the calcite altered phenocrysts are albite (An_{5-10}) & plagioclase (An_{34-54})
CP1-92	albite (An_{1-3})		K-feldspar (Or_{95} & Or_{98})	Ti-oxide, illitic clay, mixed-layer Fe-K clay, significant fine-grained calcite	intermediate	
CP1-92	plagioclase		plagioclase	Fe-smectite, Na-smectite	intermediate	
CP1-92			albite (An_0)	mixed-layer Fe-K clay, illitic clay, fine-grained calcite	intermediate	

Table B-1 continued

Sample	Phenocrysts	Phenocryst Alteration/ Replacement	Groundmass Crystals	Groundmass Alteration	Groundmass Composition	Comments
CP1-92		calcite altered albite (An_{1-2}), kaolinite altered albite (An_{1-2})	quartz	mixed-layer Fe-K clay, chlorite, calcite	intermediate	
CP1-92	feldspar			illitic clay	felsic	
CP1-92			quartz	mixed-layer Fe-K clay	felsic	
CP1-11	plagioclase (An_{24-33}), albite (An_0)			mixed-layer Fe-K clay	felsic	
CP1-11	plagioclase, albite (An_0)			mixed-layer K-Na clay, mixed-layer K-Ca clay, chloritic clay, and Ti-oxide	intermediate	
CP1-11	albite (An_1)		quartz, albite (An_1)	mixed-layer Fe-K clay	felsic	
CP1-11	K-feldspar (Or_{85} & Or_{91})		quartz	Na-smectite, smectite	felsic	
CP1-11	quartz		quartz, albite (An_5)	clay	felsic	
GB1-3890	plagioclase (An_{43} & An_{47})		quartz(?), K-feldspar (Or_{64} & Or_{68})		felsic	
GB1-3890	quartz		quartz, plagioclase (An_{28})		felsic	
GB1-3890	plagioclase (An_{45} & An_{60})		plagioclase (An_{43} & An_{46})	fine-grained silicious material, Fe-smectite	felsic	
GB1-3890	plagioclase (An_{50-53})		plagioclase (An_{39-50})	mixed-layer Fe-K clay	intermediate	
GB1-3890	plagioclase (An_{46-57})		quartz, plagioclase (An_{37-50}), K-feldspar (Or_{42})		felsic	

Table B-1 continued

Sample	Phenocrysts	Phenocryst Alteration/ Replacement	Groundmass Crystals	Groundmass Alteration	Groundmass Composition	Comments
GB1-3890	plagioclase (An_{49})		plagioclase (An_{44} & An_{45})	fine-grained silicious material, smectite	felsic	
GB1-3890	quartz		quartz, K-feldspar (Or_{95}), albite (An_{7})	mixed-layer Fe-K clay	felsic	
GB1-3890			quartz(?), K-feldspar(?), albite(?)	smectite, mixed-layer Fe-K clay, Ti-oxide	felsic	
GB1-3890	K-feldspar (Or_{90} & Or_{97}), albite (An_{2-3})		plagioclase (An_{14})	chlorite, illitic clay, mixed-layer Na-K clay	intermediate	prehnite amygdule fill, feldspar laths present
GB1-3890	plagioclase (An_{60-69}), hornblende (Mg_{61})	zoned plagioclase (An_{57-83}) with mixed-layer Fe-K clay alteration	plagioclase (An_{36} & An_{49}) laths	Fe-oxide	felsic	
GB1-5464			quartz, K-feldspar (Or_{96}), albite (Or_{4-6})	illite	felsic	
GB1-6083	plagioclase	sericite altered feldspar	quartz, albite (An_{9}), apatite	Na-rich clay	felsic	
GB1-9823	albite (An_{10})	chlorite & chloritic clay altered hornblende	quartz, K-feldspar (Or_{92}), albite		felsic	
GB1-9823			quartz, K-feldspar, albite (An_{3})	chlorite	felsic	
GB1-9823	albite (An_{2-3}) laths		quartz, K-feldspar(?), albite(?)	chlorite, chloritic clay, Ti-oxide	felsic	
NAC1-4195	plagioclase (An_{21}) laths		quartz, K-feldspar, albite		felsic	
NAC1-4195	plagioclase (An_{34} & An_{42})		quartz	mixed-layer clay(?), Fe-smectite, Ti-oxide	felsic(?)	

Table B-1 continued

Sample	Phenocrysts	Phenocryst Alteration/ Replacement	Groundmass Crystals	Groundmass Alteration	Groundmass Composition	Comments
NAC1-4195	quartz, plagioclase laths (An_{53-60})			smectite, Fe-smectite, Ti-oxide	intermediate	quartz phenocrysts are rounded
NAC1-4195	plagioclase (An_{56}) phenocrysts, including one zoned			ilmenite	felsic	groundmass mixed with limonite
NAC1-4195	zoned plagioclase (An_{45-49}), orthopyroxene(?)		quartz, plagioclase laths (An_{31} & An_{33})	mixed-layer Fe-K clay	felsic	
NAC1-4195	plagioclase (An_{50} & An_{51}), orthopyroxene (Mg_{66})		quartz, feldspar microlites		felsic	
NAC1-4197	plagioclase (An_{45-59}), including one zoned			Fe-smectite(?)		
NAC1-4197	plagioclase (An_{61-68})		plagioclase (An_{39})	illitic clay	intermediate	groundmass illitic clay is mixed with limonite
NAC1-4197	plagioclase (An_{52-61})			mixed-layer Fe-K clay	intermediate	
NAC1-4197	plagioclase (An_{42})		plagioclase (An_{30}) & K-feldspar (Or_{31-39}) laths	mixed-layer Fe-K clay, illitic clay		
NAC1-4197	plagioclase (An_{34-38})		quartz, K-feldspar, albite(?)		felsic	
NAC1-4197	K-feldspar (Or_{89} & Or_{94}), albite (An_{2-6}), clinopyroxene (Mg_{66})		albite (An_1)	illitic clay, Fe-smectite, chloritic clay, pyrite	intermediate	
NAC1-4197	plagioclase laths (An_{18-25})		quartz, K-feldspar(?), albite(?)		felsic	

Table B-1 continued

Sample	Phenocrysts	Phenocryst Alteration/ Replacement	Groundmass Crystals	Groundmass Alteration	Groundmass Composition	Comments
NAC1-4197	zoned plagioclase (An_{20} & An_{23} near rim), plagioclase laths (An_{18-25})		quartz, K-feldspar, albite	Fe-oxide, Ti-oxide	felsic	
NAC1-4197	plagioclase (An_{34-39}) laths		quartz, K-feldspar, albite	clay(?), Fe-oxide, and Ti-oxide	felsic	
NAC1-4197	plagioclase (An_{55-71})		plagioclase laths (An_{56})	mixed-layer Fe-K clay	intermediate	
NAC1-4197	plagioclase (An_{51-54}) laths, clinopyroxene (Mg_{76})			clay, Ti-oxide	intermediate	
NAC1-4198			quartz, K-feldspar, albite	Fe-oxide, Ti-oxide	felsic	laths present in groundmass
NAC1-4198	plagioclase (An_{37-49}) laths		quartz, K-feldspar(?)	illitic clay, Ti-oxide	felsic	illitic clay in groundmass is mixed with limonite
NAC1-4198	plagioclase (An_{53-59}) laths			illitic clay	intermediate	illitic clay in groundmass is mixed with limonite
NAC1-4198	plagioclase laths (An_{35} & An_{36})		quartz, K-feldspar(?), albite(?)		felsic	
NAC1-4198	plagioclase (An_{80} & An_{86})		plagioclase laths	Ti-oxide	intermediate	
NAC1-4198	zoned plagioclase (An_{47-72})		plagioclase (An_{49})	Ti-oxide, Fe-oxide		
NAC1-4198			plagioclase laths (An_{29-33})		felsic	

APPENDIX C

X-RAY FLORESCENCE ANALYTICAL METHODS AND DATA

Rainer Newberry performed semi-quantitative major and minor element analyses on polished slabs (sample billets) of fine- to coarse-grained sandstone from the Bear Lake Formation via X-Ray Fluorescence (XRF) at the Advanced Instrumentation Laboratory at the University of Alaska Fairbanks using a Panalytical 4 kW Wavelength Dispersive Axios Spectrometer. Instrument conditions included count times of 10 to 30 seconds for major elements and 40 to200 seconds for trace elements, accelerating voltage of 32 kV for light elements and 60 kV for heavy elements, and beam current of 66 mA for light elements and 125 mA for heavy elements. Natural International rock standards were employed for elemental standardization. Precision, based on replicate analyses, is < 1% of the amount present for concentrations ≥ 10x the detection limit. Tests comparing slabs of fine-grained rocks to powder pellets (Hicks et al., 2003) indicate that accuracy is approximately ±10% for concentrations > 20 ppm and ± for concentrations > 0.5%. Table C-1 and Table C-2 report the major oxide and minor element XRF geochemical data.

Table C-1 Major oxide chemistry of Bear Lake Formation sandstones. Measured by X-Ray Fluorescence.

Sample	SiO_2	Al_2O_3	BaO	CaO	FeO	K_2O	MgO	MnO	Na_2O	P_2O_5	TiO_2
BL-5-95	56.2	7.21	0.1	27	3.66	1.12	1.2	1.3	1.52	0.24	0.339
BL5-92	50.7	8.24	0.103	30.1	4.46	1.22	1.26	1.5	1.54	0.217	0.472
BL5-52	75.6	10.3	0.0411	2.24	5.87	1.69	1.47	0.229	1.31	0.186	0.496
LH1-164	52.1	8.03	0.104	28.5	4.55	1.16	1.18	0.745	2.01	0.893	0.652
LH1-120	63.3	9.8	0.116	14	2.98	1.48	1.77	0.174	2.9	0.0783	0.408
LH1-66.5	57.6	8.31	0.0958	22.3	5.29	0.866	1.9	0.267	2.31	0.409	0.445
BL1-5	51.5	12	0.113	27.3	3.06	1.46	0.887	0.159	2.33	0.154	0.857
BL1-155	46.5	9.46	0.112	33.1	3.49	1.1	2.28	0.739	2.12	0.204	0.494
BL3-272	63.6	15.6	0.103	2.41	8.08	1.6	3.94	0.076	3.27	0.206	0.915
BL-3-205	67.1	15	0.129	2.33	6.41	1.7	3	0.0523	3.24	0.171	0.733
BL3-193	61.7	17	0.0942	2.25	9.34	1	3.14	0.0623	4.2	0.238	0.809
BL-3-36	53.5	14.5	0.0605	15.5	9.23	0.937	1.72	0.187	3.21	0.191	0.833
CP1-185	62.5	14.9	0.0945	5.29	7.51	0.93	2.2	0.117	3.73	0.338	1.38
CP1-92	65.6	17.3	0.0391	2.02	6.85	2.03	1.93	0.0618	2.87	0.21	0.96
NAC1-4197	63.6	14.4	0.141	2.76	8.25	2.4	2.59	0.0713	2.5	0.152	0.959
GB1-4945	72.4	17.1	0.0945	0.798	2.59	2.39	1.04	0.0288	2.25	0.143	0.72
GB1-6083	71.5	15.3	0.0501	1.12	4.1	2.4	1.43	0.0536	2.44	0.206	0.664
GB1-8236	69.5	16.5	0.101	0.725	6.08	1.86	1.9	0.0469	2.12	0.156	0.805
GB1-9823	72.4	16.2	0.0951	0.776	1.91	1.26	0.828	0.0356	4.95	0.132	1.21

Table C-2 Minor element chemistry of Bear Lake Formation sandstones. Measured by X-Ray Fluorescence.

Sample	As	Cr	Cu	Ni	Pb	Rb	S	Sr	V	Y	Zn	Zr
BL-5-95	5	87	41	60	40	48	710	242	235	24	59	52
BL5-92	5	119	20	5	28	61	474	238	161	36	74	99
BL5-52	5	78	89	40	32	50	855	465	186	18	98	73
LH1-164	5	70	80	87	45	56	171	432	126	14	56	122
LH1-120	5	143	5	74	- -	56	1950	484	172	15	63	90
LH1-66.5	5	57	31	5	- -	38	1020	537	67	31	58	97
BL1-5	18	136	74	11	34	57	446	458	126	17	71	167
BL1-155	5	85	80	80	36	53	1160	568	115	17	76	75
BL3-272	5	145	69	44	27	52	371	546	292	19	129	142
BL-3-205	77	126	68	59	31	57	129	455	213	20	99	91
BL3-193	73	109	41	124	25	30	466	581	290	18	86	98
BL-3-36	5	175	91	113	30	43	311	474	191	18	111	118
CP1-185	22	45	65	89	57	35	462	323	189	24	82	156
CP1-92	84	100	81	14	49	55	471	282	167	21	124	91
NAC1-4197	183	183	198	55	55	123	19700	364	308	28	180	172
GB1-4945	95	114	105	140	50	82	3750	184	111	13	100	183
GB1-6083	160	118	89	59	40	85	5580	199	198	18	203	116
GB1-8236	34	109	78	25	57	78	647	247	158	24	101	174
GB1-9823	59	146	86	5	52	36	1200	454	119	11	36	76